Morphological and molecular characterization of columnar cholinergic neurotransmission onto T5 cells of *Drosophila*

Eleni Samara

Graduate School of
Systemic Neurosciences
LMU Munich

Dissertation at the
Graduate School of Systemic Neurosciences
Ludwig-Maximilians-Universität München

19th of February 2025

First Reviewer and Supervisor
Prof. Dr. Alexander Borst, Max Planck Institute for Biological Intelligence

Second Reviewer
Prof. Dr. Martin Biel, Ludwig Maximilians University

External Reviewer
Prof. Dr. Claude Desplan, New York University

Date of Submission: *19th of February 2025*
Date of Defense: *23th of May 2025*

Ἂν μένει πάντα κάποια γῦρις
στὰ τελειωμένα πράγματα
γιὰ τὴν ἐπικονίαση
τῆς ἐμπειρίας, τῆς λύπης
καὶ τῆς ποίησης.
Αυτοσυντήρηση, Κ. Δημουλά

If there is always some pollen left
in finished things
for the pollination of experience,
of sorrow and of poetry.
Self-preservation, K. Dimoula

ABSTRACT

Sensory feedback initiates bottom-up brain processing, which in line activates top-down processing. Vision is a major sensory input in this processing loop, that eventually leads to perception and decision making. Navigating the environment while choosing attractive visual cues over aversive ones, evaluating ego-motion to stabilize a course, chromatically and achromatically detect objects, are some of the tasks that visual systems perform. To elucidate the cellular and molecular mechanisms of such neural computations and the resulting behaviors, more simplistic, yet powerful, visual systems have been explored. Being a genetically tractable model organism that exhibits high neuronal and behavioral diversity, *Drosophila melanogaster* serves this purpose well. Neuronal connectivity is now accessible thanks to connectomic approaches, but the morphological and molecular identities of each chemical connection are still quite elusive.

This cumulative-style doctoral thesis consists of two manuscripts that explore chemical synapses in the OFF-motion vision circuitry of *Drosophila*. The first manuscript investigates the polyadic morphology of chemical synapses between the primary motion detectors in the OFF pathway, T5 cells, and their columnar cholinergic inputs Tm1, Tm2, Tm4 and Tm9. In this work, I used the open-data connectomics database FlyWire and identified the Tm-to-T5 wiring via various polyadic synapse types. Then, I focused on the T5 dendritic distribution of the different polyadic types and found differences in their spatial patterns. Lastly, I showed that the polyadic morphology is setting a directional wiring architecture at the T5 network level. This work demonstrated the subsynaptic level of complexity in Tm-to-T5 connectivity.

In the second manuscript of my doctoral thesis, we investigated the molecular identity of each Tm-to-T5 chemical connection. Fast ionotropic nicotinic (nAChRs) and slow metabotropic muscarinic (mAChRs) acetylcholine receptors are expressed in the brain of *Drosophila*, but the contribution of different AChRs to visual information processing remained poorly understood. We used a suit of genetic tools and gained accessibility to AChRs, thus finding the nAChRα1, nAChRα3, nAChRα4, nAChRα5, nAChRα7 and nAChRβ1 subunits and the mAChR-B receptor localizing on T5 dendrites. Mapping the most highly expressed nAChR subunits across Tm-to-T5 synapses showed the

nAChRα5 prevalence in Tm1-, Tm2- and Tm4-to-T5 synapses and of nAChRα7 in Tm9-to-T5 synapses. *In vivo* functional characterization of nAChRα4, nAChRα5, nAChRα7 and mAChR-B revealed alterations in the fly optomotor response and T5 directional tuning after AChR knock-down. Collectively, this work exhibited the complexity of cholinergic neurotransmission and consequently of preferred direction enhancement in T5 cells, which is introduced by the different receptor categories, subunit stoichiometries, isoforms and their synaptic localization.

CONTENTS

LIST OF FIGURES

1 | INTRODUCTION

1.1 *DROSOPHILA* AS A MODEL ORGANISM

Drosophila melanogaster, most commonly known as the fruit fly, is an arthropod belonging to the order diptera, first described by the German entomologist Johann Wilhelm Meigen (Keller, 2007; Meigen, 1818). While this classification is shared with hundreds of thousands other species, *D. melanogaster* holds a unique position in scientific research. William E. Castle, Frank Lutz Fernandus Payne and Thomas H. Morgan were the first to identify the fruit fly's potential (Ashburner, 1989; Carlson, 2013; Jennings, 2011). The short life cycle, fast reproduction rates, genetic tractability, affordability and ethical accessibility, are some of the organism's valuable traits that still resonate in the scientific community. As an outcome, knowledge in genetics, immunology, developmental biology and bioengineering has been accumulating over a century now, rendering *Drosophila* an ideal model organism.

Drosophila in Neuroscience

The contributions of *Drosophila* research in neuroscience have been equally prominent. The effects of *Notch* in neurodevelopment (Morgan & Bridges, 1916; Poulson, 1950), the exploration of the behavioral molecular basis (Benzer, 1967) and the discovery of the first ever potassium channel *Shaker* (Jan & Jan, 1976; Jan et al., 1977), have been research milestones (Bellen et al., 2010). Recently, a neuronal wiring diagram of the adult female fly was completed, paving new ways in the field of connectomics and systems neuroscience (Dorkenwald et al., 2024; Schlegel et al., 2024).

Insect research can contribute to neuroscience questions across classes. *Drosophila* is used as a model for neurodegenerative diseases, including Alzheimer's and Parkinson's disease (Jeibmann & Paulus, 2009). The characterization of a plethora of exo- and endo-cytosis proteins in the fruit fly allowed for the comprehension of synaptic neurotransmission proteins in vertebrates (Bellen et al., 2010; Richmond & Broadie, 2002; Schwarz, 2006; Südhof, 2004). Importantly, *Drosophila* has offered valuable insights in sensory neuroscience thanks to the level of resolution it achieves, helping the advancement of its mammalian counterpart (Clark & Demb, 2016; Masse et al., 2009).

1.2 VISUAL SYSTEMS

Vision is a fundamental sensory modality for the navigation, socialization and ultimately for the survival of the individual. The variety of the elicited behavioral responses after visual information processing, is one of the reasons why visual systems have been -and continue to be- heavily researched across taxa (Exner, 1891).

The first step in the visual processing cascade, is the receival of sensory information by the eyes. Insects have multi-lensed compound eyes comprising of hexagonal ommatidia (Figure 1A), while mammals have single-lensed camera-like eyes (Land & Nilsson, 2012). Retinal photoreceptors are the neuronal substrate for phototransduction. Light energy i.e photons, are absorbed by visual pigment proteins and then translate into neural signals as changes in membrane conductance (Rayer et al., 1990). Rods in mammals and R1-R6 photoreceptors in the fly ommatidia are responsible for achromatic vision, while cones and R7-R8 photoreceptors are responsible for chromatic vision (Dacey, 2000; Hardie, 1979; Zuker et al., 1987; Zuker et al., 1985). Mammalian cones and rods then form connections with horizontal and bipolar cells, with the later connecting to amacrine cells and the final output retinal neurons, the retinal ganglion cells (RGCs). RGCs project to the lateral geniculate nucleus (LGN), with LGN neurons connecting to the primary visual cortex (V1)(Sanes & Zipursky, 2010). R1-R6 photoreceptors in the retina of the fly connect to neurons in the lamina neuropil, while R7-R8 photoreceptors connect with neurons in the medulla neuropil. Then visual information enters the lobula and lobula plate neuropils until it finally reaches the protocerebrum via visual projection neurons (Sanes & Zipursky, 2010). All the aforementioned neuropils belong to the optic lobe of the fly's brain, which follows a retinotopic organization (Figure 1A-C). The latter organization describes that a circuitry starting at a retinal ommatidium, expanding to a lamina cartridge and then progressing to a medulla and lobula column is recapitulated across the ~850 facets of the compound eye (Borst & Euler, 2011; Surkova et al., 2021).

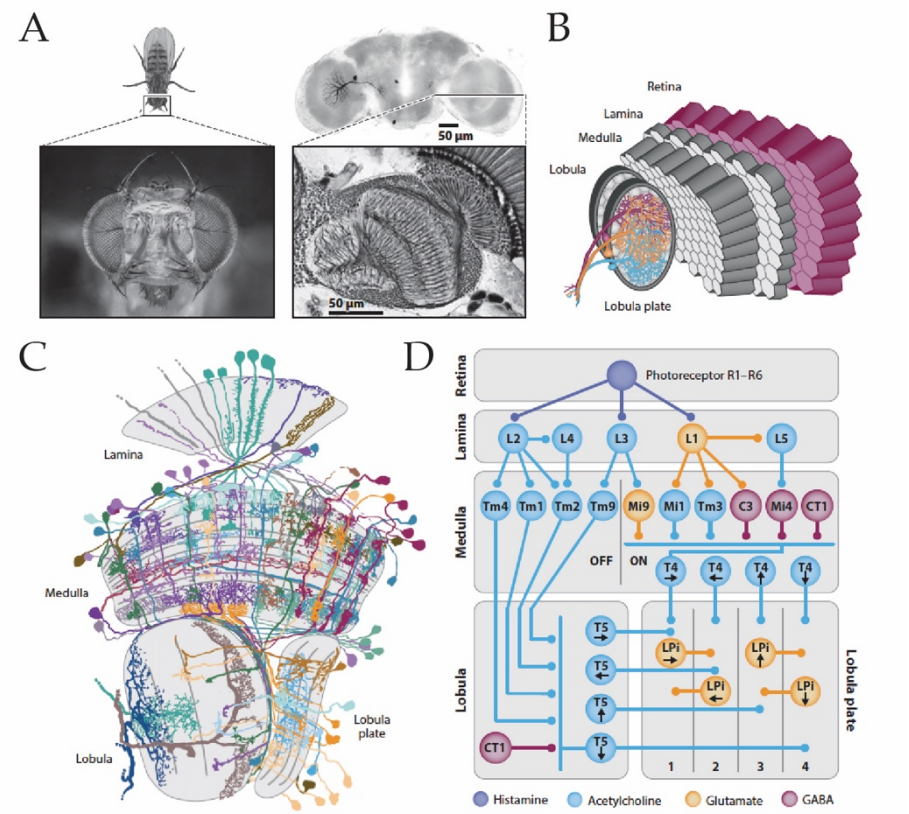

Figure 1. Anatomy of the fly optic lobe. (A) Micrograph of a *Drosophila* head with a facet eye on either side (left). (Right) Frontal cross section of a *Drosophila* brain with a single lobula plate tangential cell stained after a patch-clamp recording (top) and horizontal cross section of the optic lobe stained by Bodian's method, showing the columnar organization (bottom). Scale bars: 50 µm. Panel A adapted with permission from Takemura et al. (2008). Photo of the fly head provided by Florian Richter. (B) Schematic of the optic lobe. In the lobula plate, three tangential cells are shown. Panel b adapted with permission from Borst & Euler (2011). (C) Collection of different cell types in the Drosophila optic lobe. Panel C adapted with permission from Borst et al. (2020). (D) Schematic diagram of the motion vision circuit. Photoreceptors connect to lamina (L) cells that split signals into an ON and an OFF pathway. Transmedullary (Tm), medulla intrinsic (Mi), centrifugal (C), and complex tangential (CT) cells relay temporally filtered signals to the dendrites of T4 cells in the medulla and of T5 cells in the lobula. Different types of T4 and T5 cells send their axons to one out of four layers of the lobula plate, where they synapse onto lobula plate intrinsic (LPi) and lobula plate tangential cells (not shown). Some connections and cell types have been omitted for clarity. Figure and figure caption with permission from Borst and Groschner (2023).

1.2.1 Motion vision

Among the different visual modalities in *Drosophila* such as color vision, depth perception, feature perception and polarization vision, motion vision is the best-studied modality. The

importance of motion vision in navigating the environment so as to approach a mate and avoid a predator, while simultaneously perceiving self-motion, are some of the reasons for the excessive research focus (Borst, 2014).

Luminance changes perceived by retinal photoreceptors R1-R6 are split into two pathways: the ON-pathway computing luminance increments and the OFF-pathway for luminance decrements (Joesch et al., 2010; Strother et al., 2014) (Figure 1D). Thanks to advancements in connectomics, we now have a cell-type-specific identification of the cellular components in each pathway. In the ON-pathway, L1 neurons connect to the cholinergic inputs Mi1 and Tm3, and L3 neurons connect to the glutamatergic input Mi9 (Shinomiya et al., 2015, 2019; Takemura et al., 2013; Takemura et al., 2017). Mi1, Tm3, Mi9 together with the GABAergic C3, Mi4 and CT1 cells connect to the bushy T4 cells (Fischbach & Dittrich, 1989; Shinomiya et al., 2019). In the OFF-pathway, L2 neurons connect to the cholinergic Tm1, Tm2 and Tm4 cells, while L3 neurons connect to the also cholinergic Tm9 cells (Shinomiya et al., 2014, 2019; Takemura et al., 2011). Together with CT1, Tm1, Tm2, Tm4 and Tm9 cells connect to the bushy T5 cells (Fischbach & Dittrich, 1989; Shinomiya et al., 2019). The increased variety of cholinergic inputs in T5 compared to T4 cells has so far been addressed at the intrinsic cellular level, where Tm9 exhibits longer response time constants compared to Tm1, Tm2 and Tm4 (Serbe et al., 2016).

Elementary motion detectors

The first neuronal populations that can extract directional information are T4 cells in the ON-pathway and T5 cells in the OFF-pathway (Fisher et al., 2015; Maisak et al., 2013). T4 and T5 function is intertwined with their morphology, as both of them exist in four subtypes per column: a, b, c and d. Each subtype has its dendrite oriented in one of the four cardinal directions and responds selectively to front-to-back, back-to-front, upward or downward motion, respectively (Maisak et al., 2013). In mammals, we encounter a bigger variety of direction-selective cells. Specifically, there exist three groups of direction-selective retinal ganglion cells: a. the ON-OFF ganglion cells, with four subtypes according to their preferred direction along one of the four cardinal directions (Elstrott et al., 2008; Oyster & Barlow, 1967), b. the ON ganglion cells, with three subtypes and 120 degrees separation between their preferred directions (Oyster & Barlow, 1967; Sun et al., 2006), and c. the OFF JAM-B cells, all of which prefer upward motion (Borst & Helmstaedter, 2015; Kim et al., 2008).

1.2.2 Algorithmic models for motion vision

The direction-selective computations of T4 and T5 cells can be algorithmically explained and interpreted. The best algorithmic representation of this neuronal computation is the correlator model. Visual systems correlate in time and space: the brightness values measured at two adjacent image points are correlated with each other after one of them has been filtered in time (Borst & Euler, 2011) (Figure 2A,B). Using the optomotor response of the beetle *Cholorphanus* as a behavioral measure, Hassenstein and Reichardt proposed the first correlation detector consisting of two mirror-symmetrical subunits (Borst, 2000; Hassenstein & Reichardt, 1956; Reichardt, 1961, 1987) (Figure 2C). In each subunit, a delayed and a non-delayed signal deriving from two neighboring inputs are multiplied with each other, with the final detector response being given by the difference of the output subunit signals (Borst & Euler, 2011; Clark & Demb, 2016). The Hassenstein and Reichardt correlator responds positively to motion in the preferred direction and negatively to motion in the non-preferred 'null' direction. Another correlator detector was the one proposed by Barlow and Levick from their work in the rabbit retina (Barlow & Levick, 1965) (Figure 2D). Compared to the Hassenstein and Reichardt model, the Barlow and Levick correlator consists of one subunit with two neighboring temporally offset inputs that are not multiplied, but divided by the application of an AND-NOT or veto gate. Motion in the null direction first activates the delayed veto input and both signals arrive simultaneously at the AND-NOT gate, thus silencing the detector's activity. Motion in the preferred direction first activates the non-delayed input followed by the veto input, hence the detector gets activated (Borst & Euler, 2011). Recordings from *Drosophila melanogaster* motion-sensitive neurons showed a combination of these two correlator models into a three-arm detector model (Haag et al., 2016; Leong et al., 2016) (Figure 2E). The detector receives three input lines, one direct non-delayed line flanked by two delayed ones. The algorithmic representation of direction selectivity can be described with a multiplication of the delayed input on the preferred side with the central direct line and its consecutive division with the delayed input line at the null side of the neuron's receptive field (Borst & Groschner, 2023). Sixty years after the first proposal of these correlator models, we are now able to allocate the neural correlates of direction-selectivity both in the ON and the OFF motion pathway (Shinomiya et al., 2019).

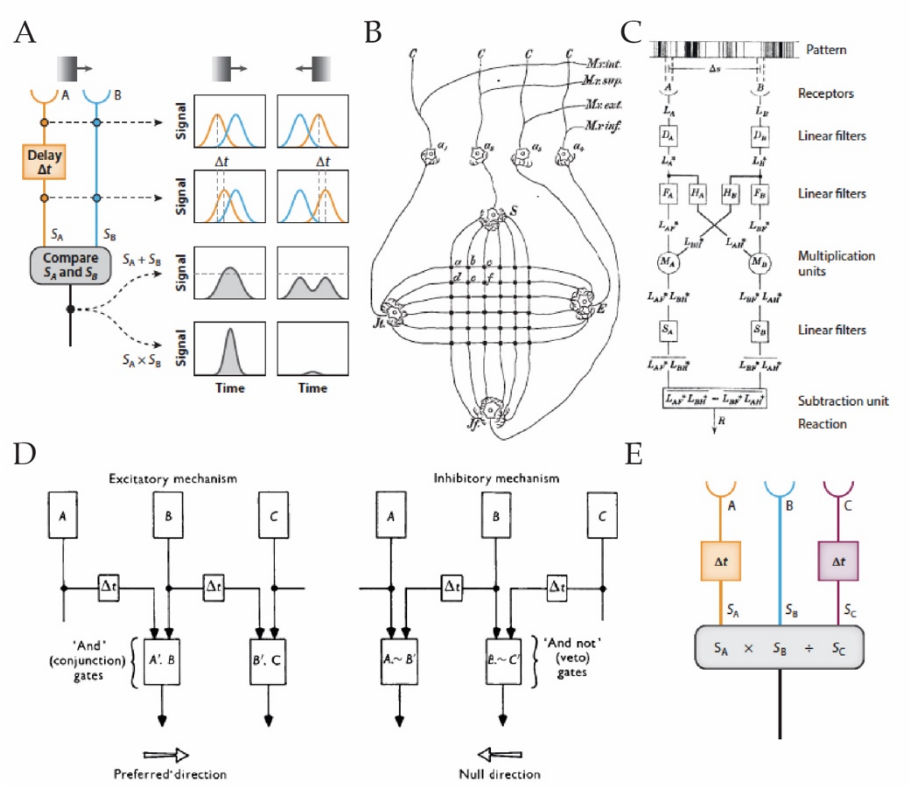

Figure 2. Models of motion detection. (A) A visual motion detector requires at least two input signals (SA and SB) from adjacent photoreceptors (A and B). The signals are differentially delayed by t so that they coincide at the detector only if A is activated prior to B, as is the case for motion in the preferred direction (rightward) but not for motion in the opposite direction. A nonlinear interaction is required to detect the coincidence of SA and SB. The bottom two rows of graphs show a signal summation (SA + SB) followed by a threshold (horizontal dashed line) and a signal multiplication (SA × SB). (B) Early proposal of a motion detection circuit. Panel b reproduced from Exner (1894) (public domain). (C) Correlation or Hassenstein–Reichardt detector. Photoreceptor signals from adjacent image points are differentially filtered in time (F and H) and multiplied (M) in a mirror-symmetrical way. The outputs of the multipliers are subtracted. Panel c reproduced with permission from Reichardt (1961); copyright 1961, Massachusetts Institute of Technology. All rights reserved. (D) Preferred direction excitation and null direction inhibition, realized by AND (left) and ANDNOT (right) gates, respectively, as two alternate mechanisms underlying direction selectivity in the rabbit retina. Panel d reproduced with permission from Barlow & Levick (1965). (E) A combination of the two mechanisms within one stage, as proposed by Haag et al. (2016, 2017) and Leong et al. (2016). Figure and figure caption with permission from Borst and Groschner (2023).

1.2.3 Motion vision and behavior

Flies visually navigate the world by rotating or translating and have evolved a set of corrective manoeuvres so as to maintain

their walking or flight trajectories. The optomotor response is such an example when flies are presented to rotatory visual motion (Mauss & Borst, 2020). It encompasses at least three neural algorithms: the detection of local motion, the detection of optic flow and the motor output (Götz, 1964, 1968, 1970; Hecht & Wald, 1934; Ryu et al., 2022). T4 and T5 cells are the neural correlates of local motion detection (Leonte et al., 2021), while lobula plate tangential cells (LPTCs) of the horizontal and the vertical system (HS/VS) are the neural correlates of widefield motion detection (Fujiwara et al., 2017; Haikala et al., 2013; Heisenberg et al., 1978). HS/VS neurons connect to the descending neurons HS1/OVS1, with the latter terminating at the prothoracic region in the ventral nerve cord (VNC), which controls neck muscles and head movement (Namiki et al., 2018; Suver et al., 2016). Interestingly, there are indications that the head optomotor response visual pathway differentiates from the wing optomotor response one (Kim et al., 2017). Nevertheless, the optomotor response is solely driven by the motion vision circuitry. Object-fixation, on the other hand, is regulated by the position and motion vision circuit (Bahl et al., 2013). In fixation behavior, flies tend to keep a long vertical bar in front of them during locomotion. This has been identified by closed loop experiments, where the fly's rotation is fed back to a servo motor control (Heisenberg, 1984; Reichardt, 1961). Another motion-vision driven behavior is the avoidance behavior. Flies can either take-off, start walking backwards, begin landing or escape manoeuvres depending on the velocity of the approaching object (Ache, Namiki, et al., 2019; Ache, Polsky, et al., 2019; Sen et al., 2017). However, it is important to study visually-induced fly behaviors under more natural conditions. As the latter are more complex than the visual stimuli used in laboratory conditions, the engineering of new devices for visual stimulation is fundamental (Prech et al., 2024).

1.3 NEUROTRANSMISSION

Neurons communicate via chemical, electrical and ephaptic connections. Electrical connections are formed by gap junctions and allow the bidirectional flow of ions and metabolites (Ammer et al., 2022; Furshpan & Potter, 1957; Nielsen et al., 2012), while ephaptic connections take place in anatomically and electrically proximate neurons through modulation of the extracellular potential (Kamermans & Fahrenfort, 2004). Chemical communication happens in juxtapositions known as chemical synapses and exhibit unparalleled levels of modulation, thus

driving cognitive processes as learning and memory (Kandel & Squire, 2000).

Presynapse

From the initial discovery of chemical communication (Loewi, 1921), neurotransmission has been heavily researched, primarily due to its compartmentalized complexity. Neurotransmitters are released from the presynaptic compartment, diffuse in the synaptic cleft and are received by neurotransmitter receptors at the postsynaptic site. At the presynaptic site, neurotransmitters are stored in secretory vesicles that get transferred close to the plasma membrane for a Ca^{2+}-regulated fusion. The molecular machinery responsible for vesicular fusion are the membrane associated SNARE proteins, comprising of the vesicular SNARE Synaptobrevin 2, the target SNARE Syntaxin 1 and the Synaptosomal associated protein of 25 kilodaltons (SNAP-25) across species (Sauvola & Littleton, 2021; Söllner et al., 1993). Another level of vesicular fusion regulation in *Drosophila* comes with the SNARE regulatory proteins, amid whom Unc13, Synaptotagmin 1, Rab3-interacting molecule (RIM) and Tomosyn offer temporal and spatial control of secretion (Sauvola & Littleton, 2021; Südhof & Rothman, 2009). Remarkably, two Unc13 isoforms spatially differ in presynapses which might account for release differences (Böhme et al., 2016; Piao & Sigrist, 2022). The specific presynaptic localization of fusion and release is referred to as an active zone (AZ), while multiple AZs can be found at a single presynaptic bouton in the *Drosophila* neuromuscular junction (NMJ) (Van Vactor & Sigrist, 2017). In the fruit fly, AZs are characterized by a T-bar structure (Duhart & Mosca, 2022; Hamanaka & Meinertzhagen, 2010; Meinertzhagen, 1996; Prokop & Meinertzhagen, 2006) formed by the proteins Bruchpilot (Brp) and RIM (Acuna et al., 2016; Duhart & Mosca, 2022; Fouquet et al., 2009; Hallermann et al., 2010; Kittel et al., 2006; Liu et al., 2011; Scholz et al., 2019; Wagh et al., 2006).

Postsynapse

The postsynaptic components are understudied compared to their presynaptic counterparts. Based on the synapse's neurotransmitter identity, different receptors either ionotropic or metabotropic localize postsynaptically. Discs large (Dlg) is a member of the membrane-associated guanylate kinase (MAGUK) family (Harris & Littleton, 2015) and together with Drep-2 have been found to localize at postsynaptic sites in *Drosophila* (Andlauer et al., 2014; Duhart & Mosca, 2022).

Even though the pre- and post-synaptic compartments are structurally discrete, they are not functionally disconnected. Retrograde signaling offers an additional level of regulation. The

target SNARE Syx4 was found to regulate the localization of synaptic proteins in the postsynaptic compartment at the *Drosophila* NMJ (Harris et al., 2016, 2018). Neurexin (Nrx) and Neuroligin (Nlg) are transsynaptic adhesion proteins important for the formation, maturation, and organization of synapses, with Nrx being the presynaptic partner and Nlg the postsynaptic partner (Bang & Owczarek, 2013; Harris & Littleton, 2015). Nonetheless, Nrx has a postsynaptic role at the NMJ (Chen et al., 2010), and Nlg-2 is required both pre- and post-synaptically (Chen et al., 2012; Harris & Littleton, 2015). Another set of transsynaptic adhesion proteins are Teneurins (Ten) and interact with Nrx-1 and Nlg-1 in synaptic organization, while Ten-a is presynaptic and Ten-m is predominantly postsynaptic (Harris & Littleton, 2015; Mosca et al., 2012). Collectively, chemical synapses are sites of extreme complexity that dynamically regulate neuronal communication.

1.3.1 Cholinergic neurotransmission

Depending on the identity of the neurotransmitter that is transported in synaptic vesicles, neurotransmission in *Drosophila* can be cholinergic, GABAergic, glutamatergic, dopaminergic, serotoninergic, octopaminergic and histaminergic (Kolodziejczyk et al., 2008; Shin et al., 2018; Stuart, 1999; Yasuyama & Salvaterra, 1999). Apart from being the first neurotransmitter ever identified (Dale & Dudley, 1929), acetylcholine is the most widely used neurotransmitter in *Drosophila* synapses (Eckstein et al., 2024) and is produced by choline acetylase (ChAT) after the transfer of an acetyl group from acetyl coenzyme A to choline (Buchner et al., 1986; Nachmansohn & Machado, 1943; Smallman & Pal, 1957). Interestingly, acetylcholine can act as a fast neurotransmitter via ionotropic receptors or as a neuromodulator via metabotropic receptors, showing once more the complexity of chemical communication (Ito, 2008; Picciotto et al., 2012).

1.3.2 Acetylcholine receptors

The presynaptic release of acetylcholine is followed by its binding at the postsynaptic site by acetylcholine receptors (AChRs). AChRs include two categories across bilaterians and cnidarians (Faltine-Gonzalez & Layden, 2018): the fast ionotropic nicotinic receptors (nAChRs) and the slow metabotropic muscarinic receptors (mAChRs).

nAChRs

nAChRs are activated by acetylcholine (ACh) and the agonist nicotine and belong to the cys-loop ligand-gated ion channel superfamily, forming functional pentamers of various subunit stoichiometries, homomeric or heteromeric (Hogg et al., 2003). Cys-loop receptors are named after a 13-amino-acid loop within the extracellular domain (ECD) that is enclosed by a pair of disulphide-bonded Cys residues (Thompson et al., 2010). The ECD contains the ligand-binding site, the transmembrane domain (TMD) consists of four membrane-spanning a-helices (M1–M4) that enable ions to cross the membrane, while the intracellular domain (ICD) is primarily formed by the M3–M4 intracellular loop (Thompson et al., 2010) (Figure 3). In *Drosophila* the pentameric nAChR formation is achieved from a pool of seven α and three β subunits (Dupuis et al., 2012; Littleton & Ganetzky, 2000; Thompson et al., 2010). In mammals, nicotinic AChRs comprise nine α subunits (α1-7,9,10), four β subunits (β1-4), one γ, one δ and one ε subunits (Albuquerque et al., 2009). Nevertheless, both in the fruit fly and in mammals, the two adjacent extracellular cysteines (Cys-Cys) are the ones responsible for binding ACh (Rosenthal & Yuan, 2021). The extracellular Cys-Cys motif is a characteristic of the α subunits and sets them apart from the remaining β, γ, δ and ε subunits. The stoichiometry of nAChRs still remains elusive. The neuromuscular nAChR in mammals was the first stoichiometry to be identified, with four different subunits forming a functional pentameric receptor $\alpha_2\beta\gamma\delta$ (Karlin et al., 1983; Thompson et al., 2010). Another level of stoichiometrical diversity comes between different isoforms, as different arrangements may exist even with the same subunit types (Gotti et al., 2007; Millar & Gotti, 2009; Millar & Harkness, 2008; Olsen & Sieghart, 2009). For example, the α4β2 nAChR may be of an $(\alpha4)_2(\beta2)_3$ or $(\alpha4)_3(\beta2)_2$ isoform, resulting in distinct pharmacologies and channel conductance (Moroni et al., 2006; Moroni & Bermudez, 2006). Interestingly, it has been found that fast (τ=50ms) and slow desensitizing (τ=539 ms) nAChRs exist in the honeybee brain (Dupuis et al., 2011). This has been attributed to the nAChRα7 subunit, showing once more the temporal regulation that different stoichiometries can introduce.

mAChRs

mAChRs are G protein-coupled receptors (GPCRs), activated by ACh and the agonist muscarine and have three types, A, B and C in *Drosophila* (Bielopolski et al., 2019; Malloy et al., 2019; Xia et al., 2016). These mAChR types activate different signaling cascades, with the mAChR-A and mAChR-C being coupled to the $G_{q/11}$ signaling cascade and the mAChR-B to the $G_{i/0}$ (Collin et al., 2013; Malloy et al., 2019; Ren et al., 2015). In mammals, a

greater variety of mAChRs is encountered, as they consist of five M (M1-5) types (Abrams et al., 2006). G-proteins are composed of three subunits: α, β, and γ. When the muscarinic receptor is bound by acetylcholine, it will change its conformation, causing the α subunit to release the natively bound guanosine diphosphate molecule (GDP) and trade it for guanosine triphosphate (GTP) (Sam & Bordoni, 2025). Once GTP binds to the α subunit, the α subunit will dissociate from the β and γ subunits and interact with other downstream effector molecules. The α subunit has intrinsic GTPase activity and will eventually catalyze GTP back into GDP, thus turning the second messenger system "off" intrinsically with time (Sam & Bordoni, 2025).

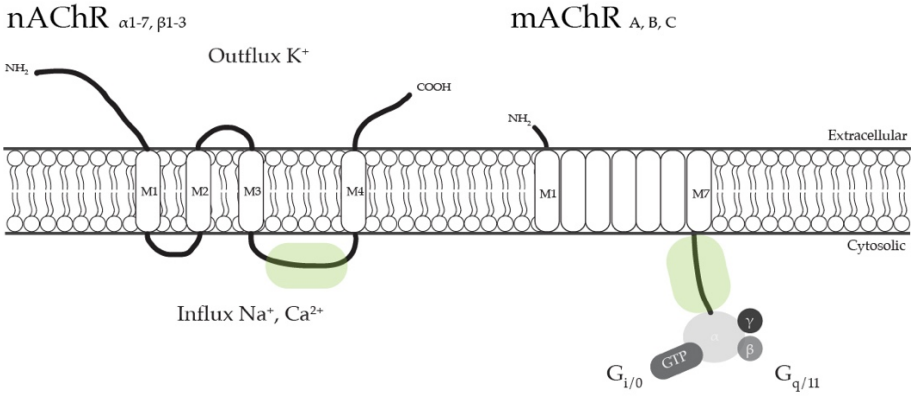

Figure 3. Nicotinic (nAChR) and muscarinic (mAChR) receptors in *Drosophila*. nAChRs have four transmembrane domains and allow the influx of sodium and calcium and the outflux of potassium. The pentameric active channel is formed from a pool of seven α and three β subunits. mAChRs have seven transmembrane domains and are G-protein coupled receptors that activate secondary signaling cascades. A, B, C types activate different signaling pathways. The intracellular sites mostly used for protein engineering with fluorescent proteins are depicted in green.

1.4 NEURONAL CIRCUITS

Neuronal circuits responsible for certain behaviors can be explored with high resolution in *Drosophila*. From the cellular morphology up to the individual connections and their function, the fruit fly is a powerful model organism for systems neuroscience.

1.4.1 Genetic tools

GAL4/UAS

A significant breakthrough in *Drosophila* genetics was the development of the GAL4/UAS system for targeted gene expression (Brand & Perrimon, 1993). GAL4 is a transcription

factor that was first identified in the yeast *Saccharomyces cerevisiae*, and regulates gene expression by binding to 17 base pair sites termed the Upstream Activating Sequences (UAS) (Duffy, 2002; Giniger et al., 1985; Laughon et al., 1984; Laughon & Gesteland, 1984). The extensive use of the GAL4/UAS binary gene expression system lead to the identification of other binary expression systems like the LexA/LexAop (Lai & Lee, 2006; Szüts & Bienz, 2000), tTA/TRE (Bello et al., 1998), and the Q-system (Potter et al., 2010). Such a toolbox of various expression systems allows for the simultaneous use of two binary expression systems and consequently for the simultaneous accessibility in distinct neuronal populations. To constrain the expression of GAL4 drivers in neurons of interest, the split-GAL4 system has been developed (Luan et al., 2006). DNA-binding (DBD) and transcription activation (AD) domains of GAL4 were fused to heterodimerizing leucine zippers. This allows for the independent targeting of the DBD and AD domains to different cells using distinct enhancers. Only those cells in which both enhancers were active would express the DBD and AD GAL4 domains and hence reconstitute GAL4 activity (Luan et al., 2020).

RNAi

Another advancement was the generation of resources for transgenic RNA interference (RNAi) in *Drosophila* (Echeverri & Perrimon, 2006). Double-stranded long- and short-hairpin RNA are two approaches where RNA silencing can be induced. For the long-hairpin RNA approach (Ni et al., 2008, 2009), an inverted repeat of the target mRNA is transgenically expressed, which triggers the activation of the Dicer ribonuclease of the RISC complex and then eventually leads to the double-stranded (dsRNA) cleavage in small RNAs (siRNA)(Bernstein et al., 2001; Kavi et al., 2005). For the short-hairpin RNAs, the same activation cascade with the long-hairpin version applies, but is more effective in silencing genes during oogenesis (Ni et al., 2011). In general, RNA interference in *Drosophila* is essential for reverse genetic experiments, but parameters such as gene knock-down efficiency, off-target effects and temperature-dependence should always be kept in mind.

Protein tags

The morphological aspects of neuronal connectivity can currently be addressed from the cellular up to the molecular level. Promoter-enhancer sequences for specific neuronal types (Jenett et al., 2012; Tirian & Dickson, 2017) are used in combination with binary expression systems and allow for the targeted expression of various effector genes. Fundamental proteins of the presynaptic machinery such as Bruchpilot can be fused with fluorescent proteins (Berger-Müller et al., 2013;

Christiansen et al., 2011; Owald et al., 2010; Schmid et al., 2008), GFP reconstitution across synaptic partners (GRASP) techniques offer transsynaptic accessibility (Feinberg et al., 2008; Macpherson et al., 2015; Shearin et al., 2018), whilst postsynaptic proteins as neurotransmitter receptors can finally be identified. Molecular engineering advancements allowed for tagging receptor genes at the endogenous locus with fluorescent proteins or peptide tags (Chen et al., 2014; Fendl et al., 2020; Pribbenow et al., 2022; Sanfilippo et al., 2024). Currently, this is achieved through the RNA-guided CRISPR-Cas nuclease system for targeted genome engineering (Jinek et al., 2012; Ran et al., 2013). Thus, receptor overexpression artifacts induced by the transgene insertion can now mostly be avoided.

Neuronal suppression

The gene *shibire* encodes dynamin, a GTPase required late in the process of endocytosis and synaptic vesicle recycling, that is responsible for fission of the vesicle from the membrane (Kroll et al., 2015; Van Der Bliek & Meyerowrtz, 1991). *shibire*^{ts} holds a temperature-sensitive missense mutation in the GTPase domain of the protein. When flies are heated to the restrictive temperature (~29°), nerve terminals become completely depleted of synaptic vesicles, paralyzing the flies (Koenig et al., 1983; Kroll et al., 2015; Van Der Bliek & Meyerowrtz, 1991). When flies are returned to permissive temperatures, dynamin resumes normal function, therefore, temperature allows for conditional control of synaptic release. Another means of suppressing neuronal activity, is by the overexpression of the Kir2.1 inward rectifying potassium channel (Baines et al., 2001). Kir2.1 hyperpolarizes the neuron and importantly, permits the suppression of not only chemical but electrical neuronal communication via gap junctions, a restriction of the *shibire*^{ts} approach.

GECIs

Genetically encoded calcium indicators (GECIs) are used for optically reading out neuronal activity, by reporting cytoplasmic Ca^{2+} levels as changes in fluorescence intensity (Miyawaki et al., 1997; Nakai et al., 2001; Tian et al., 2009). Specifically, in the cases of the green fluorescent protein (GFP)-based GCaMP sensors, Ca^{2+} binds to calmodulin (CaM) and conformational changes due to the Ca^{2+}-CaM-M13 (myosin light chain kinase) interaction induce a subsequent conformational change in GFP (Crivici & Ikura, 1995; Miyawaki et al., 1997). Importantly, GCaMP sensors with improved kinetics have been generated, bringing the scientific community one step closer to tracking the millisecond-timescale electrical communication (Zhang et al., 2023). For the

in vivo use of GECIs, two-photon microscopy is the imaging method of choice as it is ideal for three-dimensional and deep tissue imaging. Two-photon excitation arises from the simultaneous fluorophore absorption of two infrared photons in a single event, with the emission spectrum being exactly the same as that generated in normal one-photon excitation (Denk et al., 1990, 1995). Due to the quadratic dependence of two-photon absorption on excitation intensity, the probability of two-photon absorption at the center of the focus is substantially greater than outside of the focus, and thus significant two-photon absorption occurs only at the center of the focus (Benninger & Piston, 2013).

1.4.2 Connectivity

Neuronal connectivity dictates and coordinates neuronal function. Understanding the strength of neural connections in terms of synapse number, discovering feedforward and feedback interactions, are crucial for exploring neuronal systems. The seminal work in *Caenorhabditis elegans* brought the first complete wiring diagram of a living organism (White et al., 1986). To advance from the level of 302 neurons in *C. elegans* to ~140.000 neurons in the adult *Drosophila melanogaster*, a combination of novel imaging and analysis techniques were used. 7,062 serial ~40-nm thin sections were cut to span the ~250 µm depth of the entire fly brain and imaged with a serial section transmission electron miscroscope (ssTEM)(Zheng et al., 2018). Then, methods for automatic synapse detection were generated (Buhmann et al., 2021; Dorkenwald et al., 2017) and an open-access online proofreading community was built thanks to the FlyWire interface (Dorkenwald et al., 2022). These collaborative steps lead to the release of a complete neuronal wiring diagram of the adult female fly brain (Dorkenwald et al., 2024; Schlegel et al., 2024) (Figure 4). Importantly, the rapid evolution of the connectomics field in *Drosophila* creates new possibilities for comparative studies across individuals, for example between female brains (Dorkenwald et al., 2024; Scheffer et al., 2020), and across sexes, for instance between the ventral nerve cord of males and females (Azevedo et al., 2024; Takemura et al., 2024). Finally, the morphology of each synaptic connection can now be addressed in microcircuits of interest.

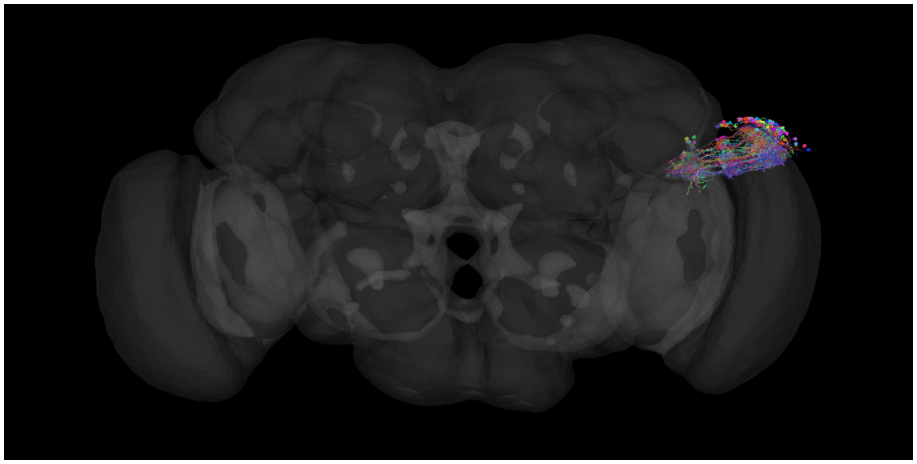

Figure 4. Neuronal reconstructions in the fruit fly brain. Snippet from the FlyWire Neuroglancer (flywire.ai). Neuronal reconstructions correspond to neuronal IDs used in Manuscript 2.

1.5 CONCLUSION

This cumulative-style doctoral dissertation uses the powerful model organism *Drosophila melanogaster* to explore the morphological and molecular characteristics of cholinergic neurotransmission in T5 direction-selective neurons of the visual system. In **Manuscript 1**, we use the open-access female connectome and explore the effects of polyadic morphology in single T5 neurons and in the T5 network. In **Manuscript 2**, we explore the postsynaptic acetylcholine receptor variety across Tm-to-T5 synapses and their functional implications in the visual microcircuit of interest. Collectively, my PhD work gave us insights on the complexity of the T5 direction-selective computations, this time at the single chemical synapse level.

2 | MANUSCRIPTS

2.1 POLYADIC SYNAPSES INTRODUCE UNIQUE WIRING ARCHITECTURES IN T5 CELLS OF *DROSOPHILA*

Abstract

Connectomes provide neuronal wiring diagrams and allow for investigating the detailed synaptic morphology of each connection. In the visual system of Drosophila, T5 cells are the primary motion-sensing neurons in the OFF-pathway. Apart from the spatial wiring of the excitatory Tm1, Tm2, Tm4, Tm9 and the inhibitory CT1 neurons on T5 dendrites, the connectivity implementations of the abundant in the fly nervous system polyadic synapses have not been addressed. In this study, we use the FlyWire database and identify that Tm and CT1 cells wire on T5a dendrites via different polyadic synapse types. We then explore the distribution of the various synapse types on T5a dendrites and find differences in their spatial patterns. Finally, we show that the polyadic morphology is setting a directional wiring architecture at the T5 network level. Our work showcases the complexity that polyadic synapses introduce in T5 connectivity.

Authors

Eleni Samara and Alexander Borst.

Author contributions

Eleni Samara and Alexander Borst conceived this study. Eleni Samara performed the data extraction and analysis. Eleni Samara and Alexander Borst wrote and edited this manuscript.

Polyadic synapses introduce unique wiring architectures in T5 cells of *Drosophila*

Eleni Samara[1,2*] and Alexander Borst[1,3*]

[1]Max Planck Institute for Biological Intelligence, Department of Circuits-Computation-Models, Martinsried, Germany

[2]Graduate School of Systemic Neurosciences, LMU Munich, Martinsried, Germany

[3] Lead contact

*Correspondence: eleni.samara@bi.mpg.de, alexander.borst@bi.mpg.de.

Abstract

Connectomes provide neuronal wiring diagrams and allow for investigating the detailed synaptic morphology of each connection. In the visual system of *Drosophila*, T5 cells are the primary motion-sensing neurons in the OFF-pathway. Apart from the spatial wiring of the excitatory Tm1, Tm2, Tm4, Tm9 and the inhibitory CT1 neurons on T5 dendrites, the connectivity implementations of the abundant in the fly nervous system polyadic synapses have not been addressed. In this study, we use the FlyWire database and identify that Tm and CT1 cells wire on T5a dendrites via eight polyadic synapse types. We then explore the distribution of the different synapse types on T5a dendrites and find differences in their spatial patterns. Finally, we show that the polyadic morphology is setting a directional wiring architecture at the T5 network level. Our work showcases the complexity that polyadic synapses introduce in T5 connectivity.

Introduction

One of the major goals in Neuroscience is to better understand the structure-function relationship of neuronal circuits. This goal could be reached more easily by gaining access to brain-wide

neuronal connectivity, namely the connectome. Recently, a female adult brain wiring diagram of *Drosophila melanogaster* has been completed from electron-microscope reconstructions [1–3]. The dataset offers morphological access to approximately 10^5 neurons and provides information on the connectivity between all neurons via approximately 10^8 chemical synapses [4]. Interestingly, the majority of these chemical synapses are polyadic, i.e. one presynaptic site forms connections with multiple postsynaptic sites [3]. Therefore, polyadic synapses result in the formation of a diverging connection at the single bouton level. Polyads were also encountered at the neuromuscular junction of *C. elegans* [5] and the photoreceptor synapse of the vertebrate retina [6]. In *Drosophila*, their numerical prevalence, as well as their functional implications in neural circuits, still remain speculative. Thanks to the accumulated knowledge [7–14], the early visual processing center of *Drosophila*, i.e. the optic lobe, is the ideal place to first address the polyadic synapse morphology.

The optic lobe is divided in four neuropils: the lamina, the medulla, the lobula and the lobula plate. Each of these neuropils is built from about 850 columns repeating the columnar structure of the facet eye in a retinotopic way [15]. Among visual modalities, motion detection and consequently the circuit that extracts directional information from either luminance increments (ON-pathway) or luminance decrements (OFF-pathway) has been the focus of study for the past two decades [16–19]. Within the visual processing stream, the first neurons that compute directional information are the bushy T4 cells in the ON-pathway and the bushy T5 cells in the OFF-pathway [18]. Both T4 and T5 cells exist in four morphologically discrete subtypes a, b, c and d: each subtype has its dendrite oriented into one of the four cardinal directions and sends its axon terminals into one of the four layers of the lobula plate [7,20,21]. Aligned with their morphology, each subtype responds to either front-to-back, back-to-front, upward

or downward motion, respectively [18]. T5 cells receive inputs mainly from the excitatory cholinergic cells Tm1, Tm2, Tm4 and Tm9 and from the inhibitory GABAergic CT1 cell [7,10,22–30] lacking glutamatergic inputs and exhibiting a greater cholinergic input variety than T4 cells. The distinct spatial distribution of T5 inputs follows their directional preference and contributes to the cells' sharp directional tuning [31,32]. Nonetheless, the role of polyadic synapses in T5 wiring and function has not been addressed so far.

Here, we study the polyadic morphology in Tm1, Tm2, Tm4- Tm9 and CT1 synapses onto T5a dendrites. We first identify the different polyadic types and then explore their T5a dendritic distributions. Ultimately, we show that polyadic synapses introduce a directional wiring motif at the T5 network level.

Materials and methods

Data and code availability

This paper analyzes a dataset from FlyWire (flywire.ai). Data for analysis are publicly available at the at the Edmond Open Research Data Repository of the Max Planck Society. Any additional information required to reanalyze the data reported in this paper is available from the lead contact upon request.

Synapse proofreading

The full adult fly brain (FAFB) TEM-generated dataset, corresponding to a later version compared to the 783 public release version, was analyzed via FlyWire [1–4]. The upstream circuitry (Tm1, Tm2, Tm4, Tm9, CT1) of five reconstructed T5a dendrites from the dorsal part of the right optic lobe were identified via Codex (synapse threshold≥5) and the 'connectivity analysis' function in FlyWire (no synapse threshold). Codex cell type annotations were used together with morphological

information [7] for the cell type identification. Inputs with less than five synapses to T5a dendrites from the 'connectivity analysis' function were also included to the analysis. Neuronal reconstructions were performed by FlyWire users. The majority of orphan twigs belonging to T5a dendritic spines were traced back to their neuron of origin for the purposes of this study. Synapse number Buhmann predictions [33] between the T5a neuron of interest and its respective input neurons were acquired from FlyWire's connectivity viewer. Cleft score was set to 50, so as to eliminate synaptic redundancy resulting from the combination of synaptic connections between the same neurons when their presynaptic locations are within $100nm^2$. Synapse coordinates were manually allocated to the presynaptic T-bar and compared with the automatic synapse coordinates from Codex corresponding to postsynaptic sites to correct for potential false positive and false negative synaptic sites. Manual synaptic proofreading was based on the existence of four morphological markers: a. synaptic vesicles, b. protein dense T-bar structure, c. synaptic cleft, and d. postsynaptic densities (or postsynaptic domains). Complex synaptic cases and their proofreading outcome are extensively described in Fig S1. Dendritic spines that could not be traced back to their neuron of origin were classified as non-traced and could belong to T5s or other cell types (Fig 1J). All synapses in this study correspond to manually proofread synapses.

Allocation of polyadic synapse types

Apart from T5a, b, c and d subtypes, dendritic spines corresponding to Tm1, Tm9 and CT1 cells were found across Tm-, CT1-to-T5 synapses [29] and were not included in the allocation of polyadic T5 synapse types. Synapse types were allocated qualitatively, regardless of the dendritic spine number (eg. synapse type *abcd* can include 1a, 2b, 1c and 2d T5 spines).

Spatial distribution of polyadic types

Synapse type distributions across the anterior-posterior T5a dendritic axis (Fig 2) were addressed by plotting the horizontal distance of every synapse from the root of the dendrite. The root was set manually as the first branching point of the dendrite. Distances were calculated by dividing the z coordinates of each T-bar with 40 (voxel=4x4x40).

Lobula distribution of co-T5s

For the spatial distribution of T5 subtypes residing at the same postsynaptic site with the T5a of analysis (namely co-T5s) in lobula layer 1 (LO1), the horizontal distance of each co-T5 root from the T5a root of analysis was calculated. For every T5a dendrite of analysis, we evaluated the co-T5s per input type rather than per input cell (eg. Tm1 connections in one T5a dendrite can consist of three Tm1 cells). To exclude any bias from co-T5 overrepresentation due to connection strength, we counted each co-T5s once, regardless of the number of boutons it appeared into. We controlled for duplicates resulting from neuronal ID updates in FlyWire by looking at the 3D reconstructions in Neuroglancer.

Immunohistochemistry and confocal microscopy

Flies at early pupa stages were heat-shocked for 30 minutes at 37° to activate the Multi-color FlpOut cassette [34]. Fly brains (aged 2-5 days) were dissected in cold phosphate-buffered saline (PBS) and fixed in 4% paraformaldehyde (in PBS with 0.1% Triton X-100) for 24 minutes at room temperature, followed by three 10-minute washes in PBT (PBS and 0.3% Triton X-100). Brains were then incubated with primary antibodies in PBT for 48 hours at 4°C. After being incubated for 2 hours at room temperature, brains were washed four times for 15 minutes each in PBT and then incubated with secondary antibodies diluted in PBT for 48 hours at 4°C. After being incubated for 2 hours at

room temperature and four 15 minutes PBT washes, brains were mounted with SlowFade Gold Antifade (Cat#S36936) for immediate sample viewing. Images were acquired in a Leica Stellaris 5 laser scanning confocal microscope with a 20x glycerol 0.75 NA HC Plan-apochromat and 63x glycerol immersive 1.3 NA HC Plan-apochromat objective at 2048 x 2048 x 0.4µm image resolution.

Statistical analysis

Detailed analysis is reported in figure legends and was performed in GraphPad Prism v.9.3.0 and in Python v.3.9.18 with the use of seaborn 0.12.2, pandas 1.5.3, numpy 1.23.3 and scipy 1.9.3.

Results

Polyadic types in Tm1-, Tm2-, Tm4-, Tm9- and CT1-to-T5 connections

For our analysis, we used five, dorsally located, reconstructed T5a neurons as representatives of the horizontal motion detection system. Together with FlyWire annotations and previously attained morphological information [7,10], we identified the majority of Tm1, Tm2, Tm4, Tm9 and CT1 cells connecting to T5a dendrites of analysis (Fig 1A and 1B). Polyadic synapses are characterized by a single presynaptic bouton with multiple postsynaptic compartments adjacent to it. Throughout our manual proofreading, we encountered Tm- and CT1-to-T5a synapses with multiple postsynaptic compartments, belonging to dendritic spines of different T5 subtypes (Fig 1C). Therefore, we allocated eight synapse types, namely *a*, *ab*, *ac*, *ad*, *abc*, *abd*, *acd* and *abcd* based on the T5 subtypes present in the respective postsynaptic sites (Fig 1D). Importantly, all eight polyadic types were encountered across the five T5a neuronal inputs. Additionally, we report certain complex synapse examples during

the proofreading process. We treated two dendritic spines of the same T5 cell across one presynapse in the same or sequential z-plane as one polyadic synapse (Fig S1A,B). In two examples of multiple T-bars at the vicinity, we treated them as one and two synapses respectively based on their distinct synaptic clefts (Fig S1C,D). Finally, the number of postsynaptic densities in Tm and CT1 boutons did not vary across the five neuronal input types (Fig S1E). This indicated the lack of synapse strength regulation at the level of postsynaptic density abundancy.

Do Tm1-, Tm2-, Tm4-, Tm9- and CT1-to-T5 connections differ in terms of the polyadic types they use? The *abcd* type exhibited higher abundance compared to the other polyadic synapse types across the five neuronal inputs and was particularly enriched in Tm1 and Tm2 synapses (Fig 1E-I). Polyadic type allocation is susceptible to dendritic spine reconstruction, hence the number of non-traced dendritic spines could affect our allocation. To test this, we calculated the average number of non-traced dendritic spines in all Tm and CT1 boutons across the T5a neurons of analysis (Fig 1J). One up to two dendritic spines were not traced in each postsynaptic density of analysis. This could result in quantitative differences, eg. *abcd* type where a T5d spine is not traced, or qualitative differences, eg. *abc* type where a T5d spine is not traced, and currently cannot be further resolved. In summary, visual information that is computed by a single Tm and CT1 neuronal bouton, could in principle be simultaneously transmitted to T5a, b, c, d neurons.

Polyadic types introduce unique wiring patterns on T5 dendrites

The compartmentalized wiring of Tm1, Tm2, Tm4, Tm9 and CT1 cells on T5 dendrites has been extensively described at the morphological and functional level [10,29,31,32,35]. CT1 wires proximally to the dendrite root, Tm1, Tm2, Tm4 and Tm9 wire at

the central dendritic compartment, while Tm9 extends to the most distal dendritic parts (Fig 2A). This compartmentalized wiring will from now on be referred to as typical wiring. Consequently, we wondered if the typical wiring was recapitulated by the different polyadic synapse types. The *a* polyadic type did not mirror the typical wiring, as the Tm9 extension to the distal dendritic site was concealed (Fig 2B). The *ab* polyadic type diverged from the typical wiring in the case of CT1, while the *ac* and *ad* types mirrored the typical wiring principles (Fig 2C-E). The *abc* and *acd* polyadic types deviated from the typical wiring in the cases of Tm1 and Tm4 respectively, whereas the *abd* and *abcd* types followed the typical wiring (Fig 2F-I). Collectively, our results show that the typical wiring of the various input neurons on T5a dendrites is not preserved across all polyadic types. It is thus possible that different polyadic types serve unique functional purposes in T5a computation.

Polyadic types introduce unique wiring patterns in the T5 network

The polyadic types imply the simultaneous binding of neurotransmitters by transmitter receptors located on the dendrites of multiple T5 cells. We named as 'co-T5s' the remaining T5 dendritic spines residing at the same postsynaptic density with the T5a spine of analysis (Fig 3A, synaptic level). The co-T5 spines belong to T5 cells that are proximal to the T5a cell of analysis, contributing to the T5 network in the lobula (Fig 3A, columnar & neuropil level, Fig 3B). Hence, we wanted to understand if there was an underlying wiring architecture imposed by the co-T5s. We focused on the posterior-anterior distribution of these co-T5s with respect to the T5a of analysis and calculated the horizontal distances between the T5a and co-T5 roots. In CT1-T5a polyads of analysis, the co-T5s localized more on the anterior side of T5a dendrites, while in Tm1-, Tm2-, Tm4-, Tm9-T5a polyads, the co-T5s localized more on the

posterior side of T5a dendrites (Fig 3C-H). We conclude that CT1-derived co-T5s distributions significantly differed from the Tm1, Tm2, Tm4 and Tm9-derived co-T5s distributions.

Discussion

The outcome of connectome analyses is usually represented by connectivity matrices, rather than the morphology of those connections. Even though in *Drosophila melanogaster* the most abundant synapse morphology is that of polyadic synapses [3], they have been heavily understudied. Here, we report for the first time the wiring architectures that can be introduced by polyadic synapses. The connection of Tm1, Tm2, Tm4, Tm9 and CT1 with T5 dendrites has been known for almost a decade and lead to the extensive functional exploration of the circuitry [10,22,24–30]. Another level of complexity is added by polyadic synapses, as all T5 neuronal inputs use eight synapse types, *a*, *ab*, *ac*, *ad*, *abc*, *abd*, *acd* and *abcd*, for their connections. Acetylcholine receptor (AChRs) differences in expression levels across the different T5 subtypes [36], could potentially introduce functional differences among the different polyadic types. This is further corroborated by recent work, showing that the AChR profiles among Tm1, Tm2, Tm4 and Tm9 inputs differ, which could also expand among different boutons of the same input [35]. Therefore, the polyadic types we report here could be indicative of such inter-bouton AChR variety. Lastly, the polyadic synapse arrangements could potentially affect the single bouton output, as changes in release probability depending on the postsynaptic partner have been previously observed in mammals [37,38].

Do the different synapse identities affect the spatial wiring of the five neuronal input types? We tackled this question by looking at the distributions of different polyadic types across the T5a anterior-posterior arborization axis. Different polyadic types

introduced diversions from the typical wiring. Consequently, the possible functional differences among polyadic types, together with their spatial differences might account for more compartmentalized synaptic effects. Importantly, the polyadic morphology denotes the synchronous activation of postsynaptic T5 neurons, from neighboring positions which might not necessarily be visually activated. Such 'co-T5s' from the GABAergic input neuron CT1 localized closer to the anterior side of the analyzed T5a cells, whereas co-T5s from cholinergic Tm cells localized closer to the posterior side of the analyzed T5a cells, resembling an excitation-inhibition (E/I) polarization along their axis. When a front-to-back motion stimulus activates the T5a neuron of interest, the majority of co-T5s posterior to that T5a would be activated and the majority of co-T5s anterior would be inhibited. Such a local adaptation mechanism could, for example, compensate for contrast fluctuations.

Polyadic synapses might play an important role in visual processing, as well as in the development of the visual system. Therefore, it is crucial to explore them in depth. Our work represents a first step towards that direction. By addressing connectivity architectures that emerge from the polyadic synapse morphology in the OFF-edge motion pathway, we are eventually moving from the single neuron to the single synapse wiring diagram era[39].

Acknowledgments

The authors thank N. Drummond for discussions. We are grateful to the Princeton FlyWire team and members of the Murthy and Seung labs for development and maintenance of FlyWire (supported by BRAIN Initiative grant MH117815 to Murthy and Seung) and to the Imaging Facility of the MPI for Biological Intelligence-Martinsried. E. Samara is a member of the Graduate

school of Systemic Neurosciences (GSN) Munich. This work was funded by the Max Planck Society.

References

1. Zheng, Z. *et al.* A complete electron microscopy volume of the Brain of adult *Drosophila melanogaster*. *Cell* **174**, 730-743.e22 (2018).
2. Dorkenwald, S. *et al.* FlyWire: online community for whole-brain connectomics. *Nat Methods* **19**, 119–128 (2022).
3. Dorkenwald, S. *et al.* Neuronal wiring diagram of an adult brain. *Nature* **634**, 124–138 (2024).
4. Schlegel, P. *et al.* Whole-brain annotation and multi-connectome cell typing of *Drosophila*. *Nature* **634**, 139–152 (2024).
5. Liu, Q., Chen, B., Hall, D. H. & Wang, Z. A quantum of neurotransmitter causes minis in multiple postsynaptic cells at the *Caenorhabditis elegans* neuromuscular junction. *Developmental Neurobiology* **67**, 123–128 (2007).
6. Rao-Mirotznik, R., Buchsbaum, G. & Sterling, P. Transmitter concentration at a three-dimensional synapse. *Journal of Neurophysiology* **80**, 3163–3172 (1998).
7. Fischbach, K.-F. & Dittrich, A. P. M. The optic lobe of *Drosophila melanogaster*. I. A Golgi analysis of wild-type structure. *Cell Tissue Res.* **258**, (1989).
8. Kondo, S. *et al.* Neurochemical organization of the *Drosophila* brain visualized by endogenously tagged neurotransmitter receptors. *Cell Reports* **30**, 284-297.e5 (2020).
9. Shinomiya, K. *et al.* A common evolutionary origin for the ON- and OFF-edge motion detection pathways of the *Drosophila* visual system. *Front. Neural Circuits* **9**, (2015).

10. Shinomiya, K. *et al.* Comparisons between the ON- and OFF-edge motion pathways in the *Drosophila* brain. *eLife* **8**, e40025 (2019).
11. Behnia, R. & Desplan, C. Visual circuits in flies: beginning to see the whole picture. *Curr Opin Neurobiol* **34**, 125–132 (2015).
12. Borst, A. & Groschner, L. N. How flies see motion. *Annu. Rev. Neurosci.* **46**, 17–37 (2023).
13. Lappalainen, J. K. *et al.* Connectome-constrained networks predict neural activity across the fly visual system. *Nature* (2024) doi:10.1038/s41586-024-07939-3.
14. Matsliah, A. *et al.* Neuronal “parts list” and wiring diagram for a visual system. Preprint at https://doi.org/10.1101/2023.10.12.562119 (2023).
15. Surkova, S., Görne, J., Nuzhdin, S. & Samsonova, M. Interplay between sex determination cascade and major signaling pathways during *Drosophila* eye development: Perspectives for future research. *Developmental Biology* **476**, 41–52 (2021).
16. Joesch, M., Schnell, B., Raghu, S. V., Reiff, D. F. & Borst, A. ON and OFF pathways in *Drosophila* motion vision. *Nature* **468**, 300–304 (2010).
17. Strother, J. A., Nern, A. & Reiser, M. B. Direct observation of ON and OFF pathways in the *Drosophila* visual system. *Current Biology* **24**, 976–983 (2014).
18. Maisak, M. S. *et al.* A directional tuning map of *Drosophila* elementary motion detectors. *Nature* **500**, 212–216 (2013).
19. Fisher, Y. E., Silies, M. & Clandinin, T. R. Orientation selectivity sharpens motion detection in *Drosophila*. *Neuron* **88**, 390–402 (2015).
20. Pinto-Teixeira, F. *et al.* Development of concurrent retinotopic maps in the fly motion detection circuit. *Cell* **173**, 485-498.e11 (2018).

21. Apitz, H. & Salecker, I. Spatio-temporal relays control layer identity of direction-selective neuron subtypes in *Drosophila*. *Nat Commun* **9**, 2295 (2018).
22. Meier, M. & Borst, A. Extreme compartmentalization in a *Drosophila* amacrine cell. *Current Biology* **29**, 1545-1550.e2 (2019).
23. Davis, F. P. *et al.* A genetic, genomic, and computational resource for exploring neural circuit function. *eLife* **9**, e50901 (2020).
24. Behnia, R., Clark, D. A., Carter, A. G., Clandinin, T. R. & Desplan, C. Processing properties of ON and OFF pathways for *Drosophila* motion detection. *Nature* **512**, 427–430 (2014).
25. Takemura, S. *et al.* Cholinergic circuits integrate neighboring visual signals in a *Drosophila* motion detection pathway. *Curr Biol* **21**, 2077–2084 (2011).
26. Shinomiya, K. *et al.* Candidate neural substrates for OFF-edge motion detection in *Drosophila*. *Current Biology* **24**, 1062–1070 (2014).
27. Serbe, E., Meier, M., Leonhardt, A. & Borst, A. Comprehensive characterization of the major presynaptic elements to the *Drosophila* OFF motion detector. *Neuron* **89**, 829–841 (2016).
28. Meier, M. *et al.* Neural circuit components of the *Drosophila* OFF motion vision pathway. *Current Biology* **24**, 385–392 (2014).
29. Braun, A., Borst, A. & Meier, M. Disynaptic inhibition shapes tuning of OFF-motion detectors in *Drosophila*. *Curr Biol* **33**, 2260-2269.e4 (2023).
30. Ramos-Traslosheros, G. & Silies, M. The physiological basis for contrast opponency in motion computation in *Drosophila*. *Nat Commun* **12**, 4987 (2021).

31. Borst, A. A biophysical mechanism for preferred direction enhancement in fly motion vision. *PLoS Comput Biol* **14**, e1006240 (2018).
32. Haag, J., Arenz, A., Serbe, E., Gabbiani, F. & Borst, A. Complementary mechanisms create direction selectivity in the fly. *eLife* **5**, e17421 (2016).
33. Buhmann, J. *et al.* Automatic detection of synaptic partners in a whole-brain *Drosophila* electron microscopy data set. *Nat Methods* **18**, 771–774 (2021).
34. Nern, A., Pfeiffer, B. D. & Rubin, G. M. Optimized tools for multicolor stochastic labeling reveal diverse stereotyped cell arrangements in the fly visual system. *Proc Natl Acad Sci USA* **112**, E2967–E2976 (2015).
35. Samara, E. *et al.* Columnar cholinergic neurotransmission onto T5 cells of *Drosophila*. *bioRxiv* 2024.08.28.610055 (2024) doi:10.1101/2024.08.28.610055.
36. Hoermann, N. *et al.* A combinatorial code of transcription factors specifies subtypes of visual motion-sensing neurons in *Drosophila*. *Development* dev.186296 (2020) doi:10.1242/dev.186296.
37. Zilberter, Y., Kaiser, K. M. M. & Sakmann, B. Dendritic GABA release depresses excitatory transmission between layer 2/3 pyramidal and bitufted neurons in rat neocortex. *Neuron* **24**, 979–988 (1999).
38. Aldahabi, M. *et al.* Different priming states of synaptic vesicles underlie distinct release probabilities at hippocampal excitatory synapses. *Neuron* **110**, 4144-4161.e7 (2022).
39. Seung, H. S. Multi-output computation by single neuron biophysics in a visual system. *bioRxiv* 2025.02.02.636137 (2025) doi:10.1101/2025.02.02.636137.

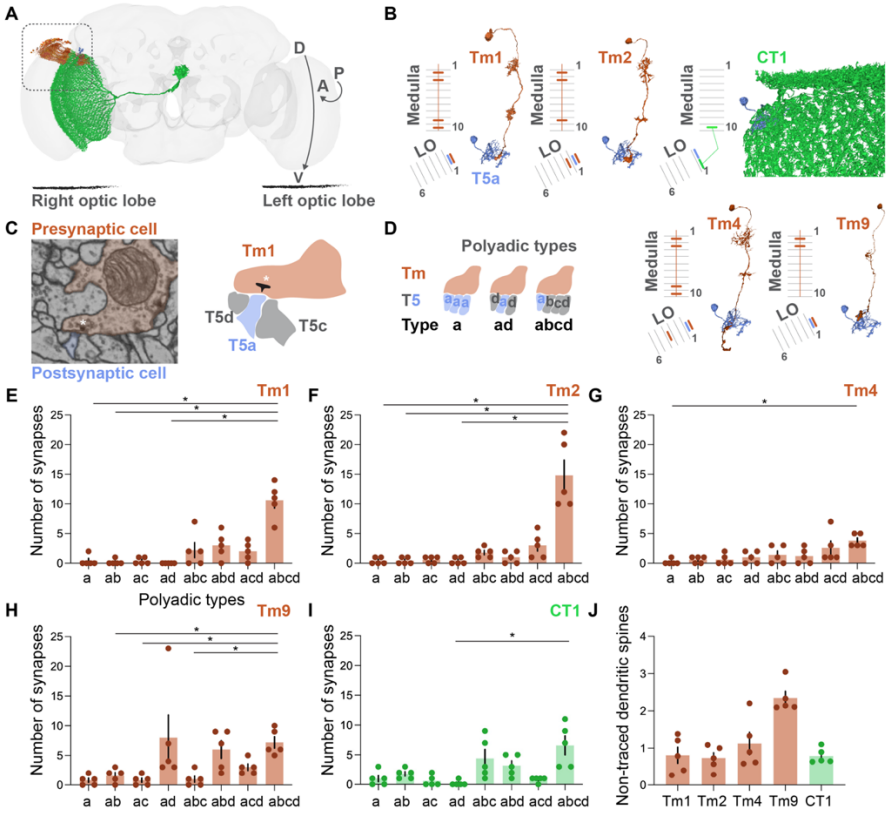

Figure 1. Polyadic Tm1-, Tm2-, Tm4-, Tm9-, CT1-to-T5a synapses

(A) Schematic representation of the circuit of analysis in the right optic lobe of the fly brain (flywire.ai).

(B) Dendritic ramifications in medulla layers and axonal terminals in lobula (LO) layers of Tm1, Tm2, Tm4 and Tm9 cells (orange). Dendritic ramifications in medulla layer 10 and lobula layer 1 (LO1) of CT1 cell (green). T5a dendrites in LO1 (blue). FlyWire IDs as in (A).

(C) Electron microscopy snapshot of a polyadic Tm1-T5 synapse from flywire.ai (left). Synapse coordinates: x=181940, y=46900, z=4912. Asterisk indicates the presynaptic T-bar. Schematic representation of one presynaptic Tm1 bouton wiring to a T5d, T5a and T5c dendritic spine (right).

(D) Schematic representation of polyadic Tm-T5 synapse types.

(E-I) Number of *a*, *ab*, *ac*, *ad*, *abc*, *abd*, *acd* and *abcd* polyadic types in Tm1-, Tm2-, Tm4-, Tm9-, CT1-to-T5a synapses (nT5a=5). The normality of distribution was assessed with the use of Shapiro-Wilk test. Friedman test followed by Dunn's post hoc test (Tm1, Tm2, Tm4, CT1), One- way ANOVA followed by Tukey's post hoc test (Tm9); *p<0.05. Data is mean ± SEM.

(J) Average number of non-traced dendritic spines in Tm1-, Tm2-, Tm4-, Tm9- and CT1-to-T5a synapses of analysis (nT5a=5). Data is mean ± SEM.

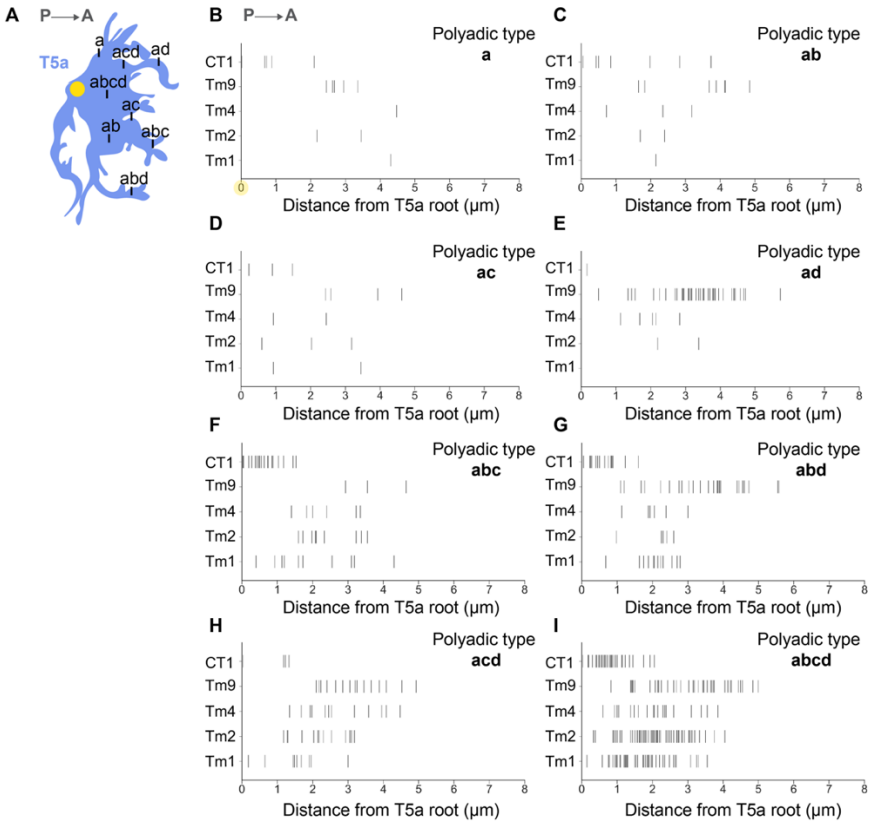

Figure 2. Spatial organization of polyadic types on T5 dendrites

(A) Schematic representation of polyadic Tm-T5 synapse types on a T5a dendrite (blue). Horizontal distances of polyadic types were measured from the T5a dendritic root (yellow circle).

(B) Horizontal distance of *a* polyadic types from the root of T5a dendrites (nT5a=5) across Tm1-, Tm2-, Tm4-, Tm9- and CT1-to-T5a synapses.

(C-I) Same as in (B) for *ab*, *ac*, *ad*, *abc*, *abd*, *acd and abcd* polyadic types.

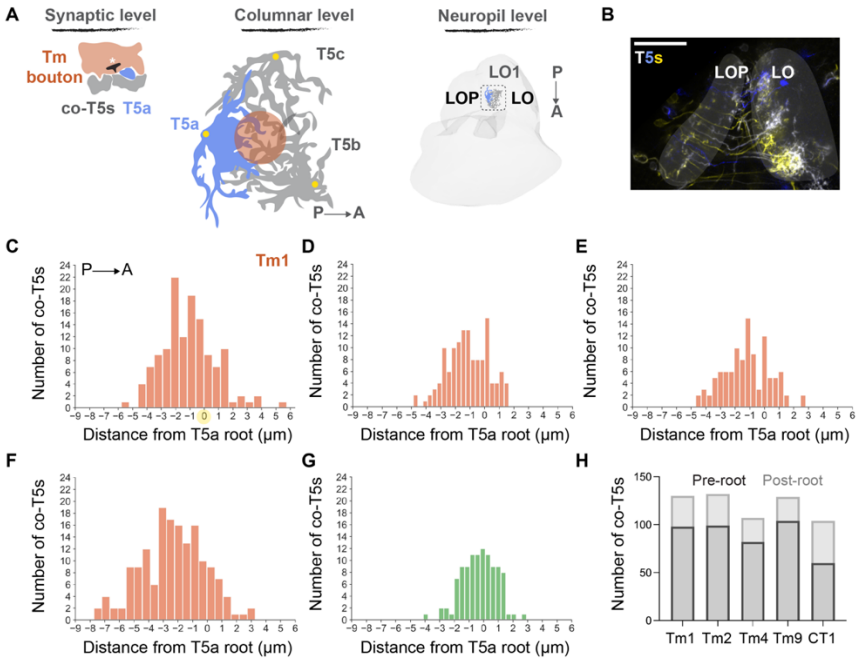

Figure 3. co-T5 organization in lobula layer 1

(A) Schematic representation of polyadic morphology from the synaptic to the neuropil level. Asterisk indicates the presynaptic T-bar. Dendritic roots in yellow circles.

(B) Sparse T5 subtype labelling via the multi-color FlpOut approach. Scale bar 40µm.

(C-G) co-T5 distribution from the root of T5a dendrites (nT5a=5) across Tm1-, Tm2-, Tm4-, Tm9- and CT1-to-T5a polyadic synapses. Dendritic root of T5a of analysis in yellow circle. The normality of distribution was assessed with the use of Shapiro-Wilk test. Unpaired Student's t-test, C to G p=0.000161, D to G p=0.000001, E to G p=0.000003, F to G p=0.000000.

(H) Number of co-T5s posterior (pre-root) and anterior (post-root) to the T5a root across Tm1- , Tm2-, Tm4-, Tm9- and CT1-to-T5a polyadic synapses.

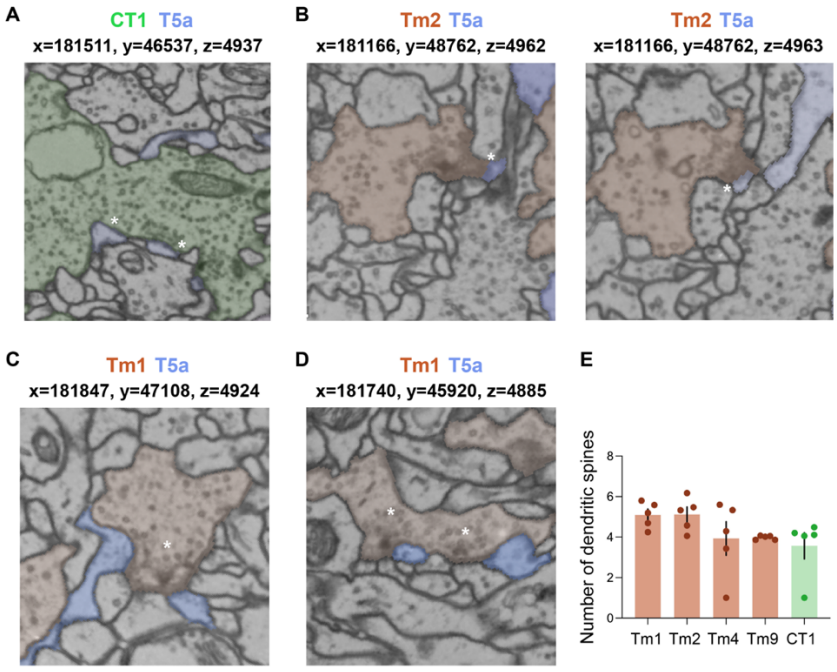

Figure S1. Synaptic proofreading in Tm1-, Tm2-, Tm4-, Tm9-, CT1-to-T5 synapses

(A) Electron microscopy snapshot of one polyadic CT1-T5a synapse at a single z-plane. Asterisks indicate the two T5a dendritic spines at the same CT1 presynaptic site.

(B) Electron microscopy snapshot of one polyadic Tm2-T5a synapse at two sequential z-planes. Asterisks indicate the two T5a dendritic spines at the same Tm2 presynaptic site.

(C) Electron microscopy snapshot of one polyadic Tm1-T5a synapse at a single z-plane. Asterisk indicates the three presynaptic T-bars.

(D) Electron microscopy snapshot of two polyadic Tm1-T5a synapses at a single z-plane. Asterisks indicate the two presynaptic T-bars.

(E) Average number per neuronal input type of dendritic spines in Tm1-, Tm2-, Tm4- , Tm9- and CT1-to-T5a polyadic synapses of analysis. The normality of distribution was assessed with the use of Shapiro-Wilk test. Friedman test followed by Dunn's post hoc test. Data is mean ± SEM.

T5a	720575940643169933 **(Fig.1A,1C, S1A, S1C, S1D)**	720575940625654759	720575940616396703 **(Fig.S1B)**	720575940621106368	720575940626820538
Tm1	720575940620976493 (Fig. S1D) 720575940608883465 (Fig.1A, 1C, S1C) 720575940623583428 720575940627201308 720575940619723643 720575940640955088 720575940627479836	720575940622364961 720575940621146733 720575940608883465 720575940613587935 720575940616994134	720575940620523540 720575940608195339 720575940613587935 720575940634579135	720575940621146733 720575940633875117 720575940643191949	720575940616994134 720575940621146733 720575940613587935
Tm2	720575940630551670 720575940622364961 (Fig.1A) 720575940640230259 720575940621868276 720575940623081942	720575940632142904 720575940640453437 720575940640230259	720575940630308663 (Fig.S1B) 720575940640947152 720575940619708888 720575940632142904	720575940625164327 720575940615731359 720575940640453437	720575940619708888 720575940632142904 720575940615731359
Tm4	720575940637976666 (Fig.1A) 720575940620745163	720575940621582401 720575940620745163 720575940620782171 720575940637976666	720575940639445582 720575940620782171 720575940614824338 720575940627035198	720575940625442492 720575940621582401 720575940615720258 720575940613610642	720575940638140506 720575940620782171 720575940615720258 720575940639445582 720575940620745163
Tm9	720575940616384742 (Fig.1A) 720575940628740039 720575940613374873 720575940617906589 720575940620814356 720575940630425564 720575940624565296	720575940613374873 720575940620814356 720575940609254851 720575940626242348 720575940623771061	720575940610056654 720575940637539806 720575940626242348 720575940620680277 720575940631934039 720575940626578965 720575940653151649 720575940625797936	720575940626254892 720575940620814356 720575940623771061 720575940621776664 720575940626242348 720575940617906589	720575940625797936 720575940626242348 720575940623771061 720575940610056654 720575940620814356
CT1	720575940626979621 (Fig.1A, S1A)	720575940626979621	720575940626979621	720575940626979621	720575940626979621

Table S1. Analyzed neuronal IDs from FlyWire.

2.2 COLUMNAR CHOLINERGIC NEUROTRANSMISSION ONTO T5 CELLS OF *DROSOPHILA*

Abstract

Several nicotinic and muscarinic acetylcholine receptors (AChRs) are expressed in the brain of *Drosophila melanogaster*. However, the contribution of different AChRs to visual information processing remains poorly understood. T5 cells are the primary motion-sensing neurons in the OFF pathway and receive input from four different columnar cholinergic neurons, Tm1, Tm2, Tm4 and Tm9. We reasoned that different AChRs in T5 postsynaptic sites might contribute to direction selectivity, a central feature of motion detection. We show that the nicotinic nAChRα1, nAChRα3, nAChRα4, nAChRα5, nAChRα7 and nAchβ1 subunits localize on T5 dendrites. By targeting synaptic markers specifically to each cholinergic input neuron, we find a prevalence of the nAChRα5 in Tm1-, Tm2- and Tm4-to-T5 synapses and of nAChRα7 in Tm9-to-T5 synapses. Knock-down of nAChRα4, nAChRα5, nAChRα7, or mAChR-B individually in T5 cells alters the optomotor response and reduces T5 directional selectivity. Our findings indicate the contribution of a consortium of postsynaptic receptors to input visual processing and, thus, to the computation of motion direction in T5 cells.

Authors

Eleni Samara, Tabea Schilling, Inês M. A. Ribeiro, Juergen Haag, Maria-Bianca Leonte, Alexander Borst

Author contributions

Eleni Samara and Alexander Borst conceived this study. Eleni Samara, Tabea Schilling and Inês M. A. Ribeiro designed the experiments. Eleni Samara and Tabea Schilling contributed to the receptor synaptic localization experiments and analysis. Eleni Samara and Maria-Bianca Leonte contributed to the optomotor response experiments. Eleni Samara and Juergen Haag contributed to the calcium imaging analysis. Eleni Samara, Inês M. A. Ribeiro and Alexander Borst wrote and edited this paper, and all authors contributed edits to this manuscript.

Columnar cholinergic neurotransmission onto T5 cells of *Drosophila*

Eleni Samara[1,2*], Tabea Schilling[1], Inês M. A. Ribeiro[1,3], Juergen Haag[1], Maria-Bianca Leonte[1,2], Alexander Borst[1,4*]

[1] Max Planck Institute for Biological Intelligence, Department of Circuits-Computation-Models, Am Klopferspitz 18, 82152 Planegg, Germany

[2] Graduate School of Systemic Neurosciences, Department Biology II Neurobiology, LMU Munich, Grosshaderner Strasse 2, 82152 Planegg, Germany

[3] Institute of Medical Psychology, Medical Faculty, LMU Munich, Goethestrasse 31, 80336 Munich, Germany

[4] Lead contact

*Correspondence: eleni.samara@bi.mpg.de (E.S.), alexander.borst@bi.mpg.de (A.B.)

Summary

Several nicotinic and muscarinic acetylcholine receptors (AChRs) are expressed in the brain of *Drosophila melanogaster*. However, the contribution of different AChRs to visual information processing remains poorly understood. T5 cells are the primary motion-sensing neurons in the OFF pathway and receive input from four different columnar cholinergic neurons, Tm1, Tm2, Tm4 and Tm9. We reasoned that different AChRs in T5 postsynaptic sites might contribute to direction selectivity, a central feature of motion detection. We show that the nicotinic nAChRα1, nAChRα3, nAChRα4, nAChRα5, nAChRα7 and nAChβ1 subunits localize on T5 dendrites. By targeting synaptic markers specifically to each cholinergic input neuron, we find a prevalence of the nAChRα5 in Tm1-, Tm2- and Tm4-to-T5 synapses and of nAChRα7 in Tm9-to-T5 synapses. Knock-down of nAChRα4, nAChRα5, nAChRα7, or mAChR-B individually in T5 cells alters the optomotor response and reduces T5

directional selectivity. Our findings indicate the contribution of a consortium of postsynaptic receptors to input visual processing and, thus, to the computation of motion direction in T5 cells.

Introduction

Neurotransmission is fundamental for neuronal communication, entailing the release of neurotransmitter from the presynaptic terminal and its binding by receptors on the postsynaptic membrane. In *Drosophila melanogaster*, the neurotransmitters acetylcholine, GABA, glutamate, dopamine, serotonin, octopamine[1] and histamine[2] are used for neuronal tasks. Amongst them, the prime excitatory neurotransmitter is acetylcholine[3–5], which can bind to a multitude of structurally diverse acetylcholine receptors (AChRs)[6–9]. How this structural variety supports specific neural computations is not understood.

AChRs comprise two categories in bilaterians and cnidarians[10]: fast ionotropic nicotinic receptors (nAChRs) and slow metabotropic muscarinic receptors (mAChRs). nAChRs are activated by acetylcholine (ACh) and the agonist nicotine and belong to the cys-loop ligand-gated ion channel superfamily, forming functional pentamers of various subunit stoichiometries, homomeric or heteromeric. In *Drosophila* the pentameric nAChR formation is achieved from a pool of seven α and three β subunits[11–13]. mAChRs are G protein-coupled receptors (GPCRs), activated by ACh and the agonist muscarine and comprise three types, A, B and C in *Drosophila*[14–16]. These mAChR types activate different signaling cascades, with mAChR-A and mAChR-C coupling to the $G_{q/11}$ and mAChR-B to the $G_{i/0}$[15,17,18]. Although the variety of AChRs has been thoroughly addressed at the biochemical level[18,19], our understanding at the circuit level and consequently in behavioral output is only starting to advance[14,15,20–23].

Among sensory modalities, vision contributes the most synaptic input to the *Drosophila* central brain[24]. Visual processing starts at the retina of the compound eye, whose retinotopic organization leads to a repetitive circuitry across its ~850 facets[25,26], and progresses to the lamina, medulla, lobula and lobula plate neuropils of the optic lobe. Next to color and polarization vision[27], motion vision has been most thoroughly investigated. The photoreceptor-derived information is split into two pathways: the ON-pathway for luminance increments and the OFF-pathway for luminance decrements[28,29]. The first neurons that compute directional information are T4 cells in the ON- and T5 cells in the OFF-pathway[30,31].

Both T4 and T5 cells bifurcate, with the dendrite giving rise to the soma and axonal terminal fiber[32]. T4 dendrites are located in medulla layer ten (M10) and T5 dendrites in lobula layer one (LO1). T4 and T5 cells exist in four subtypes: a, b, c and d. Each subtype has its dendrite oriented in one of the four cardinal directions and responds selectively to front-to-back, back-to-front, upward or downward motion, respectively[31–34]. Furthermore, each subtype has its axonal terminals in one of the four layers in lobula plate[32]. For their directional responses, T4 and T5 cells rely on the visual information they receive from input neurons. The major T4 upstream columnar neurons are the excitatory cholinergic Mi1 and Tm3, the glutamatergic Mi9 and the inhibitory GABAergic CT1, C3 and Mi4[35–43]. For T5 cells, the main columnar input neurons are the excitatory cholinergic Tm1, Tm2, Tm4 and Tm9 and the inhibitory GABAergic CT1[37,39–41,44–49]. T4 and T5 cells collect their inputs in a distinct spatial order[37] reflecting their specific directional tuning[50,51].

T4/T5 direction-selectivity is based on two mechanisms: preferred direction (PD) enhancement and null direction (ND)

suppression[51–53]. In both processes, the luminance signal from one point in visual space is delayed and interacts with the instantaneous signal from a neighboring image point. For PD enhancement, the delayed signal is from the preferred side of the cell and amplifies the central signal. For ND suppression, the delayed signal is from the opposite side and suppresses the central signal. In T4 cells, PD enhancement is biophysically implemented by a release from shunting inhibition, mediated by the glutamatergic, inhibitory OFF-center cell Mi9, which amplifies the central excitatory input from Mi1 and Tm3 neurons[42,54]. For ND suppression, the inhibitory neurons CT1, Mi4 and C3 act in concert to inhibit the Mi1-Tm3 signal. In T5 cells, CT1 is responsible for ND suppression[48]. It is, however, unclear how the different cholinergic inputs accomplish the PD enhancement. While the functional consequences of the different T5 cholinergic inputs have been addressed in the past[45,49,55], the implications of an input-specific AChR composition on T5 dendrites have not been considered.

In this study, we address the variety of AChRs in T5 cells. We show the existence of the nAChRα1, nAChRα3, nAChRα4, nAChRα5, nAChRα7 and nAChRβ1 subunits on T5 dendrites. We then target synaptic markers to each T5 cholinergic input and find a differential distribution of nAChRs in T5 postsynaptic sites. Through a combinatorial approach of neuronal input spatial wiring and synaptic receptor mapping, we demonstrate the complex columnar cholinergic spatial wiring on T5 dendrites and hypothesize about the intra- and inter-bouton nAChR variety. Finally, we show that nAChRα4, nAChRα5, nAChRα7 and mAChR-B affect the optomotor response and T5 direction-selectivity.

Results

Expression of AChRs in T5 cells

Information about the AChR expression in T5 cells is available at the RNA[40,56,57] and lacks at the protein level. We evaluated the endogenous expression of the nAChRα1, nAChRα2, nAChRα3, nAChRα4, nAChRα5, nAChRα6, nAChRα7 and nAChRβ1 subunits on T5 dendrites residing in LO1 together with other cell types[32] (Figure 1A,B). We used nAChRα subunits endogenously tagged with an enhanced version of the green fluorescent protein (EGFP) generated by Pribbenow et al.[22] and the nAChRα3 and nAChRβ1 subunits endogenously tagged with peptide tags (ALFA and HA accordingly) from Sanfilippo et al.[58]. Such receptor lines minimize the mistargeting error that can occur with receptor overexpression and allow for assessing protein expression levels. To test for mistargeting events caused by the protein tagging, we compared the nAChRα7 EGFP-tagged subunit expression pattern to the endogenous nAChRα7 with an antibody[59] and to the nAChRα7 ALFA-tagged expression pattern (Figure S1A,B). The nAChRα7 EGFP expression pattern was recapitulated by both the nAChRα7 antibody and nAChRα7 ALFA. Importantly, the EGFP and ALFA tag were inserted in the same amino acid position, allowing us to compare the tag effects in nAChRα7 localization. To test for functional alterations caused by the tagging events, we focused on fly behavior. When stimulated by rotatory visual motion, flies perform corrective steering maneuvers in their trajectories, a behavior called the optomotor response[60–62]. Wild type and nAChRα5 EGFP-tagged flies were exposed to a set of OFF edges moving in sixteen directions, while walking on an air-suspended ball (Figure S1C). No significant differences between their angular velocities were observed, acting as a first indication of minor-to-none functional alterations by the EGFP-tagging event.

Next, we verified the T5 localization of nAChRs by co-localizing the receptor puncta with the membrane-bound tdTomato expressed in T5 dendrites. We found the nAChRα1, nAChRα3, nAChRα4, nAChRα5, nAChRα6, nAChRα7 and nAChRβ1 subunits on T5 dendrites, while nAChRα2 was not detected (Figure 1C-K). To ensure the T5-specific lack of nAChRα2 expression, we confirmed its expression in other lobula layers (Figure S1D). By quantifying the nAChRα subunit density in regions of interest (ROIs) on T5 dendrites in LO1, we observed the nAChRα5 prevalence and low co-localization levels for nAChRα2 and nAChRα6, in agreement with previous RNA-seq levels[40,56] (Figure 1L, Figure S1E-G). Subsequently, we sought to identify the nAChRα expression patterns in T5 axonal terminals. Both T4 and T5 populations were targeted and due to the lack of neuropil distinction between T4/T5 axonal terminals, our results cannot be attributed explicitly to T5 cells. nAChRα1, nAChRα5, nAChRα6, nAChRα7 and nAChRβ1 were detected in T4/T5 terminals, nAChRα2 and nAChRα4 were not and nAChRα3 showed a distinct expression pattern in LOP3 where T4/T5c subtypes reside (Figure S2A-I). Additionally, we observed the reduction of the nAChRα1, nAChRα3, nAChRα5 and nAChRα7 subunits in LOP after a T4/T5 specific subunit knock-down, indicative of their T4/T5 axonal terminal localization (Figure S2L, S3A,B,D,E).

To study the T5 mAChR expression, we used a UAS-mAChR-B line. The overexpressed mAChR-B protein localized exclusively on T5 dendrites (Figure 1M, S2J), however this might be the outcome of ectopic expression leading to dendritic protein targeting. We reasoned that if mAChR-B was mistargeted to T5 dendrites, this mistargeting would be observed in other cells and that over-expression of mAChR-B with a pan-neuronal driver would result in the presence of ectopic mAChR-B in all the dendrites of neurons in the fly brain (Figure S2K). Instead, the

mAChR-B type followed an enrichment in M10 and LO1, where T4 and T5 dendrites reside respectively, while being absent from LOP. In summary, the dendritic and axonal terminal protein expression patterns differ between ionotropic and metabotropic AChRs and even within the same AChR (Figure S2M).

To investigate the expression of AChRs where we lacked endogenously tagged lines, and to verify the expression profiles reported in Figure 1, we used enhancer-trap Gal4 lines[63] (Figure S4A-L). By comparing RNA-seq datasets[40,56] with the enhancer trap and the endogenously tagged experiments here and in previous studies[58], we concluded that nAChRα1, nAChRα3, nAChRα4, nAChRα5, nAChRα7 and nAChRβ1 as well as mAChR-A and mAChR-B are expressed in T5 cells, while the nAChRα2, nAChRα6, nAChRβ2 and nAChRβ3 subunits exhibit low expression levels or are not expressed at all (Figure S4M). Finally, transcriptomics suggest low mAChR-C expression levels in the fly brain[14,20,64].

Morphological identification of cholinergic T5 input neurons and synapse visualization

nAChRα1, nAChRα3, nAChRα4, nAChRα5, nAChRα7 and nAChRβ1 might contribute to T5 directional responses by localizing to all cholinergic synapses linking Tm1, Tm2, Tm4 and Tm9 to T5 dendrites, or to only a subset of these. To discern between these possibilities, we assessed the protein localization of nAChRα subunits in specific synaptic pairs (Figure 2). We first evaluated the genetic access to the four Tm neurons. The morphology of these neurons has been extensively studied via Golgi staining[32] and EM reconstructions[36,37,44,47,65–67], thus we used this knowledge to cross-validate our light microscopy screening of potential Tm-specific enhancer lines (Figure S5A,D,G,J). The efficacy of Gal4 and LexA driver lines[68,69], used in functional studies[45,48], was assessed in terms of neuronal

specificity and whole population targeting. To achieve sparse and stochastic neuronal labelling, we used the MCFO approach[70] and observed axonal terminals in lobula layer 1 for Tm1 (Figure S5A), up to layer 2 for Tm2 (Figure S5D), up to layer 4 for Tm4 (Figure S5G), and in layer 1 for Tm9 (Figure S5J), as expected from previous studies[32,37]. To exclude the developmental bias as well as the non-neuronal targeting induced by the heat-shock-activated flipase[71] in the MCFO approach (Figure S5G), we supplemented our single cell labelling with whole population labelling of the Tm-Gal4 lines (Figure S5B,E,H,K). Gal4 driver lines were cell-type specific and targeted the whole population of Tm1, Tm2, Tm4 and Tm9 cells. For the LexA[69,72] driver lines, the whole Tm1 population was targeted, but after comparing the results with the analogous Gal4 driver line, dendritic ramifications in M4 that do not correspond to Tm1, were observed (Figure S5C). Tm2, Tm4 and Tm9 LexA lines displayed sparse neuronal labelling and could not target the whole neuronal population (Figure S5F,I,L). Based on this morphological screening, we chose the Gal4 driver lines for the Tm-T5 synapse visualization.

To visualize Tm-to-T5 synapses, we screened for the available reporter tools. We first explored methods of trans-synaptic labelling such as GRASP[73], where the GFP_{1-10} and GFP_{11} fragments are targeted to the cell membranes of the pre- and post-synaptic compartment respectively. The targeted GRASP (t-GRASP)[74] allowed to capture all synapses between Tm and T5 cells (Figure S5M). The presence of reconstituted GFP signal in the inner optic chiasm, likely due to the ectopic reconstitution in the Tm4-T5 synapses, led us to exclude this genetic method. The next reporter tool was the activity GRASP (syb-GRASP)[75]. The reconstituted GFP signal was indicative of the given synaptic activity at the point of the dissection, as the GFP_{1-10} fragment is tethered to the vesicular protein synaptobrevin, thus resulting in the syb-GRASP reconstitution being sparser than the t-GRASP

reconstitution (Figure S5N). This approach was excluded because it did not allow for a quantitative analysis, as its activity dependency reports only the at the given-timepoint active synapses introducing false negatives in the total synapse count. Finally, we tested the truncated version of the presynaptic active zone marker Brp, namely Brp^{short} [76,77] (Figure S5O). Brp is one of the major protein participants of the protein-dense T-bar[78,79], a ubiquitous presynaptic component of *Drosophila* visual synapses (as in previously[80] and from the current EM analysis), while Brp^{short} depends on endogenous Brp levels and does not modify them[77,81]. This Brp^{short}::GFP line labelled only the presynaptic sites of the Tm synapses, regardless of their activity, without labelling their postsynaptic sites. In conclusion, Brp^{short} was selected for the evaluation of the nAChR synaptic localization.

To validate the synaptic specificity of Brp^{short}, we assessed two different, well described synapses: the glutamatergic Mi9-T4 and the cholinergic Tm3-T4 synapse (Figure S6A-D). Mi9-driven Brp$^{short::mCherry}$ [82] puncta lacked trans-synaptic alignment with nAChRα5 in M10 (Figure S6A,D), while they trans-synaptically aligned with the glutamatergic receptor GluClα[42] known to localize in Mi9-T4 synapses (Figure S6B,D). Tm3-driven Brp$^{short::mCherry}$ puncta also showed no trans-synaptic alignment with the GABAergic receptor Rdl in Tm3-T4 synapses (Figure S6C). To confirm the synaptic localization of Brp$^{short::mStraw}$, a chimera that has the same truncated form of Brp as in Brp$^{short::mCherry}$ but is instead fused with mStrawberry[83], we used an antibody against the endogenous Brp that detects amino acids absent from the truncated Brp^{short} form (Figure S6E). This approach revealed the presynaptic alignment of the endogenous Brp (Anti-Brp) with the Tm1, Tm2, Tm4 and Tm9 boutons (Brp$^{short::mStraw}$). These results, together with previous studies[76], speak in favor of Brp$^{short::mStraw}$ as an effective presynaptic marker in our circuit of interest.

The synaptic localization of the nAChRα5 subunit differs among the four cholinergic inputs

With genetic access to the major cholinergic T5 inputs and $Brp^{short::mStraw}$ as a presynaptic marker, we evaluated the localization of the most highly expressed subunits, nAChRα1, nAChRα3, nAChRα4, nAChRα5, nAChRα7 and nAChRβ1 along Tm-to-T5 synapses. ROIs were restricted to LO1 so as to include the Tm-T5 synaptic connections (Figure S7A). We found all the tested subunits localizing to Tm1, Tm2, Tm4 and Tm9 synapses in LO1 (Figure 2A-D, Figure S7B). Tm synapses in LO1 might account for other output neurons apart from T5 cells, hence we used the FlyWire connectome data explorer (Codex) for the full adult fly brain (FAFB) dataset[65–67] in order to find the output neurons of Tm1, Tm2, Tm4 and Tm9 synapses in LO1. T5 cells were found as the principal neuronal outputs across all four Tm types in LO1 (Figure S8A). Therefore, the quantification of the nAChRα synaptic localization in LO1 principally corresponded to Tm-to-T5 synapses. Importantly, by calculating the synapse occupancy index (number of nAChR puncta with Brp co-localization/number of Brp puncta), we found that not all Tm input neurons had the same synaptic receptor profiles. Tm1-, Tm2- and Tm4-to-T5 synapses primarily used the nAChRα5, whereas Tm9-to-T5 synapses mainly used the nAChRα7 subunit (Figure 2E-H). Interestingly, Tm9 synapses had increased index values along the nAChRα1, nAChRα3, nAChRα4, nAChRα7 and nAChRβ1 subunits compared to the other Tm neurons, depicting a greater nAChR variety in Tm9 synapses.

As the GABAergic neuron CT1 was a considerable Tm9 output in terms of synapse number in LO1 (Figure S8A), we wondered if the Tm9-nAChRα7 subunit trans-synaptic alignment (Figure 2H) could be attributed to Tm9-to-T5 synapses as well. We generated new flies to employ a C-RASP approach, which follows the activity GRASP principles, but instead of a GFP_{1-10}

uses a CFP_{1-10} fragment. This method showed the nAChRα7 localization in Tm9-to-T5 synapses (Figure S8B). Finally, we calculated the total synapse counts of Tm1, Tm2, Tm4 and Tm9 neurons in LO1 (flywire.ai) and, with the exception of Tm2, found a similar tendency with the $Brp^{short::mStraw}$ counts in the LO1 voxels we previously quantified (Figure S8C). This is an additional testament to the localization and quantitative specificity of $Brp^{short::mStraw}$, as its localization depends on the endogenous Brp[77] (Figure S6E) and the majority of the endogenous Brp is accompanied by $Brp^{short::mStraw}$ [81,84] (Figure S8C).

Whether Tm neurons differ from one another by differentially using muscarinic receptors as well, is currently unknown. T5 mAChR-B overexpression led to mAChR-B localization in Tm9-to-T5 synapses (Figure S8D), which was more evident when compared to nAChRα5 (Figure S8E). The apparent lack of a generalized cellular mistargeting of the mAChR-B overexpression line (Figure S2K) does not exclude the existence of synaptic mistargeting events. Consequently, the Tm9-mAChR-B results are indicative rather than definitive. Overall, our Tm-nAChR mapping in LO1 revealed that Tm1, Tm2 and Tm4 additionally differ from Tm9 cells at the postsynaptic level.

Spatial organization and variety of Tm-nAChRα synapses on T5 dendrites

The compartmentalization of inputs and subsequently of receptors on T5 dendrites is essential for T5 direction-selectivity[50,51]. Thus far, receptor localization in Tm-to-T5 synapses has been addressed by combining single-cell receptor localization and neuronal input spatial wiring information[58,85]. To advance this, we analyzed T5a and T5c dendrites as representatives of the two directional systems from the FAFB[65] dataset via the FlyWire (flywire.ai)[66,67] interface. Manual proofreading of predicted synapses[86,87] revealed the differences

in connection strengths across Tm1, Tm2, Tm4 and Tm9 as reported before[37,48] (Figure 3A,B). To account for these Tm-to-T5 differences in synapse counts, we measured the synapse occupancy index that represents the proportion of Brp puncta colocalizing with nAChR subunits (Figure 2E-H). Next, we sought to identify the spatial wiring of the four Tm neurons on T5 dendrites. Tm1, Tm2, Tm4 and importantly, also Tm9 wire to the central dendritic compartment, with Tm9 synapses extending to the distal compartment as previously shown[37,48] (Figure 3C,D).

Tm9 synapses spatially differentiate from Tm1, Tm2, Tm4 synapses on T5 dendrites, preferentially use nAChRα7 over nAChRα5 and exhibit a pronounced nAChR variety (Figure 2H, Figure 3J). Whether such variety could result from an intra- or inter-bouton nAChR variety is not known. To address the latter possibility, we focused on the localization of nAChR pairs in LO1 and encountered increased co-localization events between nAChRα3 and nAChRβ1 (Figure 3E,I). We used the nAChRα5 and nAChRβ1 subunits as a negative control, since their Tm1-, Tm2-, Tm4-nAChRα5 and Tm9-nAChRβ1 localization profiles implies their spatial separation (Figure 2E-H). nAChRα5 and nAChRβ1 were indeed found primarily in different locations in LO1 (Figure 3F,I). Subsequently, we compared the nAChRα3 and nAChRβ1 localization with that of the Tm9-prevalent nAChRα7 subunit and encountered sparse co-localization events (Figure 3G-I). These results suggest a Tm9 inter-bouton nAChR variety, where some boutons prefer the nAChRα7 subunit and others the nAChRα3 and nAChRβ1 subunits. In conclusion, the polyadic synapse morphology (i.e. one Tm9 presynapse corresponds to multiple T5 postsynaptic sites) suggests a rather complex intra-bouton AChR variety. In an example Tm9-T5c,T5a connection, the T5c postsynaptic site might occupy nAChRα3 in a homomeric or a heteromeric nAChRβ1 formation and mAChR-

B, while the T5a one might occupy the heteromeric nAChRα3-nAChRβ1 formation (Figure 3K).

AChRs differentially affect the optomotor response

The optomotor response is a sensory-induced locomotion where flies correct their trajectories when presented to rotational motion. T4 and T5 cells are indispensable for its manifestation in the ON and the OFF pathway accordingly[88–91], therefore, molecular alterations that are crucial for proper T5 function should be reflected in the fly's behavior. Using RNAi knock-down, we tested whether nAChRα1, nAChRα3, nAChRα4, nAChRα5, nAChRα7 and mAChR-B were required for the optomotor response on the 'fly-on-ball' set up. Given that each receptor has a unique developmental onset of expression (Figure S1G), we used a T4/T5 driver line that was active from the third larval stage onwards[88,92,] and raised flies in 29°C[93,94] to achieve a strong knock-down of protein levels. The driver line targeted all T5 subtypes and allowed for the RNAi induction prior to the peak of AChR expression (Figure S3I,J). Finally, we confirmed the RNAi-induced reduction in AChR expression with immunohistochemistry (Figure S3A-H). To test if the nAChR knock-down reduced synapse counts rather than only affecting neurotransmission, we counted Brp puncta in LO1 among different genetic backgrounds (Figure S3K). Brp counts in T4/T5-specific RNAi against the nAChRα5 or the nAChRα7 subunit were similar to the control T4/T5-specific RNAi against mCherry. Tm9-specific expression of the apoptotic gene *hid* led to a significant reduction in Brp counts and served as a positive control. Our results indicate that synapse formation is unaffected upon T4/T5 knock-down of nAChRα5 or nAChRα7.

Tethered walking flies were exposed to a set of OFF edges moving in sixteen directions, eliciting a typical profile of turning velocities, with the highest amplitudes to horizontal motion and

lowest to vertical motion[42] (Figure 4A). Knock-down of nAChRα1 or nAChRα3 did not alter the response profile to OFF edges (Figure 4B,C,H). Knock-down of nAChRα4 or mAChR-B resulted in a response increase (Figure 4D,G,H), whereas knock-down of nAChRα5 or nAChRα7 led to a response decrease to horizontal moving edges (Figure 4E,F,H). Knock-down of nAChRβ1 and mAChR-A did not affect the response profile (Figure S9A-C). However, the RNAi efficiency against the nAChRβ1 subunit was low and for the mAChR-A could not be verified (Figure S3F,H). Therefore, these AChRs should not be excluded from playing an important role in the optomotor response. Each AChR knock-down was compared to four control types: the UAS-AChR RNAi effector, the T4/T5-Gal4 driver, the T4/T5-specific mCherry RNAi (Valium 10 and Valium 20 depending on the respective AChR RNAi) and wild type flies (Canton S) (Figure 4H, Figure S9D-F). We excluded the T4/T5-Gal4 driver to be the one inducing the angular velocity reduction observed in nAChRα5 and nAChRα7 knock-down flies, as nAChRα3, nAChRα4 and mAChR-B knock-downs exhibit different angular velocities from T4/T5-Gal4 driver flies. Notably, the T4/T5-specific mCherry RNAi Valium 10 phenotypes did not differ from the T4/T5-specific mCherry RNAi Valium 20 ones. The UAS-mCherry RNAi Valium 10 effector did not differ from the T4/T5-specific mCherry RNAi Valium 10, in contrast to the Valium 20 control.

Subunit compensation mechanisms have been previously reported[95,96], but it is not known whether they extend to T5 cells. To address this, we focused on nAChRα5 and nAChRα7 subunits as they dominate in Tm1-, Tm2-, Tm4-to-T5 and in Tm9-to-T5 synapses, respectively. Knock-down of both nAChRα5 and nAChRα7 attenuated the flies' responses similar to the individual subunit knock-downs (Figure S9G). The optomotor response was not abolished upon double knock-down, in contrast to T5 silencing[88], indicating the importance of other nAChRs for T5

function. Moreover, nAChRα5 counts in LO1 were decreased after nAChRα7 knock-out[97], in alignment with previous work pointing towards the nAChRα5-nAChRα7 co-assembly[98] (Figure S9H-J). Collectively, our results indicate the lack of compensation mechanisms between nAChRα5 and nAChRα7 in T5 cells.

The observed enrichment of nAChRα5 and nAChRα7 in specific sets of Tm-to-T5 synapses suggests that there might be a dominant nAChR subunit, responsible for most of neurotransmission at that synapse. To test whether this is the case for the abundant in Tm9-to-T5 synapses nAChRα7 subunit, we compared behavioral responses to OFF edges presented in different directions upon thermogenetic silencing of Tm9 with *shibire*^{ts} and nAChRα7 knock-down (Figure S9K). We observed a reduction in the angular velocity under the two conditions, with the nAChRα7-induced reduction being stronger than the Tm9-induced one. This can be primarily explained by an incomplete thermogenetic silencing with *shibire*^{ts} and the lack of absolute exclusivity of the nAChRα7 subunit in Tm9-to-T5 synapses. We conclude that it is difficult to assign single nAChR subunit function to input function. Nonetheless, creating synaptic maps of nAChR subunits certainly helps to discriminate among the different possibilities.

Directional tuning of T5 cells changes after AChR knock-down

nAChRα5 and nAChRα7 localize on T5 dendrites and axonal terminals (Figure 1H,J, Figure S2F,H). The behavioral effects to OFF-edge horizontal motion that were observed upon nAChRα5 or nAChRα7 knock-down (Figure 4E,F,H) could either be due to functional roles in T5 dendrites or axonal terminals. To discern between these possibilities, we measured calcium responses in T5 terminals. We performed two-photon calcium imaging in T5c

neurons, which are sensitive to upward motion as the preferred motion direction[31]. nAChRα4, nAChRα5, nAChRα7 or mAChR-B knock-down flies were stimulated by dark edges moving in sixteen different directions, while calcium responses were monitored in T5c axonal terminals in LOP3 (Figure 5A, Figure S10A-C). As in behavioral experiments, RNA interference was induced prior to peak receptor expression with the use of a T4/T5 promoter active from the third larval stage[92], and raising flies in 29°C[93,94]. Knock-down of nAChRα4 led to a slight increase in calcium responses in response to the non-preferred direction (270°) (Figure 5B). Similarly, knock-down of nAChRα5 resulted in higher calcium responses to the edge moving in the non-preferred direction (Figure 5C), suggesting nAChRα5, and to a lesser extent, nAChRα4 contribute to directional tuning in T5c neurons. Knock-down of nAChRα7 resulted in a calcium response increase to the null and mostly to the preferred motion direction (Figure 5D). Knock-down of mAChR-B caused an overall increase of T5 calcium responses across all presented stimuli directions (Figure 5E). Individual fly responses in Figure S10D, show the nAChRα4 and nAChRα5 subunit knock-down flies exhibiting high inter-fly variability, whereas the nAChRα7, mAChR-B and mCherry RNAi flies display more stable response patterns. In general, nAChRα4, nAChRα5 and mAChR-B significantly influenced T5 directional tuning by altering the directionality index (Figure 5F). However, T5 cells exhibit increased responses to edges in the preferred direction after nAChRα7 knock-down compared to controls, a phenotype also observed in mAChR-B knock-down flies. Taken together, an interplay of nAChRs and mAChRs shapes T5 direction-selectivity.

Cholinergic neurotransmission in T5 cells takes place in two distinct locations: the dendrite in LO1, where T5-T5 dendro-dendritic synapses[37] reside, and the axonal terminals in LOP3,

where T4/T5 and T5-T5 axo-axonic synapses reside[99]. Calcium responses in nAChRα5 knock-down flies were different in LO1 and LOP3 (Figure S10E-G). Dendritic calcium responses were of lower amplitude, while axonal terminal responses increased in response to the non-preferred direction (270°) in nAChRα5 knock-down compared to control mCherry RNAi flies (Figure S10F,G). Such differences imply distinct nAChR roles in the two T5 compartments.

Discussion

In this study, we investigated the columnar cholinergic neurotransmission onto T5 neurons of *Drosophila*. We found a variety of AChRs on their dendrites, which, surprisingly, are differentially distributed across the cholinergic Tm1-, Tm2-, Tm4-, Tm9-to-T5 synapses. This acetylcholine receptor variety translated into a functional variety, as portrayed by both the optomotor response and T5 directional tuning.

In mammals, nAChRs comprise nine α subunits (α1-7,9,10), four β subunits (β1-4), one γ, one δ and one ε subunits[100], whereas mAChRs consist of five M (M1-5) types[101]. This AChR variety is also found, but to a lesser extent, in *Drosophila melanogaster*, with its ten nAChR subunits and three mAChR types. Does this structural variety directs differences in neuronal function? nAChRα5 was found to be required in M4/6 mushroom body output neurons (MBONs) for coding immediate appetitive memories[22]. mAChR-A was observed on Kenyon cell dendrites, mediating aversive olfactory learning in adult flies[14]. Moreover, a study in *Drosophila* larvae showed the glutamatergic interneuron glu-lOLP mediating OFF detection via mAChR-B signaling[23], while the interplay of nAChRs and mAChRs in regulating acetylcholine modulation of larval locomotion has been pharmacologically assessed with bath application of AChR

agonists and antagonists[15]. Our study provides another example of diverse AChR functions, this time in the visual system of the adult fly.

AChR expression on T5 dendrites

AChRs in the visual system of *Drosophila* have been investigated for long[58,85,102–104]. Advancements in genomics and molecular engineering now give access to AChRs of interest by endogenously tagging them[22,58,85]. This allows for qualitatively and quantitatively assessing the neuronal expression of AChRs, avoiding the ambiguity of studies where electrophysiology was combined with antagonist application in order to identify specific AChRs[105]. We identified the nAChRα1, nAChRα3, nAChRα4, nAChRα5, nAChRα7 and nAChRβ1 subunits on T5 dendrites, where nAChRα1 and nAChRβ1 were also found co-localizing[58]. Whether this co-localization depicts a pentameric co-organization as speculated in lobula[102] remains to be proven, but it certainly indicates the stoichiometrical nAChR complexity that exists in the optic lobe[106,107]. For the mAChR-mediated neurotransmission, our results and previous RNA-seq studies[40,56,57] indicate the T5 mAChR-B expression .

nAChRα subunits in Tm-to-T5 synapses

Verifying the explicit genetic access to Tm1, Tm2, Tm4 and Tm9 neurons allowed us to use Brp^{short} for synapse labelling. While mapping the most highly expressed nAChRα1, nAChRα3, nAChRα4, nAChRα5, nAChRα7 and nAChRβ1 subunits across Tm synapses in LO1, we found nAChRα5 preferentially localizing to Tm1, Tm2, Tm4 rather than Tm9 synapses. Tm9 is functionally different from Tm1, Tm2 and Tm4 with respect to its response dynamics: the latter respond to light decrements in a transient way, while Tm9 reveals a sustained low-pass filter response with rather large time-constant[45,46,55]. Tm9-to-T5 synapses use a different and more diverse nAChR set for their cholinergic

neurotransmission than the other Tm cells. This suggests that the computation of motion direction in T5 cells is shaped by the different time-courses of the input signals they receive and by molecular mechanisms at the postsynaptic site. Such molecular mechanisms might expand to the subunit stoichiometry and isoform, even up to the inter-bouton receptor variety level. Moreover, the potential mAChR-B localization in Tm9-T5 synapses, together with the nAChRα1, nAChRα3, nAChRα4, nAChRα7, nAChRαβ1 and to a lesser extend nAChRα5 localization, points towards an interplay between ionotropic and metabotropic receptors. The role of such receptor interactions is still unclear, but recent examples indicate a potentiation of nAChR responses[20]. Finally, it is crucial to appreciate the multi-level functional diversity of Tm-to-T5 connections. Apart from the intrinsic neuronal input properties and the postsynaptic receptors, functional diversity might be introduced at the single, input-specific, bouton level by unique molecular ‘‘design principles’’[84] expanding from the pre- to the post-synaptic site. Here, we encounter the nAChR variety in Tm9-to-T5 connections translating to inter-bouton variety, displaying once more the pivotal computational role of the single synapse.

Together with previous reports[37,48], our EM analysis shows a spatial overlap of Tm synapses on T5 dendrites, specifically on the central dendritic compartment. It is therefore risky to draw conclusions about receptor localization in Tm-to-T5 synapses via single-cell receptor localization experiments, especially due to the shared cholinergic nature of the input neurons and their spatial overlap. In this study, we introduce a new methodology, where EM-derived neuronal input spatial wiring and synaptic receptor mapping are combined to extract pre-, post-synaptic and spatial wiring information. Ultimately, single synapse-to-single dendrite approaches will improve the resolution of connectivity studies, leading to a T5 AChR-connectome[108].

AChRs roles in the OFF-motion pathway

Do these individual nAChRs and mAChRs control T5 motion detection? We found that both ionotropic and metabotropic AChR signaling contribute to T5 function, implying that an unforeseen complexity of cholinergic neurotransmission underlies motion detection in the OFF pathway. Notably, nAChRα5 and nAChRα7 localization in T5 axonal terminals in addition to dendrites, could result in behavioral alterations deriving from other than dendritic computations. As the behavioral output involves many T5 downstream partners[62,109,110], compensatory mechanisms might also be in place, masking immediate effects in T5 cells.

Calcium imaging in T5c neurons revealed an increase in ND responses among all nAChRα4, nAChRα5, nAChRα7 and mAChR-B knock-down flies. In contrast, the nAChRα7 or mAChR-B knock-down led to amplified PD responses. We expected the nAChRα5 subunit knock-down, while being the most highly expressed subunit along Tm1-, Tm2-, and Tm4-to-T5 synapses, to severely attenuate T5 PD responses. However, this was not the case, suggesting an important role for nAChRα1, nAChRα4 and nAChRα7 in preserving Tm1-, Tm2- and Tm4-to-T5 function. Further proof was the preservation of the optomotor response and not its abolishment after simultaneously knocking-down nAChRα5 and nAChRα7. Lastly, the mAChR-B knock-down-induced effects resemble that of a raised inhibition, which align with the receptor's reported inhibitory role[23]. Our results show an interplay of nicotinic and muscarinic AChRs taking place on T5 dendrites, but whether that derives from an intra- or inter-bouton receptor localization is not known. Nevertheless, the complexity of the ionotropic neurotransmission i.e. receptor stoichiometries, isoforms, inter-bouton variety, does not allow us to attribute subunit-specific functions in T5 computation, but

rather understand which nAChR subunits are good candidates for further *in vitro* exploration.

Fast (τ=50ms) and slow desensitizing (τ=539 ms) nAChRs have been found in Kenyon cells and antennal lobe cells of honeybees, respectively[111]. The participating subunits were identified as the nAChRα2, nAChRα8 and nAChRβ1, while their heteromeric or homomeric formation remained unknown. Interestingly, the presence of nAChRα7 in antennal lobe cells and absence from Kenyon cells appears to dictate the differences in kinetics between the two cell types[111], implying that a single nAChR subunit suffices to alter cell physiology. In mammals, the α4β2 nAChR gating kinetics change in a stoichiometry-dependent manner in the presence of calcium and magnesium[112], while stoichiometrical isoforms dictate the receptor responses to different ACh concentrations[113] ($(\alpha4)_3(\beta2)_2$ compared to $(\alpha4)_2(\beta2)_3$). The previously described invertebrate and mammalian examples are indicative of how subunit stoichiometry differences affect receptor function. Therefore, future investigation of the stoichiometries and ionic properties of nAChR subunits in *Drosophila* will be a major asset to understand the molecular mechanisms underlying T5 direction selectivity.

Multiple aspects should be taken into account when interpreting RNAi experiments. Firstly, nAChR subunit compensation[96] might take place, concealing the true receptor subunit function, however it was not present between nAChRα5 and nAChRα7. Secondly, the calcium imaging location (T5 dendrites or axonal terminals) should be considered. T5-T5 dendro-dendritic synapses, T5-T5 and T4/T5 axo-axonic synapses[99] are cholinergic. nAChRα5 and nAChRα7 knock-down will affect such synapses as well, potentially confounding our conclusions on T5 dendrites. To address this, we observed different responses in

T5 dendrites compared to axonal terminals, potentially deriving from differences in the density of ionotropic AChRs and other voltage gated calcium channels between the two T5 compartments or from an uncharacterized influence of T5-T5 dendro-dendritic and T5-T5 and T4/T5 axo-axonic synapses (Figure S10). Moreover, nAChRα1, nAChRα3 and nAChRβ1 are expressed on T5 dendrites and do not elicit distinct behavioral phenotypes. This might be an outcome of RNAi efficiency, as it results in a knock-down rather than a knock-out, especially in the nAChRβ1 case where RNAi efficiency was low. nAChRα1 and nAChRβ1 were found to co-localize[58] and restrict to the distal T5 dendritic compartment where T5-T5 dendro-dendritic synapses form, but the roles of such connections in directional computations are still unexplored. nAChRβ1 and nAChRα3 localized in Tm9-to-T5 synapses and co-localized in LO1. Therefore, it is possible that a nAChRα1-nAChRα3-nAChRβ1 heteromer exists in Tm9 synapses, corroborated by previous studies in the OL[105–107], and unknown subunit regulatory mechanisms are activated post-knock-down. Finally, we used standardized conditions for RNAi experiments, but fly-to-fly variability was encountered in nAChRα4 and nAChRα5 knock-downs (Figure S10). This encouraged us to believe that RNAi efficiency may differ across individuals and compensation mechanisms at the individual level might be activated.

RESOURCE AVAILABILITY

Lead contact

Further information and requests for data should be directed to and will be fulfilled by the Lead Contact, Alexander Borst (alexander.borst@bi.mpg.de).

Materials availability

The study generated a new fly line and is available from lead contact upon request.

Data and code availability

- This paper analyzes existing, publicly available data from FlyWire (flywire.ai).
- Data and code for analysis are publicly available at the at the Edmond Open Research Data Repository of the Max Planck Society: https://doi.org/10.17617/3.QFJ7U2.
- Any additional information required to reanalyze the data reported in this paper is available from the lead contact upon request.

ACKNOWLEDGMENTS

The authors thank D. Owald, C.H. Lee, S. Russell, F. Pinto-Teixeira, H.J. Bellen, the Bloomington Drosophila Stock Center, the Vienna Drosophila Stock Center and the Developmental Studies Hybridoma Bank for flies and antibodies. We are grateful to the Princeton FlyWire team and members of the Murthy and Seung labs for development and maintenance of FlyWire (supported by BRAIN Initiative grant MH117815 to Murthy and Seung) and to the Imaging Facility of the MPI for Biological Intelligence-Martinsried. We are thankful to B. Zuidinga for technical assistance with behavioral experiments and calcium imaging analysis; M. Sauter for technical assistance with fly dissections; R. Kutlesa for technical assistance with behavioral experiments; S. Prech for technical assistance with experimental setups; R.M. Vieira and J. Pujol-Martí for discussions. We thank Julia Kuhl for creating the graphical abstract. E. Samara is a member of the Graduate school of Systemic Neurosciences

(GSN) Munich. I.M.A.R. was funded by LMU and the DFG grant nr RI 3644/2-1. This work was funded by the Max Planck Society.

AUTHOR CONTRIBUTIONS

E.S. and A.B. conceived this study. E.S., T.S. and I.M.A.R. designed the experiments. E.S. and T.S. contributed to the receptor synaptic localization experiments and analysis. E.S. and M.B.L contributed to the optomotor response experiments. E.S. and J.H. contributed to the calcium imaging analysis. E.S., I.M.A.R. and A.B. wrote and edited this paper, and all authors contributed edits to this manuscript.

DECLARATION OF INTERESTS

The authors declare no competing interests.

FIGURE TITLES AND LEGENDS

Figure 1. AChR expression on T5 dendrites

(A) Schematic representation of T5 dendrites (blue), among other cell types, residing in lobula layer 1 (LO1) of the *Drosophila* optic lobe (OL).
(B) Schematic representation of nicotinic ionotropic (magenta) and muscarinic metabotropic (cyan) AChRs in *Drosophila*. Out of the seven nAChRα subunits, six were tagged with EGFP[22] and the nAChRα3 with the ALFA tag[58]. The nAChRβ1 subunit[58] and the mAChR-B (C.H. Lee) were tagged with the HA peptide tag.
(C) OL (Anti-Brp, grey) with T4 and T5 dendrites (R42F06-Gal4>UAS-myr::tdTomato, blue) in M10 and LO1 accordingly. Scale bar 40µm.
(D-K) nAChRα1, nAChRα2, nAChRα3, nAChRα4, nAChRα5, nAChRα6, nAChRα7 and nAChRβ1 (nAChRα1,2,4,5,6,7::EGFP, nAChRα3::ALFA, nAChRβ1::HA, magenta) subunit expression on T5 dendrites (R42F06-Gal4>UAS-myr::tdTomato, blue). Scale bar 10µm, inset 5µm. See also Figures S1-S4. Detailed genotypes are reported in Table S1.

(L) Density of nAChR subunit expression on T5 dendrites across 30 ROIs in LO1 (optic lobes n=6). nAChRβ2 and nAChRβ3 subunits were not addressed. Subunits with the lowest expression levels are in grey. Data is mean ± SEM.

(M) Overexpression of mAChR-B (UAS-mAChR-B::HA, cyan) on T5 dendrites (R42F06-Gal4>UAS-myr::tdTomato, blue). Scale bar 10µm, inset 5µm.

Figure 2. Differential synaptic localization of nAChRα subunits in Tm synapses

(A-D) Trans-synaptic alignment of Tm1, Tm2, Tm4 and Tm9 boutons (Tm-Gal4> UAS-Brp$^{short::mStraw}$, green) with the endogenously tagged nAChRα1, nAChRα3, nAChRα4, nAChRα5, nAChRα7 and nAChRβ1 subunits (nAChRα1,4,5,7::EGFP, nAChRα3::ALFA, nAChRβ1::HA, magenta) in LO1. Arrows indicate the Brp$^{short::mStraw}$-receptor punctum trans-synaptic alignment. Scale bar 1µm. See also Figures S5-S8.

(E-H) Synapse occupancy of Tm1, Tm2, Tm4 and Tm9 boutons with nAChRα1 (pale purple), nAChRα3 (pale magenta), nAChRα4 (light magenta), nAChRα5 (magenta), nAChRα7 (dark magenta) and nAChRβ1 (violet) subunits in LO1 (optic lobes n=4, ROIs N=20, for Tm4-nAChRα5 n=3, N=15). Data is mean ± SEM.

Figure 3. Wiring of Tm1, Tm2, Tm4 and Tm9 on T5 dendrites and nAChR pairs in LO1

(A) Counts of Tm1, Tm2, Tm4 and Tm9 synapses on T5a dendrites (T5a cells n=5, flywire.ai) (left). Counts of predicted (n=663) to proofread (n=479) Tm synapses on T5a dendrites (right). Data is mean ± SEM. Detailed neuronal IDs used for the synapse proofreading are reported in Table S3.

(B) As in (A) for T5c dendrites (T5c cells n=5, flywire.ai) (left). Counts of predicted (n=621) to proofread (n=488) Tm synapses on T5c dendrites (right). Data is mean ± SEM.

(C) Dendritic localization of Tm synapses across the T5a anterior-posterior axis (T5a cells n=5). Root is considered the first dendritic branch point.

(D) Dendritic localization of Tm synapses across the T5c dorso-ventral axis (T5c cells n=5).
(E) Localization of the nAChRα3 to the nAChRβ1 subunit in LO1 (nAChRα3::ALFA green, nAChRβ1::HA magenta). Scale bar 10μm, zoom-in 5μm.
(F-H) As in (E) for nAChRα5-nAChRβ1, nAChRα7-nAChRα3, nAChRα7-nAChRβ1 subunits (nAChRα5,7::EGFP, nAChRα3::ALFA and nAChRβ1::HA).
(I) Co-localization index of nAChR pairs from Figure 3E-H (optic lobes n=2, ROIs N=10). The normality of distribution was assessed with the use of Shapiro-Wilk test. *p<0.05, ***p<0.001, ****p<0.0001. Data is mean ± SEM. Detailed statistical analysis is reported in Table S2.
(J) Schematic representation of Tm synapse distribution on T5 dendrites (Tm1, Tm2, Tm4 green, Tm9 pale green) (top). Postsynaptic receptor heterogeneity between Tm1, Tm2, Tm4 and Tm9 neurons in terms of the most abundant nAChR subunit as in Figure 2E-H (bottom).
(K) Schematic representation of postsynaptic receptor heterogeneity across axonal boutons (inter-bouton heterogeneity, red and black boxes) and within one bouton (intra-bouton heterogeneity, black box) of an example Tm9-T5 connection. Tm9-T5 synapses are polyadic, with each postsynaptic site comprising of T5 spines belonging to different T5 subtypes.

Figure 4. Fly optomotor response post-AChR knock-down

(A) Schematic workflow representation for the behavioral assessment of AChR knock-down flies.
(B) Trajectory (angular velocity) of T4/T5-specific nAChRα1 knock-down flies (R42F06-p65.AD; VT043070-Gal4.DBD>UAS-nAChRα1-RNAi, pale purple, flies n=20) while presented to a sequence of upward to rightward to downward to leftward OFF-edge motion compared to the parental control flies (UAS-nAChRα1-RNAi, grey n=21). The dark lines represent the mean ± SEM. See also Figure S3 and Figure S9.
(C-G) Same as in (B) for the nAChRα3 (pale magenta n=18, grey n=20), nAChRα4 (light magenta n=19, grey n=20), nAChRα5 (magenta n=18, grey n=21), nAChRα7 (dark magenta n=21, grey n=20), mAChR-B (cyan n=20, grey n=20) knock-down flies.

(H) Average angular velocity across OFF edges moving in sixteen directions of control UAS-nAChRα-RNAi (grey, 1 to 6), control T4/T5 driver (R42F06-p65.AD; VT043070-Gal4.DBD, grey n=20 A), control mCherry Valium 10 (black n=19, grey n=18 B), mCherry Valium 20 (black n=18, grey n=18 C), control Canton S (black n=15 D) and T4/T5-specific AChR knock-down flies (star). The normality of distribution was assessed with the use of Shapiro-Wilk test. *p<0.05, **p<0.01, ***p<0.001, ****p<0.0001. Data is mean ± SEM. Detailed statistical analysis is reported in Table S2.

Figure 5. Directional tuning of T5 cells post-AChR knock-down

(A) Schematic workflow representation for the two-photon calcium imaging in AChR knock-down T5 cells.

(B) Polar plot of the maximum responses (ΔF/F) across sixteen OFF edge directions (º) of T5c cells for mCherry Valium 20 control (black, flies n=7, ROIs N=85, shown as grey in C, D and E) and nAChRα4 RNAi (light magenta, n=7, N=61) conditions (R39H12-Gal4>UAS-AChR-RNAi, VT50384-LexA>LexAop-IVS-GCaMP6m). The dark lines represent the mean (68% CI). See also Figure S3 and Figure S10.

(C) Same as in (B) for nAChRα5 RNAi flies (magenta, n=7, N=82).

(D) Same as in (B) for nAChRα7 RNAi flies (dark magenta, n=7, N=60).

(E) Same as in (B) for mAChR-B RNAi flies (cyan, n=7, N=54).

(F) Directional tuning index (Ldir). Flies n=7. The normality of distribution was assessed with the use of Shapiro-Wilk test. *p<0.05, ***p<0.001. Data is mean ± SEM. Detailed statistical analysis is reported in Table S2.

STAR★Methods

EXPERIMENTAL MODEL AND SUBJECT DETAILS

Fly husbandry

All flies were raised on corneal agar medium under standard conditions (25°C, 60% humidity, 12h light/dark cycle). For the

interference experiments (RNAi), flies (control and RNAi) at early pupa stages were transferred from 25 to 29°C. For the MCFO experiments, flies at early pupa stages were heat-shocked for 30 minutes at 37°C. Detailed fly genotypes used per figure are reported in Table S1.

METHOD DETAILS

Generation of UAS-CRASP line

The pQUAST-syb-spCFP1-10 vector[75] and the pJFRC7-20XUAS-IVS-mCD8::GFP vector[114] were digested with XhoI and XbaI restriction enzymes and the syb-spCFP1-10 DNA fragment was extracted and T4-ligated in the pJFRC7 vector. The AGGCACACCGAAACGACTAA and CAGTTCCATAGGTTGGAATCTAAAA primers were used for sequencing the successful insertion of the DNA fragment. Embryo injections were performed by BestGene Inc (Chino Hills, CA, USA) in the VK00027 attp landing site.

RNAi experiments

To ensure high interference efficiency, given that both long dsRNA (nAChRα1, nAChRα4 and nAChRβ1, Valium 10) and short shRNA (nAChRα3, nAChRα5 and nAChRα7, mAChR-A, mAChR-B, Valium 20) were used, flies were raised (at early pupa stages) at 29°C[93,94] and the RNAi was induced prior to the receptor expression peak. Dicer was not used for the long dsRNA experiments as previous studies[22,115,116] showed positive AChR-RNAi induction without dicer co-expression. Our immunohistochemical screening spoke in favor of the nAChRα1, nAChRα3, nAChRα4, nAChRα5, nAChRα7 and mAChR-B RNAi effectiveness (Figure S3).

Thermogenetics

Flies expressing *shibire^{ts}* were raised in 25°, so that neuronal silencing is not induced prior to experiments. Activation of *shibire^{ts}* was achieved by the airflow temperature of 34 ± 0.1°C during the behavioral experiments.

Immunohistochemistry

Fly brains (aged 2-5 days, for G-and C-RASP experiments aged 10-12 days) were dissected in cold phosphate-buffered saline (PBS) and fixed in 4% paraformaldehyde (in PBS with 0.1% Triton X-100) for 24 minutes at room temperature, followed by three 10-minute washes in PBT (PBS and 0.3% Triton X-100). Brains were then incubated with primary antibodies in PBT for 48 hours at 4°C. After being incubated for 2 hours at room temperature, brains were washed four times for 15 minutes each in PBT and then incubated with secondary antibodies diluted in PBT for 48 hours at 4°C. After being incubated for 2 hours at room temperature and four 15 minutes PBT washes, brains were mounted for immediate sample viewing. For the subunit mapping (Figure 3), brains were blocked in 5% normal goat serum (NGS) in PBT for 1 hour at room temperature and then incubated with the primary and secondary antibodies for 24 hours instead of 48 hours.

Confocal microscopy

Images were acquired in a Leica Stellaris 5 laser scanning confocal microscope with a 20x glycerol 0.75 NA HC Plan-apochromat and 63x glycerol immersive 1.3 NA HC Plan-apochromat objective at 2048 x 2048 x 0.4µm image resolution. The deconvolution setting (Lightning) of this microscope was used for the acquisitions in Figure 3. Image analysis was performed with Fiji (ImageJ)[117]. For the acquisitions in Figure S4, a Leica SP8 laser scanning confocal microscope with a 63x oil

immersive 1.3 NA HCX Plan-apochromat objective was used at 2048 x 2048 x 0.4μm image resolution.

Behavior

To avoid behavioral effects introduced by sexual dimorphism[26], only female flies, 1-3 days old, were used in our experiments. Flies were attached to a pin post-cold anaesthetization with the use of light-curing glue and dental curing light (440 nm, New Woodpecker). Each locomotor recorder, out of the four that were simultaneously used, consisted of an air-suspended sphere (6mm in diameter and 40 mg weight) made of polyurethane foam and coated with polyurethane spray[89,118]. A constant airflow by a rotary vane pump (G6/01-K-EB9L Gardner Denver Thomas) allowed for the free rotation of the sphere on the ball-shaped sphere holder. The sphere's rotation was tracked by two optical tracking sensors, focusing two 1-mm^2 equatorial spots at ±30° from the center of the infrared LED-illuminated (JET-800-10, Roithner Electronics) sphere. Rotational data were tracked at 4 kHz and digitized at 200 Hz[119]. To achieve a successful fly positioning on the sphere, a camera (GRAS-20S4M-C, Point Grey Research) was used. A custom-made Peltier system (QC-127-1.4-6.0MS, Quick-Cool) controlled the airflow temperature at 34 ± 0.1°C, based on the readouts deriving from a thermometer placed just below the sphere, so as to ensure prolonged walking. A U-shaped visual arena comprising of three 120-Hz LCD screens (Samsung 2233 RZ) (reaching a maximum luminance of 131 cd m^{-2}), allowed for the presentation of visual stimuli spanning approximately 270° in azimuth and 120° in elevation of the fly's visual field at a resolution of <0.1°. Panda3D was used in Python v.2.7 for the visual stimulus generation[89].

Two-photon microscopy

For functional imaging experiments, we used a custom-build two photon laser scanning microscope equipped with a 40x water

0.80 NA IR-Achroplan objective (Zeiss)[31]. Flies (1-3 days) were cold-anaesthetized and the legs and thorax were glued on a Plexiglas holder with the use of light-curing glue. The head was bend down, fitted in an aluminum opening and the holder was clamped in a recording chamber. Saline solution (PBS; 137 mM NaCl, 3 mM KCl, 8 mM Na_2HPO_4, 1.5 mM KH_2PO_4, pH 7.3) was introduced and the posterior side of the fly's optic lobe was exposed by a small incision of the head. Muscles, adipose tissue and trachea were manually removed. Images were acquired at a 64 x 64-pixel resolution and a frame rate of 15 Hz in Matlab R2013b (MathWorks) using ScanImage 3.8 software (Vidrio Technologies, LLC).

Visual stimulation

For the behavioral experiments, OFF edges (50% contrast) moved at 16 evenly spaced directions with a velocity of 60° s^{-1}, were randomized and crossed the whole arena span within 5s. Each experiment lasted for ~55 min, including 35 trials of OFF edges, of which the first 15 trials were excluded from analysis, as they were appointed to temperature stabilization and fly accommodation. The same inclusion criteria as in a previous study[42] were used.

For the calcium imaging experiments, we used a custom-built projector-based arena[55], where two micro-projectors (TI DLP Lightcrafter 3000) projected visual stimuli, with a refresh rate of 180 Hz and maximum luminance of 276 ± 48 cd/m^2, onto the back of a cylindrical screen. The arena covered 180° in azimuth and 105° in elevation of the fly's visual field. OFF edges (92% contrast) moved at 16 evenly spaced directions with a velocity of 30° s^{-1}, were randomized and repeated four times.

Trans-synaptic alignment

To assess the trans-synaptic alignment between the receptors and the synapses of interest, we calculated the fluorescence intensity values (later normalized to the maximum pixel intensity value) in a 1 μm line positioned across the synapse punctum in a single z plane using Fiji-ImageJ[117]. Data analysis was performed with Python v.3.9.18 with the use of seaborn 0.12.2, pandas 1.5.3 and numpy 1.23.3.

EM analysis

For the Tm-T5 wiring, we used the FAFB volume[65] via the FlyWire (flywire.ai) proofreading environment[66,67] and chose five reconstructed T5a and five T5c neurons from the right optic lobe (Table S3). T5 and Tm1, Tm2, Tm4, Tm9 identities were verified by users' annotations and by comparison with previous electron microscopy[37] and our light microscopy reconstructions. Synapse number Buhmann predictions[86,87] between the T5 neuron of interest and its respective input neurons were acquired from FlyWire's connectivity viewer. Cleft score was set to 50, so as to eliminate synaptic redundancy resulting from the combination of synaptic connections between the same neurons when their presynaptic locations are within 100nm^2. For each synapse, we sought four morphological markers: a. synaptic vesicles, b. the protein dense T-bar structure, c. synaptic cleft, and d. postsynaptic densities (or postsynaptic domains). Every synaptic locus was assessed in a volume of five up to seven brain slices, 40nm each. Only synapses that displayed all four morphological markers were included in our dataset. We treated proofread synapses as points in T5 dendrite space by collecting the x,y,z coordinates of each T-bar (presynapse). FlyWire predictions correspond to postsynaptic densities (eg. one T-bar to three postsynaptic densities, synapse prediction=3), while in the same example our proofread synapse number would be 1. Hence, our proofread synapse counts are bound to be lower compared to

the predicted synapse counts. Synapse numbers in this study correspond to manually proofread synapses.

For synapse distributions across the anterior-posterior and dorso-ventral dendritic arborization axis (Figure 3C,D), we measured the Euclidean distance of every synapse from the root (first branching point) of the dendrite. Distances in µm were calculated by multiplying the y and z coordinates of each T-bar with 4 and 40 accordingly (voxel=4x4x40nm). To correct for anterior-posterior and dorsal-ventral dendrite length differences, we normalized each synapse-to-root Euclidean distance to the longest T5a and T5c dendrite.

For the identification of Tm1, Tm2, Tm4 and Tm9 synaptic partners in LO1 (Figure S8), we used Codex[65,66,67]. We searched for all the Tm output neurons in five Tm1 (FlyWire ID: 720575940620976493,720575940608883465,720575940623583428, 720575940632600647,720575940621146733), Tm2 (FlyWire ID: 720575940632142904,720575940640453437,720575940640230259,720575940630551670,720575940622364961), Tm4 (FlyWire ID: 720575940637976666, 720575940620745163, 720575940621582401, 720575940626612228, 720575940620782171) and Tm9 (FlyWire ID: 720575940613374873, 720575940620814356, 720575940609254851, 720575940626242348, 720575940623771061) cells, and selected only those outputs whose Tm synapses were restricted in LO1 (excluding all Tm medullary output neurons). For the output neurons that only formed connections with Tm neurons in LO1, we used the predicted synapse number, but for those output neurons that made Tm connections in other LO layers as well, we manually proofread the LO1 synapses. The reconstructed neurons for Figure S5 correspond to FlyWire IDs 720575940621338038, 720575940614527742, 720575940623

16041926 and 720575940616813142 for Tm1, Tm2, Tm4 and Tm9 respectively.

QUANTIFICATION AND STATISTICAL ANALYSIS

nAChRα density

Receptor puncta that localized in T5 dendrites were quantified along 8µm x 8µm x 4µm voxels in Fiji-ImageJ[117]. The total number of puncta divided to the analyzed LO1 volume resulted in the nAChRα density.

Synapse occupancy

The total number of Brp-receptor co-localizing puncta in voxels of 8µm x 8µm x 4µm in Fiji-ImageJ[117] was counted via the *Cell counter* plugin and was divided to the number of Brp puncta, resulting in the synapse occupancy index.

nAChR co-localization

The total number of nAChR co-localizing puncta in voxels of 8µm x 8µm x 4µm in Fiji-ImageJ[117] was counted via the *Cell counter* plugin and was divided to total number of nAChR puncta, resulting in the co-localization index.

RNAi efficiency

The mean grey value of ten 8µm x 8µm ROIs per optic lobe in LO1 and LOP (layer 1 and 2) was measured via Fiji-ImageJ[117] and was normalized by subtracting the mean grey value of one 8µm x 8µm ROI in the inner optic chiasm.

Brp counts in LO1

The total number of Brp puncta in LO1 voxels of 8µm x 8µm x 4µm was counted via the *Cell counter* plugin in Fiji-ImageJ[117] (Figure S3K).

Behavior

The optomotor response was quantified as the absolute average angular velocity during 5 s of edge motion in each direction. Data analysis was performed with Python v.3.9.18 using seaborn 0.12.2, pandas 1.5.3 and numpy 1.23.3.

Calcium imaging

Calcium imaging data were analyzed as described in[55] with a custom written software in Python v.2.7. ROIs were drawn manually across LO layer 1 and LOP layer 3. Only ROIs that repeatedly responded to the given visual stimulus and exhibited consistent-across the four repetitions-responses, were included in the dataset. For each ROI, the time courses of relative fluorescence changes (ΔF/F) were calculated and responses to stimulus were baseline-subtracted and averaged over repetitions. Maximum responses were aligned to 90°. The directional tuning index (Figure 5F, Ldir) was calculated as the magnitude of the resultant vector divided by the sum of the individual vectors' magnitudes:

$$Ldir = \left| \frac{\sum_{\varphi} \overrightarrow{v(\varphi)}}{\sum_{\varphi} \overrightarrow{|v(\varphi)|}} \right|$$

Statistical analysis

Detailed analysis is reported in figure legends and Table S2 and was performed in GraphPad Prism v.9.3.0.

SUPPLEMENTAL INFORMATION

Document S1. Figures S1–S10, Table S3 and supplemental references

Table S1. List of fly experimental genotypes, related to STAR Methods

Table S2. Statistical analysis, related to STAR Methods

REFERENCES

1. Shin, M., Copeland, J.M., and Venton, B.J. (2018). *Drosophila* as a model system for neurotransmitter measurements. ACS Chem. Neurosci. *9*, 1872–1883. https://doi.org/10.1021/acschemneuro.7b00456.
2. Stuart, A.E. (1999). From fruit flies to barnacles, histamine is the neurotransmitter of arthropod photoreceptors. Neuron *22*, 431–433. https://doi.org/10.1016/S089 6-6273(00)80699-6.
3. Kolodziejczyk, A., Sun, X., Meinertzhagen, I.A., and Nässel, D.R. (2008). Glutamate, GABA and acetylcholine signaling components in the lamina of the *Drosophila* visual system. PLoS ONE *3*, e2110. https://doi.org/10.1371/journal .pone.0002110.
4. Yasuyama, K., and Salvaterra, P.M. (1999). Localization of choline acetyltransferase-expressing neurons in *Drosophila* nervous system. Microsc Res Tech *45*, 65–79. https://doi.org/10.1002/(SICI)1097-0029(19990415)45:2<65::AID-JEMT2>3.0.CO;2-0.
5. Eckstein, N., Bates, A.S., Champion, A., Du, M., Yin, Y., Schlegel, P., Lu, A.K.-Y., Rymer, T., Finley-May, S., Paterson, T., et al. (2024). Neurotransmitter classification from electron microscopy images at synaptic sites in

Drosophila melanogaster. Cell *187*, 2574-2594.e23. https://doi.org/10.1016/j.cell.2024. 03.016.

6. Breer, H., and Sattelle, D.B. (1987). Molecular properties and functions of insect acetylcholine receptors. Journal of Insect Physiology *33*, 771–790. https://doi.org/10.1016/0022-1910(87)90025-4.

7. Sattelle, D.B., Jones, A.K., Sattelle, B.M., Matsuda, K., Reenan, R., and Biggin, P.C. (2005). Edit, cut and paste in the nicotinic acetylcholine receptor gene family of *Drosophila melanogaster*. Bioessays *27*, 366–376. https://doi.org/10.1002/ bies.20207.

8. Rosenthal, J.S., and Yuan, Q. (2021). Constructing and tuning excitatory cholinergic synapses: The multifaceted functions of nicotinic acetylcholine receptors in *Drosophila* neural development and physiology. Front. Cell. Neurosci. *15*, 720560. https://doi.org/10.3389/fncel.2021.720560.

9. Thany, S.H., Lenaers, G., Raymond-Delpech, V., Sattelle, D.B., and Lapied, B. (2007). Exploring the pharmacological properties of insect nicotinic acetylcholine receptors. Trends Pharmacol Sci *28*, 14–22. https://doi.org/10.1016/j.tips. 2006.11.006.

10. Faltine-Gonzalez, D.Z., and Layden, M.J. (2018). The origin and evolution of acetylcholine signaling through AchRs in metazoans. Preprint,

https://doi.org/10.1101/424804

https://doi.org/10.1101/424804.

11. Littleton, J.T., and Ganetzky, B. (2000). Ion channels and synaptic organization: analysis of the *Drosophila* genome. Neuron *26*, 35–43. https://doi.org/ 10.1016/s0896-6273(00)81135-6.

12. Thompson, A.J., Lester, H.A., and Lummis, S.C.R. (2010). The structural basis of function in Cys-loop receptors. Quart. Rev. Biophys. *43*, 449–499. https://doi.org/10.1017/S0033583510000168.

13. Dupuis, J., Louis, T., Gauthier, M., and Raymond, V. (2012). Insights from honeybee (*Apis mellifera*) and fly (*Drosophila melanogaster*) nicotinic acetylcholine receptors: From genes to behavioral functions. Neuroscience & Biobehavioral Reviews *36*, 1553–1564. https://doi.org/10.1016/j.neubiorev. 2012.04.003.

14. Bielopolski, N., Amin, H., Apostolopoulou, A.A., Rozenfeld, E., Lerner, H., Huetteroth, W., Lin, A.C., and Parnas, M. (2019). Inhibitory muscarinic acetylcholine receptors enhance aversive olfactory learning in adult *Drosophila*. eLife *8*, e48264. https://doi.org/10.7554/eLife.48264.

15. Malloy, C.A., Somasundaram, E., Omar, A., Bhutto, U., Medley, M., Dzubuk, N., and Cooper, R.L. (2019). Pharmacological identification of cholinergic receptor

subtypes: modulation of locomotion and neural circuit excitability in *Drosophila* larvae. Neuroscience *411*, 47–64. https://doi.org/10.1016/j.neuroscience. 2019.05.016.

16. Xia, R. -Y., Li, M. -Q., Wu, Y. -S., Qi, Y. -X., Ye, G. -Y., and Huang, J. (2016). A new family of insect muscarinic acetylcholine receptors. Insect Molecular Biology *25*, 362–369. https://doi.org/10.1111/imb.12229.

17. Collin, C., Hauser, F., De Valdivia, E.G., Li, S., Reisenberger, J., Carlsen, E.M.M., Khan, Z., Hansen, N.Ø., Puhm, F., Søndergaard, L., et al. (2013). Two types of muscarinic acetylcholine receptors in *Drosophila* and other arthropods. Cell. Mol. Life Sci. *70*, 3231–3242. https://doi.org/10.1007/s00018-013-1334-0.

18. Ren, G.R., Folke, J., Hauser, F., Li, S., and Grimmelikhuijzen, C.J.P. (2015). The A- and B-type muscarinic acetylcholine receptors from *Drosophila melanogaster* couple to different second messenger pathways. Biochemical and Biophysical Research Communications *462*, 358–364. https://doi.org/10.1016/j.bbrc. 2015.04.141.

19. Perry, T., Chen, W., Ghazali, R., Yang, Y.T., Christesen, D., Martelli, F., Lumb, C., Bao Luong, H.N., Mitchell, J., Holien, J.K., et al. (2021). Role of nicotinic acetylcholine receptor subunits in the mode of action of neonicotinoid, sulfoximine and spinosyn insecticides in *Drosophila*

melanogaster. Insect Biochem Mol Biol *131*, 103547. https://doi.org/10.1016/j.ibmb.2021.103547.

20. Rozenfeld, E., Tauber, M., Ben-Chaim, Y., and Parnas, M. (2021). GPCR voltage dependence controls neuronal plasticity and behavior. Nat Commun *12*, 7252. https://doi.org/10.1038/s41467-021-27593-x.

21. Manoim, J.E., Davidson, A.M., Weiss, S., Hige, T., and Parnas, M. (2022). Lateral axonal modulation is required for stimulus-specific olfactory conditioning in Drosophila. Curr Biol *32*, 4438-4450.e5. https://doi.org/10.1016/j.cub.2022. 09.007.

22. Pribbenow, C., Chen, Y., Heim, M.-M., Laber, D., Reubold, S., Reynolds, E., Balles, I., Fernández-d V Alquicira, T., Suárez-Grimalt, R., Scheunemann, L., et al. (2022). Postsynaptic plasticity of cholinergic synapses underlies the induction and expression of appetitive and familiarity memories in *Drosophila*. eLife *11*, e80445. https://doi.org/10.7554/eLife.80445.

23. Qin, B., Humberg, T.-H., Kim, A., Kim, H.S., Short, J., Diao, F., White, B.H., Sprecher, S.G., and Yuan, Q. (2019). Muscarinic acetylcholine receptor signaling generates OFF selectivity in a simple visual circuit. Nat Commun *10*, 4093. https://doi.org/10.1038/s41467-019-12104-w.

24. Schlegel, P., Yin, Y., Bates, A.S., Dorkenwald, S., Eichler, K., Brooks, P., Han, D.S., Gkantia, M., Dos Santos, M., Munnelly, E.J., et al. (2024). Whole-brain annotation and multi-connectome cell typing of *Drosophila*. Nature *634*, 139–152. https://doi.org/10.1038/s41586-024-07686-5.

25. Borst, A., and Euler, T. (2011). Seeing things in motion: Models, circuits, and mechanisms. Neuron *71*, 974–994. https://doi.org/10.1016/j.neuron.2011. 08.031.

26. Surkova, S., Görne, J., Nuzhdin, S., and Samsonova, M. (2021). Interplay between sex determination cascade and major signaling pathways during *Drosophila* eye development: Perspectives for future research. Developmental Biology *476*, 41–52. https://doi.org/10.1016/j.ydbio.2021.03.005.

27. Behnia, R., and Desplan, C. (2015). Visual circuits in flies: beginning to see the whole picture. Curr Opin Neurobiol *34*, 125–132. https://doi.org/10.1016/j.conb. 2015.03.010.

28. Joesch, M., Schnell, B., Raghu, S.V., Reiff, D.F., and Borst, A. (2010). ON and OFF pathways in *Drosophila* motion vision. Nature *468*, 300–304. https://doi.org/10.1038/nature09545.

29. Strother, J.A., Nern, A., and Reiser, M.B. (2014). Direct observation of ON and OFF pathways in the *Drosophila* visual system. Current Biology *24*, 976–983. https://doi.org/10.1016/j.cub.2014.03.017.

30. Fisher, Y.E., Silies, M., and Clandinin, T.R. (2015). Orientation selectivity sharpens motion detection in *Drosophila*. Neuron *88*, 390–402. https://doi.org/10.1016/j.neuron.2015.09.033.

31. Maisak, M.S., Haag, J., Ammer, G., Serbe, E., Meier, M., Leonhardt, A., Schilling, T., Bahl, A., Rubin, G.M., Nern, A., et al. (2013). A directional tuning map of *Drosophila* elementary motion detectors. Nature *500*, 212–216. https://doi.org/10.1038/nature12320.

32. Fischbach, K.-F., and Dittrich, A.P.M. (1989). The optic lobe of *Drosophila melanogaster*. I. A Golgi analysis of wild-type structure. Cell Tissue Res. *258*. https://doi.org/10.1007/BF00218858.

33. Pinto-Teixeira, F., Koo, C., Rossi, A.M., Neriec, N., Bertet, C., Li, X., Del-Valle-Rodriguez, A., and Desplan, C. (2018). Development of concurrent retinotopic maps in the fly motion detection circuit. Cell *173*, 485-498.e11. https://doi.org/10.1016/j.cell.2018.02.053.

34. Apitz, H., and Salecker, I. (2018). Spatio-temporal relays control layer identity of direction-selective neuron subtypes in *Drosophila*. Nat Commun *9*, 2295. https://doi.org/10.1038/s41467-018-04592-z.

35. Takemura, S.-Y., Nern, A., Chklovskii, D.B., Scheffer, L.K., Rubin, G.M., and Meinertzhagen, I.A. (2017). The comprehensive connectome of a neural substrate for “ON”

motion detection in *Drosophila*. Elife *6*, e24394. https://doi.org/10.7554/eLife.24394.

36. Shinomiya, K., Takemura, S., Rivlin, P.K., Plaza, S.M., Scheffer, L.K., and Meinertzhagen, I.A. (2015). A common evolutionary origin for the ON- and OFF-edge motion detection pathways of the *Drosophila* visual system. Front. Neural Circuits *9*. https://doi.org/10.3389/fncir.2015.00033.

37. Shinomiya, K., Huang, G., Lu, Z., Parag, T., Xu, C.S., Aniceto, R., Ansari, N., Cheatham, N., Lauchie, S., Neace, E., et al. (2019). Comparisons between the ON- and OFF-edge motion pathways in the *Drosophila* brain. eLife *8*, e40025. https://doi.org/10.7554/eLife.40025.

38. Takemura, S., Bharioke, A., Lu, Z., Nern, A., Vitaladevuni, S., Rivlin, P.K., Katz, W.T., Olbris, D.J., Plaza, S.M., Winston, P., et al. (2013). A visual motion detection circuit suggested by *Drosophila* connectomics. Nature *500*, 175–181. https://doi.org/10.1038/nature12450.

39. Meier, M., and Borst, A. (2019). Extreme compartmentalization in a *Drosophila* amacrine cell. Current Biology *29*, 1545-1550.e2. https://doi.org/10.1016/j.cub. 2019.03.070.

40. Davis, F.P., Nern, A., Picard, S., Reiser, M.B., Rubin, G.M., Eddy, S.R., and Henry, G.L. (2020). A genetic, genomic, and computational resource for exploring neural

circuit function. eLife *9*, e50901. https://doi.org/10.7554/eLife.50901.

41. Behnia, R., Clark, D.A., Carter, A.G., Clandinin, T.R., and Desplan, C. (2014). Processing properties of ON and OFF pathways for *Drosophila* motion detection. Nature *512*, 427–430. https://doi.org/10.1038/nature13427.

42. Groschner, L.N., Malis, J.G., Zuidinga, B., and Borst, A. (2022). A biophysical account of multiplication by a single neuron. Nature *603*, 119–123. https://doi.org/10.1038/s41586-022-04428-3.

43. Ammer, G., Leonhardt, A., Bahl, A., Dickson, B.J., and Borst, A. (2015). Functional specialization of neural input elements to the *Drosophila* ON motion detector. Current Biology *25*, 2247–2253. https://doi.org/10.1016/j.cub.2015.07.014.

44. Takemura, S., Karuppudurai, T., Ting, C.-Y., Lu, Z., Lee, C.-H., and Meinertzhagen, I.A. (2011). Cholinergic circuits integrate neighboring visual signals in a *Drosophila* motion detection pathway. Curr Biol *21*, 2077–2084. https://doi.org/10.1016/j.cub.2011.10.053.

45. Serbe, E., Meier, M., Leonhardt, A., and Borst, A. (2016). Comprehensive characterization of the major presynaptic elements to the *Drosophila* OFF motion detector. Neuron *89*, 829–841. https://doi.org/10.1016/j.neuron.2016.01.006.

46. Meier, M., Serbe, E., Maisak, M.S., Haag, J., Dickson, B.J., and Borst, A. (2014). Neural circuit components of the *Drosophila* OFF motion vision pathway. Current Biology *24*, 385–392. https://doi.org/10.1016/j.cub.2014.01.006.

47. Shinomiya, K., Karuppudurai, T., Lin, T.-Y., Lu, Z., Lee, C.-H., and Meinertzhagen, I.A. (2014). Candidate neural substrates for OFF-edge motion detection in *Drosophila*. Current Biology *24*, 1062–1070. https://doi.org/10.1016/j.cub.2 014.03.051.

48. Braun, A., Borst, A., and Meier, M. (2023). Disynaptic inhibition shapes tuning of OFF-motion detectors in *Drosophila*. Curr Biol *33*, 2260-2269.e4. https://doi.org/ 10.1016/j.cub.2023.05.007.

49. Ramos-Traslosheros, G., and Silies, M. (2021). The physiological basis for contrast opponency in motion computation in *Drosophila*. Nat Commun *12*, 4987. https://doi.org/10.1038/s41467-021-24986-w.

50. Borst, A. (2018). A biophysical mechanism for preferred direction enhancement in fly motion vision. PLoS Comput Biol *14*, e1006240. https://doi.org/10.1371/j ournal.pcbi.1006240.

51. Haag, J., Arenz, A., Serbe, E., Gabbiani, F., and Borst, A. (2016). Complementary mechanisms create direction

selectivity in the fly. eLife *5*, e17421. https://doi.org/10.7554/eLife.17421.

52. Haag, J., Mishra, A., and Borst, A. (2017). A common directional tuning mechanism of *Drosophila* motion-sensing neurons in the ON and in the OFF pathway. eLife *6*, e29044. https://doi.org/10.7554/eLife.29044.

53. Leong, J.C.S., Esch, J.J., Poole, B., Ganguli, S., and Clandinin, T.R. (2016). Direction selectivity in *Drosophila* emerges from preferred-direction enhancement and null-direction suppression. Journal of Neuroscience *36*, 8078–8092. https://doi.org/10.1523/JNEUROSCI.1272-16.2016.

54. Gruntman, E., Romani, S., and Reiser, M.B. (2018). Simple integration of fast excitation and offset, delayed inhibition computes directional selectivity in *Drosophila*. Nat Neurosci *21*, 250–257. https://doi.org/10.1038/s41593-017-0046-4.

55. Arenz, A., Drews, M.S., Richter, F.G., Ammer, G., and Borst, A. (2017). The temporal tuning of the *Drosophila* motion detectors is determined by the dynamics of their input elements. Current Biology *27*, 929–944. https://doi.org/ 10.1016/j.cub.2017.01.051.

56. Hoermann, N., Schilling, T., Haji Ali, A., Serbe, E., Mayer, C., Borst, A., and Pujol-Martí, J. (2020). A combinatorial code of transcription factors specifies subtypes of visual

motion-sensing neurons in *Drosophila*. Development, dev.186296. https://doi.org/10.1242/dev.186296.

57. Özel, M.N., Simon, F., Jafari, S., Holguera, I., Chen, Y.-C., Benhra, N., El-Danaf, R.N., Kapuralin, K., Malin, J.A., Konstantinides, N., et al. (2021). Neuronal diversity and convergence in a visual system developmental atlas. Nature *589*, 88–95. https://doi.org/10.1038/s41586-020-2879-3.

58. Sanfilippo, P., Kim, A.J., Bhukel, A., Yoo, J., Mirshahidi, P.S., Pandey, V., Bevir, H., Yuen, A., Mirshahidi, P.S., Guo, P., et al. (2024). Mapping of multiple neurotransmitter receptor subtypes and distinct protein complexes to the connectome. Neuron *112*, 942-958.e13. https://doi.org/10.1016/j.neuron.2023. 12.014.

59. Fayyazuddin, A., Zaheer, M.A., Hiesinger, P.R., and Bellen, H.J. (2006). The nicotinic acetylcholine receptor Dα7 is required for an escape behavior in *Drosophila*. PLoS Biol *4*, e63. https://doi.org/10.1371/journal.pbio.0040063.

60. Mauss, A.S., and Borst, A. (2020). Optic flow-based course control in insects. Current Opinion in Neurobiology *60*, 21–27. https://doi.org/10.1016/j.conb. 2019.10.007.

61. Götz, K.G. (1968). Flight control in *Drosophila* by visual perception of motion. Kybernetik *4*, 199–208. https://doi.org/10.1007/BF00272517.

62. Ryu, L., Kim, S.Y., and Kim, A.J. (2022). From photons to behaviors: Neural implementations of visual behaviors in *Drosophila*. Front. Neurosci. *16*, 883640. https://doi.org/10.3389/fnins.2022.883640.

63. Kondo, S., Takahashi, T., Yamagata, N., Imanishi, Y., Katow, H., Hiramatsu, S., Lynn, K., Abe, A., Kumaraswamy, A., and Tanimoto, H. (2020). Neurochemical organization of the *Drosophila* brain visualized by endogenously tagged neurotransmitter receptors. Cell Reports *30*, 284-297.e5. https://doi.org/10.1016/j.celrep.2019.12.018.

64. Davie, K., Janssens, J., Koldere, D., De Waegeneer, M., Pech, U., Kreft, Ł., Aibar, S., Makhzami, S., Christiaens, V., Bravo González-Blas, C., et al. (2018). A single-cell transcriptome atlas of the aging *Drosophila* brain. Cell *174*, 982-998.e20. https://doi.org/10.1016/j.cell.2018.05.057.

65. Zheng, Z., Lauritzen, J.S., Perlman, E., Robinson, C.G., Nichols, M., Milkie, D., Torrens, O., Price, J., Fisher, C.B., Sharifi, N., et al. (2018). A complete electron microscopy volume of the brain of adult *Drosophila melanogaster*. Cell *174*, 730-743.e22. https://doi.org/10.1016/j.cell.2018.06.019.

66. Dorkenwald, S., McKellar, C.E., Macrina, T., Kemnitz, N., Lee, K., Lu, R., Wu, J., Popovych, S., Mitchell, E.,

Nehoran, B., et al. (2022). FlyWire: online community for whole-brain connectomics. Nat Methods *19*, 119–128. https://doi.org/10.1038 /s41592-021-01330-0.

67. Dorkenwald, S., Matsliah, A., Sterling, A.R., Schlegel, P., Yu, S., McKellar, C.E., Lin, A., Costa, M., Eichler, K., Yin, Y., et al. (2024). Neuronal wiring diagram of an adult brain. Nature *634*, 124–138. https://doi.org/10.1038/s41586-024-07558-y.

68. Jenett, A., Rubin, G.M., Ngo, T.-T.B., Shepherd, D., Murphy, C., Dionne, H., Pfeiffer, B.D., Cavallaro, A., Hall, D., Jeter, J., et al. (2012). A GAL4-driver line resource for *Drosophila* neurobiology. Cell Reports *2*, 991–1001. https://doi.org /10.1016/j.celrep.2012.09.011.

69. Tirian, L., and Dickson, B.J. (2017). The VT GAL4, LexA, and split-GAL4 driver line collections for targeted expression in the *Drosophila* nervous system. Preprint, https://doi.org/10.1101/198648 https://doi.org/10.1101/198648.

70. Nern, A., Pfeiffer, B.D., and Rubin, G.M. (2015). Optimized tools for multicolor stochastic labeling reveal diverse stereotyped cell arrangements in the fly visual system. Proc Natl Acad Sci USA *112*, E2967–E2976. https://doi.org/ 10.1073/pnas.1506763112.

71. Meissner, G.W., Nern, A., Dorman, Z., DePasquale, G.M., Forster, K., Gibney, T., Hausenfluck, J.H., He, Y., Iyer,

N.A., Jeter, J., et al. (2023). A searchable image resource of *Drosophila* GAL4 driver expression patterns with single neuron resolution. eLife *12*, e80660. https://doi.org/10.7554/eLife.80660.

72. Diegelmann, S., Bate, M., and Landgraf, M. (2008). Gateway cloning vectors for the LexA-based binary expression system in *Drosophila*. Fly *2*, 236–239. https://doi.org/10.4161/fly.6817.

73. Feinberg, E.H., VanHoven, M.K., Bendesky, A., Wang, G., Fetter, R.D., Shen, K., and Bargmann, C.I. (2008). GFP reconstitution across synaptic partners (GRASP) defines cell contacts and synapses in living nervous systems. Neuron *57*, 353–363. https://doi.org/10.1016/j.neuron.2007.11.030.

74. Shearin, H.K., Quinn, C.D., Mackin, R.D., Macdonald, I.S., and Stowers, R.S. (2018). t-GRASP, a targeted GRASP for assessing neuronal connectivity. Journal of Neuroscience Methods *306*, 94–102. https://doi.org/10.1016/j.jneumeth. 2018.05.014.

75. Macpherson, L.J., Zaharieva, E.E., Kearney, P.J., Alpert, M.H., Lin, T.-Y., Turan, Z., Lee, C.-H., and Gallio, M. (2015). Dynamic labelling of neural connections in multiple colours by trans-synaptic fluorescence complementation. Nat Commun *6*, 10024. https://doi.org/10.1038/ncomms10024.

76. Schmid, A., Hallermann, S., Kittel, R.J., Khorramshahi, O., Frölich, A.M.J., Quentin, C., Rasse, T.M., Mertel, S., Heckmann, M., and Sigrist, S.J. (2008). Activity-dependent site-specific changes of glutamate receptor composition in vivo. Nat Neurosci *11*, 659–666. https://doi.org/10.1038/nn.2122.

77. Christiansen, F., Zube, C., Andlauer, T.F.M., Wichmann, C., Fouquet, W., Owald, D., Mertel, S., Leiss, F., Tavosanis, G., Farca Luna, A.J., et al. (2011). Presynapses in Kenyon cell dendrites in the mushroom body calyx of *Drosophila*. Journal of Neuroscience *31*, 9696–9707. https://doi.org/10.1523/JNEUROSCI. 6542-10.2011.

78. Wagh, D.A., Rasse, T.M., Asan, E., Hofbauer, A., Schwenkert, I., Dürrbeck, H., Buchner, S., Dabauvalle, M.-C., Schmidt, M., Qin, G., et al. (2006). Bruchpilot, a protein with homology to ELKS/CAST, is required for structural integrity and function of synaptic active zones in *Drosophila*. Neuron *49*, 833–844. https://doi.org/10.1016/j.neuron.2006.02.008.

79. Mosca, T.J., and Luo, L. (2014). Synaptic organization of the *Drosophila* antennal lobe and its regulation by the Teneurins. Elife *3*, e03726. https://doi.org/10.7554 /eLife.03726.

80. Prokop, A., and Meinertzhagen, I.A. (2006). Development and structure of synaptic contacts in *Drosophila*. Seminars in Cell & Developmental Biology *17*, 20–30. https://doi.org/10.1016/j.semcdb.2005.11.010.

81. Kremer, M.C., Christiansen, F., Leiss, F., Paehler, M., Knapek, S., Andlauer, T.F.M., Förstner, F., Kloppenburg, P., Sigrist, S.J., and Tavosanis, G. (2010). Structural long-term changes at mushroom body input synapses. Current Biology *20*, 1938–1944. https://doi.org/10.1016/j.cub.2010.09.060.

82. Berger-Müller, S., Sugie, A., Takahashi, F., Tavosanis, G., Hakeda-Suzuki, S., and Suzuki, T. (2013). Assessing the role of cell-surface molecules in central synaptogenesis in the *Drosophila* visual system. PLoS ONE *8*, e83732. https://doi.org/10.1371/journal.pone.0083732.

83. Owald, D., Fouquet, W., Schmidt, M., Wichmann, C., Mertel, S., Depner, H., Christiansen, F., Zube, C., Quentin, C., Körner, J., et al. (2010). A Syd-1 homologue regulates pre- and postsynaptic maturation in *Drosophila*. Journal of Cell Biology *188*, 565–579. https://doi.org/10.1083/jcb.200908055.

84. Fulterer, A., Andlauer, T.F.M., Ender, A., Maglione, M., Eyring, K., Woitkuhn, J., Lehmann, M., Matkovic-Rachid, T., Geiger, J.R.P., Walter, A.M., et al. (2018). Active zone scaffold protein ratios tune functional diversity across

brain synapses. Cell Reports *23*, 1259–1274. https://doi.org/10.1016/j.celrep.2018.03.126.

85. Fendl, S., Vieira, R.M., and Borst, A. (2020). Conditional protein tagging methods reveal highly specific subcellular distribution of ion channels in motion-sensing neurons. eLife *9*, e62953. https://doi.org/10.7554/eLife.62953.

86. Buhmann, J., Sheridan, A., Malin-Mayor, C., Schlegel, P., Gerhard, S., Kazimiers, T., Krause, R., Nguyen, T.M., Heinrich, L., Lee, W.-C.A., et al. (2021). Automatic detection of synaptic partners in a whole-brain *Drosophila* electron microscopy data set. Nat Methods *18*, 771–774. https://doi.org/10.1038/s41592-021-01183-7.

87. Heinrich, L., Funke, J., Pape, C., Nunez-Iglesias, J., and Saalfeld, S. (2018). Synaptic cleft segmentation in non-isotropic volume electron microscopy of the complete *Drosophila* brain. Preprint at arXiv, https://doi.org/10.48550/ARXIV .1805.02718.

88. Leonte, M.-B., Leonhardt, A., Borst, A., and Mauss, A.S. (2021). Aerial course stabilization is impaired in motion-blind flies. Journal of Experimental Biology *224*, jeb242219. https://doi.org/10.1242/jeb.242219.

89. Bahl, A., Ammer, G., Schilling, T., and Borst, A. (2013). Object tracking in motion-blind flies. Nat Neurosci *16*, 730–738. https://doi.org/10.1038/nn.3386.

90. Schnell, B., Raghu, S.V., Nern, A., and Borst, A. (2012). Columnar cells necessary for motion responses of wide-field visual interneurons in *Drosophila*. J Comp Physiol A *198*, 389–395. https://doi.org/10.1007/s00359-012-0716-3.

91. Schilling, T., and Borst, A. (2015). Local motion detectors are required for the computation of expansion flow-fields. Biology Open *4*, 1105–1108. https://doi.org/10.1242/bio.012690.

92. Schilling, T., Ali, A.H., Leonhardt, A., Borst, A., and Pujol-Martí, J. (2019). Transcriptional control of morphological properties of direction-selective T4/T5 neurons in *Drosophila*. Development, dev.169763. https://doi.org/10.1242/dev. 169763.

93. Ni, J.-Q., Liu, L.-P., Binari, R., Hardy, R., Shim, H.-S., Cavallaro, A., Booker, M., Pfeiffer, B.D., Markstein, M., Wang, H., et al. (2009). A *Drosophila* resource of transgenic RNAi lines for neurogenetics. Genetics *182*, 1089–1100. https://doi.org/10.1534/genetics.109.103630.

94. Ni, J.-Q., Zhou, R., Czech, B., Liu, L.-P., Holderbaum, L., Yang-Zhou, D., Shim, H.-S., Tao, R., Handler, D., Karpowicz, P., et al. (2011). A genome-scale shRNA resource for transgenic RNAi in *Drosophila*. Nat Methods *8*, 405–407. https://doi.org/10.1038/nmeth.1592.

95. Raghu, S.V., Joesch, M., Sigrist, S.J., Borst, A., and Reiff, D.F. (2009). Synaptic organization of lobula plate tangential cells in *Drosophila:* Dα7 cholinergic receptors. Journal of Neurogenetics *23*, 200–209. https://doi.org/10.1080 /01677060802471684.

96. Komori, Y., Takayama, K., Okamoto, N., Kamiya, M., Koizumi, W., Ihara, M., Misawa, D., Kamiya, K., Yoshinari, Y., Seike, K., et al. (2023). Functional impact of subunit composition and compensation on *Drosophila melanogaster* nicotinic receptors-targets of neonicotinoids. PLoS Genet *19*, e1010522. https://doi.org /10.1371/journal.pgen.1010522.

97. Korona, D., Dirnberger, B., Giachello, C.N., Queiroz, R.M., Popovic, R., Müller, K.H., Minde, D.-P., Deery, M.J., Johnson, G., Firth, L.C., et al. (2022). *Drosophila* nicotinic acetylcholine receptor subunits and their native interactions with insecticidal peptide toxins. eLife *11*, e74322. https://doi.org/10.7554/eLife.74322.

98. Lansdell, S.J., Collins, T., Goodchild, J., and Millar, N.S. (2012). The *Drosophila* nicotinic acetylcholine receptor subunits Dα5 and Dα7 form functional homomeric and heteromeric ion channels. BMC Neurosci *13*, 73. https://doi.org/10.1186/ 1471-2202-13-73.

99. Shinomiya, K., Nern, A., Meinertzhagen, I.A., Plaza, S.M., and Reiser, M.B. (2022). Neuronal circuits integrating

visual motion information in *Drosophila melanogaster*. Curr Biol *32*, 3529-3544.e2. https://doi.org/10.1016/j.cub.2022.06.061.

100. Albuquerque, E.X., Pereira, E.F.R., Alkondon, M., and Rogers, S.W. (2009). Mammalian nicotinic acetylcholine receptors: from structure to function. Physiol Rev *89*, 73–120. https://doi.org/10.1152/physrev.00015.2008.

101. Abrams, P., Andersson, K.-E., Buccafusco, J.J., Chapple, C., de Groat, W.C., Fryer, A.D., Kay, G., Laties, A., Nathanson, N.M., Pasricha, P.J., et al. (2006). Muscarinic receptors: their distribution and function in body systems, and the implications for treating overactive bladder. Br J Pharmacol *148*, 565–578. https://doi.org/10.1038/sj.bjp.0706780.

102. Schuster, R., Phannavong, B., Schröder, C., and Gundelfinger, E.D. (1993). Immunohistochemical localization of a ligand-binding and a structural subunit of nicotinic acetylcholine receptors in the central nervous system of *Drosophila melanogaster*. J of Comparative Neurology *335*, 149–162. https://doi.org/10.1002/cne.903350202.

103. Gundelfinger, E.D. (1992). How complex is the nicotinic receptor system of insects? Trends Neurosci *15*, 206–211. https://doi.org/10.1016/0166-2236(92)90035-7.

104. Jonas, P.E., Phannavong, B., Schuster, R., Schröder, C., and Gundelfinger, E.D. (1994). Expression of the ligand-binding nicotinic acetylcholine receptor subunit Dα2 in the *Drosophila* central nervous system. J. Neurobiol. *25*, 1494–1508. https://doi.org/10.1002/neu.480251203.

105. Thany, S.H. (2010). Electrophysiological studies and pharmacological properties of insect native nicotinic acetylcholine receptors. In insect nicotinic acetylcholine receptors advances in experimental medicine and biology., S. H. Thany, ed. (Springer New York), pp. 53–63. https://doi.org/10.1007/978-1-4419-6445-8_5.

106. Chamaon, K., Smalla, K., Thomas, U., and Gundelfinger, E.D. (2002). Nicotinic acetylcholine receptors of *Drosophila* : three subunits encoded by genomically linked genes can co-assemble into the same receptor complex. Journal of Neurochemistry *80*, 149–157. https://doi.org/10.1046/j.0022-3042.2001.00685.x.

107. Chamaon, K., Schulz, R., Smalla, K.-H., Seidel, B., and Gundelfinger, E.D. (2000). Neuronal nicotinic acetylcholine receptors of *Drosophila melanogaster* : the α-subunit Dα3 and the β-type subunit ARD co-assemble within the same receptor complex. FEBS Letters *482*, 189–192. https://doi.org/10.1016/S0014-5793(00)02057-3.

108. Deng, B., Li, Q., Liu, X., Cao, Y., Li, B., Qian, Y., Xu, R., Mao, R., Zhou, E., Zhang, W., et al. (2019). Chemoconnectomics: Mapping chemical transmission in *Drosophila*. Neuron *101*, 876-893.e4. https://doi.org/10.1016/j.neuron.2019.01. 045.

109. Bahl, A., Serbe, E., Meier, M., Ammer, G., and Borst, A. (2015). Neural mechanisms for *Drosophila* contrast vision. Neuron *88*, 1240–1252. https://doi.org/10.1016/j.neuron.2015.11.004.

110. Namiki, S., Dickinson, M.H., Wong, A.M., Korff, W., and Card, G.M. (2018). The functional organization of descending sensory-motor pathways in *Drosophila*. eLife *7*, e34272. https://doi.org/10.7554/eLife.34272.

111. Dupuis, J.P., Gauthier, M., and Raymond-Delpech, V. (2011). Expression patterns of nicotinic subunits α2, α7, α8, and β1 affect the kinetics and pharmacology of ACh-induced currents in adult bee olfactory neuropiles. Journal of Neurophysiology *106*, 1604–1613. https://doi.org/10.1152/jn.00126.2011.

112. Mazzaferro, S., Strikwerda, J.R., and Sine, S.M. (2022). Stoichiometry-selective modulation of α4β2 nicotinic ACh receptors by divalent cations. British J Pharmacology *179*, 1353–1370. https://doi.org/10.1111/bph.15723.

113. Weltzin, M.M., George, A.A., Lukas, R.J., and Whiteaker, P. (2019). Distinctive single-channel properties of α4β2-

nicotinic acetylcholine receptor isoforms. PLoS ONE *14*, e0213143. https://doi.org/10.1371/journal.pone.0213143.

114. Pfeiffer, B.D., Ngo, T.-T.B., Hibbard, K.L., Murphy, C., Jenett, A., Truman, J.W., and Rubin, G.M. (2010). Refinement of tools for targeted gene expression in *Drosophila*. Genetics *186*, 735–755. https://doi.org/10.1534/genetics.110. 119917.

115. Raccuglia, D., Huang, S., Ender, A., Heim, M.-M., Laber, D., Suárez-Grimalt, R., Liotta, A., Sigrist, S.J., Geiger, J.R.P., and Owald, D. (2019). Network-specific synchronization of electrical slow-wave oscillations regulates sleep drive in *Drosophila*. Curr Biol *29*, 3611-3621.e3. https://doi.org/10.1016/j.cub.2019. 08.070.

116. Jin, X., Tian, Y., Zhang, Z.C., Gu, P., Liu, C., and Han, J. (2021). A subset of DN1p neurons integrates thermosensory inputs to promote wakefulness via CNMa signaling. Curr Biol *31*, 2075-2087.e6. https://doi.org/10.1016/j.cub.2021. 02.048.

117. Schindelin, J., Arganda-Carreras, I., Frise, E., Kaynig, V., Longair, M., Pietzsch, T., Preibisch, S., Rueden, C., Saalfeld, S., Schmid, B., et al. (2012). Fiji: an open-source platform for biological-image analysis. Nat Methods *9*, 676–682. https://doi.org/10.1038/nmeth.2019.

118. Buchner, E. (1976). Elementary movement detectors in an insect visual system. Biol. Cybernetics *24*, 85–101. https://doi.org/10.1007/BF00360648.

119. Seelig, J.D., Chiappe, M.E., Lott, G.K., Dutta, A., Osborne, J.E., Reiser, M.B., and Jayaraman, V. (2010). Two-photon calcium imaging from head-fixed *Drosophila* during optomotor walking behavior. Nat Methods *7*, 535–540. https://doi.org/10.1038/nmeth.1468.

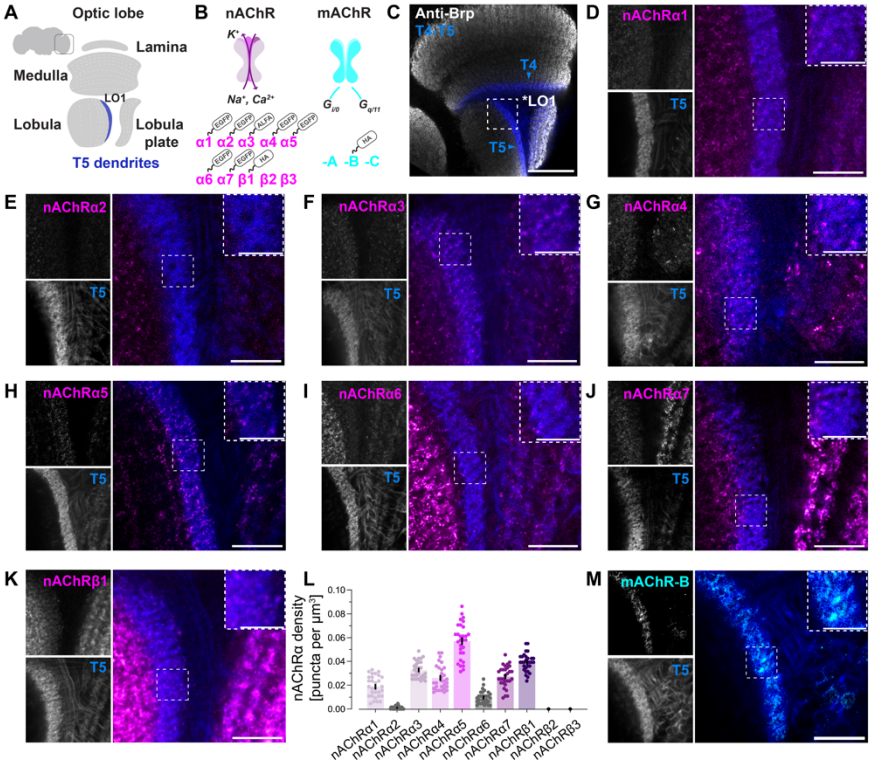

Figure 1. AChR expression on T5 dendrites

(A) Schematic representation of T5 dendrites (blue), among other cell types, residing in lobula layer 1 (LO1) of the *Drosophila* optic lobe (OL). (B) Schematic representation of nicotinic ionotropic (magenta) and muscarinic metabotropic (cyan) AChRs in *Drosophila*. Out of the seven nAChRα subunits, six were tagged with EGFP[22] and the nAChRα3 with the ALFA tag[58]. The nAChRβ1 subunit[58] and the mAChR-B (C.H. Lee) were tagged with the HA peptide tag.

(C) OL (Anti-Brp, grey) with T4 and T5 dendrites (R42F06-Gal4>UAS-myr::tdTomato, blue) in M10 and LO1 accordingly. Scale bar 40µm.
(D-K) nAChRα1, nAChRα2, nAChRα3, nAChRα4, nAChRα5, nAChRα6, nAChRα7 and nAChRβ1 (nAChRα1,2,4,5,6,7::EGFP, nAChRα3::ALFA, nAChRβ1::HA, magenta) subunit expression on T5 dendrites (R42F06-Gal4>UAS-myr::tdTomato, blue). Scale bar 10µm, inset 5µm. See also Figures S1-S4. Detailed genotypes are reported in Table S1.
(L) Density of nAChR subunit expression on T5 dendrites across 30 ROIs in LO1 (optic lobes n=6). nAChRβ2 and nAChRβ3 subunits were not addressed. Subunits with the lowest expression levels are in grey. Data is mean ± SEM.
(M) Overexpression of mAChR-B (UAS-mAChR-B::HA, cyan) on T5 dendrites (R42F06-Gal4>UAS-myr::tdTomato, blue). Scale bar 10µm, inset 5µm.

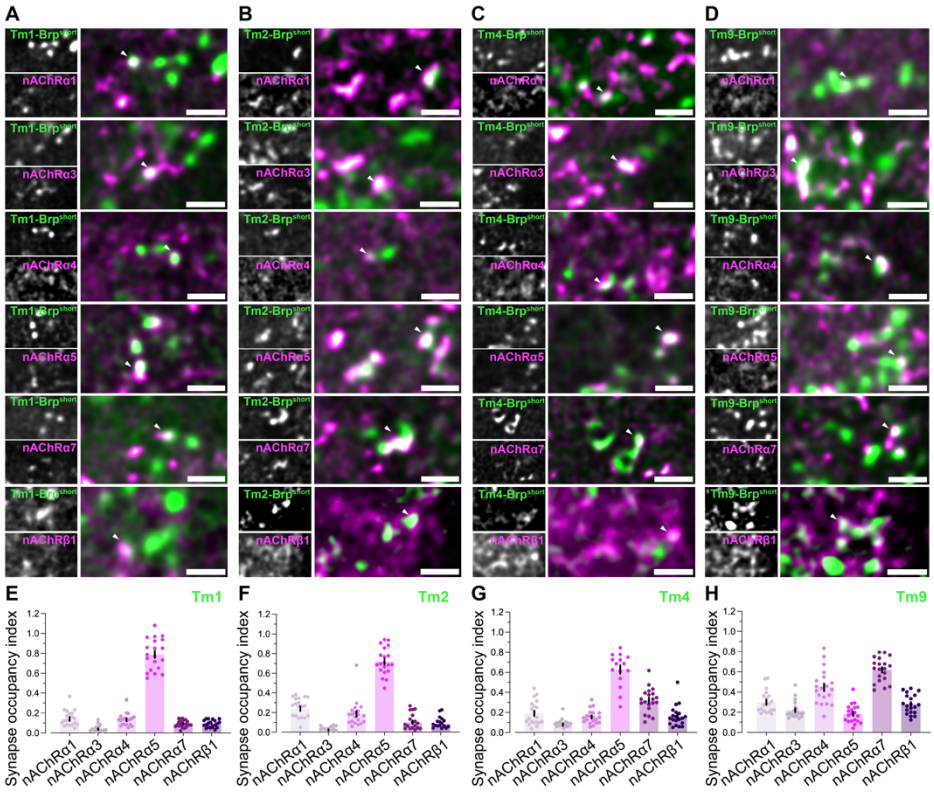

Figure 2. Differential synaptic localization of nAChRα subunits in Tm synapses

(A-D) Trans-synaptic alignment of Tm1, Tm2, Tm4 and Tm9 boutons (Tm-Gal4> UAS-Brp$^{short::mStraw}$, green) with the endogenously tagged nAChRα1, nAChRα3, nAChRα4, nAChRα5, nAChRα7 and nAChRβ1

subunits (nAChRα1,4,5,7::EGFP, nAChRα3::ALFA, nAChRβ1::HA, magenta) in LO1. Arrows indicate the Brp$^{short::mStraw}$-receptor punctum trans-synaptic alignment. Scale bar 1µm. See also Figures S5-S8.
(E-H) Synapse occupancy of Tm1, Tm2, Tm4 and Tm9 boutons with nAChRα1 (pale purple), nAChRα3 (pale magenta), nAChRα4 (light magenta), nAChRα5 (magenta), nAChRα7 (dark magenta) and nAChRβ1 (violet) subunits in LO1 (optic lobes n=4, ROIs N=20, for Tm4-nAChRα5 n=3, N=15). Data is mean ± SEM.

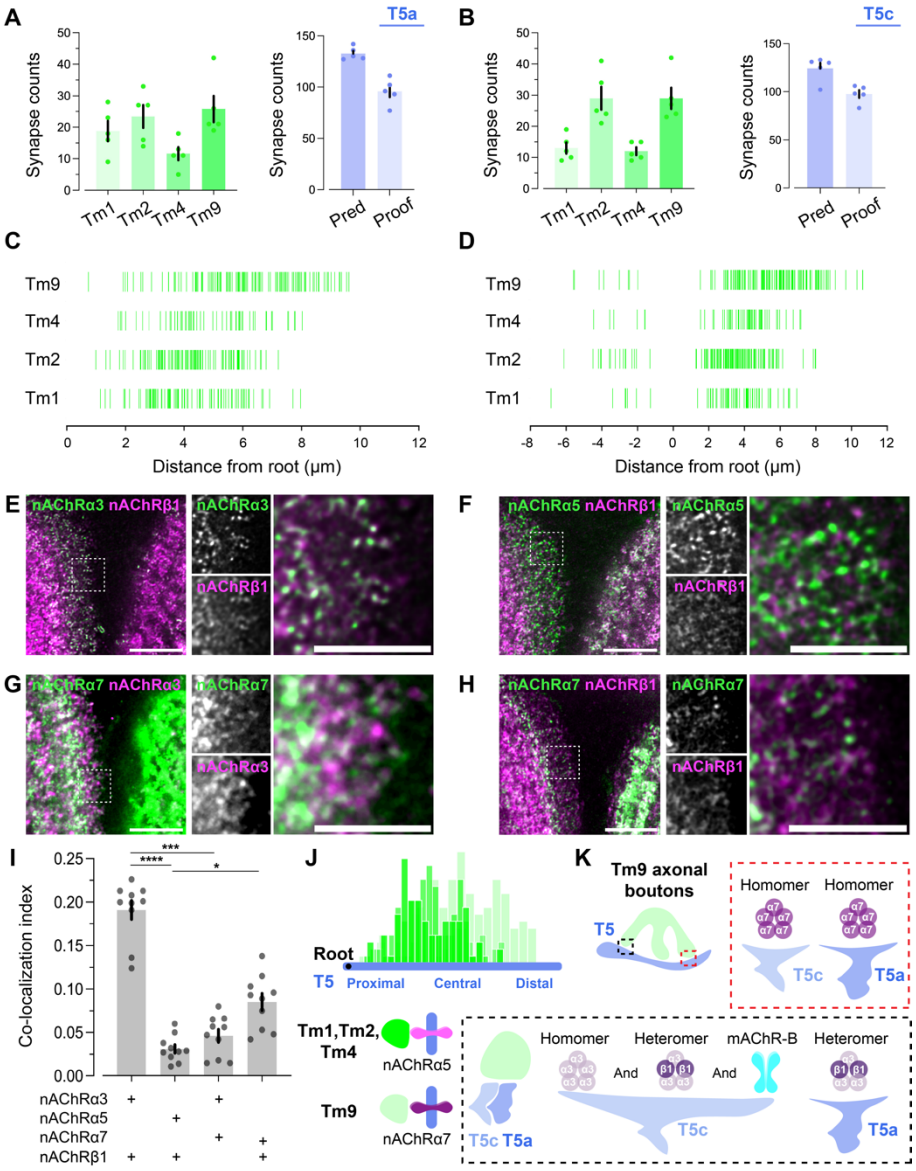

Figure 3. Wiring of Tm1, Tm2, Tm4 and Tm9 on T5 dendrites and nAChR pairs in LO1

(A) Counts of Tm1, Tm2, Tm4 and Tm9 synapses on T5a dendrites (T5a cells n=5, flywire.ai) (left). Counts of predicted (n=663) to proofread (n=479) Tm synapses on T5a dendrites (right). Data is mean

± SEM. Detailed neuronal IDs used for the synapse proofreading are reported in Table S3.

(B) As in (A) for T5c dendrites (T5c cells n=5, flywire.ai) (left). Counts of predicted (n=621) to proofread (n=488) Tm synapses on T5c dendrites (right). Data is mean ± SEM.

(C) Dendritic localization of Tm synapses across the T5a anterior-posterior axis (T5a cells n=5). Root is considered the first dendritic branch point.

(D) Dendritic localization of Tm synapses across the T5c dorso-ventral axis (T5c cells n=5).

(E) Localization of the nAChRα3 to the nAChRβ1 subunit in LO1 (nAChRα3::ALFA green, nAChRβ1::HA magenta). Scale bar 10μm, zoom-in 5μm.

(F-H) As in (E) for nAChRα5-nAChRβ1, nAChRα7-nAChRα3, nAChRα7-nAChRβ1 subunits (nAChRα5,7::EGFP, nAChRα3::ALFA and nAChRβ1::HA).

(I) Co-localization index of nAChR pairs from Figure 3E-H (optic lobes n=2, ROIs N=10). The normality of distribution was assessed with the use of Shapiro-Wilk test. *p<0.05, ***p<0.001, ****p<0.0001. Data is mean ± SEM. Detailed statistical analysis is reported in Table S2.

(J) Schematic representation of Tm synapse distribution on T5 dendrites (Tm1, Tm2, Tm4 green, Tm9 pale green) (top). Postsynaptic receptor heterogeneity between Tm1, Tm2, Tm4 and Tm9 neurons in terms of the most abundant nAChR subunit as in Figure 2E-H (bottom).

(K) Schematic representation of postsynaptic receptor heterogeneity across axonal boutons (inter-bouton heterogeneity, red and black boxes) and within one bouton (intra-bouton heterogeneity, black box) of an example Tm9-T5 connection. Tm9-T5 synapses are polyadic, with each postsynaptic site comprising of T5 spines belonging to different T5 subtypes.

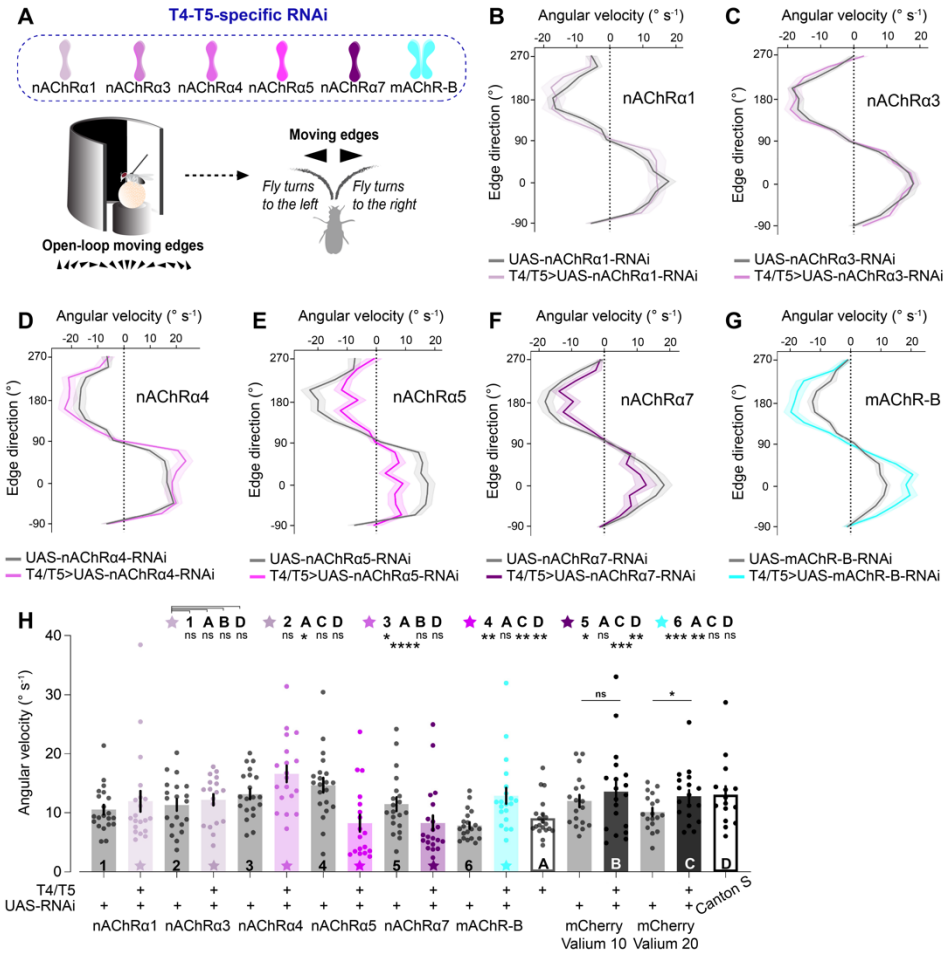

Figure 4. Fly optomotor response post-AChR knock-down

(A) Schematic workflow representation for the behavioral assessment of AChR knock-down flies.

(B) Trajectory (angular velocity) of T4/T5-specific nAChRα1 knock-down flies (R42F06-p65.AD; VT043070-Gal4.DBD>UAS-nAChRα1-RNAi, pale purple, flies n=20) while presented to a sequence of upward to rightward to downward to leftward OFF-edge motion compared to the parental control flies (UAS-nAChRα1-RNAi, grey n=21). The dark lines represent the mean ± SEM. See also Figure S3 and Figure S9.

(C-G) Same as in (B) for the nAChRα3 (pale magenta n=18, grey n=20), nAChRα4 (light magenta n=19, grey n=20), nAChRα5 (magenta n=18, grey n=21), nAChRα7 (dark magenta n=21, grey n=20), mAChR-B (cyan n=20, grey n=20) knock-down flies.

(H) Average angular velocity across OFF edges moving in sixteen directions of control UAS-nAChRα-RNAi (grey, 1 to 6), control T4/T5 driver (R42F06-p65.AD; VT043070-Gal4.DBD, grey n=20 A), control mCherry Valium 10 (black n=19, grey n=18 B), mCherry Valium 20

(black n=18, grey n=18 C), control Canton S (black n=15 D) and T4/T5-specific AChR knock-down flies (star). The normality of distribution was assessed with the use of Shapiro-Wilk test. *p<0.05, **p<0.01, ***p<0.001, ****p<0.0001. Data is mean ± SEM. Detailed statistical analysis is reported in Table S2.

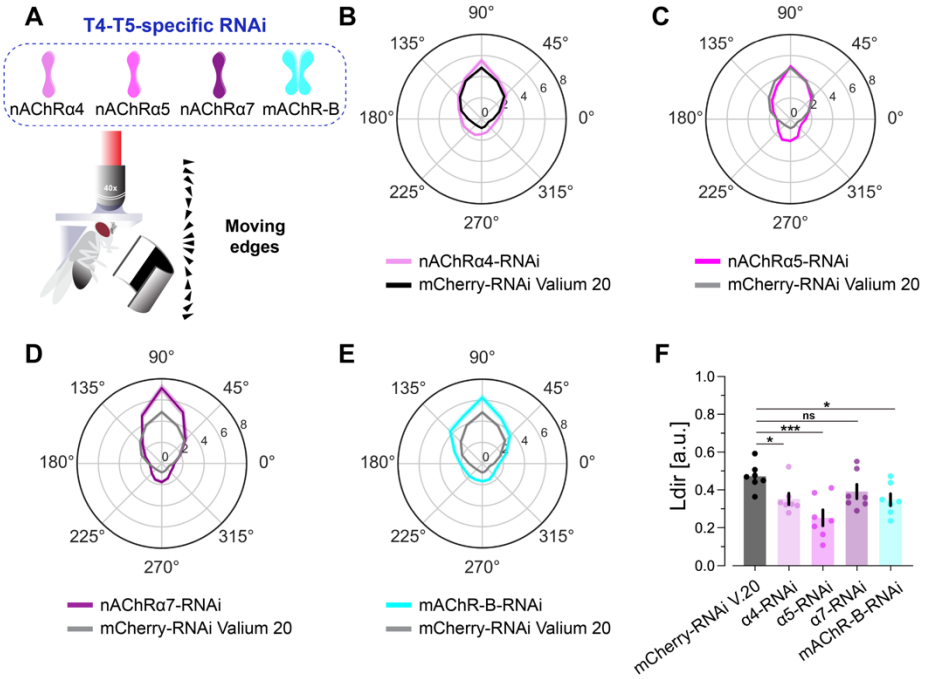

Figure 5. Directional tuning of T5 cells post-AChR knock-down

(A) Schematic workflow representation for the two-photon calcium imaging in AChR knock-down T5 cells.

(B) Polar plot of the maximum responses (ΔF/F) across sixteen OFF edge directions (º) of T5c cells for mCherry Valium 20 control (black, flies n=7, ROIs N=85, shown as grey in C, D and E) and nAChRα4 RNAi (light magenta, n=7, N=61) conditions (R39H12-Gal4>UAS-AChR-RNAi, VT50384-LexA>LexAop-IVS-GCaMP6m). The dark lines represent the mean (68% CI). See also Figure S3 and Figure S10.

(C) Same as in (B) for nAChRα5 RNAi flies (magenta, n=7, N=82).

(D) Same as in (B) for nAChRα7 RNAi flies (dark magenta, n=7, N=60).

(E) Same as in (B) for mAChR-B RNAi flies (cyan, n=7, N=54).

(F) Directional tuning index (Ldir). Flies n=7. The normality of distribution was assessed with the use of Shapiro-Wilk test. *p<0.05, ***p<0.001. Data is mean ± SEM. Detailed statistical analysis is reported in Table S2.

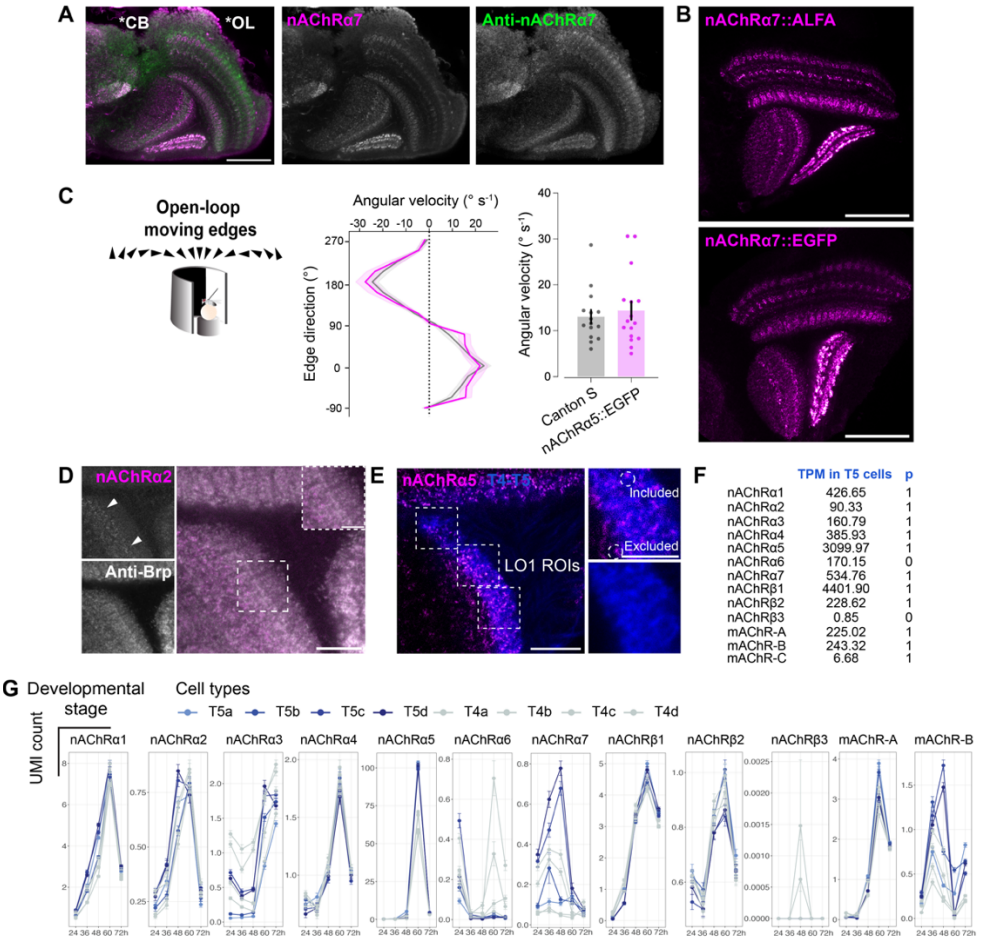

Figure S1. AChR expression in T5 cells-Related to Figure 1

(A) Localization of the nAChRα7 subunit in LO1 by an endogenous tag (nAChRα7::EGFP, magenta) and by antibody labelling (Anti-nAChRα7 from H.J. Bellen, green). Scale bar 40µm.

(B) Localization of the nAChRα7 subunit in LO1 by an endogenous EGFP [S1] (nAChRα7::EGFP) and ALFA [S2] tag (nAChRα7::ALFA). Scale bar 40µm.

(C) Angular velocity of control Canton S (grey n=15) and nAChRa5::EGFP tagged (magenta n=16) flies. The normality of distribution was assessed with the use of Shapiro-Wilk test. Data is mean ± SEM.

(D) nAChRα2 expression in LO. Arrows indicate the LO layers of expression past the LO1. Scale bar 10µm, inset 5µm.

(E) Example ROIs in LO1 for quantification as in Figure 1L. Scale bar 10µm, zoom-in 5µm.

(F) Bulk RNAseq of AChR expression (transcripts per million, TPM) in T5 cells and probability of expression (p) [S3].

(G) scRNAseq of AChR expression in T4 (grey) and T5 (blue) cells across five developmental stages (hours correspond to APF-after puparium formation) [S4].

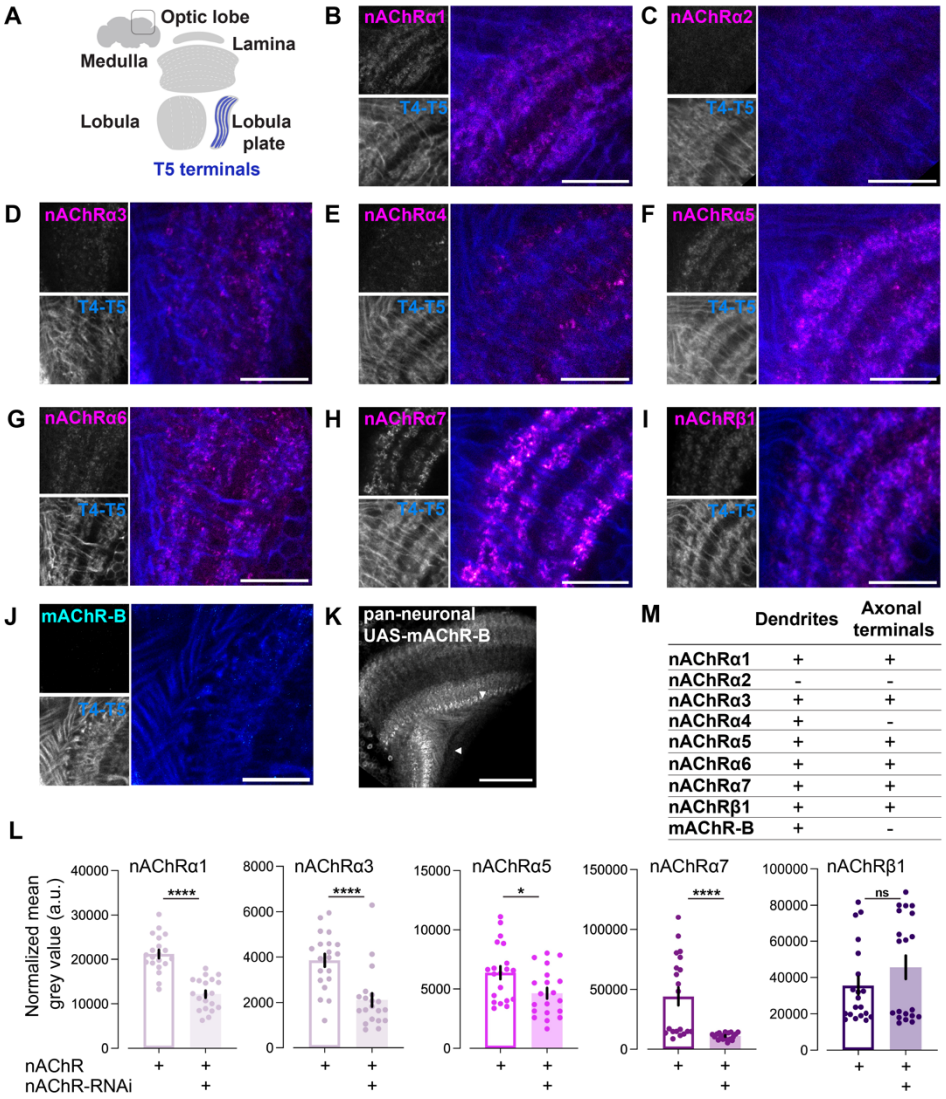

Figure S2. AChR expression in T4/T5 axonal terminals-Related to Figure 1
(A) Schematic representation of T5 axonal terminals, among other cell types, residing in lobula plate (LOP1-4) of the *Drosophila* optic lobe (OL).
(B-I) Expression of nAChRα1, nAChRα2, nAChRα3, nAChRα4, nAChRα5, nAChRα6, nAChRα7 and nAChRβ1 (nAChRα1,2,4,5,6,7::EGFP, nAChRα3::ALFA, nAChRβ1::HA, magenta) in T4/T5 axonal terminals (R42F06-Gal4>UAS-myr::tdTomato, blue). Scale bar 10μm.
(J) Overexpression of mAChR-B (cyan) in T4/T5 axonal terminals (R42F06-Gal4>UAS-myr::tdTomato, UAS-mAChR-B::HA). Scale bar 10μm.
(K) Pan-neuronal expression of mAChR-B in OL (GMR57C10-Gal4>UAS-mAChR-B::HA). Scale bar 40μm.
(L) Normalized mean grey value of nAChR subunits in LOP (layers 1 and 2) before and after RNAi induction (optic lobes n=2, ROIs N=20, for nAChRα1 n=1). The normality of distribution was assessed with the use of Shapiro-Wilk test. *p<0.05, ****p<0.0001. Data is mean ± SEM.
(M) Summarized expression patterns of nAChRα1, nAChRα2, nAChRα3, nAChRα4, nAChRα5, nAChRα6, nAChRα7 and nAChRβ1 subunits and the mAChR-B type on T5 dendrites and in T4/T5 axonal terminals.

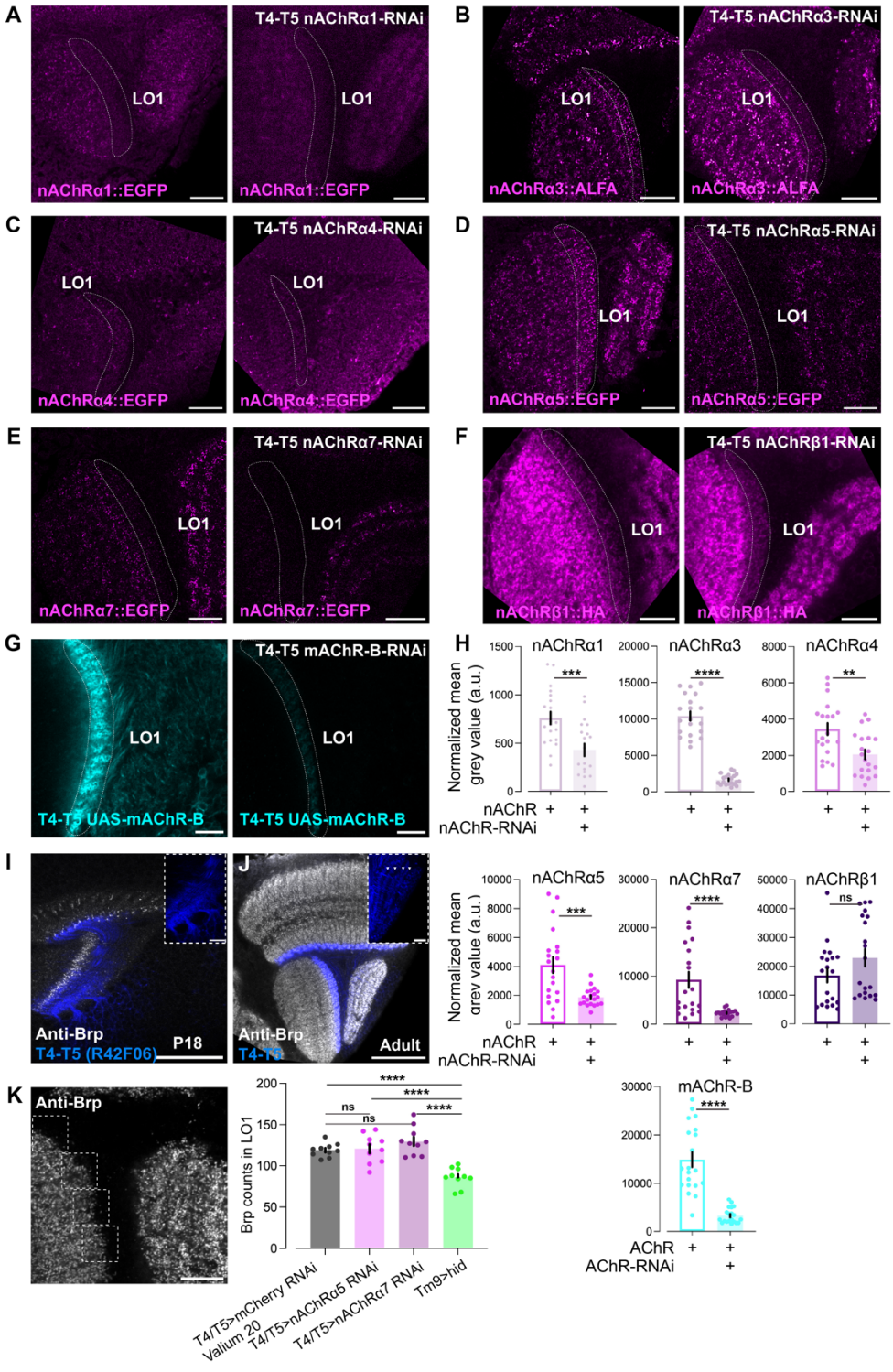

Figure S3. RNA interference against AChRs in T5 cells-Related to Figure 1, 4 and 5

(A) Expression of the nAChRα1 subunit (nAChRα1::EGFP, magenta) in LO1 before (left panel) and after (right panel) the RNAi induction (R42F06-Gal4>UAS-AChR-RNAi). Scale bar 10μm.

(B-G) As in (A) for the nAChRα3, nAChRα4, nAChRα5, nAChRα7, nAChRβ1 subunits and the mAChR-B type (nAChRα4,5,7::EGFP, nAChRα3::ALFA, nAChRβ1::HA, magenta and UAS-mAChR-B::HA, cyan).
(H) Normalized mean grey value of AChRs in LO1 before and after RNAi induction (optic lobes n=2, ROIs N=20). The normality of distribution was assessed with the use of Shapiro-Wilk test. **p<0.01, ***p<0.001, ****p<0.0001. Data is mean ± SEM.
(I) Developmental onset (P18) of the R42F06 promoter used for the split T4/T5 line in all behavioral experiments (R42F06-Gal4> UAS-myr::tdTomato). Scale bar 40µm, inset 10µm.
(J) Split T4/T5 line (R42F06-p65.AD; VT043070-Gal4.DBD>UAS-CD4::tdGFP) used in all behavioral experiments. Arrows indicate the four LOP layers. Scale bar 40µm, inset 10µm.
(K) Antibody labelling against Brp and example ROI selection in LO1 (left). Scale bar 10µm. Counts of Brp puncta (Anti-Brp) in LO1 (optic lobes n=2, ROIs N=10) under control (R42F06-Gal4>UAS-mCherry RNAi Valium 20) and induced conditions (R42F06-Gal4>UAS-nAChRα5 RNAi, R42F06-Gal4>UAS-nAChRα7 RNAi, VT065303-Gal4>UAS-hid)(right). The normality of distribution was assessed with the use of Shapiro-Wilk test. ****p<0.0001. Data is mean ± SEM.

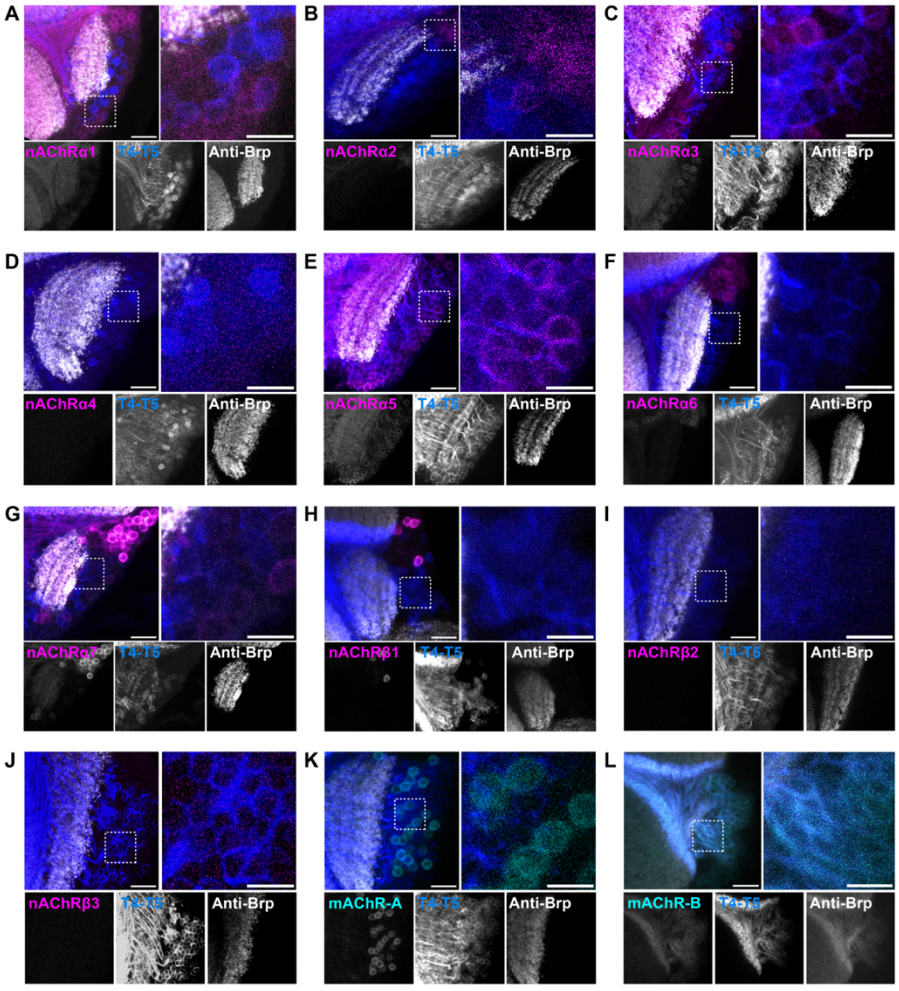

M

	scRNA-seq	Bulk-seq	Enhancer trap	Tagged
nAChRα1	+	+	+	+
nAChRα2	-	+	-	-
nAChRα3	+	+	+	+
nAChRα4	+	+		+
nAChRα5	+	+	+	+
nAChRα6	-	-	-	+
nAChRα7	-	+	+	+
nAChRβ1	+	+	-	+
nAChRβ2	-	+	-	
nAChRβ3	-	-	-	
mAChR-A	+	+	-	
mAChR-B	+	+	+	

Figure S4. Enhancer-trap verification of AChR expression in T4/T5 cells- Related to Figure 1

(A-L) Enhancer-trap lines for the nAChRα1, nAChRα2, nAChRα3, nAChRα4, nAChRα5, nAChRα6, nAChRα7, nAChRβ1, nAChRβ2, nAChRβ3 subunits and mAChR-A and mAChR-B receptors (AChR-Mi or T2A-Gal4>UAS-CD8::GFP, magenta and cyan). Signal overlap with T4/T5 somata (R42F06-LexA>LexAop-CD8::RFP, blue) denoted the T4/T5 AChR expression. The nAChRα4 line did not show expression across all brain areas. Images are z-projections. Scale bar 40µm, inset 10µm.

(M) AChR expression in T5 cells across scRNA-seq [S4], Bulk-seq [S3], enhancer trap and endogenously tagged receptor experiments.

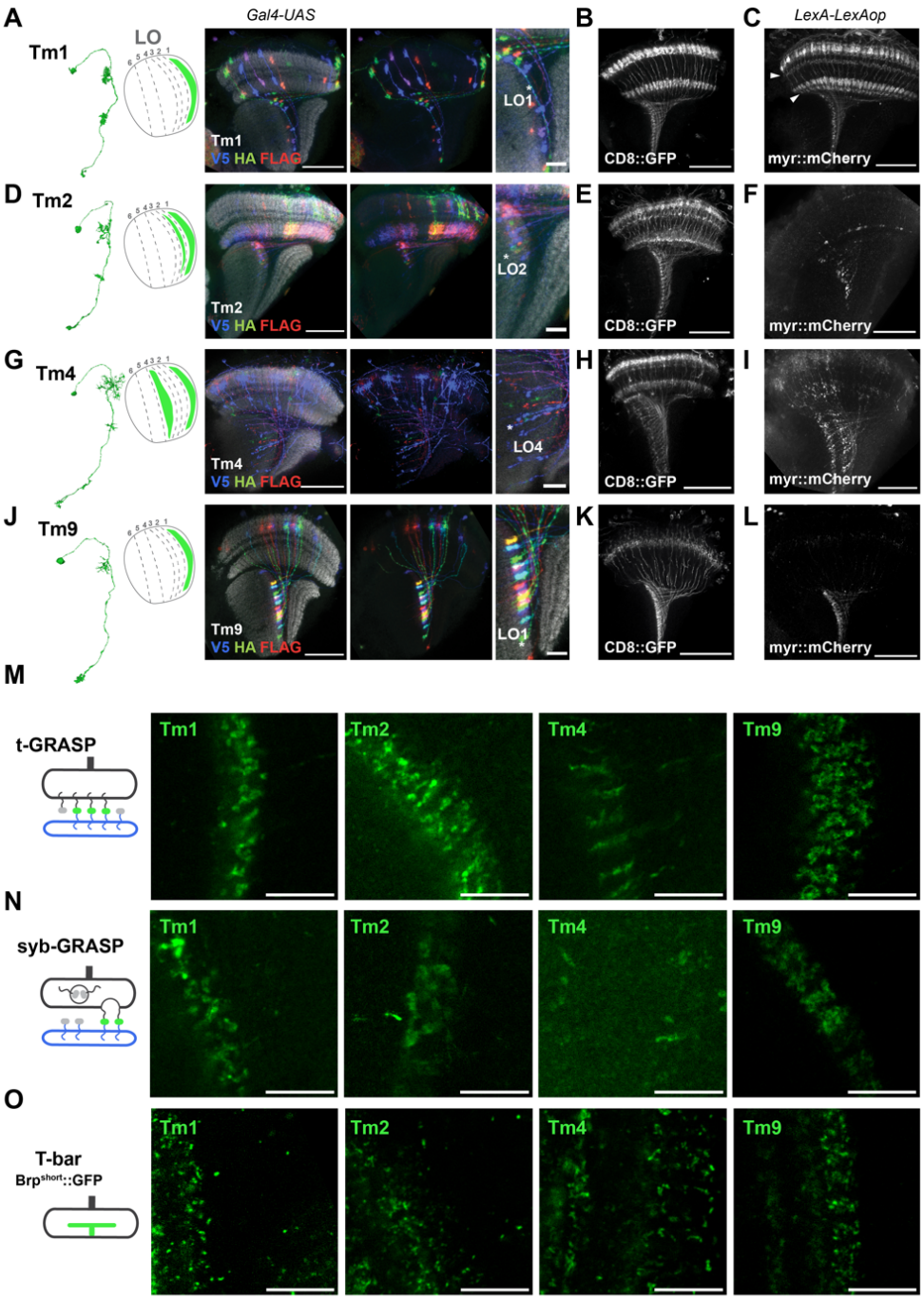

Figure S5. Morphological identification of the four columnar T5 cholinergic input neurons and screening of genetic approaches for synapse visualization- Related to Figure 2

(A) Electron microscopy (EM)(flywire.ai) reconstruction of a Tm1 neuron reveals two loci of arborization in medulla. Schematic representation of the Tm1 axonal terminal localization in LO1. Tm1-Gal4 expression of the MultiColor FlpOut cassette (V5, HA, FLAG) and axonal localization in LO. Scale bar 40µm and 10µm.

(B) Whole population labelling of Tm1 neurons (R74G01-Gal4>UAS-CD8::GFP). Scale bar 40µm.

(C) Whole population labelling of Tm1-LexA neurons (VT041034-LexAGAD>LexAop-myr::mCherry). Arrows represent additional dendritic ramifications that lack in (B). Scale bar 40µm.
(D-F) As in (A-C), but for Tm2 neurons (VT012282-Gal4, VT058650-LexAGAD).
(G-I) As in (A-C), but for Tm4 neurons (R35H01-Gal4, R53C02-LexAGAD).
(J-L) As in (A-C), but for Tm9 neurons (VT065303-Gal4, R24C08-LexAp65).
(M) t-GRASP expression in Tm1, Tm2, Tm4 and Tm9-T5 synapses (Tm1, Tm2, Tm4, Tm9-Gal4>UAS-pre-t-GRASP, VT25965-LexAp65>LexAop-post-t-GRASP). Scale bar 10µm. Ectopic reconstitution is observed in Tm4-T5 synapses.
(N) Activity GRASP (syb-GRASP) in Tm1, Tm2, Tm4 and Tm9-T5 synapses (Tm1, Tm2, Tm4, Tm9-Gal4>UAS-nSyb-spGFP1-10, VT25965-LexAp65>LexAop-CD4-spGFP11). Scale bar 10µm.
(O) Brp$^{short::GFP}$ expression in Tm1, Tm2, Tm4 and Tm9 boutons (Tm1, Tm2, Tm4, Tm9-Gal4>UAS-Brp$^{short::GFP}$). Scale bar 10µm.

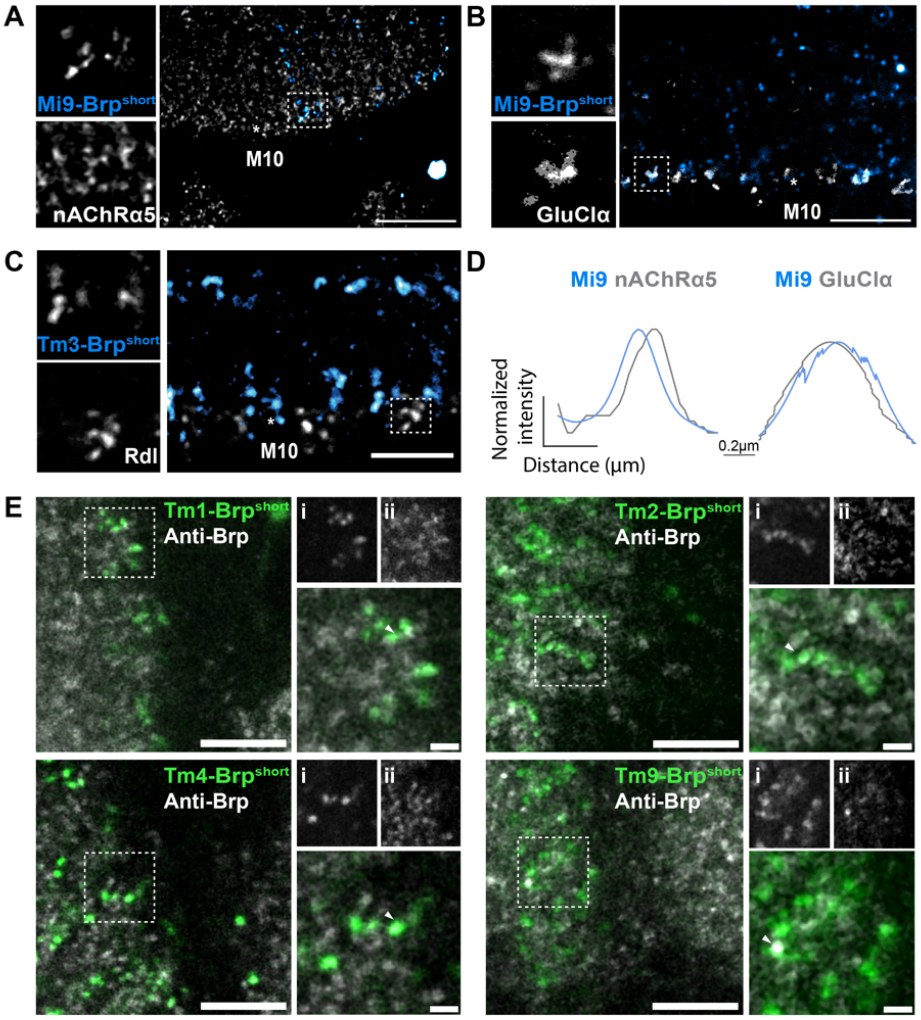

Figure S6. Validation of Brp^{short} as a precise presynaptic marker-Related to Figure 2
(A) Mi9-Brp$^{short::mCherry}$(blue) and the acetylcholine receptor subunit nAChRa5 (grey) in medulla layer 10 (GMR48A07-LexA>LexAop-Brp$^{short::mCherry}$, nAChRa5::EGFP). Scale bar 10µm.
(B) Mi9-Brp$^{short::mCherry}$(blue) and the glutamatergic GluClα receptor (grey) in the glutamatergic Mi9-T4 synapse (GMR48A07-LexA>LexAop-Brp$^{short::mCherry}$, R42F06-Gal4>UAS-GluClα::GFP). Scale bar 10µm.

(C) Tm3-Brp$^{short::mCherry}$(blue) and the GABAergic Rdl receptor (grey) in the cholinergic Tm3-T4 synapse (GMR13E12-LexA>LexAop-Brp$^{short::mCherry}$, R42F06-Gal4>UAS-Rdl::GFP). Scale bar 10µm.
(D) Line profile analysis for the assessment of trans-synaptic alignment of Brp$^{short::mCherry}$ puncta (blue) and the nAChRα5 subunit (grey, analyzed puncta n=10)(left). Line profile analysis for the assessment of trans-synaptic alignment of Brp$^{short::mCherry}$ puncta (blue) and the GluClα receptor (grey, analyzed puncta n=10)(right). The dark lines represent the mean values.
(E) Localization of Brp$^{short::mStraw}$ in Tm1, Tm2, Tm4 and Tm9 boutons (green, i) and endogenous Brp (grey, ii) identified by the Anti-Brp staining. Arrows correspond to the signal overlap between the Tm-Brp^{short} and the Anti-Brp. Scale bar 5 and 1µm.

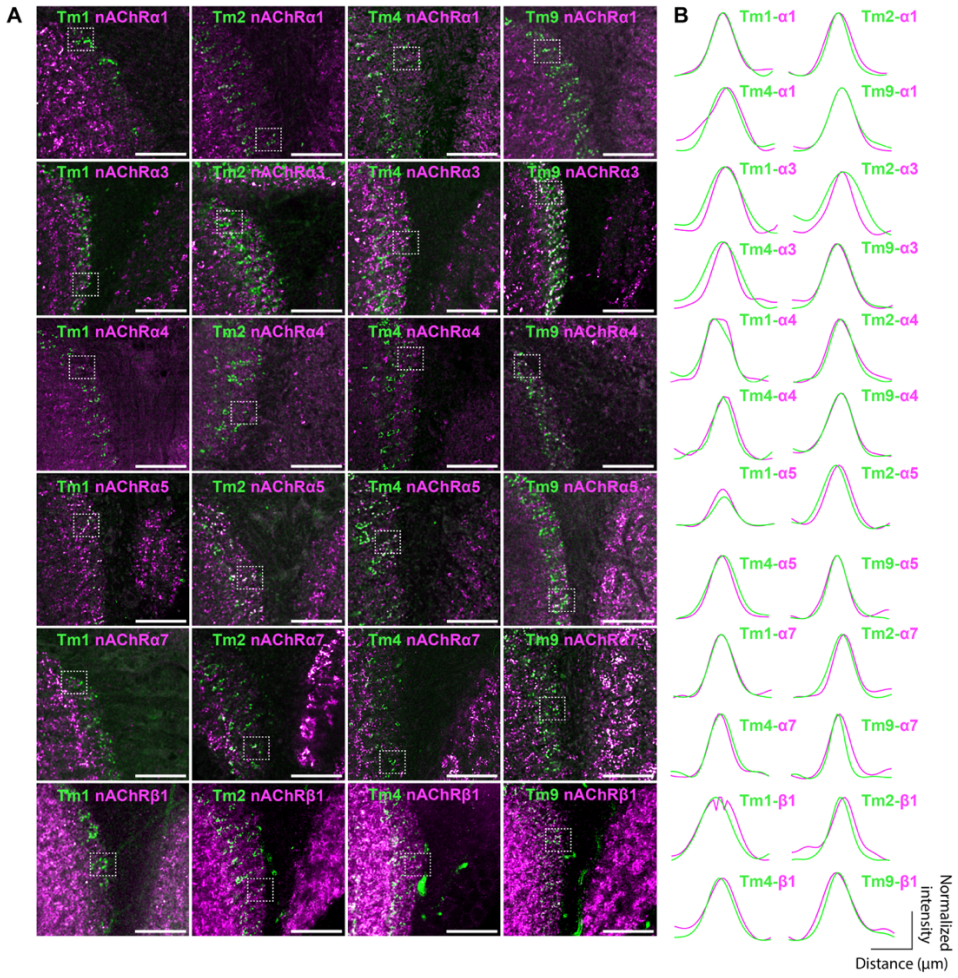

Figure S7. Localization of nAChRα subunits in Tm synapses-Related to Figure 2
(A) LO1 loci that were used for Figure 2A-D. Scale bar 10µm.
(B) Line profile analysis for the assessment of trans-synaptic alignment of Brp$^{short::mStraw}$ puncta (green) and nAChRα and nAChRβ puncta (magenta) across Tm1, Tm2, Tm4 and Tm9 synapses (analyzed puncta n=10). The dark lines represent the mean values.

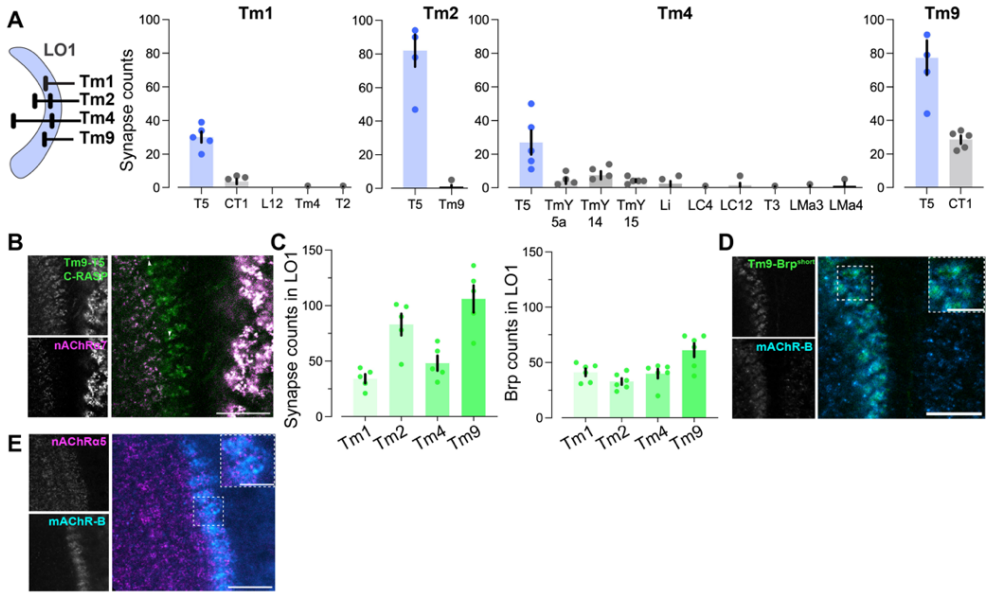

Figure S8. Neuronal outputs of Tm1, Tm2, Tm4 and Tm9 cells in LO1 and mAChR-B receptor localization on T5 dendrites-Related to Figure 2

(A) Schematic representation of Tm1, Tm2, Tm4 and Tm9 axonal terminals in relation to LO1 (left). Primary Tm1, Tm2, Tm4 and Tm9 output neuronal types in LO1 (Tm cells n=5, Codex) (right). Data is mean ± SEM.

(B) C-RASP for the Tm9-T5 synapse visualization (Tm9-Gal4>UAS-IVS-syb-spCFP1-10, VT25965-LexAp65>LexAop-CD4-spGFP11, green) of the nAChRα7 subunit (nAChRα7::EGFP, magenta). Arrows correspond to Tm9-nAChRα7 trans-synaptic alignment. Scale bar 10μm.

(C) Total synapse counts of Tm1, Tm2, Tm4 and Tm9 neurons in LO1 (data from Figure S8A)(left). Tm1-, Tm2-, Tm4-, Tm9-Brp$^{short::mStraw}$ counts in LO1 (data from Figure 2E-H)(right). Each circle corresponds to the average among 20 ROIs Brp$^{short::mStraw}$ counts along the six Tm-nAChR genotypes.

(D) mAChR-B localization (R42F06-Gal4>UAS-mAChR-B::HA, cyan) in Tm9-T5 synapses (Tm9-LexA>LexAop-Brp$^{short::mCherry}$, green). Scale bar 10μm, inset 5μm.

(E) nAChRα5 subunit (nAChRα5::EGFP, magenta) localization pattern compared to mAChR-B (R42F06-Gal4>UAS-mAChR-B::HA, cyan) in LO1. Scale bar 10μm, inset 5μm.

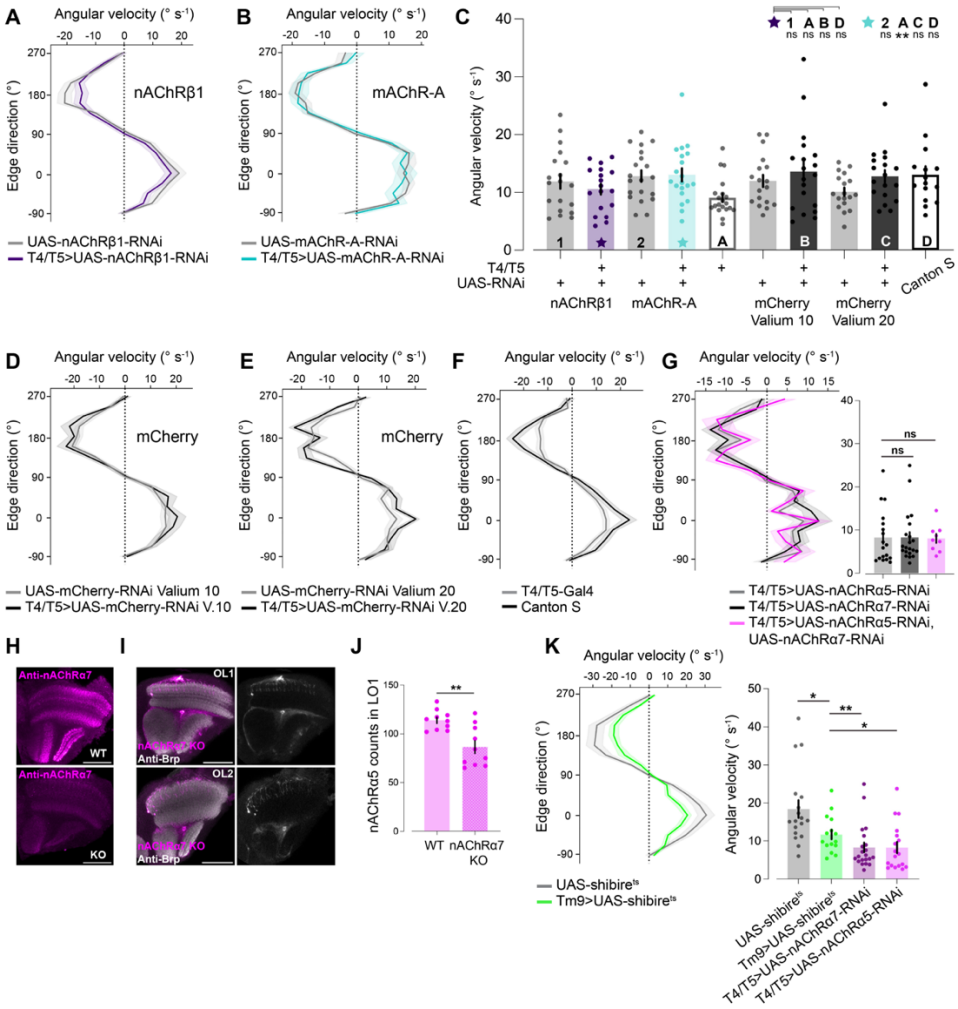

Figure S9. Fly optomotor response after AChR knock-down, Tm9 silencing and double AChR knock-down-Related to Figure 4

(A) Trajectory (angular velocity) of nAChRβ1 knock-down flies (42F06-p65.AD; VT043070-Gal4.DBD>UAS-nAChRβ1-RNAi, violet n=18) while presented to a sequence of upward to rightward to downward to leftward OFF-edge motion compared to the parental control flies (UAS-nAChRβ1-RNAi, grey n=19). The dark lines represent the mean ± SEM.

(B) Same as in (A) for the mAChR-A (teal n=20, grey n=20) knock-down flies.

(C) Average angular velocity across OFF edges moving in sixteen directions of control UAS-AChR-RNAi (grey, 1 to 2), control T4/T5 driver (R42F06-p65.AD; VT043070-Gal4.DBD, grey n=20 A), control mCherry Valium 10 (black n=19, grey n=18 B), mCherry Valium 20 (black n=18, grey n=18 C), control Canton S (black n=15 D) and T4/T5-specific AChR knock-down flies (star) (as in Figure 4H). The normality of distribution was assessed with the use of Shapiro-Wilk test. *p<0.05, **p<0.01, ***p<0.001, ****p<0.0001. Data is mean ± SEM.

(D-F) Trajectory (angular velocity) of control mCherry Valium 10, control mCherry Valium 20, control T4/T5 driver and control Canton S flies as in Figure 4H and S9C.

(G) Trajectory (angular velocity) of T4/T5-specific nAChRα5 knock-down flies (R42F06-p65.AD; VT043070-Gal4.DBD>UAS-nAChRα5-RNAi, grey n=18), of T4/T5-specific nAChRα7 knock-down flies (R42F06-p65.AD; VT043070-Gal4.DBD>UAS-nAChRα7-RNAi, grey n=21) and of T4/T5-specific nAChRα5 & nAChRα7 knock-down flies (R42F06-p65.AD; VT043070-Gal4.DBD>UAS-nAChRα5-RNAi & UAS-nAChRα7-RNAi, magenta n=9) (left). Average angular velocity across the three conditions (right). The normality of distribution was assessed with the use of Shapiro-Wilk test. Data is mean ± SEM.

(H) Antibody staining against the nAChRα7 subunit in Canton S (WT) and nAChRα7 knock-out (KO) flies. Scale bar 40µm.
(I) Verification of the nAChRα7 knock-out expression in OLs used for analysis. nAChRα7 knock-out flies express DsRed under control of the eye-specific 3xP3 promoter, leading to distinct photoreceptor staining. Scale bar 40µm.
(J) nAChRα5 counts in LO1 in wild type nAChRα5::EGFP expressing flies and nAChRα7 knock-out nAChRα5::EGFP expressing flies as in Figure S9I. The normality of distribution was assessed with the use of Shapiro-Wilk test. **p<0.01. Data is mean ± SEM.
(K) Trajectories and angular velocities of flies after thermogenetically silencing Tm9 (VT065303-Gal4>UAS-shibire^{ts}, green n=15) compared to parental control flies (UAS-shibire^{ts}, grey n=18), nAChRα7 subunit knock-down flies (42F06-p65.AD; VT043070-Gal4.DBD>UAS-nAChRα7-RNAi, dark magenta n=21) and nAChRα5 subunit knock-down flies (42F06-p65.AD; VT043070-Gal4.DBD>UAS-nAChRα5-RNAi, magenta n=18). The normality of distribution was assessed with the use of Shapiro-Wilk test. *p<0.05 and **p<0.01. Data is mean ± SEM.

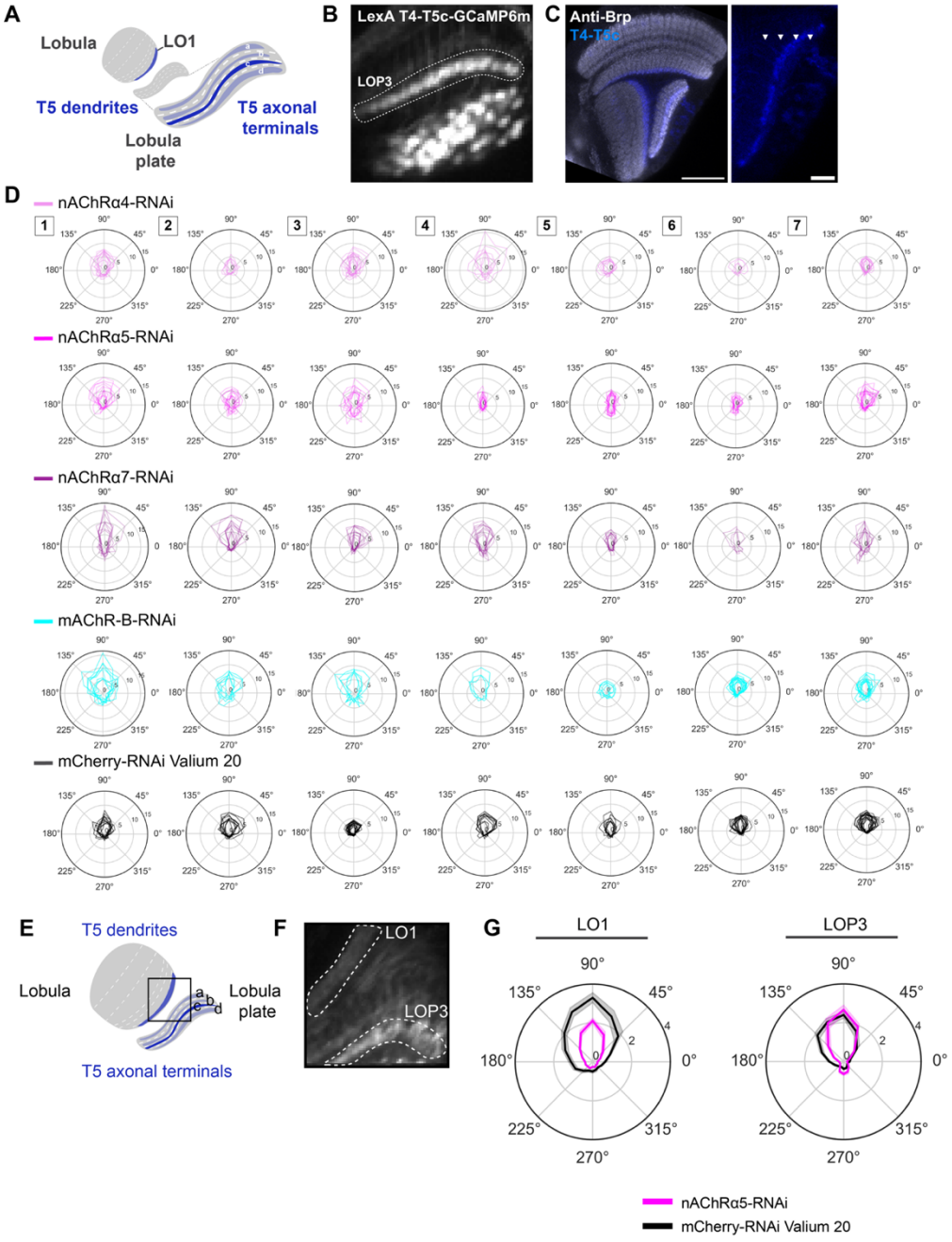

Figure S10. Two-photon calcium imaging in T5 cells-Related to Figure 5
(A) Schematic representation of LO1 (where T5 dendrites reside) and of LOP3 (where T5c axonal terminals reside).
(B) Two-photon view of LOP3 (VT50384-LexA>LexAop-IVS-GCaMP6m).
(C) T4/T5c specific targeting (VT50384-Gal4>UAS-CD8::GFP). Arrows indicate the four LOP layers. Scale bars 40 and 10μm.
(D) Polar plots of the maximum responses (ΔF/F) -along seven flies- across sixteen OFF edge directions (°) of T5c cells under nAChRα4 RNAi (light magenta), nAChRα5 RNAi (magenta), nAChRα7 RNAi (dark magenta), mAChR-B RNAi (cyan) and control mCherry RNAi Valium 20 (black) conditions.
(E) Zoom-in schematic representation of LO1 (where T5 dendrites reside) and of LOP3 (where T5c axonal terminals reside).
(F) Two-photon view of the LO1 and LOP3 layers (VT50384-LexA>LexAop-IVS-GCaMP6m).
(G) Polar plots of the maximum responses (ΔF/F) across sixteen OFF edge directions (°) of T5c cells under mCherry control (black, flies n=5, ROIs N=10) and nAChRα5 RNAi (magenta, n=5, N=13) conditions in LO1 (left) and in LOP3 (right). The dark lines represent the mean (68% CI).

Figure	Short name	Genotype
Figure 1C	T4/T5>td Tomato	w-; UAS-myr::tdTomato/+; R42F06-Gal4/+
Figure 1D	T4/T5>td Tomato, nAChRα1	w-; UAS-myr::tdTomato/+; R42F06-Gal4/nAChRα1::EGFP
Figure 1E	T4/T5>td Tomato, nAChRα2	w-; UAS-myr::tdTomato/+; R42F06-Gal4/nAChRα2::EGFP
Figure 1F	T4/T5>td Tomato, nAChRα3	nAChRα3::ALFA/w-; UAS-myr::tdTomato/+; R42F06-Gal4/+
Figure 1G	T4/T5>td Tomato, nAChRα4	w-; UAS-myr::tdTomato/+; R42F06-Gal4/nAChRα4::EGFP
Figure 1H	T4/T5>td Tomato, nAChRα5	w-; UAS-myr::tdTomato/ nAChRα5::EGFP; R42F06-Gal4/+
Figure 1I	T4/T5>td Tomato, nAChRα6	w-; UAS-myr::tdTomato/ nAChRα6::EGFP; R42F06-Gal4/+
Figure 1J	T4/T5>td Tomato, nAChRα7	nAChRα7::EGFP/w-; UAS-myr::tdTomato/+; R42F06-Gal4/+
Figure 1K	T4/T5>td Tomato, nAChRβ1	w-; UAS-myr::tdTomato/+; R42F06-Gal4/nAChRβ1::HA
Figure 1M	T4/T5>td Tomato, mAChR-B	w-; UAS-myr::tdTomato/ UAS-mAChR-B::HA; R42F06-Gal4/+
Figure 2A	Tm1> Brp^{short}, nAChRα1, nAChRα3, nAChRα4, nAChRα5, nAChRα7, nAChRβ1	w-; UAS-Brp^{short}::mStrawberry/+; R74G01-Gal4/ nAChRα1::EGFP nAChRα3::ALFA/w-; UAS-Brp^{short}::mStrawberry/+; R74G01-Gal4/+ w-; UAS-Brp^{short}::mStrawberry/+; R74G01-Gal4/ nAChRα4::EGFP w-; UAS-Brp^{short}::mStrawberry/ nAChRα5::EGFP; R74G01-Gal4/+ nAChRα7::EGFP/w-; UAS-Brp^{short}::mStrawberry/+; R74G01-Gal4/+ w-; UAS-Brp^{short}::mStrawberry/+; R74G01-Gal4/ nAChRβ1::HA
Figure 2B	Tm2> Brp^{short}, nAChRα1, nAChRα3, nAChRα4, nAChRα5, nAChRα7, nAChRβ1	w-; UAS-Brp^{short}::mStrawberry/+; VT012282-Gal4/ nAChRα1::EGFP nAChRα3::ALFA/w-; UAS-Brp^{short}::mStrawberry/+; VT012282-Gal4/+ w-; UAS-Brp^{short}::mStrawberry/+; VT012282-Gal4/ nAChRα4::EGFP

		w-; UAS-Brp^{short}::mStrawberry/ nAChRα5::EGFP; VT012282-Gal4/+ nAChRα7::EGFP/w-; UAS-Brp^{short}::mStrawberry/+; VT012282-Gal4/+ w-; UAS-Brp^{short}::mStrawberry/+; VT012282-Gal4/ nAChRβ1::HA
Figure 2C	Tm4> Brp^{short}, nAChRα1, nAChRα3, nAChRα4, nAChRα5, nAChRα7, nAChRβ1	w-; UAS-Brp^{short}::mStrawberry/+; R35H01-Gal4/ nAChRα1::EGFP nAChRα3::ALFA/w-; UAS-Brp^{short}::mStrawberry/+; R35H01-Gal4/+ w-; UAS-Brp^{short}::mStrawberry/+; R35H01-Gal4/ nAChRα4::EGFP w-; UAS-Brp^{short}::mStrawberry/ nAChRα5::EGFP; R35H01-Gal4/+ nAChRα7::EGFP/w-; UAS-Brp^{short}::mStrawberry/+; R35H01-Gal/+ w-; UAS-Brp^{short}::mStrawberry/+; R35H01-Gal4/ nAChRβ1::HA
Figure 2D	Tm9> Brp^{short}, nAChRα1, nAChRα3, nAChRα4, nAChRα5, nAChRα7, nAChRβ1	w-; UAS-Brp^{short}::mStrawberry/+; VT065303-Gal4/ nAChRα1::EGFP nAChRα3::ALFA/w-; UAS-Brp^{short}::mStrawberry/+; VT065303-Gal4/+ w-; UAS-Brp^{short}::mStrawberry/+; VT065303-Gal4/ nAChRα4::EGFP w-; UAS-Brp^{short}::mStrawberry/ nAChRα5::EGFP; VT065303-Gal4/+ nAChRα7::EGFP/w-; UAS-Brp^{short}::mStrawberry/+; VT065303-Gal4/+ w-; UAS-Brp^{short}::mStrawberry/+; VT065303-Gal4/ nAChRβ1::HA
Figure 3E	nAChRα3, nAChRβ1	nAChRα3::ALFA/w-; +; nAChRβ1::HA/+
Figure 3F	nAChRα5, nAChRβ1	w-; nAChRα5::EGFP/+; nAChRβ1::HA/+
Figure 3G	nAChRα3, nAChRα7	nAChRα7::EGFP/nAChRα3::ALFA; +; +
Figure 3H	nAChRα7, nAChRβ1	nAChRα7::EGFP/+; +; nAChRβ1::HA/+
Figure 4B	T4/T5> nAChRα1 RNAi, nAChRα1 RNAi (Ctrl)	w+; R42F06-p65.AD/+; VT043070-Gal4.DBD/ UAS-nAChRα1 RNAi w+; +; UAS-nAChRα1 RNAi/+
Figure 4C	T4/T5> nAChRα3 RNAi, nAChRα3 RNAi (Ctrl)	w+; R42F06-p65.AD/ UAS-nAChRα3 RNAi; VT043070-Gal4.DBD/ + w+; UAS-nAChRα3 RNAi/+; +
Figure 4D	T4/T5> nAChRα4 RNAi, nAChRα4 RNAi (Ctrl)	w+; R42F06-p65.AD/+; VT043070-Gal4.DBD/ UAS-nAChRα4 RNAi w+; +; UAS-nAChRα4 RNAi/+
Figure 4E	T4/T5> nAChRα5 RNAi, nAChRα5 RNAi (Ctrl)	w+; R42F06-p65.AD/+; VT043070-Gal4.DBD/ UAS-nAChRα5 RNAi w+; +; UAS-nAChRα5 RNAi/+
Figure 4F	T4/T5> nAChRα7 RNAi, nAChRα7 RNAi (Ctrl)	w+; R42F06-p65.AD/ UAS-nAChRα7 RNAi; VT043070-Gal4.DBD/ + w+; UAS-nAChRα7 RNAi/+; +
Figure 4G	T4/T5> mAChR-B RNAi, mAChR-B RNAi (Ctrl)	w+; R42F06-p65.AD/+; VT043070-Gal4.DBD/ UAS-mAChR-B RNAi w+; +; UAS-mAChR-B RNAi/+
Figure 5B	T4/T5c>GCaMP6m T4/T5> nAChRα4 RNAi, T4/T5c>GCaMP6m T4/T5>mCherry RNAi (Ctrl)	w+; R39H12-GAL4/+; VT50384-LexA, 13xLexAop-IVS-GCaMP6m/ UAS-nAChRα4 RNAi w+; R39H12-GAL4/+; VT50384-LexA, 13xLexAop-IVS-GCaMP6m/ UAS-mCherry RNAi Valium 20

Figure 5C	T4/T5c>GCaMP6m T4/T5> nAChRα5 RNAi, T4/T5c>GCaMP6m T4/T5>mCherry RNAi (Ctrl)	w+; R39H12-GAL4/+; VT50384-LexA, 13xLexAop-IVS-GCaMP6m/ UAS-nAChRα5 RNAi w+; R39H12-GAL4/+; VT50384-LexA, 13xLexAop-IVS-GCaMP6m/ UAS-mCherry RNAi Valium 20
Figure 5D	T4/T5c>GCaMP6m T4/T5> nAChRα7 RNAi, T4/T5c>GCaMP6m T4/T5>mCherry RNAi (Ctrl)	w+; R39H12-GAL4/ UAS-nAChRα7 RNAi; VT50384-LexA, 13xLexAop-IVS-GCaMP6m/ + w+; R39H12-GAL4/+; VT50384-LexA, 13xLexAop-IVS-GCaMP6m/ UAS-mCherry RNAi Valium 20
Figure 5E	T4/T5c>GCaMP6m T4/T5> mAChR-B RNAi, T4/T5c>GCaMP6m T4/T5>mCherry RNAi (Ctrl)	w+; R39H12-GAL4/+; VT50384-LexA, 13xLexAop-IVS-GCaMP6m/ UAS-mAChR-B RNAi w+; R39H12-GAL4/+; VT50384-LexA, 13xLexAop-IVS-GCaMP6m/ UAS-mCherry RNAi Valium 20
Figure S1A	nAChRα7	nAChRα7::EGFP; +; +
Figure S1B	nAChRα7	nAChRα7::EGFP; +; + nAChRα7::ALFA; +; +
Figure S1C	nAChRα5, Canton S	w+; nAChRα5::EGFP; + w+; +; +
Figure S1D	nAChRα2	w-; +; nAChRα2::EGFP
Figure S1E	T4/T5>td Tomato, nAChRα5	w-; UAS-myr::tdTomato/ nAChRα5::EGFP; R42F06-Gal4/+
Figure S2B	T4/T5>td Tomato, nAChRα1	w-; UAS-myr::tdTomato/+; R42F06-Gal4/nAChRα1::EGFP
Figure S2C	T4/T5>td Tomato, nAChRα2	w-; UAS-myr::tdTomato/+; R42F06-Gal4/nAChRα2::EGFP
Figure S2D	T4/T5>td Tomato, nAChRα3	nAChRα3::ALFA/w-; UAS-myr::tdTomato/+; R42F06-Gal4/+
Figure S2E	T4/T5>td Tomato, nAChRα4	w-; UAS-myr::tdTomato/+; R42F06-Gal4/nAChRα4::EGFP
Figure S2F	T4/T5>td Tomato, nAChRα5	w-; UAS-myr::tdTomato/ nAChRα5::EGFP; R42F06-Gal4/+
Figure S2G	T4/T5>td Tomato, nAChRα6	w-; UAS-myr::tdTomato/ nAChRα6::EGFP; R42F06-Gal4/+
Figure S2H	T4/T5>td Tomato, nAChRα7	nAChRα7::EGFP/w-; UAS-myr::tdTomato/+; R42F06-Gal4/+
Figure S2I	T4/T5>td Tomato, nAChRβ1	w-; UAS-myr::tdTomato/+; R42F06-Gal4/nAChRβ1::HA
Figure S2J	T4/T5>td Tomato, mAChR-B	w-; UAS-myr::tdTomato/ UAS-mAChR-B::HA; R42F06-Gal4/+
Figure S2K	Pan-neuronal> mAChR-B	w-; UAS-mAChR-B::HA/+; GMR57C10-Gal4 /+
Figure S3A	T4/T5> nAChRα1 RNAi, nAChRα1 (Ctrl)	w-; +; nAChRα1::EGFP w-; R42F06-Gal4/+; nAChRα1::EGFP/UAS-nAChRα1 RNAi
Figure S3B	T4/T5> nAChRα3 RNAi, nAChRα3 (Ctrl)	nAChRα3::ALFA; +;+ nAChRα3::ALFA; UAS-nAChRα3 RNAi/+; R42F06-Gal4/+
Figure S3C	T4/T5> nAChRα4 RNAi, nAChRα4 (Ctrl)	w-; +; nAChRα4::EGFP w-; R42F06-Gal4/+; nAChRα4::EGFP/UAS-nAChRα4 RNAi

Figure S3D	T4/T5> nAChRα5 RNAi, nAChRα5 (Ctrl)	w-; nAChRα5::EGFP; + w-; nAChRα5::EGFP/ R42F06-Gal4; UAS-nAChRα5 RNAi/+
Figure S3E	T4/T5> nAChRα7 RNAi, nAChRα7 (Ctrl)	nAChRα7::EGFP; +; + nAChRα7::EGFP/w-; UAS-nAChRα7 RNAi/+; R42F06-Gal4/+
Figure S3F	T4/T5> nAChRβ1 RNAi, nAChRβ1 (Ctrl)	w-; +; nAChRβ1::HA w-; R42F06-Gal4/+; UAS-nAChRβ1 RNAi/ nAChRβ1::HA
Figure S3G	T4/T5> mAChR-B RNAi, mAChR-B (Ctrl)	w-; UAS-mAChR-B::HA/cyo; R42F06-Gal4/TM6B w-; UAS-mAChR-B::HA/ UAS-mAChR-B RNAi; R42F06-Gal4/+
Figure S3I	T4/T5>td Tomato	w-; UAS-myr::tdTomato/+; R42F06-Gal4/+
Figure S3J	T4/T5>td GFP	w-; R42F06-p65.AD /sp; VT043070-Gal4.DBD/ UAS-CD4::tdGFP
Figure S3K	T4/T5>mCherry RNAi (Ctrl), T4/T5>nAChRα5 RNAi, T4/T5>nAChRα7 RNAi, Tm9>hid	w-; +; R42F06-Gal4/UAS-mCherry RNAi Valium 20 w-; +; R42F06-Gal4/UAS-nAChRα5 RNAi w-; UAS-nAChRα7 RNAi/+; R42F06-Gal4/+ w-; +; UAS-hid/VT065303-Gal4
Figure S4A	nAChRα1>GFP, T4/T5>RFP	w-; R42F06-LexA, LexAop-CD8::RFP,UAS-CD8::GFP/+; nAChRα1 Mi-GAL4/mkrs or Tm6b
Figure S4B	nAChRα2>GFP, T4/T5>RFP	w-; R42F06-LexA, LexAop-CD8::RFP,UAS-CD8::GFP/+; nAChRα2 T2A-GAL4/mkrs or Tm6b
Figure S4C	nAChRα3>GFP, T4/T5>RFP	nAChRα3 T2A-GAL4/+; R42F06-LexA, LexAop-CD8::RFP,UAS-CD8::GFP/+; mkrs or +/ Tm6b or +
Figure S4D	nAChRα4>GFP, T4/T5>RFP	w-; R42F06-LexA, LexAop-CD8::RFP,UAS-CD8::GFP/nAChRα4-Gal4; mkrs or +/ Tm6b or +
Figure S4E	nAChRα5>GFP, T4/T5>RFP	w-; R42F06-LexA, LexAop-CD8::RFP,UAS-CD8::GFP/nAChRα5 Mi-GAL4; mkrs or +/ Tm6b or +
Figure S4F	nAChRα6>GFP, T4/T5>RFP	w-; R42F06-LexA, LexAop-CD8::RFP,UAS-CD8::GFP/ nAChRα6 Mi-GAL4; mkrs or +/ Tm6b or +
Figure S4G	nAChRα7>GFP, T4/T5>RFP	nAChRα7 Mi-GAL4/+; R42F06-LexA, LexAop-CD8::RFP,UAS-CD8::GFP/+; mkrs or +/ Tm6b or +
Figure S4H	nAChRβ1>GFP, T4/T5>RFP	w-; R42F06-LexA, LexAop-CD8::RFP,UAS-CD8::GFP/+; nAChRβ1-GAL4/mkrs or Tm6b
Figure S4I	nAChRβ2>GFP, T4/T5>RFP	w-; R42F06-LexA, LexAop-CD8::RFP,UAS-CD8::GFP/+; nAChRβ2 T2A-GAL4 /mkrs or Tm6b
Figure S4J	nAChRβ3>GFP, T4/T5>RFP	w-; R42F06-LexA, LexAop-CD8::RFP,UAS-CD8::GFP/ nAChRβ3 T2A-GAL4; mkrs or +/ Tm6b or +

Figure S4K	mAChR-A>GFP, T4/T5>RFP	w-; R42F06-LexA, LexAop-CD8::RFP,UAS-CD8::GFP/+; mAChR-A Mi-GAL4/mkrs or Tm6b
Figure S4L	mAChR-B>GFP, T4/T5>RFP	w-; R42F06-LexA, LexAop-CD8::RFP,UAS-CD8::GFP/+; mAChR-B T2A-GAL4 /mkrs or Tm6b
Figure S5A	Tm1 (Gal4) >MCFO	hs-FLPG5.PEST/w-; +; 10xUAS(FRT.stop)myr::smGdP-HA,10xUAS(FRT.stop)myr::smGdP-V5-THS, 10xUAS(FRT.stop)myr::smGdP-FLAG/ R74G01-Gal4
Figure S5B	Tm1 (Gal4) >GFP	w-; UAS-CD8::GFP/+; R74G01-Gal4/+
Figure S5C	Tm1 (LexA) >mCherry	w-; LexAop-myr::mCherry/ VT041034-LexAGAD; +
Figure S5D	Tm2 (Gal4) >MCFO	hs-FLPG5.PEST/w-; +; 10xUAS(FRT.stop)myr::smGdP-HA,10xUAS(FRT.stop)myr::smGdP-V5-THS, 10xUAS(FRT.stop)myr::smGdP-FLAG/ VT012282-Gal4
Figure S5E	Tm2 (Gal4) >GFP	w-; UAS-CD8::GFP/+; VT012282-Gal4/+
Figure S5F	Tm2 (LexA) >mCherry	w-; LexAop-myr::mCherry/ VT058650-LexAGAD; +
Figure S5G	Tm4 (Gal4) >MCFO	hs-FLPG5.PEST/w-; +; 10xUAS(FRT.stop)myr::smGdP-HA,10xUAS(FRT.stop)myr::smGdP-V5-THS, 10xUAS(FRT.stop)myr::smGdP-FLAG/ R35H01-Gal4
Figure S5H	Tm4 (Gal4) >GFP	w-; UAS-CD8::GFP/+; R35H01-Gal4/+
Figure S5I	Tm4 (LexA) >mCherry	w-; LexAop-myr::mCherry/ R53C02-LexAGAD; +
Figure S5J	Tm9 (Gal4) >MCFO	hs-FLPG5.PEST/w-; +; 10xUAS(FRT.stop)myr::smGdP-HA,10xUAS(FRT.stop)myr::smGdP-V5-THS, 10xUAS(FRT.stop)myr::smGdP-FLAG/ VT065303-Gal4
Figure S5K	Tm9 (Gal4) >GFP	w-; UAS-CD8::GFP/+; VT065303-Gal4/+
Figure S5L	Tm9 (LexA) >mCherry	w-; LexAop-myr::mCherry/ GMR13E12-LexA; +
Figure S5M	Tm1, Tm2, Tm4, Tm9>tGRASP	w-; VT25965-LexAGAD/+; 13xLexAop2-post-t-GRASP, 20xUAS-pre-t-GRASP/ R74G01-Gal4 w-; VT25965-LexAGAD/+; 13xLexAop2-post-t-GRASP, 20xUAS-pre-t-GRASP/ VT012282-Gal4 w-; VT25965-LexAGAD/+; 13xLexAop2-post-t-GRASP, 20xUAS-pre-t-GRASP/ R35H01-Gal4 w-; VT25965-LexAGAD/+; 13xLexAop2-post-t-GRASP, 20xUAS-pre-t-GRASP/ VT065303-Gal4
Figure S5N	Tm1, Tm2, Tm4, Tm9>sybGRASP	w-; UAS-nSyb-spGFP1-10, lexAop-CD4-spGFP11; VT25965-LexAp65/ R74G01-Gal4

		w-; UAS-nSyb-spGFP1-10, lexAop-CD4-spGFP11; VT25965-LexAp65/ VT012282-Gal4 w-; UAS-nSyb-spGFP1-10, lexAop-CD4-spGFP11; VT25965-LexAp65/ R35H01-Gal4 w-; UAS-nSyb-spGFP1-10, lexAop-CD4-spGFP11; VT25965-LexAp65/ VT065303-Gal4
Figure S5O	Tm1, Tm2, Tm4, Tm9> Brp^{short}	w-; UAS-Brp^{short}::GFP/+; R74G01-Gal4/+ w-; UAS-Brp^{short}::GFP/+; VT012282-Gal4 /+ w-; UAS-Brp^{short}::GFP/+; R35H01-Gal4/+ w-; UAS-Brp^{short}::GFP/+; VT065303-Gal4/+
Figure S6A	Mi9>Brp^{short}, nAChRα5	w-; nAChRα5::EGFP/8xLexAop2-Brp^{short}::mcherry; GMR48A07-LexA/+
Figure S6B	Mi9>Brp^{short}, T4/T5>GluClα	w-; UAS-GluClα::GFP/8xLexAop2-Brp^{short}::mcherry; R42F06 Gal4/GMR48A07-LexA
Figure S6C	Tm3>Brp^{short}, T4/T5>Rdl	w-; UAS-Rdl::GFP/8xLexAop2-Brp^{short}::mcherry; R42F06-Gal4/ GMR13E12-LexA
Figure S6E	Tm1, Tm2, Tm4, Tm9> Brp^{short}	w-; UAS-Brp^{short}::mStrawberry/+; R74G01-Gal4/ + w-; UAS-Brp^{short}::mStrawberry/+; VT012282-Gal4/ + w-; UAS-Brp^{short}::mStrawberry/+; R35H01-Gal4/ + w-; UAS-Brp^{short}::mStrawberry/+; VT065303-Gal4/ +
Figure S7A		As in Figure 2A-D.
Figure S8B	Tm9>sybCRASP, nAChRα7	nAChRα7::EGFP /w-; VT25965-LexAGAD/ LexAop-CD4-spGFP11; VT065303-Gal4/ UAS-syb-spCFP1-10
Figure S8D	Tm9>Brp^{short}, T4/T5>mAChR-B	w-; R24C08-LexAp65/ UAS-mAChR-B::HA, 8xLexAop2- Brp^{short}::mCherry; R42F06-Gal4/+
Figure S8E	T4/T5>mAChR-B, nAChRα5	w-; UAS-mAChR-B::HA / nAChRα5::EGFP; R42F06-Gal4/+
Figure S9A	T4/T5> nAChRβ1 RNAi, nAChRβ1 RNAi (Ctrl)	w+; R42F06-p65.AD/+; VT043070-Gal4.DBD/ UAS- nAChRβ1 RNAi w+; +; UAS-nAChRβ1 RNAi/+
Figure S9B	T4/T5> mAChR-A RNAi, mAChR-A RNAi (Ctrl)	w+; R42F06-p65.AD/+; VT043070-Gal4.DBD/ UAS-mAChR-A RNAi w+; +; UAS-mAChR-A RNAi/+
Figure S9D	T4/T5> mCherry V.10 RNAi, mCherry V.10 RNAi (Ctrl)	w+; R42F06-p65.AD/+; VT043070-Gal4.DBD/ UAS-mCherry RNAi Valium 10 w+; +; UAS-mCherry RNAi Valium 10/+
Figure S9E	T4/T5> mCherry V.20 RNAi, mCherry V.20 RNAi (Ctrl)	w+; R42F06-p65.AD/+; VT043070-Gal4.DBD/ UAS-mCherry RNAi Valium 20 w+; +; UAS-mCherry RNAi Valium 20/+
Figure S9F	T4/T5, Canton S	w+; R42F06-p65.AD/+; VT043070-Gal4.DBD/+ w+; +; +

Figure S9G	T4/T5> nAChRα5 RNAi, T4/T5> nAChRα7 RNAi, T4/T5> nAChRα5 RNAi & nAChRα7 RNAi	w+; R42F06-p65.AD/+; VT043070-Gal4.DBD/ UAS-nAChRα5 RNAi w+; R42F06-p65.AD/ UAS-nAChRα7 RNAi; VT043070-Gal4.DBD/ + w+; R42F06-p65.AD/ UAS-nAChRα7 RNAi; VT043070-Gal4.DBD/ UAS-nAChRα5 RNAi
Figure S9H	Canton S, nAChRα7-KO	w+; +; + nAChRα7-KO; +; +
Figure S9I	nAChRα7-KO	nAChRα7-KO; +; +
Figure S9J	nAChRα5, nAChRα5 nAChRα7-KO	w-; nAChRα5::EGFP; + nAChRα7-KO; nAChRα5::EGFP/+; +
Figure S9K	Tm9> Shibire, Shibire (Ctrl)	w+; UAS-Shibire^{ts}/+; VT065303-Gal4/+ w+; UAS-Shibire^{ts}/+; +
Figure S10B	T4/T5c>GCaMP6m	w+; R39H12-GAL4/+; VT50384-LexA, 13xLexAop-IVS-GCaMP6m/ +
Figure S10C	T4/T5c>GFP	w-; UAS-CD8::GFP/+; VT50384-Gal4/+
Figure S10D		As in Figure 5B-E.
Figure S11B	T4/T5c>GCaMP6m T4/T5>mCherry RNAi	w+; R39H12-GAL4/+; VT50384-LexA, 13xLexAop-IVS-GCaMP6m/ UAS-mCherry RNAi Valium 20
Figure S11C	T4/T5c>GCaMP6m T4/T5> nAChRα5 RNAi, T4/T5c>GCaMP6m T4/T5>mCherry RNAi (Ctrl)	w+; R39H12-GAL4/+; VT50384-LexA, 13xLexAop-IVS-GCaMP6m/ UAS-nAChRα5 RNAi w+; R39H12-GAL4/+; VT50384-LexA, 13xLexAop-IVS-GCaMP6m/ UAS-mCherry RNAi Valium 20

Table S1. List of fly experimental genotypes, related to STAR Methods.

Figure	Comparison	Statistical test	p-value	Significance
Figure 3I	nAChRα3, nAChRα5, nAChRα7 and nAChRβ1 pairs	Kruskal-Wallis test followed by Dunn's post hoc test	p<0.0001	****
Figure 4H	UAS-nAChRα1-RNAi with nAChRα1 knock-down	Two-tailed Mann–Whitney U-test	p=0.7865	ns
	T4/T5 with nAChRα1 knock-down	Two-tailed Mann–Whitney U-test	p=0.3141	ns
	mCherry Valium 10 knock-down with nAChRα1 knock-down	Two-tailed Mann–Whitney U-test	p=0.2990	ns
	Canton S with nAChRα1 knock-down	Two-tailed Mann–	p=0.2143	ns

		Whitney U-test		
	UAS-nAChRα3-RNAi with nAChRα3 knock-down	Two-tailed unpaired Student's t-test	p=0.5286	ns
	T4/T5 with nAChRα3 knock-down	Two-tailed Mann–Whitney U-test	p=0.022	*
	mCherry Valium 20 knock-down with nAChRα3 knock-down	Two-tailed unpaired Student's t-test	p=0.6835	ns
	Canton S with nAChRα3 knock-down	Two-tailed Mann–Whitney U-test	p=0.9788	ns
	UAS-nAChRα4-RNAi with nAChRα4 knock-down	Two-tailed unpaired Student's t-test	p=0.0429	*
	T4/T5 with nAChRα4 knock-down	Two-tailed Mann–Whitney U-test	p<0.0001	****
	mCherry Valium 10 knock-down with nAChRα4 knock-down	Two-tailed unpaired Student's t-test	p=0.1789	ns
	Canton S with nAChRα4 knock-down	Two-tailed Mann–Whitney U-test	p=0.0592	ns
	UAS-nAChRα5-RNAi with nAChRα5 knock-down	Two-tailed Mann–Whitney U-test	p=0.0023	**
	T4/T5 with nAChRα5 knock-down	Two-tailed Mann–Whitney U-test	p=0.1579	ns
	mCherry Valium 20 knock-down with nAChRα5 knock-down	Two-tailed Mann–Whitney U-test	p=0.0087	**
	Canton S with nAChRα5 knock-down	Two-tailed Mann–Whitney U-test	p=0.0094	**
	UAS-nAChRα7-RNAi with nAChRα7 knock-down	Two-tailed Mann–Whitney U-test	p=0.0107	*
	T4/T5 with nAChRα7 knock-down	Two-tailed Mann–Whitney U-test	p=0.0617	ns

	mCherry Valium 20 knock-down with nAChRα7 knock-down	Two-tailed Mann–Whitney U-test	p=0.0008	***
	Canton S with nAChRα7 knock-down	Two-tailed Mann–Whitney U-test	p=0.0019	**
	UAS-mAChR-B-RNAi with mAChR-B knock-down	Two-tailed Mann–Whitney U-test	p=0.0006	***
	T4/T5 with mAChR-B knock-down	Two-tailed Mann–Whitney U-test	p=0.0093	**
	mCherry Valium 20 knock-down with mAChR-B knock-down	Two-tailed Mann–Whitney U-test	p=0.7557	ns
	Canton S with mAChR-B knock-down	Two-tailed Mann–Whitney U-test	p=0.8238	ns
	UAS-mCherry Valium 10 RNAi with mCherry Valium 10 knock-down	Two-tailed unpaired Student's t-test	p=0.4173	ns
	UAS-mCherry Valium 20 RNAi with mCherry Valium 20 knock-down	Two-tailed unpaired Student's t-test	p=0.0464	*
	mCherry Valium 10 knock-down with mCherry Valium 20 knock-down	Two-tailed unpaired Student's t-test	p=0.6839	ns
Figure 5F	nAChRα4-RNAi with mCherry-RNAi Valium 20	Two-tailed Mann–Whitney U-test	p=0.0262	*
	nAChRα5-RNAi with mCherry-RNAi Valium 20	Two-tailed unpaired Student's t-test	p=0.0008	***
	nAChRα7-RNAi with mCherry-RNAi Valium 20	Two-tailed unpaired Student's t-test	p=0.1061	ns
	mAChR-B-RNAi - RNAi with mCherry-RNAi Valium 20	Two-tailed unpaired Student's t-test	p=0.0111	*
Figure S1C	Canton S with nAChRα5::EGFP	Two-tailed Mann–Whitney U-test	p=0.9224	ns

Figure S2L	nAChRα1 EGFP to nAChRα1-EGFP & UAS-nAChRα1-RNAi	Two-tailed unpaired Student's t-test	p<0.0001	****
	nAChRα3 EGFP to nAChRα3-EGFP & UAS-nAChRα3-RNAi	Two-tailed unpaired Student's t-test	p<0.0001	****
	nAChRα5 EGFP to nAChRα5-EGFP & UAS-nAChRα5-RNAi	Two-tailed unpaired Student's t-test	p=0.016	*
	nAChRα7 EGFP to nAChRα7-EGFP & UAS-nAChRα7-RNAi	Two-tailed Mann–Whitney U-test	p<0.0001	****
	nAChRβ1 EGFP to nAChRβ1-EGFP & UAS-nAChRβ1-RNAi	Two-tailed Mann–Whitney U-test	p=0.5468	ns
Figure S3H	nAChRα1 EGFP to nAChRα1-EGFP & UAS-nAChRα1-RNAi	Two-tailed unpaired Student's t-test	p=0.0009	***
	nAChRα3 EGFP to nAChRα3-EGFP & UAS-nAChRα3-RNAi	Two-tailed unpaired Student's t-test	p<0.0001	****
	nAChRα4 EGFP to nAChRα4-EGFP & UAS-nAChRα4-RNAi	Two-tailed unpaired Student's t-test	p=0.0022	**
	nAChRα5 EGFP to nAChRα5-EGFP & UAS-nAChRα5-RNAi	Two-tailed unpaired Student's t-test	p=0.0004	***
	nAChRα7 EGFP to nAChRα7-EGFP & UAS-nAChRα7-RNAi	Two-tailed Mann–Whitney U-test	p<0.0001	****
	nAChRβ1 EGFP to nAChRβ1-EGFP & UAS-nAChRβ1-RNAi	Two-tailed Mann–Whitney U-test	p=0.0810	ns
	mAChR-B::HA to mAChR-B::HA & UAS- mAChR-B-RNAi	Two-tailed Mann–Whitney U-test	p<0.0001	****
Figure S3K	mCherry knock-down with nAChRα5 knock-down	Two-tailed unpaired Student's t-test	p=0.7696	ns
	mCherry knock-down with nAChRα7 knock-down	Two-tailed unpaired Student's t-test	p=0.0928	ns
	mCherry knock-down with apoptotic Tm9	Two-tailed unpaired	p<0.0001	****

		Student's t-test		
	nAChRα5 knock-down with apoptotic Tm9	Two-tailed unpaired Student's t-test	p<0.0001	****
	nAChRα7 knock-down with apoptotic Tm9	Two-tailed unpaired Student's t-test	p<0.0001	****
Figure S9C	UAS-nAChRβ1-RNAi with nAChRβ1 knock-down	Two-tailed unpaired Student's t-test	p=0.4021	ns
	T4/T5 with nAChRβ1 knock-down	Two-tailed Mann–Whitney U-test	p=0.1833	ns
	mCherry Valium 10 knock-down with nAChRβ1 knock-down	Two-tailed unpaired Student's t-test	p=0.1258	ns
	Canton S with nAChRβ1 knock-down	Two-tailed Mann–Whitney U-test	p=0.2400	ns
	UAS-mAChR-A-RNAi with mAChR-A knock-down	Two-tailed unpaired Student's t-test	p=0.8898	ns
	T4/T5 with mAChR-A knock-down	Two-tailed Mann–Whitney U-test	p=0.0029	**
	mCherry Valium 20 knock-down with mAChR-A knock-down	Two-tailed unpaired Student's t-test	p=0.8733	ns
	Canton S with mAChR-A knock-down	Two-tailed Mann–Whitney U-test	p=0.8307	ns
Figure S9G	nAChRα5 knock-down with nAChRα5 & nAChRα7 knock-down	Two-tailed Mann–Whitney U-test	p=0.4948	ns
	nAChRα7 knock-down with nAChRα5 & nAChRα7 knock-down	Two-tailed Mann–Whitney U-test	p=0.4488	ns
Figure S9J	nAChRα5 WT with nAChRα5-nAChRα7 knock-out	Two-tailed unpaired Student's t-test	p=0.0014	**
Figure S9K	Tm9 shibire^{ts} with nAChRα7 knock-down	Two-tailed Mann–	p=0.0092	**

		Whitney U-test		
	Tm9 shibire^{ts} with nAChRα5 knock-down	Two-tailed Mann–Whitney U-test	p=0.0437	*
	shibire^{ts} with Tm9 shibire^{ts}	Two-tailed Mann–Whitney U-test	p=0.0247	*

Table S2. Statistical analysis, related to STAR Methods.

T5a	720575940643169933	720575940625654759	720575940616396703	720575940621106368	720575940626820538
Tm1	720575940620976493 720575940608883465 720575940623583428 720575940627201308 720575940619723643 720575940640955088 720575940627479836	720575940622364961 720575940621146733 720575940608883465 720575940613587935 720575940616994134	720575940620523540 720575940608195339 720575940613587935 720575940634579135 720575940616994134	720575940621146733 720575940633875117 720575940643191949	720575940616994134 720575940621146733 720575940613587935
Tm2	720575940630551670 720575940622364961 720575940640230259 720575940621868276 720575940623081942	720575940632142904 720575940640453437 720575940640230259	720575940630308663 720575940640947152 720575940619708888 720575940632142904 720575940615716418	720575940625164327 720575940615731359 720575940640453437	720575940619708888 720575940632142904 720575940615731359
Tm4	720575940637976666 720575940620745163	720575940621582401 720575940620745163 720575940620782171 720575940637976666	720575940639445582 720575940620782171 720575940614824338 720575940638140506 720575940627035198	720575940625442492 720575940621582401 720575940615720258 720575940613610642	720575940638140506 720575940620782171 720575940615720258 720575940639445582 720575940620745163
Tm9	720575940616384742 720575940628740039 720575940613374873 720575940617906589 720575940620814356 720575940630425564 720575940624565296	720575940613374873 720575940620814356 720575940609254851 720575940626242348 720575940623771061 720575940626578965	720575940610056654 720575940637539806 720575940626242348 720575940620680277 720575940631934039 720575940626578965 720575940653151649 720575940625797936	720575940626254892 720575940620814356 720575940623771061 720575940621776664 720575940626242348 720575940617906589 720575940610056654	720575940625797936 720575940626242348 720575940623771061 720575940610056654 720575940620814356
T5c	720575940625825424	720575940618172121	720575940621915558	720575940619398981	720575940644937160
Tm1	720575940627479836 720575940608883465 720575940630729410 720575940623583428	720575940613587935 720575940616994134 720575940643191949 720575940621146733 720575940620523540	720575940616994134 720575940620523540 720575940621146733 720575940634426905	720575940616994134 720575940633875117 720575940633395999 720575940620523540 720575940626742814	720575940608195339 720575940634426905 720575940616994134 720575940620523540 720575940614334114 720575940634579135
Tm2	720575940622364961 720575940640230259 720575940621868276 720575940632142904 720575940624518408	720575940632142904 720575940640453437 720575940624518408	720575940619708888 720575940630308663 720575940632142904 720575940640453437 720575940615731359	720575940625164327 720575940619708888 720575940615731359 720575940632142904 720575940640453437 720575940640947152	720575940640947152 720575940644137416 720575940619708888 720575940615731359 720575940630772342 720575940627321981
Tm4	720575940620745163 720575940617429977 720575940621582401 720575940614824338	720575940620782171 720575940625442492	720575940639445582 720575940620782171 720575940615720258 720575940627035198 720575940621582401	720575940615720258 720575940639445582 720575940638273513 720575940625442492 720575940620782171	720575940638140506 720575940639445582 720575940631619468
Tm9	720575940626578965 720575940609254851 720575940620814356 720575940630942551 720575940613374873 720575940630425564 720575940617906589 720575940626242348	720575940610056654 720575940626578965 720575940626242348 720575940623771061 720575940631934039 720575940620814356	720575940625797936 720575940631934039 720575940637539806 720575940610056654 720575940620680277 720575940623771061 720575940626578965 720575940626242348	720575940625797936 720575940610056654 720575940616917004 720575940620680277 720575940623771061 720575940626242348 720575940637539806	720575940620680277 720575940612259221 720575940610056654 720575940653151649 720575940613033907 720575940637539806 720575940631934039

Table S3. FlyWire neuronal IDs, related to STAR Methods.

Supplemental references

[S1] Pribbenow, C., Chen, Y., Heim, M.-M., Laber, D., Reubold, S., Reynolds, E., Balles, I., Fernández-d V Alquicira, T., Suárez-Grimalt, R., Scheunemann, L., et al. (2022). Postsynaptic plasticity of cholinergic synapses underlies the induction and expression of appetitive and familiarity memories in *Drosophila*. eLife *11*, e80445. https://doi.org/10.7554/eLife.80445.

[S2] Sanfilippo, P., Kim, A.J., Bhukel, A., Yoo, J., Mirshahidi, P.S., Pandey, V., Bevir, H., Yuen, A., Mirshahidi, P.S., Guo, P., et al. (2024). Mapping of multiple neurotransmitter receptor subtypes and distinct protein complexes to

the connectome. Neuron *112*, 942-958.e13. https://doi.org/10.1016/j. neuron. 2023.12.014.

[S3] Davis, F.P., Nern, A., Picard, S., Reiser, M.B., Rubin, G.M., Eddy, S.R., and Henry, G.L. (2020). A genetic, genomic, and computational resource for exploring neural circuit function. eLife *9*, e50901. https://doi.org/10.7554/eLife.50901.

[S4] Hoermann, N., Schilling, T., Haji Ali, A., Serbe, E., Mayer, C., Borst, A., and Pujol-Martí, J. (2020). A combinatorial code of transcription factors specifies subtypes of visual motion-sensing neurons in *Drosophila*. Development, dev.186296. https://doi.org/10.1242/dev.186296.

3 | DISCUSSION

In this doctoral thesis, I tackled the morphological and molecular characteristics of cholinergic excitatory synapses in the OFF-motion vision circuitry of *Drosophila*. First, I explored the polyadic morphology of Tm-to-T5 connections, in an effort to understand the purpose of a divergence at the single bouton level (**Manuscript 1**). With this work, I found different polyadic synapse types, which introduced distinct wiring architectures at the single T5 and T5 network level. Secondly, I studied the postsynaptic molecular identity of the four different Tm-to-T5 cholinergic synapses and found the differential distribution of the nicotinic α5 subunit across them (**Manuscript 2**). The functional implications of each subunit in the OFF-motion pathway were addressed with the use of reverse genetics, behavioral paradigms and functional imaging. Collectively, morphological and molecular data account for the complexity of the Tm-to-T5 cholinergic neurotransmission, ranging from receptor categories, receptor subunits-stoichiometries-isoforms, inter-bouton variety, up to T5 dendritic vs axonal terminal cholinergic niches. Nevertheless, my PhD work also raises a new set of questions, which I highlight in the following sections.

3.1 MORPHOLOGICAL SYNAPSE IDENTITIES

Morphological traits of synapses have been allocated to the postsynaptic compartment in terms of dendritic spine morphology. Thin, branched, mushroom and stubby spine subclasses have been characterized in the vertebrate nervous system, with each subclass serving a specific functional role (Bourne & Harris, 2007; Harris et al., 1992; Hayashi & Majewska, 2005; Hering & Sheng, 2001). In lobula plate tangential cells of the *Drosophila* optic lobe, all four subclasses have been encountered in different ratios (Leiss et al., 2009; Scott et al., 2003a, 2003b). I studied another, previously unexplored, synapse morphological trait (**Manuscript 1**), that of the polyadic morphology (Figure 5).

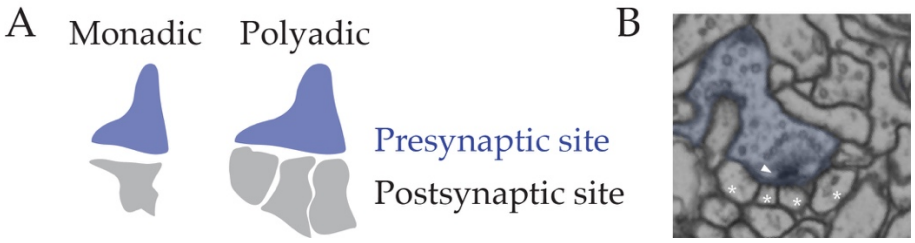

Figure 5. Polyadic synapse morphology. (A) *Drosophila* synapses are primarily polyadic, i.e. one presynaptic site forms connections with multiple postsynaptic densities of dendritic spines, instead of monadic where one presynaptic site connects with one postsynaptic density. (B) Example polyadic synapse from FlyWire (x=181521, y=46193, z=4887). Arrow indicates the presynaptic T-bar structure. Asterisks indicate postsynaptic densities that correspond to this axonal bouton.

3.1.1 Polyadic synapses in single T5 cells

Polyads have been encountered in various invertebrates (Meinertzhagen, 2016), such as the neuromuscular junction of *Caenorhabditis elegans* (Liu et al., 2007), the ascidian larva *Ciona intestinalis* (Ryan et al., 2016), the annelid *Malacoceros fuliginosus* (Seybold et al., 2025) and the photoreceptor synapse of the vertebrate retina (Rao-Mirotznik et al., 1998). Thanks to recent advancements in fruit fly wiring diagrams (Dorkenwald et al., 2024; Scheffer et al., 2020; Schlegel et al., 2024), the prevalence of the polyadic morphology across brain synapses was revealed. However, the implications of such a synapse morphology in neural wiring and function are not understood. As a first step to address this, I explored the polyadic wiring in T5a direction-selective cells of the OFF-motion pathway.

Each postsynaptic density of dendritic spines was allocated to an identity based on the T5 subtype it belonged to, eventually leading to eight combinations: a, ab, ac, ad, abc, abd, acd and abcd. Following the same allocation principles, eight combinations should be present in T5b, T5c and T5d subtypes, but this is left to future studies. An interesting question is what would be the functional consequences of polyadic synapses in T5 cells. Multiple T5 subtypes, across column borders, could be simultaneously activated by motion in one direction. Therefore, polyads might synchronize the T5 population, regardless of subtype, as previously suggested in *Caenorhabditis elegans* (Liu et al., 2007). Another important point is the characteristics of the simultaneous T5 activation. Diffusion of neurotransmitters as packages or single molecules (Rizzoli, 2014), neurotransmitter

recycling dynamics by perisynaptic glia (Chaturvedi et al., 2014) and dendritic spine location compared to the exocytotic sites spanning the active zone (transsynaptic nanocolumn) (Tang et al., 2016), might account for differences in the temporal and strength profiles of postsynaptic activation. Additionally, postsynaptic mechanisms such as receptor density and nanoarchitecture can affect dendritic spine activation properties (Caré & Soula, 2011; Sheng, 1996). Therefore, even though I identified an additional level of wiring complexity in our circuit of interest, its synaptic functional characteristics are extremely complicated. In mammals, the cholinergic neurotransmission between starbust amacrine and direction-selective retinal ganglion cells can also be achieved via a paracrine multi-directional transmission, where released transmitters diffuse relatively long distances to their target receptors (Barbour, 1994; Sethuramanujam et al., 2021; Szapiro & Barbour, 2007). One hypothesis is that the compact polyadic wiring excludes the previous mechanism and only allows for one-directional neurotransmission.

Tm1, Tm2, Tm4 and Tm9 cells have been found to wire on the central dendritic compartment of T5 dendrites, with Tm9 also extending to the most distal dendritic compartments (Braun et al., 2023; Shinomiya et al., 2019). Hence, could there be a sub-architecture within the previous wiring motif, dictated by the different polyadic types? Our work showed that the abcd polyadic synapse type was recapitulating the Tm1, Tm2, Tm4, Tm9-central and Tm9-distal dendritic arrangement, while the other types did not. A significant question is whether these polyadic type-specific dendritic arrangements extend to polyadic type-specific functions. This could potentially be addressed after morphologically characterizing each polyadic type. In the rat hippocampus, the area of the postsynaptic density dictates the number of glutamate receptors (Noguchi et al., 2005; Nusser et al., 1998), thus differences in postsynaptic density area between polyadic types may be indicative of distinct synaptic currents.

3.1.2 Polyadic synapses in the T5 population

In this thesis I showed another wiring motif introduced by the polyadic morphology, this time at the T5 network level. T5 subtypes residing at the same postsynaptic site together with the T5a neuron of analysis, namely co-T5s, exhibited oriented distributions in lobula layer one, depending on their input neuron type. Co-T5s from Tm1-, Tm2-, Tm4- and Tm9-to-T5a

connections extended posterior to the T5a of analysis and CT1-to-T5a co-T5s extended anterior (**Manuscript 1**). Therefore, excitation through the cholinergic Tm cells will progress posterior to the T5a of analysis and inhibition via the GABAergic CT1 will progress anterior. We would need more functional information to understand if this directional excitation acts to foreshadow the T5 network for an upcoming moving stimulus, while the inhibition suppresses the already activated T5 cells. Nonetheless, this shows how important it is to explore wiring motifs in a spatial embedding (Seung, 2024), such as the lobula neuropil. Therefore, the understudied polyadic synapses in *Drosophila* might hold the key for even more detailed single neuron biophysical models (Liu et al., 2022; Meier & Borst, 2019; Seung, 2025; Yang et al., 2016), where not only synapse numbers and location, but also single synapse morphology are taken into account.

3.2 MOLECULAR SYNAPSE IDENTITIES

The chemical synapse is a junction where a presynaptic site coordinates with a postsynaptic site to transmit information with a certain chemical identity. Pioneering work on characterizing connection strength pointed towards three factors: the number of synaptic contacts, the size of the postsynaptic depolarization caused by neurotransmitter release from a single synaptic vesicle (termed quantal size) and the probability of neurotransmitter release at each synapse (Branco & Staras, 2009; Del Castillo & Katz, 1954). The size of the postsynaptic depolarization as well as its dynamics is primarily coordinated by the neurotransmitter receptors at the postsynaptic density. Hence, beginning to understand the consortium of neurotransmitter receptors in postsynaptic sites of interest (**Manuscript 2**), is a key step to decode single synapse function.

3.2.1 The acetylcholine receptor variety

Acetylcholine receptors in *Drosophila* are highly heterogeneous. However, attributing their diversity in evolutionary redundancy might be a mistake (Sivilotti & Colquhoun, 1995), as their pharmacological and functional differences account for their importance. For example, the insecticidal effects of the snake venom α-Bungarotoxin can be induced only upon the presence of the α5, α6 and α7 nicotinic acetylcholine receptor subunits, as the ones bearing the respective toxin binding site (Korona et al., 2022), while the α1 subunit was found to be the main target of nicotine and neonicotinoids in *Drosophila* (Dederer et al., 2011;

Rosenthal & Yuan, 2021; Tomizawa et al., 1996; Tomizawa & Casida, 2003).

Acetylcholine receptor categories

The first level of acetylcholine receptor variety lies in their distinction into two categories: fast ionotropic nicotinic nAChRs on the one side and slow metabotropic muscarinic mAChRs on the other (Figure 6A). The major difference between the two categories is the time course of their postsynaptic effects, which can range from less than a millisecond to minutes, hours, or even days (Purves, 2001). mAChR-A and mAChR-C are coupled to the $G_{q/11}$ signalling cascade, which activates phospholipase C and an excitatory intracellular IP_3/Ca^{2+} cascade (Ren et al., 2015). However, transcriptomics suggest the low mAChR-C expression levels in the fly brain (Bielopolski et al., 2019; Davie et al., 2018; Rozenfeld et al., 2021). mAChR-B is coupled to the $G_{i/0}$ signalling cascade, which can either lead to an inhibition of adenylate cyclase resulting in a decrease of intracellular cAMP, or to the opening of a G protein-coupled potassium channel (GIRK of the Kir family), both leading to inhibition or hyperpolarisation of the target cells (Hulme et al., 1990; Kruse et al., 2014; Ren et al., 2015). Importantly, we too (Collin et al., 2013; Malloy et al., 2019; Manoim et al., 2022; Ren et al., 2015) have verified *in vivo* and for the first time in T5 cells the inhibitory role of mAChR-B (**Manuscript 2**). mAChR-B knock-down resulted in an increase of T5 calcium responses across all presented edge directions, while the rotational speed of the flies was increased, indicative of the receptor's inhibitory contribution. It would be pivotal to understand which of the two mAChR-B inhibitory mechanisms is mobilized in T5 cells. Functional imaging with cAMP indicators (Wang et al., 2022) could be used to evaluate cAMP levels pre- and post-T5 activation. Knocking-down the mAChR-B receptor while measuring ionic currents in T5 cells via the patch-clamp technique, would be ideal for identifying open potassium channels. If the latter mechanism is deployed, then mAChR-B would be an ideal candidate for better understanding the biophysical properties that govern T5 function.

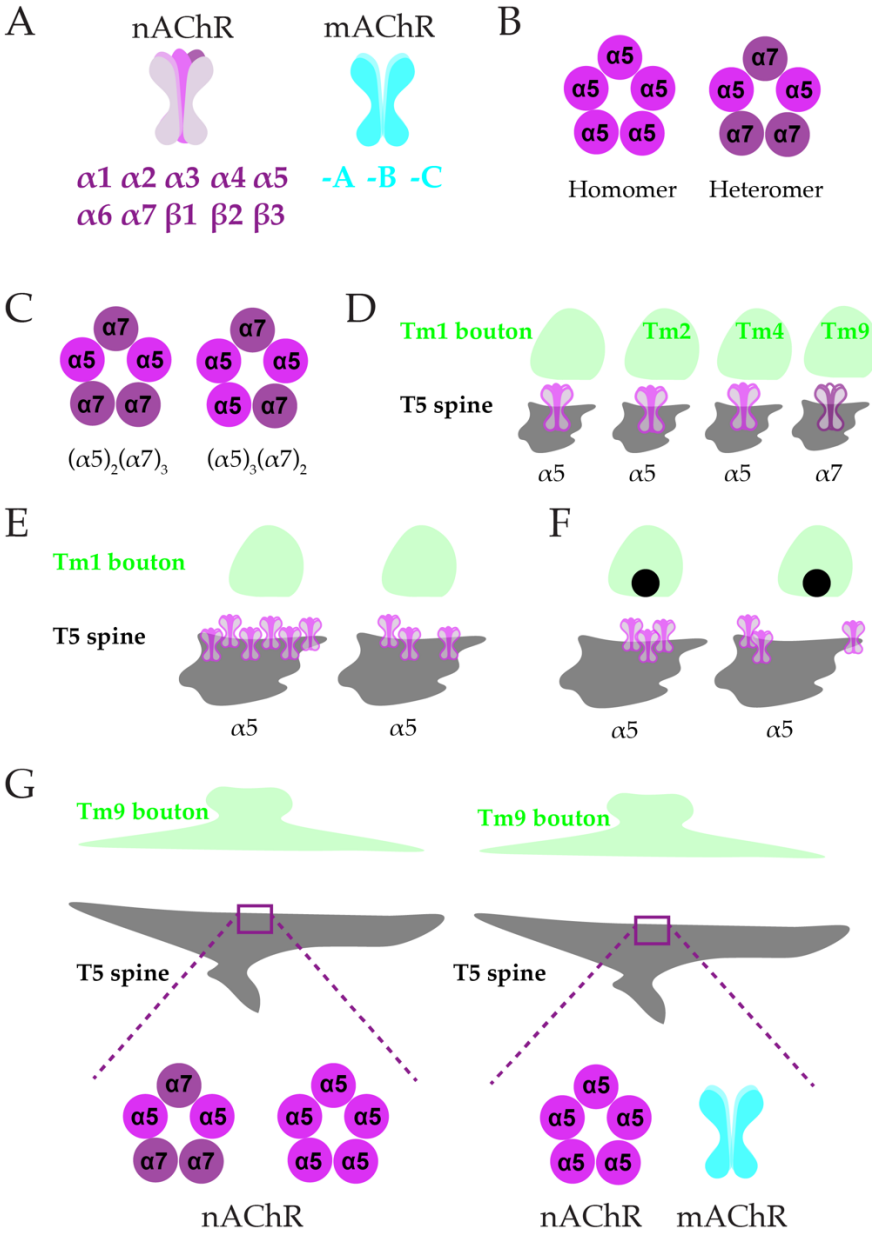

Figure 6. Acetylcholine receptor variety. (A) Acetylcholine receptors comprise of the nicotinic (nAChRs, magenta) and muscarinic (mAChRs, cyan) categories. nAChRs form pentamers from a set of seven α and three β subunits. mAChRs consist of three types, i.e. A, B and C. (B) nAChR pentamers can be formed by one subunit (homomeric) or multiple subunits (heteromeric). (C) nAChRs heteromers can exhibit different isoforms, while containing the same subunits. (D) Tm-to-T5 synapses demonstrate a differential postsynaptic receptor composition. Tm1-, Tm2-, Tm4-to-T5 synapses prefer the α5 subunit, whereas Tm9-to-T5 synapses prefer the α7 subunit. (E) Example of Tm1-to-T5 boutons where the α5 subunit displays high (left) and low (right) density. (F) Example of Tm1-to-T5 boutons where the α5 subunit localizes across the release site (black circle) (left) and further away (right). (G) Distinct axonal terminal boutons belonging to the same Tm9 neuron, might differ in their acetylcholine receptor composition. Example of a Tm9-to-T5 bouton

with nAChRs (left) and of a neighboring Tm9-to-T5 bouton with a nAChR & mAChR composition (right).

Nicotinic acetylcholine receptor stoichiometry

nAChRs contribute more to the acetylcholine receptor variety in *Drosophila* than mAChRs, primarily due to their pentameric formation. nAChRs are selective mainly to sodium, potassium and calcium and regulate their flow across the cell membrane by a tertiary conformational transition from resting to open state induced by the binding of acetylcholine (Ho et al., 2020). Multiple stoichometrical combinations can emerge from the pool of ten subunits that are expressed in the fly genome (Figure 6A,B), with subunit composition influencing the kinetics of the channel's conformational state transitions (Ho et al., 2020; Hurst et al., 2013). For example, in honeybees, the presence of the α7 subunit in antennal lobe cells and its absence from Kenyon cells controls the differences in kinetics between them (Dupuis et al., 2011). Our work (**Manuscript 2**) provided proof for the co-localization between the α3 and β1 subunit in lobula layer one. It certainly does not serve as proof for co-assembly, but it is the first *in vivo* indication for an α3 and β1 heteromer. Studies have shown that *in vitro* stoichiometries differentiate from the *in vivo* ones, and together with the lack of post-translational processing do not render *in vitro* approaches ideal for assessing nAChR function (Rosenthal & Yuan, 2021; Schloss et al., 1988, 1991). It is therefore important to explore the different receptor stoichiometries preferably *in vivo*. Only then the ionic conductance of the different nAChR stoichiometries could be measured *in vitro*. Interestingly, our experiments showed that calcium responses in T5 dendrites differed from calcium responses in T5 axonal terminals in α5 subunit knock-down flies (**Manuscript 2**). This may be the outcome of distinct α5 stoichiometries between the two T5 compartments.

Finally, one should also take into account the isoforms of each nAChR stoichiometry (Figure 6C). In mammals, the $(\alpha4)_3(\beta2)_2$ stoichiometrical isoform responds differently to various ACh concentrations compared to the $(\alpha4)_2(\beta2)_3$ (Weltzin et al., 2019). Therefore, an α3-β1 heteromer could for example correspond to a $(\alpha3)_2$ $(\beta1)_3$ or $(\alpha3)_3$ $(\beta1)_2$ isoform and exhibit different ionic conductance in response to acetylcholine binding.

Nicotinic acetylcholine receptor localization, density and synaptic organization

RNAseq data (Davis et al., 2020; Hoermann et al., 2020) are useful for understanding the extent of the nAChR variety in T5 cells.

Though helpful, mRNA levels do not follow a one-to-one relationship with protein levels, since post-transcriptional, translational and protein degradation diversifying mechanisms apply (De Sousa Abreu et al., 2009; Vogel & Marcotte, 2012). Advances in endogenous protein tagging techniques (Chen et al., 2014; Fendl et al., 2020; Venken et al., 2011) surpass the previous caveat and allow for assessing receptor localization in the single cell (Fendl et al., 2020; Sanfilippo et al., 2024) and synapse levels. In my work (**Manuscript 2**), we used such acetylcholine receptor tagged constructs to look at their synaptic localization in the light microscopy level.

While Tm1, Tm2, Tm4 and Tm9 share the same cholinergic identity, they were found to differentiate at their postsynaptic sites in terms of the nAChR subunits they use (Figure 6D). Tm1- Tm2- and Tm4-to-T5 synapses primarily use the α5 subunit, whereas Tm9-to-T5 synapses preferably use the α7 subunit. What would be the functional implications of such a distinction? To address the latter, we would first need to achieve certain milestones. Firstly, the *in vivo* stoichiometries should be established, as nAChR stoichiometries dictate both the channel's kinetic properties and ionic conductance. If this knowledge is obtained, then *in vitro* patch-clamp experiments (Sakmann & Neher, 1984) in *Drosophila* embryo cells expressing the respective nicotinic subunit could be performed. Such experiments would describe the ionic profiles of each channel and consequently enlighten the biophysical properties of the different Tm-to-T5 synapses. Secondly, the receptor's density as well as synaptic nanoarchitecture might also contribute in the single synapse biophysics (Figure 6E,F). Receptor density controls the binding of ligands (Berg & Purcell, 1977; Caré & Soula, 2011; Erickson et al., 1987), while receptor synaptic nanoarchitecture relative to the presynaptic release sites can affect postsynaptic currents (Olah et al., 2023; Tang et al., 2016). Whether these mechanisms apply to Tm-to-T5 synapses is not known, but they should not be excluded from future scientific endeavors. Lastly, we propose that Tm9-to-T5 synapses display an inter-bouton nAChR variety, which may also extend to mAChRs (Figure 6G). We found mAChR-B and the α1, α3, α4, α5, α7 and β1 subunits localizing in Tm9-to-T5 synapses. This is indicative of a potential ionotropic and metabotropic crosstalk at the single bouton level, in agreement to recent work showing a potentiation activity loop between the nAChR-mAChR-A (Rozenfeld et al., 2021). Therefore, different boutons of the same Tm9 neuron might have different functional identities, showing once more the pivotal computational role of the single synapse. In summary,

acetylcholine does not discriminate between the two acetylcholine receptor categories, hence receptor stoichiometry, localization, density and synaptic organization, together with the biophysical properties of each category will eventually define the synaptic output.

3.2.2 Acetylcholine receptors and T5 direction selectivity

Intracellular recordings in blow flies indicated the directional responses of T5 cells to visual motion (Douglass & Strausfeld, 1996; Douglass & Strausfeld, 1995) and paved the way for the discovery of T5 direction-selective cells in *Drosophila* (Maisak et al., 2013). A fundamental question is how T5 cells and their ON pathway counterparts, T4 cells, achieve their direction-selective computation. Mathematical models such as the Hassenstein-Reichardt (HR) in the beetle *Chlorophanus viridis* (Hassenstein & Reichardt, 1956) for preferred direction enhancement and the Barlow-Levick (BL) in the rabbit retina (Barlow & Levick, 1965) for null direction suppression, have been proposed as mathematical descriptions of direction-selective neuronal computations. However, a hybrid correlator encompassing both preferred direction enhancement and null direction suppression has been found in T4 cells (Haag et al., 2016). Such a hybrid correlator, namely HR/BL detector, has been proposed for T5 cells as well (Leong et al., 2016).

The hybrid correlator receives three input lines, one direct non-delayed line flanked by two delayed ones (Figure 7). The non-linear interactions between the three input lines are algorithmically described with a multiplication of the delayed input on the preferred side with the central direct line and its consecutive division with the delayed input line at the null side of the neuron's receptive field (Borst & Groschner, 2023). Hence, to decode the T4 and T5 computations it is essential to a. find the neuronal correlates of each input line, b. understand where and how the delays are implemented, and c. locate the needed non-linearities.

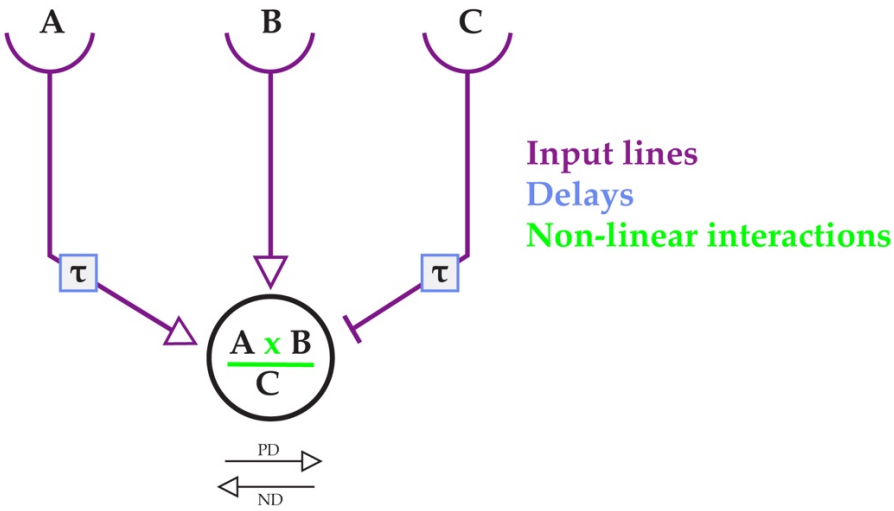

Figure 7. Three-arm hybrid correlator. Three spatially offset input lines (A,B,C purple) provide input to the motion detector and two of them (A,C) are delayed in time (τ blue) compared to the third input line (B). The three lines are non-linearly integrated by a means of a multiplication (AxB) followed by a division (AxB/C) (green). Preferred direction (PD) and null direction (ND) of a moving stimulus.

Neuronal correlates

The first prerequisite has been achieved for T5 cells by a consortium of studies ranging from the morphological (Shinomiya et al., 2014, 2019; Takemura et al., 2011) up to the functional characterization of T5 input neurons (Arenz et al., 2017; Behnia et al., 2014; Braun et al., 2023; Meier et al., 2014; Meier & Borst, 2019; Serbe et al., 2016). Tm1, Tm2, Tm4 and Tm9 are the primary cholinergic-excitatory T5 inputs, while CT1 is a GABAergic-inhibitory input. CT1 acts as the inhibitory arm of the HR/BL detector (Figure 7, 'C') (Braun et al., 2023) and the slow responses of Tm9 to moving edges render it as the delayed-excitatory arm of the hybrid detector (Figure 7, 'A'), while the fast responses of Tm1, Tm2, Tm4 make them the direct-excitatory arm (Figure 7, 'B') (Serbe et al., 2016). Nonetheless, the neuronal input sign, i.e excitatory or inhibitory, can be defined by the neurotransmitter that neurons release, but at the same time it can be controlled by the neurotransmitter receptors at the postsynaptic site. Such an example is the glutamate-gated chloride channel GluClα which acts as an inhibitory glutamate receptor in *Drosophila* (Ammer et al., 2023; Groschner et al., 2022; Liu & Wilson, 2013; Mauss et al., 2014). A similar example is the mAChR-B acetylcholine receptor which we showed to be inhibitory in T5 cells, while binding the excitatory neurotransmitter acetylcholine (**Manuscript 2**). It is thus important to fully understand which receptors mediate the Tm- and CT1-to-T5 neurotransmission.

Delays in time

The slower Tm9 responses (Serbe et al., 2016) render it the primary source of delays for preferred direction enhancement in T5 dendrites. However, the metabotropic nature of the mAChR-B receptor could potentially introduce additional delays. As a first step to apprehend in which synapses mAChR-B-introduced delays are applied, we would need to acquire information on the Tm-to-T5 localization of mAChR-B. In my work (**Manuscript 2**), we used an overexpression mAChR-B line and visualized its Tm9-to-T5 localization. The caveat of such overexpression lines is the mistargeting, at the cellular and synaptic level, that can occur, hence we cannot exclude this factor from the interpretation of our result. Another interesting possibility is that the differential nicotinic receptor subunit composition between Tm-to-T5 synapses may introduce additional delays to the circuitry. Does a α7 homomer or α7-present heteromer exhibit slower kinetics than an α5 version? To give an answer to this question, we would first need to know the *in vivo* stoichiometries of these nicotinic receptors, as previously mentioned. Additionally, the unknown effects of co-transmission should not be omitted. Neuropeptides are a diverse category of neuromodulators that act via GPCRs (Nusbaum et al., 2017). Small molecule neurotransmitter and neuropeptide co-transmission is a very common phenomenon across species (Nässel, 2018; Nusbaum et al., 2017). The latter has recently been identified in Kenyon cells of *Drosophila* between acetylcholine and the Short neuropeptide F (sNPF), with sNPF exhibiting slower kinetics (Xia & Li, 2025). Therefore, the temporal profile of Tm-to-T5 connections might be additionally regulated by neuropeptides. Research is already focused on investigating neuropeptides in the navigational center of the fruit fly, the Central Complex (Wolff et al., 2024). The next step would be to seek such information in the optic lobe and particularly in T5 cells. Lastly, it was recently found that the response time constants of CT1 make it an ideal candidate to act as the slow, inhibitory signal for null direction suppression in T5 cells (Braun et al., 2023).

Operational nonlinearities

In a seminal study from Groschner and colleagues (Groschner et al., 2022), the biophysical implementation of preferred direction enhancement in T4 cells has been described. As proposed (Borst, 2018), visual stimuli moving in the preferred direction of the T4 neuron result in the release from shunting inhibition that Mi9 imposes via the GluClα receptor. The T4 input resistance increases and this T4 state coincides and gets enhanced by the

activation of the excitatory Mi1 and Tm3 neurons, resembling an algorithmic multiplication. For null direction suppression in T4 cells, we have a first indication that it is introduced by shunting inhibition, a divisive non-linearity. Shunting inhibition takes place when the inhibitory conductance is bigger than the leak conductance of the cell, and T4 input resistance slightly decreased in response to null direction motion (Groschner et al., 2022). Whether null direction suppression in T4 cells is mediated by the GABA receptor Rdl is still an open question.

In T5 cells, the biophysical implementation of preferred direction enhancement is less clear. T5 cells do not receive a glutamatergic input as T4 cells, whilst they exhibit a higher variety of cholinergic inputs. Could it be that Tm9 connections induce an increase in T5 input resistance, while Tm1, Tm2 and Tm4 enhance this T5 state? Similar electrophysiological approaches should be followed in T5 cells as in the T4 example, however the key to the T5 preferred direction enhancement might be held by muscarinic acetylcholine receptors. The mAChR-B possible localization in Tm9-to-T5 synapses (**Manuscript 2**) and its activation, could lead to the opening of G protein-coupled potassium channels of the Kir family (Ren et al., 2015), eventually leading to an increase in T5 input resistance. Then the multiplicative enhancement would be introduced by the Tm1,Tm2,Tm4-α5 excitatory neurotransmission. Another Tm9-specific mechanism for increasing the T5 input resistance could be imposed by the α7 nicotinic receptor subunit. If the α7 homomeric or heteromeric potassium conductance is high, then it could induce a localized T5 membrane hyperpolarization. The possibility that both muscarinic and nicotinic receptors act in conjunction to control the T5 input resistance should not be excluded. Thus, key experiments would be the knock-down of the mAChR-B and/or α7 subunit, while assessing the T5 input resistance. The mechanism for null direction suppression in T5 cells has been characterized at the calcium level, where the Rdl-mediated CT1 GABAergic neurotransmission accounts for the divisive non-linearity (Braun et al., 2023). Knowing the inhibitory receptor mediator, the T5 input resistance after Rdl knock-down should be measured and the biophysical properties of this divisive nonlinearity ought to be defined.

Other nonlinearities

Voltage-gated ion channels also control the amplitude and the dynamics of the neuronal response and can introduce nonlinearities. Their activation can be mAChR-dependent or independent. In mammals, muscarinic receptors have been

found to inhibit and activate a plethora of ion channels (Brown, 2018). The voltage-activated potassium channel ether-à-go-go (eag) was inhibited after muscarinic receptor activation in human embryonic kidney cells (Stansfeld et al., 1996). In vestibular ganglion neurons of rats, muscarinic signaling cascades were found to depolarize the activation range of hyperpolarization-activated cyclic-nucleotide gated (HCN) channels (Bronson & Kalluri, 2023). This muscarinic-mediated HCN activation is another means of introducing delaying nonlinearities (Lüscher & Slesinger, 2010) and in *Drosophila* the HCN channel Ih has been found on T5 dendrites (Fendl et al., 2020). It would therefore be interesting to electrophysiologically explore T5 responses after knocking down the mAChR-B & eag and the mAChR-B & Ih. Once more, the mAChR-B receptor is a prominent candidate for future studies.

3.3 CHOLINERGIC NEUROTRANSMISSION IN DIRECTION SELECTIVE CIRCUITS IN MAMMALS

The mammalian retina comprises of three cellular layers: the photoreceptor segments in the outermost layer, the outer nuclear layer where the somata of rods and cones reside and the inner nuclear layer that contains bipolar, horizontal, starbust amacrine (SACs), Müller glial cells, and direction-selective ganglion cells (DSGCs) (Jeon et al., 1998; Todorova et al., 2022) (Figure 8A).

DSGCs respond to moving stimuli in their preferred direction, while remain silent in stimuli coming from their null direction (Figure 8B). The GABAergic SACs are the upstream partners of DSGCs and play a fundamental role in DSGC direction-selectivity (Barlow et al., 1964; Briggman et al., 2011; Taylor & Vaney, 2002; Yoshida et al., 2001), whilst being centrifugally direction-selective themselves (from the soma to the distal dendritic sites) (Euler et al., 2002; Lee & Zhou, 2006; Vlasits et al., 2016) (Figure 8C,D). SACs co-release GABA and ACh and are the only cholinergic neurons in the mouse retina (Famiglietti, 1983; Hayden et al., 1980; Yan et al., 2020). Interestingly, a recent study found the α7 nicotinic subunit localizing at the presynaptic site of the bipolar cell types 1,2,7, which provide excitatory glutamatergic input at the proximal dendrites of SACs (Hall et al., 2019). They later identified that the presynaptic α7 subunit in bipolar cells facilitated transmitter release and enhanced feedforward inhibition from SACs to DSGCs (Alkondon et al., 1996; Hellmer et al., 2021; McGehee et al., 1995). Another level of complexity in cholinergic neurotransmission between SACs and

DSGCs lies at the multi-directed form of acetylcholine transmission, where released acetylcholine from a single vesicle rapidly co-activates receptors expressed in multiple neurons located within ~1 μm of the release site (Sethuramanujam et al., 2021). The diversity of AChRs in SACs has not been addressed so far. However, a recent study found that feedforward inhibition of SACs was achieved via nicotinic and muscarinic AChRs in ON SACs and through nicotinic AChRs in OFF SACs (Gangi et al., 2024).

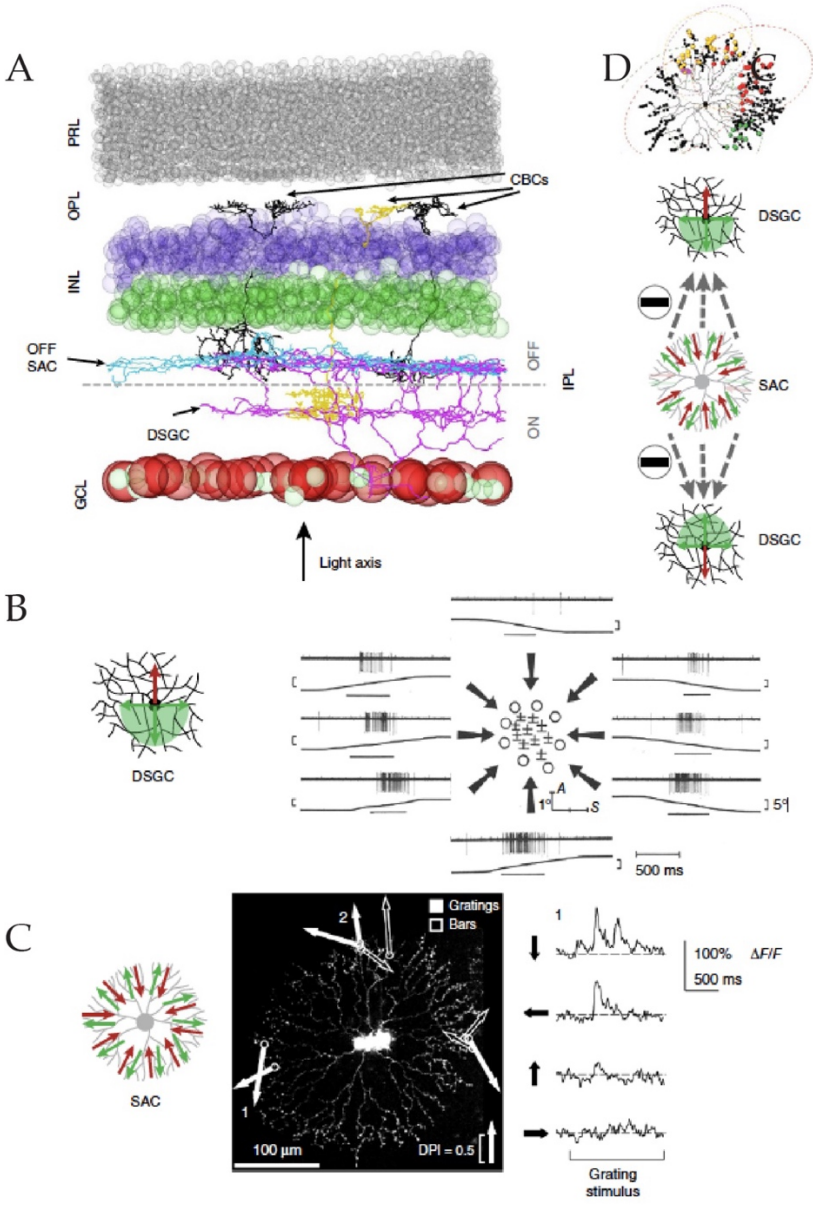

Figure 8. Motion detection in the mouse retina: direction-selective neurons and direction-specific circuits. (A) Layout of the retina from a densely reconstructed EM data set[22]. Cell body positions of photoreceptors (gray), bipolar cells (blue) and ganglion cells (red) as well as amacrine cells (green) are shown. PRL, photoreceptor layer; OPL, outer plexiform layer; INL, inner nuclear layer; IPL, inner

plexiform layer, GCL, ganglion cell layer. Reconstructions of a direction-selective ON-OFF ganglion cell (DSGC, magenta; note bistratification in ON and OFF sublayers), an OFF starburst amacrine cell (SAC, cyan) and type 2 (black), 3A (black) and 5B/C (yellow) cone bipolar cells (CBCs) are shown. All these cell types are involved in motion detection. (Adapted from ref. 22, Nature Publishing Group.) (B) Discovery of direction-selective responses in ganglion cells in rabbit retina (left, reproduced from ref. 96, John Wiley and Sons). Unit recordings (top traces) from a DSGC axon in response to moving light spots (trajectories in bottom traces) presented in eight movement directions (black arrows). ON-OFF receptive field (±) and non-responsive surround (circles) are shown (inner scale bars represent 1° for the respective in-plane directions). Horizontal lines indicate approximately when the light spot was crossing the receptive field. Left, DSGC schematic (black). One directional quadrant (the NULL direction, red) is suppressed, while the neuron stays responsive to the other directions of motion (green). (C) Discovery of direction-selective responses in starburst amacrine cell dendrites[31]. A fluorescent dye-filled SAC in the plane of the retina (center panel; DPI, directional preference index) and Ca2+ responses to moving gratings presented in four movement directions (right) are shown (center and right adapted from ref. 31, Nature Publishing Group). Left, SAC schematic (gray). Each of the radially directed dendrites has its own preferred direction of motion; this preferred direction (green) is oriented from the SAC soma to the dendrite tip. Directional preference is thus represented not just for the four cardinal directions but at a higher angular density. (D) Proof of directionally specific neuronal wiring from SAC dendrites to direction-selective ganglion cells[37] (top; adapted from ref. 37, Nature Publishing Group). The output synapses of one SAC (black) are color-coded by the directional preference of the respective postsynaptic ganglion cells (yellow, green, red and magenta for downward, upward, leftward and rightward motion, respectively). These data and the population average imply that these ganglion cells in fact inherit their direction selectivity from SACs. Bottom, schematic. A range of directions is suppressed by the inhibitory effect of SAC dendrites, which release GABA, generating the null direction in the postsynaptic direction-selective ganglion cells. Figure and figure caption with permission from Borst and Helmstaedter (2015).

3.4 CONCLUSIONS AND OUTLOOK

The past decade has been revolutionary in the exploration of direction selectivity in the ON- and the OFF-motion pathway. From the cellular identification of the elementary motion detectors (Maisak et al., 2013), up to the response properties of their columnar and non-columnar input neurons (Ammer et al., 2015; Arenz et al., 2017; Behnia et al., 2014; Braun et al., 2023; Meier & Borst, 2019; Serbe et al., 2016), and eventually the biophysical implementation of preferred direction enhancement

in T4 cells (Groschner et al., 2022), the building blocks of this computation have been defined. Nevertheless, preferred direction enhancement in T5 correlators has been understudied compared to their T4 counterparts. One step for the T5 biophysical characterization is to study the respective receptors that govern the Tm-to-T5 neurotransmission, the epicenter of my doctoral thesis. However, despite our contributions, certain questions still remain unanswered.

Multiple nicotinic acetylcholine receptor subunits were found on T5 dendrites, thus pointing to their great stoichiometrical variety. We still do not understand the *in vivo* stoichiometrical combinations of these channels and per extension their distinct kinetics and conductance profiles. T5 co-localization approaches together with co-assembly verifications via biochemical pull-downs (Korona et al., 2022), could offer valuable insights in the nicotinic receptor stoichiometry. Consequently, the functional characterization of each channel would be possible *in vitro* by combining subunit expression in cell lines and their subsequent electrophysiological description with patch-clamp (González et al., 2011; Sakmann & Neher, 1984). Together with the synaptic localization of nicotinic subunits we provided, a biophysical model for T5 preferred direction enhancement could then be implemented.

Another open question is whether T5 preferred direction enhancement is achieved via the same mechanism as in T4 cells (Groschner et al., 2022; Gruntman et al., 2018). While presenting motion in their preferred direction, the input resistance of T5 cells should be measured under control and α7 subunit and/or mAChR-B knock-down conditions. This will be a key experiment to understand the biophysical implementation of preferred direction enhancement in T5 cells. In parallel, the functional implications of T5-T5 axo-axonic and dendro-dendritic synapses (Shinomiya et al., 2019, 2022) are not known, nor their postsynaptic receptor profiles and thus, T5 network dynamics still remain unexplored.

In the era of brain wiring diagrams (Dorkenwald et al., 2024; Scheffer et al., 2020; Schlegel et al., 2024; Zheng et al., 2018), we propose a shift towards the single synapse connectivity. The functional roles of each polyadic types we identified in Tm-to-T5 synapses are currently unknown. Synaptic calcium indicators could potentially show differences in presynaptic release mechanisms of polyads (Xing & Wu, 2018). For differences in the postsynaptic machinery, new electron microscopy tools

(Sigmund et al., 2023) might allow for the ultrastructural documentation of different receptor types. We are currently in the fortunate position to explore motion vision circuits in *Drosophila* with high resolution. I believe that the final level to tackle is that of the chemical synapse. Focusing on single synapse computations will eventually grant us access to a holistic understanding of visual direction-selective computations.

4 | REFERENCES

Abrams, P., Andersson, K.-E., Buccafusco, J. J., Chapple, C., de Groat, W. C., Fryer, A. D., Kay, G., Laties, A., Nathanson, N. M., Pasricha, P. J., & Wein, A. J. (2006). Muscarinic receptors: Their distribution and function in body systems, and the implications for treating overactive bladder. *British Journal of Pharmacology*, *148*(5), 565–578. https://doi.org/10.1038/sj.bjp.0706780

Ache, J. M., Namiki, S., Lee, A., Branson, K., & Card, G. M. (2019). State-dependent decoupling of sensory and motor circuits underlies behavioral flexibility in *Drosophila*. *Nature Neuroscience*, *22*(7), 1132–1139.

Ache, J. M., Polsky, J., Alghailani, S., Parekh, R., Breads, P., Peek, M. Y., Bock, D. D., Von Reyn, C. R., & Card, G. M. (2019). Neural basis for looming size and velocity encoding in the *Drosophila* giant fiber escape pathway. *Current Biology*, *29*(6), 1073–1081.

Acuna, C., Liu, X., & Südhof, T. C. (2016). How to make an active zone: Unexpected universal functional redundancy between RIMs and RIM-BPs. *Neuron*, *91*(4), 792–807. https://doi.org/10.1016/j.neuron.2016.07.042

Albuquerque, E. X., Pereira, E. F. R., Alkondon, M., & Rogers, S. W. (2009). Mammalian nicotinic acetylcholine receptors: From structure to function. *Physiological Reviews*, *89*(1), 73–120. https://doi.org/10.1152/physrev.00015.2008

Alkondon, M., Rocha, E. S., Maelicke, A., & Albuquerque, E. X. (1996). Diversity of nicotinic acetylcholine receptors in rat brain. V. alpha-Bungarotoxin-sensitive nicotinic receptors in olfactory bulb neurons and presynaptic modulation of glutamate release. *Journal of Pharmacology and Experimental Therapeutics*, *278*(3), 1460–1471.

Ammer, G., Leonhardt, A., Bahl, A., Dickson, B. J., & Borst, A. (2015). Functional specialization of neural input elements to the *Drosophila* ON motion detector. *Current Biology*, *25*(17), 2247–2253. https://doi.org/10.1016/j.cub.2015.07.014

Ammer, G., Serbe-Kamp, E., Mauss, A. S., Richter, F. G., Fendl, S., & Borst, A. (2023). Multilevel visual motion opponency in *Drosophila*. *Nature Neuroscience*, *26*(11), 1894–1905. https://doi.org/10.1038/s41593-023-01443-z

Ammer, G., Vieira, R. M., Fendl, S., & Borst, A. (2022). Anatomical distribution and functional roles of electrical

synapses in *Drosophila*. *Current Biology*, *32*(9), 2022-2036.e4. https://doi.org/10.1016/j.cub.2022.03.040

Andlauer, T. F. M., Scholz-Kornehl, S., Tian, R., Kirchner, M., Babikir, H. A., Depner, H., Loll, B., Quentin, C., Gupta, V. K., Holt, M. G., Dipt, S., Cressy, M., Wahl, M. C., Fiala, A., Selbach, M., Schwärzel, M., & Sigrist, S. J. (2014). Drep-2 is a novel synaptic protein important for learning and memory. *eLife*, *3*, e03895. https://doi.org/10.7554/eLife.03895

Arenz, A., Drews, M. S., Richter, F. G., Ammer, G., & Borst, A. (2017). The temporal tuning of the *Drosophila* motion detectors is determined by the dynamics of their input elements. *Current Biology*, *27*(7), 929–944. https://doi.org/10.1016/j.cub.2017.01.051

Ashburner, M. (1989). *Drosophila*. Cold Spring Harbor Laboratory.

Azevedo, A., Lesser, E., Phelps, J. S., Mark, B., Elabbady, L., Kuroda, S., Sustar, A., Moussa, A., Khandelwal, A., Dallmann, C. J., Agrawal, S., Lee, S.-Y. J., Pratt, B., Cook, A., Skutt-Kakaria, K., Gerhard, S., Lu, R., Kemnitz, N., Lee, K., … Tuthill, J. C. (2024). Connectomic reconstruction of a female *Drosophila* ventral nerve cord. *Nature*, *631*(8020), 360–368. https://doi.org/10.1038/s41586-024-07389-x

Bahl, A., Ammer, G., Schilling, T., & Borst, A. (2013). Object tracking in motion-blind flies. *Nature Neuroscience*, *16*(6), 730–738. https://doi.org/10.1038/nn.3386

Baines, R. A., Uhler, J. P., Thompson, A., Sweeney, S. T., & Bate, M. (2001). Altered electrical properties in *Drosophila* neurons developing without synaptic transmission. *The Journal of Neuroscience*, *21*(5), 1523–1531. https://doi.org/10.1523/JNEUROSCI.21-05-01523.2001

Bang, M. L., & Owczarek, S. (2013). A matter of balance: Role of neurexin and neuroligin at the synapse. *Neurochemical Research*, *38*(6), 1174–1189. https://doi.org/10.1007/s11064-013-1029-9

Barbour, B. (1994). Prolonged presence of glutamate during excitatory synaptic transmission to cerebellar Purkinje cells. *Neuron*, *12*(6), 1331–1343. https://doi.org/10.1016/0896-6273(94)90448-0

Barlow, H., Hill, R., & Levick, W. (1964). Retinal ganglion cells responding selectively to direction and speed of image motion in the rabbit. *The Journal of Physiology*, *173*(3), 377.

Barlow, H., & Levick, W. R. (1965). The mechanism of directionally selective units in rabbit's retina. *The Journal of Physiology*, *178*(3), 477.

Behnia, R., Clark, D. A., Carter, A. G., Clandinin, T. R., & Desplan, C. (2014). Processing properties of ON and OFF pathways for *Drosophila* motion detection. *Nature*, *512*(7515), 427–430. https://doi.org/10.1038/nature13427

Bellen, H. J., Tong, C., & Tsuda, H. (2010). 100 years of *Drosophila* research and its impact on vertebrate neuroscience: A history lesson for the future. *Nature Reviews Neuroscience*, *11*(7), 514–522. https://doi.org/10.1038/nrn2839

Bello, B., Resendez-Perez, D., & Gehring, W. J. (1998). Spatial and temporal targeting of gene expression in *Drosophila* by means of a tetracycline-dependent transactivator system. *Development*, *125*(12), 2193–2202. https://doi.org/10.1242/dev.125.12.2193

Benninger, R. K. P., & Piston, D. W. (2013). Two-photon excitation microscopy for the study of living cells and tissues. *Current Protocols in Cell Biology*, *59*(1). https://doi.org/10.1002/0471143030.cb0411s59

Benzer, S. (1967). Behavioral mutants of *Drosophila* isolated by counter current distribution. *Proceedings of the National Academy of Sciences*, *58*(3), 1112–1119. https://doi.org/10.1073/pnas.58.3.1112

Berg, H. C., & Purcell, E. M. (1977). Physics of chemoreception. *Biophysical Journal*, *20*(2), 193–219. https://doi.org/10.1016/S0006-3495(77)85544-6

Berger-Müller, S., Sugie, A., Takahashi, F., Tavosanis, G., Hakeda-Suzuki, S., & Suzuki, T. (2013). Assessing the role of cell-surface molecules in central synaptogenesis in the *Drosophila* visual system. *PLoS ONE*, *8*(12), e83732. https://doi.org/10.1371/journal.pone.0083732

Bernstein, E., Caudy, A. A., Hammond, S. M., & Hannon, G. J. (2001). Role for a bidentate ribonuclease in the initiation step of RNA interference. *Nature*, *409*(6818), 363–366. https://doi.org/10.1038/35053110

Bielopolski, N., Amin, H., Apostolopoulou, A. A., Rozenfeld, E., Lerner, H., Huetteroth, W., Lin, A. C., & Parnas, M. (2019). Inhibitory muscarinic acetylcholine receptors enhance aversive olfactory learning in adult *Drosophila*. *eLife*, *8*, e48264. https://doi.org/10.7554/eLife.48264

Böhme, M. A., Beis, C., Reddy-Alla, S., Reynolds, E., Mampell, M. M., Grasskamp, A. T., Lützkendorf, J., Bergeron, D. D., Driller, J. H., Babikir, H., Göttfert, F., Robinson, I. M., O'Kane, C. J., Hell, S. W., Wahl, M. C., Stelzl, U., Loll, B., Walter, A. M., & Sigrist, S. J. (2016). Active zone scaffolds differentially accumulate Unc13 isoforms to tune Ca2+

channel–vesicle coupling. *Nature Neuroscience*, *19*(10), 1311–1320. https://doi.org/10.1038/nn.4364

Borst, A. (2000). Models of motion detection. *Nature Neuroscience*, *3*(S11), 1168–1168. https://doi.org/10.1038/81435

Borst, A. (2014). Fly visual course control: Behaviour, algorithms and circuits. *Nature Reviews Neuroscience*, *15*(9), 590–599. https://doi.org/10.1038/nrn3799

Borst, A. (2018). A biophysical mechanism for preferred direction enhancement in fly motion vision. *PLOS Computational Biology*, *14*(6), e1006240. https://doi.org/10.1371/journal.pcbi.1006240

Borst, A., & Euler, T. (2011). Seeing things in motion: Models, circuits, and mechanisms. *Neuron*, *71*(6), 974–994. https://doi.org/10.1016/j.neuron.2011.08.031

Borst, A., & Groschner, L. N. (2023). How flies see motion. *Annual Review of Neuroscience*, *46*(1), 17–37. https://doi.org/10.1146/annurev-neuro-080422-111929

Borst, A., & Helmstaedter, M. (2015). Common circuit design in fly and mammalian motion vision. *Nature Neuroscience*, *18*(8), 1067–1076. https://doi.org/10.1038/nn.4050

Bourne, J., & Harris, K. M. (2007). Do thin spines learn to be mushroom spines that remember? *Current Opinion in Neurobiology*, *17*(3), 381–386. https://doi.org/10.1016/j.conb.2007.04.009

Branco, T., & Staras, K. (2009). The probability of neurotransmitter release: Variability and feedback control at single synapses. *Nature Reviews Neuroscience*, *10*(5), 373–383. https://doi.org/10.1038/nrn2634

Brand, A. H., & Perrimon, N. (1993). Targeted gene expression as a means of altering cell fates and generating dominant phenotypes. *Development (Cambridge, England)*, *118*(2), 401–415.

Braun, A., Borst, A., & Meier, M. (2023). Disynaptic inhibition shapes tuning of OFF-motion detectors in *Drosophila*. *Current Biology: CB*, *33*(11), 2260-2269.e4. https://doi.org/10.1016/j.cub.2023.05.007

Briggman, K. L., Helmstaedter, M., & Denk, W. (2011). Wiring specificity in the direction-selectivity circuit of the retina. *Nature*, *471*(7337), 183–188.

Bronson, D., & Kalluri, R. (2023). Muscarinic acetylcholine receptors modulate HCN channel properties in vestibular ganglion neurons. *The Journal of Neuroscience*, *43*(6), 902–917. https://doi.org/10.1523/JNEUROSCI.2552-21.2022

Brown, D. A. (2018). Regulation of neural ion channels by muscarinic receptors. *Neuropharmacology*, *136*, 383–400. https://doi.org/10.1016/j.neuropharm.2017.11.024

Buchner, E., Buchner, S., Crawford, G., Mason, WilliamT., Salvaterra, PaulM., & Sattelle, DavidB. (1986). Choline acetyltransferase-like immunoreactivity in the brain of *Drosophila melanogaster*. *Cell and Tissue Research*, *246*(1). https://doi.org/10.1007/BF00218999

Buhmann, J., Sheridan, A., Malin-Mayor, C., Schlegel, P., Gerhard, S., Kazimiers, T., Krause, R., Nguyen, T. M., Heinrich, L., Lee, W.-C. A., Wilson, R., Saalfeld, S., Jefferis, G. S. X. E., Bock, D. D., Turaga, S. C., Cook, M., & Funke, J. (2021). Automatic detection of synaptic partners in a whole-brain *Drosophila* electron microscopy data set. *Nature Methods*, *18*(7), 771–774. https://doi.org/10.1038/s41592-021-01183-7

Caré, B. R., & Soula, H. A. (2011). Impact of receptor clustering on ligand binding. *BMC Systems Biology*, *5*(1), 48. https://doi.org/10.1186/1752-0509-5-48

Carlson, E. A. (2013). How fruit flies came to launch the chromosome theory of heredity. *Mutation Research/Reviews in Mutation Research*, *753*(1), 1–6. https://doi.org/10.1016/j.mrrev.2013.03.001

Chaturvedi, R., Reddig, K., & Li, H.-S. (2014). Long-distance mechanism of neurotransmitter recycling mediated by glial network facilitates visual function in *Drosophila*. *Proceedings of the National Academy of Sciences*, *111*(7), 2812–2817. https://doi.org/10.1073/pnas.1323714111

Chen, K., Gracheva, E. O., Yu, S.-C., Sheng, Q., Richmond, J., & Featherstone, D. E. (2010). Neurexin in embryonic *Drosophila* neuromuscular junctions. *PLoS ONE*, *5*(6), e11115. https://doi.org/10.1371/journal.pone.0011115

Chen, Y., Akin, O., Nern, A., Tsui, C. Y. K., Pecot, M. Y., & Zipursky, S. L. (2014). Cell-type-specific labeling of synapses *in vivo* through synaptic tagging with recombination. *Neuron*, *81*(2), 280–293. https://doi.org/10.1016/j.neuron.2013.12.021

Chen, Y.-C., Lin, Y. Q., Banerjee, S., Venken, K., Li, J., Ismat, A., Chen, K., Duraine, L., Bellen, H. J., & Bhat, M. A. (2012). *Drosophila* neuroligin 2 is required presynaptically and postsynaptically for proper synaptic differentiation and synaptic transmission. *The Journal of Neuroscience*, *32*(45), 16018–16030.https://doi.org/10.1523/JNEUROSCI.1685-12.2012

Christiansen, F., Zube, C., Andlauer, T. F. M., Wichmann, C., Fouquet, W., Owald, D., Mertel, S., Leiss, F., Tavosanis, G., Farca Luna, A. J., Fiala, A., & Sigrist, S. J. (2011). Presynapses in Kenyon cell dendrites in the mushroom body calyx of *Drosophila*. *Journal of Neuroscience*, *31*(26),

9696–9707. https://doi.org/10.1523/JNEUROSCI.6542-10.2011

Clark, D. A., & Demb, J. B. (2016). Parallel computations in insect and mammalian visual motion processing. *Current Biology*, *26*(20), R1062–R1072. https://doi.org/10.1016/j.cub.2016.08.003

Collin, C., Hauser, F., De Valdivia, E. G., Li, S., Reisenberger, J., Carlsen, E. M. M., Khan, Z., Hansen, N. Ø., Puhm, F., Søndergaard, L., Niemiec, J., Heninger, M., Ren, G. R., & Grimmelikhuijzen, C. J. P. (2013). Two types of muscarinic acetylcholine receptors in *Drosophila* and other arthropods. *Cellular and Molecular Life Sciences*, *70*(17), 3231–3242. https://doi.org/10.1007/s00018-013-1334-0

Crivici, A., & Ikura, M. (1995). Molecular and structural basis of target recognition by calmodulin. *Annual Review of Biophysics and Biomolecular Structure*, *24*(1), 85–116. https://doi.org/10.1146/annurev.bb.24.060195.000505

Dacey, D. M. (2000). Parallel pathways for spectral coding in primate retina. *Annual Review of Neuroscience*, *23*(1), 743–775. https://doi.org/10.1146/annurev.neuro.23.1.743

Dale, H. H., & Dudley, H. W. (1929). The presence of histamine and acetylcholine in the spleen of the ox and the horse. *The Journal of Physiology*, *68*(2), 97–123. https://doi.org/10.1113/jphysiol.1929.sp002598

Davie, K., Janssens, J., Koldere, D., De Waegeneer, M., Pech, U., Kreft, Ł., Aibar, S., Makhzami, S., Christiaens, V., Bravo González-Blas, C., Poovathingal, S., Hulselmans, G., Spanier, K. I., Moerman, T., Vanspauwen, B., Geurs, S., Voet, T., Lammertyn, J., Thienpont, B., … Aerts, S. (2018). A single-cell transcriptome atlas of the aging *Drosophila* brain. *Cell*, *174*(4), 982-998.e20. https://doi.org/10.1016/j.cell.2018.05.057

Davis, F. P., Nern, A., Picard, S., Reiser, M. B., Rubin, G. M., Eddy, S. R., & Henry, G. L. (2020). A genetic, genomic, and computational resource for exploring neural circuit function. *eLife*, *9*, e50901. https://doi.org/10.7554/eLife.50901

De Sousa Abreu, R., Penalva, L. O., Marcotte, E. M., & Vogel, C. (2009). Global signatures of protein and mRNA expression levels. *Molecular BioSystems*, 10.1039.b908315d. https://doi.org/10.1039/b908315d

Dederer, H., Werr, M., & Ilg, T. (2011). Differential sensitivity of *Ctenocephalides felis* and *Drosophila melanogaster* nicotinic acetylcholine receptor α1 and α2 subunits in recombinant hybrid receptors to nicotinoids and neonicotinoid

insecticides. *Insect Biochemistry and Molecular Biology*, *41*(1), 51–61. https://doi.org/10.1016/j.ibmb.2010.09.012

Del Castillo, J., & Katz, B. (1954). Quantal components of the end-plate potential. *The Journal of Physiology*, *124*(3), 560–573. https://doi.org/10.1113/jphysiol.1954.sp005129

Denk, W., Piston, D. W., & Webb, W. W. (1995). Two-photon molecular excitation in laser-scanning microscopy. In J. B. Pawley (Ed.), *Handbook of Biological Confocal Microscopy* (pp. 445–458). Springer US. https://doi.org/10.1007/978-1-4757-5348-6_28

Denk, W., Strickler, J. H., & Webb, W. W. (1990). Two-photon laser scanning fluorescence microscopy. *Science*, *248*(4951), 73–76. https://doi.org/10.1126/science.2321027

Dorkenwald, S., Matsliah, A., Sterling, A. R., Schlegel, P., Yu, S., McKellar, C. E., Lin, A., Costa, M., Eichler, K., Yin, Y., Silversmith, W., Schneider-Mizell, C., Jordan, C. S., Brittain, D., Halageri, A., Kuehner, K., Ogedengbe, O., Morey, R., Gager, J., … Zandawala, M. (2024). Neuronal wiring diagram of an adult brain. *Nature*, *634*(8032), 124–138. https://doi.org/10.1038/s41586-024-07558-y

Dorkenwald, S., McKellar, C. E., Macrina, T., Kemnitz, N., Lee, K., Lu, R., Wu, J., Popovych, S., Mitchell, E., Nehoran, B., Jia, Z., Bae, J. A., Mu, S., Ih, D., Castro, M., Ogedengbe, O., Halageri, A., Kuehner, K., Sterling, A. R., … Seung, H. S. (2022). FlyWire: Online community for whole-brain connectomics. *Nature Methods*, *19*(1), 119–128. https://doi.org/10.1038/s41592-021-01330-0

Dorkenwald, S., Schubert, P. J., Killinger, M. F., Urban, G., Mikula, S., Svara, F., & Kornfeld, J. (2017). Automated synaptic connectivity inference for volume electron microscopy. *Nature Methods*, *14*(4), 435–442. https://doi.org/10.1038/nmeth.4206

Douglass, J. K., & Strausfeld, N. J. (1996). Visual motion-detection circuits in flies: parallel direction- and non-direction-sensitive pathways between the medulla and lobula plate. *The Journal of Neuroscience*, *16*(15), 4551–4562. https://doi.org/10.1523/JNEUROSCI.16-15-04551.1996

Douglass, J., & Strausfeld, N. (1995). Visual motion detection circuits in flies: Peripheral motion computation by identified small-field retinotopic neurons. *The Journal of Neuroscience*, *15*(8), 5596–5611. https://doi.org/10.1523/JNEUROSCI.15-08-05596.1995

Duffy, J. B. (2002). GAL4 system in *Drosophila*: A fly geneticist's swiss army knife. *Genesis*, *34*(1–2), 1–15. https://doi.org/10.1002/gene.10150

Duhart, J. C., & Mosca, T. J. (2022). Genetic regulation of central synapse formation and organization in *Drosophila melanogaster*. *Genetics*, *221*(3), iyac078. https://doi.org/10.1093/genetics/iyac078

Dupuis, J., Louis, T., Gauthier, M., & Raymond, V. (2012). Insights from honeybee (*Apis mellifera*) and fly (*Drosophila melanogaster*) nicotinic acetylcholine receptors: From genes to behavioral functions. *Neuroscience & Biobehavioral Reviews*, *36*(6), 1553–1564. https://doi.org/10.1016/j.neubiorev.2012.04.003

Dupuis, J. P., Gauthier, M., & Raymond-Delpech, V. (2011). Expression patterns of nicotinic subunits α2, α7, α8, and β1 affect the kinetics and pharmacology of ACh-induced currents in adult bee olfactory neuropiles. *Journal of Neurophysiology*, *106*(4), 1604–1613. https://doi.org/10.1152/jn.00126.2011

Echeverri, C. J., & Perrimon, N. (2006). High-throughput RNAi screening in cultured cells: A user's guide. *Nature Reviews Genetics*, *7*(5), 373–384. https://doi.org/10.1038/nrg1836

Eckstein, N., Bates, A. S., Champion, A., Du, M., Yin, Y., Schlegel, P., Lu, A. K.-Y., Rymer, T., Finley-May, S., Paterson, T., Parekh, R., Dorkenwald, S., Matsliah, A., Yu, S.-C., McKellar, C., Sterling, A., Eichler, K., Costa, M., Seung, S., … Funke, J. (2024). Neurotransmitter classification from electron microscopy images at synaptic sites in *Drosophila melanogaster*. *Cell*, *187*(10), 2574-2594.e23. https://doi.org/10.1016/j.cell.2024.03.016

Elstrott, J., Anishchenko, A., Greschner, M., Sher, A., Litke, A. M., Chichilnisky, E. J., & Feller, M. B. (2008). Direction selectivity in the retina is established independent of visual experience and cholinergic retinal waves. *Neuron*, *58*(4), 499–506. https://doi.org/10.1016/j.neuron.2008.03.013

Erickson, J., Goldstein, B., Holowka, D., & Baird, B. (1987). The effect of receptor density on the forward rate constant for binding of ligands to cell surface receptors. *Biophysical Journal*, *52*(4), 657–662. https://doi.org/10.1016/S0006-3495(87)83258-7

Euler, T., Detwiler, P. B., & Denk, W. (2002). Directionally selective calcium signals in dendrites of starburst amacrine cells. *Nature*, *418*(6900), 845–852.

Exner, S. (1891). *Die Physiologie der facettirten Augen von Krebsen und Insecten: Eine Studie / von Sigm. Exner.* Franz Deuticke,. https://doi.org/10.5962/bhl.title.2149

Faltine-Gonzalez, D. Z., & Layden, M. J. (2018). *The origin and evolution of acetylcholine signaling through AchRs in metazoans*. https://doi.org/10.1101/424804

Famiglietti Jr, E. V. (1983). 'Starburst'amacrine cells and cholinergic neurons: Mirror-symmetric ON and OFF amacrine cells of rabbit retina. *Brain Research*, *261*(1), 138–144.

Feinberg, E. H., VanHoven, M. K., Bendesky, A., Wang, G., Fetter, R. D., Shen, K., & Bargmann, C. I. (2008). GFP Reconstitution Across Synaptic Partners (GRASP) defines cell contacts and synapses in living nervous systems. *Neuron*, *57*(3), 353–363. https://doi.org/10.1016/j.neuron.2007.11.030

Fendl, S., Vieira, R. M., & Borst, A. (2020). Conditional protein tagging methods reveal highly specific subcellular distribution of ion channels in motion-sensing neurons. *eLife*, *9*, e62953. https://doi.org/10.7554/eLife.62953

Fischbach, K.-F., & Dittrich, A. P. M. (1989). The optic lobe of *Drosophila melanogaster*. I. A Golgi analysis of wild-type structure. *Cell and Tissue Research*, *258*(3). https://doi.org/10.1007/BF00218858

Fisher, Y. E., Silies, M., & Clandinin, T. R. (2015). Orientation selectivity sharpens motion detection in *Drosophila*. *Neuron*, *88*(2), 390–402. https://doi.org/10.1016/j.neuron.2015.09.033

Fouquet, W., Owald, D., Wichmann, C., Mertel, S., Depner, H., Dyba, M., Hallermann, S., Kittel, R. J., Eimer, S., & Sigrist, S. J. (2009). Maturation of active zone assembly by *Drosophila* Bruchpilot. *Journal of Cell Biology*, *186*(1), 129–145. https://doi.org/10.1083/jcb.200812150

Fujiwara, T., Cruz, T. L., Bohnslav, J. P., & Chiappe, M. E. (2017). A faithful internal representation of walking movements in the *Drosophila* visual system. *Nature Neuroscience*, *20*(1), 72–81. https://doi.org/10.1038/nn.4435

Furshpan, E. J., & Potter, D. D. (1957). Mechanism of nerve-impulse transmission at a crayfish synapse. *Nature*, *180*(4581), 342–343. https://doi.org/10.1038/180342a0

Gangi, M., Maruyama, T., Ishii, T., & Kaneda, M. (2024). ON and OFF starburst amacrine cells are controlled by distinct cholinergic pathways. *Journal of General Physiology*, *156*(8), e202413550. https://doi.org/10.1085/jgp.202413550

Giniger, E., Varnum, S. M., & Ptashne, M. (1985). Specific DNA binding of GAL4, a positive regulatory protein of yeast.

Cell, *40*(4), 767–774. https://doi.org/10.1016/0092-8674(85)90336-8

González, M., Martín-Ruíz, I., Jiménez, S., Pirone, L., Barrio, R., & Sutherland, J. D. (2011). Generation of stable *Drosophila* cell lines using multicistronic vectors. *Scientific Reports*, *1*(1), 75. https://doi.org/10.1038/srep00075

Gotti, C., Moretti, M., Gaimarri, A., Zanardi, A., Clementi, F., & Zoli, M. (2007). Heterogeneity and complexity of native brain nicotinic receptors. *Biochemical Pharmacology*, *74*(8), 1102–1111. https://doi.org/10.1016/j.bcp.2007.05.023

Götz, K. G. (1964). Optomotorische untersuchung des visuellen systems einiger augenmutanten der fruchtfliege *Drosophila*. *Kybernetik*, *2*(2), 77–92. https://doi.org/10.1007/BF00288561

Götz, K. G. (1968). Flight control in *Drosophila* by visual perception of motion. *Kybernetik*, *4*(6), 199–208. https://doi.org/10.1007/BF00272517

Götz, K. G. (1970). Fractionation of *Drosophila* Populations According to Optomotor Traits. *Journal of Experimental Biology*, *52*(2), 419–436. https://doi.org/10.1242/jeb.52.2.419

Groschner, L. N., Malis, J. G., Zuidinga, B., & Borst, A. (2022). A biophysical account of multiplication by a single neuron. *Nature*, *603*(7899), 119–123. https://doi.org/10.1038/s41586-022-04428-3

Gruntman, E., Romani, S., & Reiser, M. B. (2018). Simple integration of fast excitation and offset, delayed inhibition computes directional selectivity in *Drosophila*. *Nature Neuroscience*, *21*(2), 250–257. https://doi.org/10.1038/s41593-017-0046-4

Haag, J., Arenz, A., Serbe, E., Gabbiani, F., & Borst, A. (2016). Complementary mechanisms create direction selectivity in the fly. *eLife*, *5*, e17421. https://doi.org/10.7554/eLife.17421

Haikala, V., Joesch, M., Borst, A., & Mauss, A. S. (2013). Optogenetic control of fly optomotor responses. *Journal of Neuroscience*, *33*(34), 13927–13934. https://doi.org/10.1523/JNEUROSCI.0340-13.2013

Hall, L. M., Hellmer, C. B., Koehler, C. C., & Ichinose, T. (2019). Bipolar cell type-specific expression and conductance of alpha-7 nicotinic acetylcholine receptors in the mouse retina. *Investigative Ophthalmology & Visual Science*, *60*(5), 1353–1361.

Hallermann, S., Kittel, R. J., Wichmann, C., Weyhersmüller, A., Fouquet, W., Mertel, S., Owald, D., Eimer, S., Depner, H., Schwärzel, M., Sigrist, S. J., & Heckmann, M. (2010).

Naked dense bodies provoke depression. *The Journal of Neuroscience*, *30*(43), 14340–14345. https://doi.org/10.1523/JNEUROSCI.2495-10.2010

Hamanaka, Y., & Meinertzhagen, I. A. (2010). Immunocytochemical localization of synaptic proteins to photoreceptor synapses of *Drosophila melanogaster*. *Journal of Comparative Neurology*, *518*(7), 1133–1155. https://doi.org/10.1002/cne.22268

Hardie, R. C. (1979). Electrophysiological analysis of fly retina. I: Comparative properties of R1-6 and R 7 and 8. *Journal of Comparative Physiology ? A*, *129*(1), 19–33. https://doi.org/10.1007/BF00679908

Harris, K., Jensen, F., & Tsao, B. (1992). Three-dimensional structure of dendritic spines and synapses in rat hippocampus (CA1) at postnatal day 15 and adult ages: Implications for the maturation of synaptic physiology and long-term potentiation [published erratum appears in J Neurosci 1992 Aug;12(8):following table of contents]. *The Journal of Neuroscience*, *12*(7), 2685–2705. https://doi.org/10.1523/jneurosci.12-07-02685.1992

Harris, K. P., & Littleton, J. T. (2015). Transmission, development, and plasticity of synapses. *Genetics*, *201*(2), 345–375. https://doi.org/10.1534/genetics.115.176529

Harris, K. P., Littleton, J. T., & Stewart, B. A. (2018). Postsynaptic Syntaxin 4 negatively regulates the efficiency of neurotransmitter release. *Journal of Neurogenetics*, *32*(3), 221–229. https://doi.org/10.1080/01677063.2018.1501372

Harris, K. P., Zhang, Y. V., Piccioli, Z. D., Perrimon, N., & Littleton, J. T. (2016). The postsynaptic t-SNARE Syntaxin 4 controls traffic of Neuroligin 1 and Synaptotagmin 4 to regulate retrograde signaling. *eLife*, *5*, e13881. https://doi.org/10.7554/eLife.13881

Hassenstein, B., & Reichardt, W. (1956). Systemtheoretische analyse der zeit-, reihenfolgen- und vorzeichenauswertung bei der bewegungsperzeption des rüsselkäfers Chlorophanus. *Zeitschrift Für Naturforschung B*, *11*(9–10), 513–524. https://doi.org/10.1515/znb-1956-9-1004

Hayashi, Y., & Majewska, A. K. (2005). Dendritic spine geometry: functional implication and regulation. *Neuron*, *46*(4), 529–532. https://doi.org/10.1016/j.neuron.2005.05.006

Hayden, S. A., Mills, J. W., & Masland, R. M. (1980). Acetylcholine synthesis by displaced amacrine cells. *Science*, *210*(4468), 435–437.

Hecht, S., & Wald, G. (1934). The visual acuity and intensity discrimination of *Drosophila*. *Journal of General Physiology*, *17*(4), 517–547. https://doi.org/10.1085/jgp.17.4.517

Heisenberg, M. (with Wolf, R.). (1984). *Vision in Drosophila: Genetics of Microbehavior*. Springer Berlin / Heidelberg.

Heisenberg, M., Wonneberger, R., & Wolf, R. (1978). Optomotor-blindH31? A *Drosophila* mutant of the lobula plate giant neurons. *Journal of Comparative Physiology ? A*, *124*(4), 287–296. https://doi.org/10.1007/BF00661379

Hellmer, C. B., Hall, L. M., Bohl, J. M., Sharpe, Z. J., Smith, R. G., & Ichinose, T. (2021). Cholinergic feedback to bipolar cells contributes to motion detection in the mouse retina. *Cell Reports*, *37*(11), 110106. https://doi.org/10.1016/j.celrep.2021.110106

Hering, H., & Sheng, M. (2001). Dentritic spines: Structure, dynamics and regulation. *Nature Reviews Neuroscience*, *2*(12), 880–888. https://doi.org/10.1038/35104061

Ho, T. N. T., Abraham, N., & Lewis, R. J. (2020). Structure-function of neuronal nicotinic acetylcholine receptor inhibitors derived from natural toxins. *Frontiers in Neuroscience*, *14*, 609005. https://doi.org/10.3389/fnins.2020.609005

Hoermann, N., Schilling, T., Haji Ali, A., Serbe, E., Mayer, C., Borst, A., & Pujol-Martí, J. (2020). A combinatorial code of transcription factors specifies subtypes of visual motion-sensing neurons in *Drosophila*. *Development*, dev.186296. https://doi.org/10.1242/dev.186296

Hogg, R. C., Raggenbass, M., & Bertrand, D. (2003). Nicotinic acetylcholine receptors: From structure to brain function. In *Reviews of Physiology, Biochemistry and Pharmacology* (Vol. 147, pp. 1–46). Springer Berlin Heidelberg. https://doi.org/10.1007/s10254-003-0005-1

Hulme, E. C., Birdsall, N. J. M., & Buckley, N. J. (1990). Muscarinic receptor subtypes. *Annual Review of Pharmacology and Toxicology*, *30*(1), 633–673. https://doi.org/10.1146/annurev.pa.30.040190.003221

Hurst, R., Rollema, H., & Bertrand, D. (2013). Nicotinic acetylcholine receptors: From basic science to therapeutics. *Pharmacology & Therapeutics*, *137*(1), 22–54. https://doi.org/10.1016/j.pharmthera.2012.08.012

Ito, H. T. (2008). Frequency-dependent signal transmission and modulation by neuromodulators. *Frontiers in Neuroscience*, *2*(2), 138–144. https://doi.org/10.3389/neuro.01.027.2008

Jan, L. Y., & Jan, Y. N. (1976). Properties of the larval neuromuscular junction in *Drosophila melanogaster*. *The*

Journal of Physiology, *262*(1), 189–214. https://doi.org/10.1113/jphysiol.1976.sp011592

Jan, Y. N., Jan, L. Y., & Dennis, M. J. (1977). Two mutations of synaptic transmission in *Drosophila*. *Proceedings of the Royal Society of London. Series B, Biological Sciences*, *198*(1130), 87–108. https://doi.org/10.1098/rspb.1977.0087

Jeibmann, A., & Paulus, W. (2009). *Drosophila melanogaster* as a model organism of brain diseases. *International Journal of Molecular Sciences*, *10*(2), 407–440. https://doi.org/10.3390/ijms10020407

Jenett, A., Rubin, G. M., Ngo, T.-T. B., Shepherd, D., Murphy, C., Dionne, H., Pfeiffer, B. D., Cavallaro, A., Hall, D., Jeter, J., Iyer, N., Fetter, D., Hausenfluck, J. H., Peng, H., Trautman, E. T., Svirskas, R. R., Myers, E. W., Iwinski, Z. R., Aso, Y., … Zugates, C. T. (2012). A GAL4-driver line resource for *Drosophila* neurobiology. *Cell Reports*, *2*(4), 991–1001. https://doi.org/10.1016/j.celrep.2012.09.011

Jennings, B. H. (2011). *Drosophila* – a versatile model in biology & medicine. *Materials Today*, *14*(5), 190–195. https://doi.org/10.1016/S1369-7021(11)70113-4

Jeon, C.-J., Strettoi, E., & Masland, R. H. (1998). The major cell populations of the mouse retina. *The Journal of Neuroscience*, *18*(21), 8936–8946. https://doi.org/10.1523/JNEUROSCI.18-21-08936.1998

Jinek, M., Chylinski, K., Fonfara, I., Hauer, M., Doudna, J. A., & Charpentier, E. (2012). A programmable dual-RNA-guided DNA endonuclease in adaptive bacterial immunity. *Science (New York, N.Y.)*, *337*(6096), 816–821. https://doi.org/10.1126/science.1225829

Joesch, M., Schnell, B., Raghu, S. V., Reiff, D. F., & Borst, A. (2010). ON and OFF pathways in *Drosophila* motion vision. *Nature*, *468*(7321), 300–304. https://doi.org/10.1038/nature09545

Kamermans, M., & Fahrenfort, I. (2004). Ephaptic interactions within a chemical synapse: Hemichannel-mediated ephaptic inhibition in the retina. *Current Opinion in Neurobiology*, *14*(5), 531–541. https://doi.org/10.1016/j.conb.2004.08.016

Kandel, E. R., & Squire, L. R. (2000). Neuroscience: Breaking down scientific barriers to the study of brain and mind. *Science*, *290*(5494), 1113–1120. https://doi.org/10.1126/science.290.5494.1113

Karlin, A., Holtzman, E., Yodh, N., Lobel, P., Wall, J., & Hainfeld, J. (1983). The arrangement of the subunits of the

acetylcholine receptor of *Torpedo californica*. *The Journal of Biological Chemistry*, *258*(11), 6678–6681.

Kavi, H. H., Fernandez, H. R., Xie, W., & Birchler, J. A. (2005). RNA silencing in *Drosophila*. *FEBS Letters*, *579*(26), 5940–5949. https://doi.org/10.1016/j.febslet.2005.08.069

Keller, A. (2007). *Drosophila melanogaster's* history as a human commensal. *Current Biology*, *17*(3), R77–R81. https://doi.org/10.1016/j.cub.2006.12.031

Kim, A. J., Fenk, L. M., Lyu, C., & Maimon, G. (2017). Quantitative predictions orchestrate visual signaling in Drosophila. *Cell*, *168*(1–2), 280-294.e12. https://doi.org/10.1016/j.cell.2016.12.005

Kim, I.-J., Zhang, Y., Yamagata, M., Meister, M., & Sanes, J. R. (2008). Molecular identification of a retinal cell type that responds to upward motion. *Nature*, *452*(7186), 478–482. https://doi.org/10.1038/nature06739

Kittel, R. J., Wichmann, C., Rasse, T. M., Fouquet, W., Schmidt, M., Schmid, A., Wagh, D. A., Pawlu, C., Kellner, R. R., Willig, K. I., Hell, S. W., Buchner, E., Heckmann, M., & Sigrist, S. J. (2006). Bruchpilot promotes active zone assembly, Ca^{2+} channel clustering, and vesicle release. *Science*, *312*(5776), 1051–1054. https://doi.org/10.1126/science.1126308

Koenig, J. H., Saito, K., & Ikeda, K. (1983). Reversible control of synaptic transmission in a single gene mutant of *Drosophila melanogaster*. *The Journal of Cell Biology*, *96*(6), 1517–1522. https://doi.org/10.1083/jcb.96.6.1517

Kolodziejczyk, A., Sun, X., Meinertzhagen, I. A., & Nässel, D. R. (2008). Glutamate, GABA and acetylcholine signaling components in the lamina of the *Drosophila* visual System. *PLoS ONE*, *3*(5), e2110. https://doi.org/10.1371/journal.pone.0002110

Korona, D., Dirnberger, B., Giachello, C. N., Queiroz, R. M., Popovic, R., Müller, K. H., Minde, D.-P., Deery, M. J., Johnson, G., Firth, L. C., Earley, F. G., Russell, S., & Lilley, K. S. (2022). *Drosophila* nicotinic acetylcholine receptor subunits and their native interactions with insecticidal peptide toxins. *eLife*, *11*, e74322. https://doi.org/10.7554/eLife.74322

Kroll, J. R., Wong, K. G., Siddiqui, F. M., & Tanouye, M. A. (2015). Disruption of endocytosis with the dynamin mutant *shibirets1* suppresses seizures in *Drosophila*. *Genetics*, *201*(3), 1087–1102. https://doi.org/10.1534/genetics.115.177600

Kruse, A. C., Kobilka, B. K., Gautam, D., Sexton, P. M., Christopoulos, A., & Wess, J. (2014). Muscarinic

acetylcholine receptors: Novel opportunities for drug development. *Nature Reviews Drug Discovery*, *13*(7), 549–560. https://doi.org/10.1038/nrd4295

Lai, S.-L., & Lee, T. (2006). Genetic mosaic with dual binary transcriptional systems in *Drosophila*. *Nature Neuroscience*, *9*(5), 703–709. https://doi.org/10.1038/nn1681

Land, M. F., & Nilsson, D.-E. (2012). *Animal eyes*. OUP Oxford.

Laughon, A., Driscoll, R., Wills, N., & Gesteland, R. F. (1984). Identification of two proteins encoded by the *Saccharomyces cerevisiae GAL4* Gene. *Molecular and Cellular Biology*, *4*(2), 268–275. https://doi.org/10.1128/mcb.4.2.268-275.1984

Laughon, A., & Gesteland, R. F. (1984). Primary structure of the *Saccharomyces cerevisiae GAL4* Gene. *Molecular and Cellular Biology*, *4*(2), 260–267. https://doi.org/10.1128/mcb.4.2.260-267.1984

Lee, S., & Zhou, Z. J. (2006). The synaptic mechanism of direction selectivity in distal processes of starburst amacrine cells. *Neuron*, *51*(6), 787–799.

Leiss, F., Koper, E., Hein, I., Fouquet, W., Lindner, J., Sigrist, S., & Tavosanis, G. (2009). Characterization of dendritic spines in the *Drosophila* central nervous system. *Developmental Neurobiology*, *69*(4), 221–234. https://doi.org/10.1002/dneu.20699

Leong, J. C. S., Esch, J. J., Poole, B., Ganguli, S., & Clandinin, T. R. (2016). Direction selectivity in *Drosophila* emerges from preferred-direction enhancement and null-direction suppression. *Journal of Neuroscience*, *36*(31), 8078–8092. https://doi.org/10.1523/JNEUROSCI.1272-16.2016

Leonte, M.-B., Leonhardt, A., Borst, A., & Mauss, A. S. (2021). Aerial course stabilization is impaired in motion-blind flies. *Journal of Experimental Biology*, *224*(14), jeb242219. https://doi.org/10.1242/jeb.242219

Littleton, J. T., & Ganetzky, B. (2000). Ion channels and synaptic organization: Analysis of the *Drosophila* genome. *Neuron*, *26*(1), 35–43. https://doi.org/10.1016/s0896-6273(00)81135-6

Liu, K. S. Y., Siebert, M., Mertel, S., Knoche, E., Wegener, S., Wichmann, C., Matkovic, T., Muhammad, K., Depner, H., Mettke, C., Bückers, J., Hell, S. W., Müller, M., Davis, G. W., Schmitz, D., & Sigrist, S. J. (2011). RIM-binding protein, a central part of the active zone, is essential for neurotransmitter release. *Science*, *334*(6062), 1565–1569. https://doi.org/10.1126/science.1212991

Liu, Q., Chen, B., Hall, D. H., & Wang, Z. (2007). A quantum of neurotransmitter causes minis in multiple postsynaptic

cells at the *Caenorhabditis elegans* neuromuscular junction. *Developmental Neurobiology*, *67*(2), 123–128. https://doi.org/10.1002/dneu.20307

Liu, T. X., Davoudian, P. A., Lizbinski, K. M., & Jeanne, J. M. (2022). Connectomic features underlying diverse synaptic connection strengths and subcellular computation. *Current Biology*, *32*(3), 559-569.e5. https://doi.org/10.1016/j.cub.2021.11.056

Liu, W. W., & Wilson, R. I. (2013). Glutamate is an inhibitory neurotransmitter in the *Drosophila* olfactory system. *Proceedings of the National Academy of Sciences of the United States of America*, *110*(25), 10294–10299. https://doi.org/10.1073/pnas.1220560110

Loewi, O. (1921). Über humorale übertragbarkeit der Herznervenwirkung: I. Mitteilung. *Pflügers Archiv für die Gesamte Physiologie des Menschen und der Tiere*, *189*(1), 239–242. https://doi.org/10.1007/BF01738910

Luan, H., Diao, F., Scott, R. L., & White, B. H. (2020). The *Drosophila* split Gal4 system for neural circuit mapping. *Frontiers in Neural Circuits*, *14*, 603397. https://doi.org/10.3389/fncir.2020.603397

Luan, H., Peabody, N. C., Vinson, C. R., & White, B. H. (2006). Refined spatial manipulation of neuronal function by combinatorial restriction of transgene expression. *Neuron*, *52*(3), 425–436. https://doi.org/10.1016/j.neuron.2006.08.028

Lüscher, C., & Slesinger, P. A. (2010). Emerging roles for G protein-gated inwardly rectifying potassium (GIRK) channels in health and disease. *Nature Reviews Neuroscience*, *11*(5), 301–315. https://doi.org/10.1038/nrn2834

Macpherson, L. J., Zaharieva, E. E., Kearney, P. J., Alpert, M. H., Lin, T.-Y., Turan, Z., Lee, C.-H., & Gallio, M. (2015). Dynamic labelling of neural connections in multiple colours by trans-synaptic fluorescence complementation. *Nature Communications*, *6*(1), 10024. https://doi.org/10.1038/ncomms10024

Maisak, M. S., Haag, J., Ammer, G., Serbe, E., Meier, M., Leonhardt, A., Schilling, T., Bahl, A., Rubin, G. M., Nern, A., Dickson, B. J., Reiff, D. F., Hopp, E., & Borst, A. (2013). A directional tuning map of *Drosophila* elementary motion detectors. *Nature*, *500*(7461), 212–216. https://doi.org/10.1038/nature12320

Malloy, C. A., Somasundaram, E., Omar, A., Bhutto, U., Medley, M., Dzubuk, N., & Cooper, R. L. (2019). Pharmacological identification of cholinergic receptor subtypes:

Modulation of locomotion and neural circuit excitability in *Drosophila* larvae. *Neuroscience*, *411*, 47–64. https://doi.org/10.1016/j.neuroscience.2019.05.016

Manoim, J. E., Davidson, A. M., Weiss, S., Hige, T., & Parnas, M. (2022). Lateral axonal modulation is required for stimulus-specific olfactory conditioning in *Drosophila*. *Current Biology: CB*, *32*(20), 4438-4450.e5. https://doi.org/10.1016/j.cub.2022.09.007

Masse, N. Y., Turner, G. C., & Jefferis, G. S. X. E. (2009). Olfactory information processing in *Drosophila*. *Current Biology*, *19*(16), R700–R713. https://doi.org/10.1016/j.cub.2009.06.026

Mauss, A. S., & Borst, A. (2020). Optic flow-based course control in insects. *Current Opinion in Neurobiology*, *60*, 21–27. https://doi.org/10.1016/j.conb.2019.10.007

Mauss, A. S., Meier, M., Serbe, E., & Borst, A. (2014). Optogenetic and pharmacologic dissection of feedforward inhibition in *Drosophila* motion vision. *Journal of Neuroscience*, *34*(6), 2254–2263. https://doi.org/10.1523/JNEUROSCI.3938-13.2014

McGehee, D. S., Heath, M. J., Gelber, S., Devay, P., & Role, L. W. (1995). Nicotine enhancement of fast excitatory synaptic transmission in CNS by presynaptic receptors. *Science*, *269*(5231), 1692–1696.

Meier, M., & Borst, A. (2019). Extreme compartmentalization in a *Drosophila* amacrine cell. *Current Biology: CB*, *29*(9), 1545-1550.e2. https://doi.org/10.1016/j.cub.2019.03.070

Meier, M., Serbe, E., Maisak, M. S., Haag, J., Dickson, B. J., & Borst, A. (2014). Neural circuit components of the *Drosophila* OFF motion vision pathway. *Current Biology*, *24*(4), 385–392. https://doi.org/10.1016/j.cub.2014.01.006

Meigen, J. W. (1818). *Systematische Beschreibung der bekannten europäischen zweiflügeligen Insekten*. Bei Friedrich Wilhelm Forstmann : Gedrukt bei Beaufort Sohn. https://doi.org/10.5962/bhl.title.12464

Meinertzhagen, I. A. (1996). Ultrastructure and quantification of synapses in the insect nervous system. *Journal of Neuroscience Methods*, *69*(1), 59–73. https://doi.org/10.1016/S0165-0270(96)00021-0

Meinertzhagen, I. A. (2016). Morphology of invertebrate neurons and synapses. *Handbook of Invertebrate Neurobiology*, 1–80.

Millar, N. S., & Gotti, C. (2009). Diversity of vertebrate nicotinic acetylcholine receptors. *Neuropharmacology*, *56*(1), 237–246. https://doi.org/10.1016/j.neuropharm.2008.07.041

Millar, N. S., & Harkness, P. C. (2008). Assembly and trafficking of nicotinic acetylcholine receptors (Review). *Molecular*

Membrane Biology, *25*(4), 279–292. https://doi.org/10.1080/09687680802035675

Miyawaki, A., Llopis, J., Heim, R., McCaffery, J. M., Adams, J. A., Ikura, M., & Tsien, R. Y. (1997). Fluorescent indicators for Ca2+based on green fluorescent proteins and calmodulin. *Nature*, *388*(6645), 882–887. https://doi.org/10.1038/42264

Morgan, T. H., & Bridges, C. B. (1916). *Sex-linked inheritance in Drosophila*. Carnegie Institution of Washington. https://doi.org/10.5962/bhl.title.54326

Moroni, M., & Bermudez, I. (2006). Stoichiometry and pharmacology of two human $\alpha 4\beta 2$ nicotinic receptor types. *Journal of Molecular Neuroscience*, *30*(1–2), 95–96. https://doi.org/10.1385/JMN:30:1:95

Moroni, M., Zwart, R., Sher, E., Cassels, B. K., & Bermudez, I. (2006). α4β2 nicotinic receptors with high and low acetylcholine sensitivity: pharmacology, stoichiometry, and sensitivity to long-term exposure to nicotine. *Molecular Pharmacology*, *70*(2), 755–768. https://doi.org/10.1124/mol.106.023044

Mosca, T. J., Hong, W., Dani, V. S., Favaloro, V., & Luo, L. (2012). Trans-synaptic Teneurin signalling in neuromuscular synapse organization and target choice. *Nature*, *484*(7393), 237–241. https://doi.org/10.1038/nature10923

Nachmansohn, D., & Machado, A. L. (1943). The formation of acetylcholine. a new enzyme: "choline acetylase." *Journal of Neurophysiology*, *6*(5), 397–403. https://doi.org/10.1152/jn.1943.6.5.397

Nakai, J., Ohkura, M., & Imoto, K. (2001). A high signal-to-noise Ca2+ probe composed of a single green fluorescent protein. *Nature Biotechnology*, *19*(2), 137–141. https://doi.org/10.1038/84397

Namiki, S., Dickinson, M. H., Wong, A. M., Korff, W., & Card, G. M. (2018). The functional organization of descending sensory-motor pathways in *Drosophila*. *eLife*, *7*, e34272. https://doi.org/10.7554/eLife.34272

Nässel, D. R. (2018). Substrates for neuronal cotransmission with neuropeptides and small molecule neurotransmitters in *Drosophila*. *Frontiers in Cellular Neuroscience*, *12*, 83. https://doi.org/10.3389/fncel.2018.00083

Ni, J.-Q., Liu, L.-P., Binari, R., Hardy, R., Shim, H.-S., Cavallaro, A., Booker, M., Pfeiffer, B. D., Markstein, M., Wang, H., Villalta, C., Laverty, T. R., Perkins, L. A., & Perrimon, N. (2009). A *Drosophila* resource of transgenic RNAi lines for

neurogenetics. *Genetics*, *182*(4), 1089–1100. https://doi.org/10.1534/genetics.109.103630

Ni, J.-Q., Markstein, M., Binari, R., Pfeiffer, B., Liu, L.-P., Villalta, C., Booker, M., Perkins, L., & Perrimon, N. (2008). Vector and parameters for targeted transgenic RNA interference in *Drosophila melanogaster*. *Nature Methods*, *5*(1), 49–51. https://doi.org/10.1038/nmeth1146

Ni, J.-Q., Zhou, R., Czech, B., Liu, L.-P., Holderbaum, L., Yang-Zhou, D., Shim, H.-S., Tao, R., Handler, D., Karpowicz, P., Binari, R., Booker, M., Brennecke, J., Perkins, L. A., Hannon, G. J., & Perrimon, N. (2011). A genome-scale shRNA resource for transgenic RNAi in *Drosophila*. *Nature Methods*, *8*(5), 405–407. https://doi.org/10.1038/nmeth.1592

Nielsen, M. S., Nygaard Axelsen, L., Sorgen, P. L., Verma, V., Delmar, M., & Holstein-Rathlou, N. (2012). Gap Junctions. In Y. S. Prakash (Ed.), *Comprehensive Physiology* (1st ed., pp. 1981–2035). Wiley. https://doi.org/10.1002/cphy.c110051

Noguchi, J., Matsuzaki, M., Ellis-Davies, G. C. R., & Kasai, H. (2005). Spine-Neck geometry determines NMDA receptor-dependent Ca2+ signaling in dendrites. *Neuron*, *46*(4), 609–622. https://doi.org/10.1016/j.neuron.2005.03.015

Nusbaum, M. P., Blitz, D. M., & Marder, E. (2017). Functional consequences of neuropeptide and small-molecule co-transmission. *Nature Reviews. Neuroscience*, *18*(7), 389–403. https://doi.org/10.1038/nrn.2017.56

Nusser, Z., Lujan, R., Laube, G., Roberts, J. D. B., Molnar, E., & Somogyi, P. (1998). Cell type and pathway dependence of synaptic AMPA receptor number and variability in the hippocampus. *Neuron*, *21*(3), 545–559. https://doi.org/10.1016/S0896-6273(00)80565-6

Olah, S. S., Kareemo, D. J., Buchta, W. C., Sinnen, B. L., Miller, C. N., Actor-Engel, H. S., Gookin, S. E., Winborn, C. S., Kleinjan, M. S., Crosby, K. C., Aoto, J., Smith, K. R., & Kennedy, M. J. (2023). Acute reorganization of postsynaptic GABAA receptors reveals the functional impact of molecular nanoarchitecture at inhibitory synapses. *Cell Reports*, *42*(11), 113331. https://doi.org/10.1016/j.celrep.2023.113331

Olsen, R. W., & Sieghart, W. (2009). GABAA receptors: Subtypes provide diversity of function and pharmacology. *Neuropharmacology*, *56*(1), 141–148. https://doi.org/10.1016/j.neuropharm.2008.07.045

Owald, D., Fouquet, W., Schmidt, M., Wichmann, C., Mertel, S., Depner, H., Christiansen, F., Zube, C., Quentin, C., Körner, J., Urlaub, H., Mechtler, K., & Sigrist, S. J. (2010). A Syd-1 homologue regulates pre- and postsynaptic maturation in *Drosophila*. *Journal of Cell Biology*, *188*(4), 565–579. https://doi.org/10.1083/jcb.200908055

Oyster, C. W., & Barlow, H. B. (1967). Direction-selective units in rabbit retina: distribution of preferred directions. *Science*, *155*(3764), 841–842. https://doi.org/10.1126/science.155.3764.841

Piao, C., & Sigrist, S. J. (2022). (M)Unc13s in active zone diversity: A *Drosophila* perspective. *Frontiers in Synaptic Neuroscience*, *13*, 798204. https://doi.org/10.3389/fnsyn.2021.798204

Picciotto, M. R., Higley, M. J., & Mineur, Y. S. (2012). Acetylcholine as a neuromodulator: Cholinergic signaling shapes nervous system function and behavior. *Neuron*, *76*(1), 116–129. https://doi.org/10.1016/j.neuron.2012.08.036

Potter, C. J., Tasic, B., Russler, E. V., Liang, L., & Luo, L. (2010). The Q system: A repressible binary system for transgene expression, lineage tracing, and mosaic analysis. *Cell*, *141*(3), 536–548. https://doi.org/10.1016/j.cell.2010.02.025

Poulson, D. F. (1950). Histogenesis, organogenesis, and differentiation in the embryo of *Drosophila melanogaster* Meigen. *Biology of Drosophila*, 168–274.

Prech, S., Groschner, L. N., & Borst, A. (2024). An open platform for visual stimulation of insects. *PloS One*, *19*(4), e0301999. https://doi.org/10.1371/journal.pone.0301999

Pribbenow, C., Chen, Y., Heim, M.-M., Laber, D., Reubold, S., Reynolds, E., Balles, I., Fernández-d V Alquicira, T., Suárez-Grimalt, R., Scheunemann, L., Rauch, C., Matkovic, T., Rösner, J., Lichtner, G., Jagannathan, S. R., & Owald, D. (2022). Postsynaptic plasticity of cholinergic synapses underlies the induction and expression of appetitive and familiarity memories in *Drosophila*. *eLife*, *11*, e80445. https://doi.org/10.7554/eLife.80445

Prokop, A., & Meinertzhagen, I. A. (2006). Development and structure of synaptic contacts in *Drosophila*. *Seminars in Cell & Developmental Biology*, *17*(1), 20–30. https://doi.org/10.1016/j.semcdb.2005.11.010

Purves, D. (Ed.). (2001). *Neuroscience* (2nd ed). Sinauer Associates.

Ran, F. A., Hsu, P. D., Wright, J., Agarwala, V., Scott, D. A., & Zhang, F. (2013). Genome engineering using the CRISPR-

Cas9 system. *Nature Protocols*, *8*(11), 2281–2308. https://doi.org/10.1038/nprot.2013.143

Rao-Mirotznik, R., Buchsbaum, G., & Sterling, P. (1998). Transmitter concentration at a three-dimensional synapse. *Journal of Neurophysiology*, *80*(6), 3163–3172. https://doi.org/10.1152/jn.1998.80.6.3163

Rayer, B., Naynert, M., & Stieve, H. (1990). New trends in photobiology. *Journal of Photochemistry and Photobiology B: Biology*, *7*(2–4), 107–148. https://doi.org/10.1016/1011-1344(90)85151-L

Reichardt, W. (1961). *Autocorrelation, a principle for evaluation of sensory information by the central nervous system*. 303–317.

Reichardt, W. (1987). Evaluation of optical motion information by movement detectors. *Journal of Comparative Physiology A*, *161*(4), 533–547.

Ren, G. R., Folke, J., Hauser, F., Li, S., & Grimmelikhuijzen, C. J. P. (2015). The A- and B-type muscarinic acetylcholine receptors from *Drosophila melanogaster* couple to different second messenger pathways. *Biochemical and Biophysical Research Communications*, *462*(4), 358–364. https://doi.org/10.1016/j.bbrc.2015.04.141

Richmond, J. E., & Broadie, K. S. (2002). The synaptic vesicle cycle: Exocytosis and endocytosis in *Drosophila* and *C. elegans*. *Current Opinion in Neurobiology*, *12*(5), 499–507. https://doi.org/10.1016/S0959-4388(02)00360-4

Rizzoli, S. O. (2014). Synaptic vesicle recycling: Steps and principles. *The EMBO Journal*, *33*(8), 788–822. https://doi.org/10.1002/embj.201386357

Rosenthal, J. S., & Yuan, Q. (2021). Constructing and tuning excitatory cholinergic synapses: The multifaceted functions of nicotinic acetylcholine receptors in drosophila neural development and physiology. *Frontiers in Cellular Neuroscience*, *15*, 720560. https://doi.org/10.3389/fncel.2021.720560

Rozenfeld, E., Tauber, M., Ben-Chaim, Y., & Parnas, M. (2021). GPCR voltage dependence controls neuronal plasticity and behavior. *Nature Communications*, *12*(1), 7252. https://doi.org/10.1038/s41467-021-27593-x

Ryan, K., Lu, Z., & Meinertzhagen, I. A. (2016). The CNS connectome of a tadpole larva of *Ciona intestinalis* (L.) highlights sidedness in the brain of a chordate sibling. *eLife*, *5*, e16962. https://doi.org/10.7554/eLife.16962

Ryu, L., Kim, S. Y., & Kim, A. J. (2022). From photons to behaviors: neural implementations of visual behaviors in Drosophila. *Frontiers in Neuroscience*, *16*, 883640. https://doi.org/10.3389/fnins.2022.883640

Sakmann, B., & Neher, E. (1984). Patch clamp techniques for studying ionic channels in excitable membranes. *Annual Review of Physiology*, *46*(1), 455–472. https://doi.org/10.1146/annurev.ph.46.030184.002323

Sam, C., & Bordoni, B. (2025). Physiology, Acetylcholine. In *StatPearls*. StatPearls Publishing. http://www.ncbi.nlm.nih.gov/books/NBK557825/

Sanes, J. R., & Zipursky, S. L. (2010). Design principles of insect and vertebrate visual systems. *Neuron*, *66*(1), 15–36. https://doi.org/10.1016/j.neuron.2010.01.018

Sanfilippo, P., Kim, A. J., Bhukel, A., Yoo, J., Mirshahidi, P. S., Pandey, V., Bevir, H., Yuen, A., Mirshahidi, P. S., Guo, P., Li, H.-S., Wohlschlegel, J. A., Aso, Y., & Zipursky, S. L. (2024). Mapping of multiple neurotransmitter receptor subtypes and distinct protein complexes to the connectome. *Neuron*, *112*(6), 942-958.e13. https://doi.org/10.1016/j.neuron.2023.12.014

Sauvola, C. W., & Littleton, J. T. (2021). SNARE regulatory proteins in synaptic vesicle fusion and recycling. *Frontiers in Molecular Neuroscience*, *14*, 733138. https://doi.org/10.3389/fnmol.2021.733138

Scheffer, L. K., Xu, C. S., Januszewski, M., Lu, Z., Takemura, S., Hayworth, K. J., Huang, G. B., Shinomiya, K., Maitlin-Shepard, J., Berg, S., Clements, J., Hubbard, P. M., Katz, W. T., Umayam, L., Zhao, T., Ackerman, D., Blakely, T., Bogovic, J., Dolafi, T., … Plaza, S. M. (2020). A connectome and analysis of the adult *Drosophila* central brain. *eLife*, *9*, e57443. https://doi.org/10.7554/eLife.57443

Schlegel, P., Yin, Y., Bates, A. S., Dorkenwald, S., Eichler, K., Brooks, P., Han, D. S., Gkantia, M., Dos Santos, M., Munnelly, E. J., Badalamente, G., Serratosa Capdevila, L., Sane, V. A., Fragniere, A. M. C., Kiassat, L., Pleijzier, M. W., Stürner, T., Tamimi, I. F. M., Dunne, C. R., … Jefferis, G. S. X. E. (2024). Whole-brain annotation and multi-connectome cell typing of *Drosophila*. *Nature*, *634*(8032), 139–152. https://doi.org/10.1038/s41586-024-07686-5

Schloss, P., Betz, H., Schroder, C., & Gundelfinger, E. D. (1991). Neuronal nicotinic acetylcholine receptors in *Drosophila*: Antibodies against an α-like and a non-α-subunit recognize the same high-affinity α-bungarotoxin binding complex. *Journal of Neurochemistry*, *57*(5), 1556–1562.

Schloss, P., Hermans-Borgmeyer, I., Betz, H., & Gundelfinger, E. (1988). Neuronal acetylcholine receptors in *Drosophila*: The ARD protein is a component of a high-affinity alpha-

bungarotoxin binding complex. *The EMBO Journal*, *7*(9), 2889–2894.

Schmid, A., Hallermann, S., Kittel, R. J., Khorramshahi, O., Frölich, A. M. J., Quentin, C., Rasse, T. M., Mertel, S., Heckmann, M., & Sigrist, S. J. (2008). Activity-dependent site-specific changes of glutamate receptor composition in vivo. *Nature Neuroscience*, *11*(6), 659–666. https://doi.org/10.1038/nn.2122

Scholz, N., Ehmann, N., Sachidanandan, D., Imig, C., Cooper, B. H., Jahn, O., Reim, K., Brose, N., Meyer, J., Lamberty, M., Altrichter, S., Bormann, A., Hallermann, S., Pauli, M., Heckmann, M., Stigloher, C., Langenhan, T., & Kittel, R. J. (2019). Complexin cooperates with Bruchpilot to tether synaptic vesicles to the active zone cytomatrix. *Journal of Cell Biology*, *218*(3), 1011–1026. https://doi.org/10.1083/jcb.201806155

Schwarz, T. L. (2006). Transmitter release at the neuromuscular junction. In *International Review of Neurobiology* (Vol. 75, pp. 105–144). Elsevier. https://doi.org/10.1016/S0074-7742(06)75006-1

Scott, E. K., Reuter, J. E., & Luo, L. (2003a). Dendritic development of *Drosophila* high order visual system neurons is independent of sensory experience. *BMC Neuroscience*, *4*(1). https://doi.org/10.1186/1471-2202-4-14

Scott, E. K., Reuter, J. E., & Luo, L. (2003b). Small GTPase Cdc42 is required for multiple aspects of dendritic morphogenesis. *The Journal of Neuroscience*, *23*(8), 3118–3123. https://doi.org/10.1523/jneurosci.23-08-03118.2003

Sen, R., Wu, M., Branson, K., Robie, A., Rubin, G. M., & Dickson, B. J. (2017). Moonwalker descending neurons mediate visually evoked retreat in *Drosophila*. *Current Biology*, *27*(5), 766–771.

Serbe, E., Meier, M., Leonhardt, A., & Borst, A. (2016). Comprehensive characterization of the major presynaptic elements to the *Drosophila* OFF motion detector. *Neuron*, *89*(4), 829–841. https://doi.org/10.1016/j.neuron.2016.01.006

Sethuramanujam, S., Matsumoto, A., deRosenroll, G., Murphy-Baum, B., Grosman, C., McIntosh, J. M., Jing, M., Li, Y., Berson, D., Yonehara, K., & Awatramani, G. B. (2021). Rapid multi-directed cholinergic transmission in the central nervous system. *Nature Communications*, *12*(1), 1374. https://doi.org/10.1038/s41467-021-21680-9

Seung, H. S. (2024). Predicting visual function by interpreting a neuronal wiring diagram. *Nature*, *634*(8032), 113–123. https://doi.org/10.1038/s41586-024-07953-5

Seung, H. S. (2025). Multi-output computation by single neuron biophysics in a visual system. *bioRxiv*, 2025.02.02.636137. https://doi.org/10.1101/2025.02.02.636137

Seybold, A., Kumar, S., Tumu, S. C., & Hausen, H. (2025). Neurons with larval synaptic targets pioneer the later nervous system in the annelid *Malacoceros fuliginosus*. *Frontiers in Neuroscience*, *18*, 1439897. https://doi.org/10.3389/fnins.2024.1439897

Shearin, H. K., Quinn, C. D., Mackin, R. D., Macdonald, I. S., & Stowers, R. S. (2018). T-GRASP, a targeted GRASP for assessing neuronal connectivity. *Journal of Neuroscience Methods*, *306*, 94–102. https://doi.org/10.1016/j.jneumeth.2018.05.014

Sheng, M. (1996). PDZs and receptor/channel clustering: rounding up the latest suspects. *Neuron*, *17*(4), 575–578. https://doi.org/10.1016/S0896-6273(00)80190-7

Shin, M., Copeland, J. M., & Venton, B. J. (2018). *Drosophila* as a model system for neurotransmitter measurements. *ACS Chemical Neuroscience*, *9*(8), 1872–1883. https://doi.org/10.1021/acschemneuro.7b00456

Shinomiya, K., Huang, G., Lu, Z., Parag, T., Xu, C. S., Aniceto, R., Ansari, N., Cheatham, N., Lauchie, S., Neace, E., Ogundeyi, O., Ordish, C., Peel, D., Shinomiya, A., Smith, C., Takemura, S., Talebi, I., Rivlin, P. K., Nern, A., … Meinertzhagen, I. A. (2019). Comparisons between the ON- and OFF-edge motion pathways in the *Drosophila* brain. *eLife*, *8*, e40025. https://doi.org/10.7554/eLife.40025

Shinomiya, K., Karuppudurai, T., Lin, T.-Y., Lu, Z., Lee, C.-H., & Meinertzhagen, I. A. (2014). Candidate neural substrates for off-edge motion detection in *Drosophila*. *Current Biology*, *24*(10), 1062–1070. https://doi.org/10.1016/j.cub.2014.03.051

Shinomiya, K., Nern, A., Meinertzhagen, I. A., Plaza, S. M., & Reiser, M. B. (2022). Neuronal circuits integrating visual motion information in *Drosophila melanogaster*. *Current Biology: CB*, *32*(16), 3529-3544.e2. https://doi.org/10.1016/j.cub.2022.06.061

Shinomiya, K., Takemura, S., Rivlin, P. K., Plaza, S. M., Scheffer, L. K., & Meinertzhagen, I. A. (2015). A common evolutionary origin for the ON- and OFF-edge motion detection pathways of the *Drosophila* visual system.

Frontiers in Neural Circuits, *9*. https://doi.org/10.3389/fncir.2015.00033

Sigmund, F., Berezin, O., Beliakova, S., Magerl, B., Drawitsch, M., Piovesan, A., Gonçalves, F., Bodea, S.-V., Winkler, S., Bousraou, Z., Grosshauser, M., Samara, E., Pujol-Martí, J., Schädler, S., So, C., Irsen, S., Walch, A., Kofler, F., Piraud, M., … Westmeyer, G. G. (2023). Genetically encoded barcodes for correlative volume electron microscopy. *Nature Biotechnology*, *41*(12), 1734–1745. https://doi.org/10.1038/s41587-023-01713-y

Sivilotti, L., & Colquhoun, D. (1995). Acetylcholine receptors: Too many channels, too few functions. *Science*, *269*(5231), 1681–1682. https://doi.org/10.1126/science.7569892

Smallman, B., & Pal, R. (1957). The activity and intracellular distribution of choline acetylase in insect nervous tissue. *Bull. Ent. Soc. Am.*, *3*, 25.

Söllner, T., Whiteheart, S. W., Brunner, M., Erdjument-Bromage, H., Geromanos, S., Tempst, P., & Rothman, J. E. (1993). SNAP receptors implicated in vesicle targeting and fusion. *Nature*, *362*(6418), 318–324. https://doi.org/10.1038/362318a0

Stansfeld, C. E., Röper, J., Ludwig, J., Weseloh, R. M., Marsh, S. J., Brown, D. A., & Pongs, O. (1996). Elevation of intracellular calcium by muscarinic receptor activation induces a block of voltage-activated rat ether-à-go-go channels in a stably transfected cell line. *Proceedings of the National Academy of Sciences*, *93*(18), 9910–9914. https://doi.org/10.1073/pnas.93.18.9910

Strother, J. A., Nern, A., & Reiser, M. B. (2014). Direct observation of ON and OFF pathways in the *Drosophila* visual system. *Current Biology*, *24*(9), 976–983. https://doi.org/10.1016/j.cub.2014.03.017

Stuart, A. E. (1999). From fruit flies to barnacles, histamine is the neurotransmitter of arthropod photoreceptors. *Neuron*, *22*(3), 431–433. https://doi.org/10.1016/S0896-6273(00)80699-6

Südhof, T. C. (2004). The synaptic vesicle cycle. *Annual Review of Neuroscience*, *27*(1), 509–547. https://doi.org/10.1146/annurev.neuro.26.041002.131412

Südhof, T. C., & Rothman, J. E. (2009). Membrane fusion: Grappling with SNARE and SM proteins. *Science*, *323*(5913), 474–477. https://doi.org/10.1126/science.1161748

Sun, W., Deng, Q., Levick, W. R., & He, S. (2006). ON direction-selective ganglion cells in the mouse retina. *The Journal of*

Physiology, *576*(1), 197–202. https://doi.org/10.1113/jphysiol.2006.115857

Surkova, S., Görne, J., Nuzhdin, S., & Samsonova, M. (2021). Interplay between sex determination cascade and major signaling pathways during *Drosophila* eye development: Perspectives for future research. *Developmental Biology*, *476*, 41–52. https://doi.org/10.1016/j.ydbio.2021.03.005

Suver, M. P., Huda, A., Iwasaki, N., Safarik, S., & Dickinson, M. H. (2016). An array of descending visual interneurons encoding self-motion in *Drosophila*. *The Journal of Neuroscience*, *36*(46), 11768–11780. https://doi.org/10.1523/JNEUROSCI.2277-16.2016

Szapiro, G., & Barbour, B. (2007). Multiple climbing fibers signal to molecular layer interneurons exclusively via glutamate spillover. *Nature Neuroscience*, *10*(6), 735–742. https://doi.org/10.1038/nn1907

Szüts, D., & Bienz, M. (2000). LexA chimeras reveal the function of *Drosophila* Fos as a context-dependent transcriptional activator. *Proceedings of the National Academy of Sciences*, *97*(10), 5351–5356. https://doi.org/10.1073/pnas.97.10.5351

Takemura, S., Bharioke, A., Lu, Z., Nern, A., Vitaladevuni, S., Rivlin, P. K., Katz, W. T., Olbris, D. J., Plaza, S. M., Winston, P., Zhao, T., Horne, J. A., Fetter, R. D., Takemura, S., Blazek, K., Chang, L.-A., Ogundeyi, O., Saunders, M. A., Shapiro, V., … Chklovskii, D. B. (2013). A visual motion detection circuit suggested by *Drosophila* connectomics. *Nature*, *500*(7461), 175–181. https://doi.org/10.1038/nature12450

Takemura, S., Hayworth, K. J., Huang, G. B., Januszewski, M., Lu, Z., Marin, E. C., Preibisch, S., Xu, C. S., Bogovic, J., Champion, A. S., Cheong, H. S., Costa, M., Eichler, K., Katz, W., Knecht, C., Li, F., Morris, B. J., Ordish, C., Rivlin, P. K., … Berg, S. (2024). *A Connectome of the Male Drosophila Ventral Nerve Cord*. https://doi.org/10.7554/eLife.97769.1

Takemura, S., Karuppudurai, T., Ting, C.-Y., Lu, Z., Lee, C.-H., & Meinertzhagen, I. A. (2011). Cholinergic circuits integrate neighboring visual signals in a *Drosophila* motion detection pathway. *Current Biology: CB*, *21*(24), 2077–2084. https://doi.org/10.1016/j.cub.2011.10.053

Takemura, S.-Y., Nern, A., Chklovskii, D. B., Scheffer, L. K., Rubin, G. M., & Meinertzhagen, I. A. (2017). The comprehensive connectome of a neural substrate for "ON" motion detection in *Drosophila*. *eLife*, *6*, e24394. https://doi.org/10.7554/eLife.24394

Tang, A.-H., Chen, H., Li, T. P., Metzbower, S. R., MacGillavry, H. D., & Blanpied, T. A. (2016). A trans-synaptic nanocolumn aligns neurotransmitter release to receptors. *Nature*, *536*(7615), 210–214. https://doi.org/10.1038/nature19058

Taylor, W. R., & Vaney, D. I. (2002). Diverse synaptic mechanisms generate direction selectivity in the rabbit retina. *Journal of Neuroscience*, *22*(17), 7712–7720.

Thompson, A. J., Lester, H. A., & Lummis, S. C. R. (2010). The structural basis of function in Cys-loop receptors. *Quarterly Reviews of Biophysics*, *43*(4), 449–499. https://doi.org/10.1017/S0033583510000168

Tian, L., Hires, S. A., Mao, T., Huber, D., Chiappe, M. E., Chalasani, S. H., Petreanu, L., Akerboom, J., McKinney, S. A., Schreiter, E. R., Bargmann, C. I., Jayaraman, V., Svoboda, K., & Looger, L. L. (2009). Imaging neural activity in worms, flies and mice with improved GCaMP calcium indicators. *Nature Methods*, *6*(12), 875–881. https://doi.org/10.1038/nmeth.1398

Tirian, L., & Dickson, B. J. (2017). The VT GAL4, LexA, and split-GAL4 driver line collections for targeted expression in the *Drosophila* nervous system. https://doi.org/10.1101/198648

Todorova, V., Merolla, L., Karademir, D., Wögenstein, G. M., Behr, J., Ebner, L. J. A., Samardzija, M., & Grimm, C. (2022). Retinal Layer Separation (ReLayS) method enables the molecular analysis of photoreceptor segments and cell bodies, as well as the inner retina. *Scientific Reports*, *12*(1), 20195. https://doi.org/10.1038/s41598-022-24586-8

Tomizawa, M., & Casida, J. E. (2003). Selective toxicity of neonicotinoids attributable to specificity of insect and mammalian nicotinic receptors. *Annual Review of Entomology*, *48*(1), 339–364.

Tomizawa, M., Latli, B., & Casida, J. E. (1996). Novel neonicotinoid-agarose affinity column for *Drosophila* and *musca* nicotinic acetylcholine receptors. *Journal of Neurochemistry*, *67*(4), 1669–1676. https://doi.org/10.1046/j.1471-4159.1996.67041669.x

Van Der Bliek, A. M., & Meyerowrtz, E. M. (1991). Dynamin-like protein encoded by the *Drosophila* shibire gene associated with vesicular traffic. *Nature*, *351*(6325), 411–414. https://doi.org/10.1038/351411a0

Van Vactor, D., & Sigrist, S. J. (2017). Presynaptic morphogenesis, active zone organization and structural plasticity in

Drosophila. *Current Opinion in Neurobiology*, *43*, 119–129. https://doi.org/10.1016/j.conb.2017.03.003

Venken, K. J. T., Schulze, K. L., Haelterman, N. A., Pan, H., He, Y., Evans-Holm, M., Carlson, J. W., Levis, R. W., Spradling, A. C., Hoskins, R. A., & Bellen, H. J. (2011). MiMIC: A highly versatile transposon insertion resource for engineering *Drosophila melanogaster* genes. *Nature Methods*, *8*(9), 737–743. https://doi.org/10.1038/nmeth.1662

Vlasits, A. L., Morrie, R. D., Tran-Van-Minh, A., Bleckert, A., Gainer, C. F., DiGregorio, D. A., & Feller, M. B. (2016). A role for synaptic input distribution in a dendritic computation of motion direction in the retina. *Neuron*, *89*(6), 1317–1330.

Vogel, C., & Marcotte, E. M. (2012). Insights into the regulation of protein abundance from proteomic and transcriptomic analyses. *Nature Reviews Genetics*, *13*(4), 227–232.

Wagh, D. A., Rasse, T. M., Asan, E., Hofbauer, A., Schwenkert, I., Dürrbeck, H., Buchner, S., Dabauvalle, M.-C., Schmidt, M., Qin, G., Wichmann, C., Kittel, R., Sigrist, S. J., & Buchner, E. (2006). Bruchpilot, a protein with homology to ELKS/CAST, is required for structural integrity and function of synaptic active zones in *Drosophila*. *Neuron*, *49*(6), 833–844. https://doi.org/10.1016/j.neuron.2006.02.008

Wang, L., Wu, C., Peng, W., Zhou, Z., Zeng, J., Li, X., Yang, Y., Yu, S., Zou, Y., Huang, M., Liu, C., Chen, Y., Li, Y., Ti, P., Liu, W., Gao, Y., Zheng, W., Zhong, H., Gao, S., … Chu, J. (2022). A high-performance genetically encoded fluorescent indicator for in vivo cAMP imaging. *Nature Communications*, *13*(1), 5363. https://doi.org/10.1038/s41467-022-32994-7

Weltzin, M. M., George, A. A., Lukas, R. J., & Whiteaker, P. (2019). Distinctive single-channel properties of α4β2-nicotinic acetylcholine receptor isoforms. *PLOS ONE*, *14*(3), e0213143. https://doi.org/10.1371/journal.pone.0213143

White, J. G., Southgate, E., Thomson, J. N., & Brenner, S. (1986). The structure of the nervous system of the nematode *Caenorhabditis elegans*. *Philosophical Transactions of the Royal Society of London. Series B, Biological Sciences*, *314*(1165), 1–340. https://doi.org/10.1098/rstb.1986.0056

Wolff, T., Eddison, M., Chen, N., Nern, A., Sundaramurthi, P., Sitaraman, D., & Rubin, G. M. (2024). Cell type-specific driver lines targeting the *Drosophila* central complex and

their use to investigate neuropeptide expression and sleep regulation. https://doi.org/10.1101/2024.10.21.619448

Xia, R. -Y., Li, M. -Q., Wu, Y. -S., Qi, Y. -X., Ye, G. -Y., & Huang, J. (2016). A new family of insect muscarinic acetylcholine receptors. *Insect Molecular Biology*, *25*(4), 362–369. https://doi.org/10.1111/imb.12229

Xia, X., & Li, Y. (2025). A high-performance GRAB sensor reveals differences in the dynamics and molecular regulation between neuropeptide and neurotransmitter release. *Nature Communications*, *16*(1), 819. https://doi.org/10.1038/s41467-025-56129-w

Xing, X., & Wu, C.-F. (2018). Unraveling synaptic GCaMP signals: differential excitability and clearance mechanisms underlying distinct Ca^{2+} dynamics in tonic and phasic excitatory, and aminergic modulatory motor terminals in *Drosophila*. *Eneuro*, *5*(1), ENEURO.0362-17.2018. https://doi.org/10.1523/ENEURO.0362-17.2018

Yan, W., Laboulaye, M. A., Tran, N. M., Whitney, I. E., Benhar, I., & Sanes, J. R. (2020). Mouse retinal cell atlas: Molecular identification of over sixty amacrine cell types. *Journal of Neuroscience*, *40*(27), 5177–5195.

Yang, H. H., St-Pierre, F., Sun, X., Ding, X., Lin, M. Z., & Clandinin, T. R. (2016). Subcellular imaging of voltage and calcium signals reveals neural processing *in vivo*. *Cell*, *166*(1), 245–257. https://doi.org/10.1016/j.cell.2016.05.031

Yasuyama, K., & Salvaterra, P. M. (1999). Localization of choline acetyltransferase-expressing neurons in *Drosophila* nervous system. *Microscopy Research and Technique*, *45*(2), 65–79. https://doi.org/10.1002/(SICI)1097-0029(19990415)45:2<65::AID-JEMT2>3.0.CO;2-0

Yoshida, K., Watanabe, D., Ishikane, H., Tachibana, M., Pastan, I., & Nakanishi, S. (2001). A key role of starburst amacrine cells in originating retinal directional selectivity and optokinetic eye movement. *Neuron*, *30*(3), 771–780.

Zhang, Y., Rózsa, M., Liang, Y., Bushey, D., Wei, Z., Zheng, J., Reep, D., Broussard, G. J., Tsang, A., Tsegaye, G., Narayan, S., Obara, C. J., Lim, J.-X., Patel, R., Zhang, R., Ahrens, M. B., Turner, G. C., Wang, S. S.-H., Korff, W. L., … Looger, L. L. (2023). Fast and sensitive GCaMP calcium indicators for imaging neural populations. *Nature*, *615*(7954), 884–891. https://doi.org/10.1038/s41586-023-05828-9

Zheng, Z., Lauritzen, J. S., Perlman, E., Robinson, C. G., Nichols, M., Milkie, D., Torrens, O., Price, J., Fisher, C. B., Sharifi,

N., Calle-Schuler, S. A., Kmecova, L., Ali, I. J., Karsh, B., Trautman, E. T., Bogovic, J. A., Hanslovsky, P., Jefferis, G. S. X. E., Kazhdan, M., … Bock, D. D. (2018). A complete electron microscopy volume of the brain of adult *Drosophila melanogaster*. *Cell*, *174*(3), 730-743.e22. https://doi.org/10.1016/j.cell.2018.06.019

Zuker, C., Montell, C., Jones, K., Laverty, T., & Rubin, G. (1987). A rhodopsin gene expressed in photoreceptor cell R7 of the *Drosophila* eye: Homologies with other signal-transducing molecules. *The Journal of Neuroscience*, *7*(5), 1550–1557. https://doi.org/10.1523/JNEUROSCI.07-05-01550.1987

Zuker, C. S., Cowman, A. F., & Rubin, G. M. (1985). Isolation and structure of a rhodopsin gene from *D. melanogaster*. *Cell*, *40*(4), 851–858. https://doi.org/10.1016/0092-8674(85)90344-7